

**A petrographic, geochemical and geochronological investigation of
deformed granitoids from SW Rajasthan: Neoproterozoic age of
formation and evidence of Pan-African imprint**

By

ANIKA M. SOLANKI

Supervisor: PROF. L. D. ASHWAL

DISSERTATION

Submitted in fulfilment of the requirements for the degree

MAGISTER SCIENTAE

in

GEOLOGY

in the

SCHOOL OF GEOSCIENCES,

FACULTY OF SCIENCE

at the

UNIVERSITY OF THE WITWATERSRAND

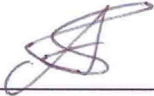
JOHANNESBURG

JUNE, 2011



DECLARATION

I, Anika. M. Solanki, declare that this dissertation thesis is my own, unaided work. It is being submitted for the degree of Master of Science in the University of the Witwatersrand, Johannesburg. It has not been submitted before for any degree or examination in any other university.



(Signature of candidate)

21 day of June 2011

ABSTRACT

Granitoid intrusions are numerous in southwestern Rajasthan and are useful because they can provide geochronological constraints on tectonic activity and geodynamic conditions operating at the time of intrusion, as well as information about deeper crustal sources. The particularly voluminous Neoproterozoic felsic magmatism in the Sirohi region of Rajasthan is of particular interest as it may have implications for supercontinental (Rodinia and Gondwana) geometry.

The Mt. Abu granitoid pluton is located between two major felsic suites, the older (~870-800 Ma) Erinpura granite and the younger (~751-771 Ma) Malani Igneous Suite (MIS). The Erinpura granite is syn- to late-orogenic and formed during the Delhi orogeny, while the MIS is classified as alkaline, anorogenic and either rift- or plume-related. This tectonic setting is contentious, as recent authors have proposed formation within an Andean-type arc setting. The Mt. Abu granitoid pluton has been mapped as partly Erinpura (deformed textural variant) and partly younger MIS (undeformed massive pink granite). As the tectonic settings of the two terranes are not compatible, confusion arises as to the classification of the Mt. Abu granitoid pluton. Poorly-constrained Rb-Sr age dating places the age of formation anywhere between 735 ± 15 and 800 ± 50 Ma. The older age is taken as evidence that the Mt. Abu intrusion was either a late phase of the Erinpura granite.

However, U-Pb zircon geochronology clearly indicates that the Mt. Abu felsic pluton is not related to- or contiguous with- the Erinpura granite suite. The major results from this study indicate that all textural variants within the Mt. Abu pluton were formed coevally at ~765 Ma. Samples of massive pink granite, mafic-foliated granite and augen gneiss from the pluton were dated using U-Pb zircon ID-TIMS at 766.0 ± 4.3 Ma, 763.2 ± 2.7 Ma and 767.7 ± 2.3 Ma, respectively.

The simple Mt. Abu pluton is considered as an enriched intermediate I- to A-type intrusion. They are not anorogenic A-types, as, although these felsic rocks have high overall alkali and incompatible element enrichment, no phase in the Mt. Abu pluton contains alkali rich amphibole or pyroxene, nor do REE diagrams for the most enriched samples show the gull-wing shape typical of highly evolved alkaline phases. The alkali-enriched magma may be explained by partial melting of a crustal source such as the high-K meta-igneous (andesite) one suggested by Roberts & Clemens (1993), not derivation from a mantle-derived mafic magma. The fairly restricted composition of Mt. Abu granitoids suggests that partial melting and a degree of assimilation/mixing may have been the major factors affecting the evolution of this granitoid pluton; fractional crystallization was not the major control on evolution of these granitoids. Revdar Rd. granitoids that are similar in outcrop appearance and petrography to Mt. Abu granitoids also conform to Mt. Abu granitoids geochemically and are classified as part of the Mt. Abu felsic pluton.

Mt. Abu samples from this study have a maximum age range of 760.5-770 Ma, placing the Mt. Abu pluton within the time limits of the Malani Igneous Suite (MIS) as well as ~750 Ma granitoids from the Seychelles. Ages of the Sindreh-Punagarh Groups are also similar. These mafic-ultramafic volcanics are thought to be remnants of an ophiolitic mélangé within a back-arc basin setting at ~750-770 Ma. The three Indian terranes are spatially and temporally contiguous. The same contiguity in space and time has been demonstrated by robust paleomagnetic data for the Seychelles and MIS. These similarities imply formation within a common geological event, the proposed Andean-type arc (Ashwal et al., 2002) on the western outboard of Rodinia. The implications are that peninsular India did not become a coherent entity until after this Neoproterozoic magmatism; Rodinia was not a static supercontinent that was completely amalgamated by 750 Ma, as subduction was occurring here simultaneously with rifting elsewhere.

The Mt. Abu pluton has undergone deformation, with much of the pluton having foliated or augen gneiss textures. The timing of some of the deformation, particularly the augen gneiss and shear zone deformation, is thought to have occurred during intrusion. The Mt. Abu and Erinpura granitoids have experienced a common regional metamorphic event, as hornblende (Mt. Abu) and biotite (Erinpura) give $^{40}\text{Ar}/^{39}\text{Ar}$ ages of 508.7 ± 4.4 Ma and 515.7 ± 4.5 Ma, respectively. This event may have reactivated older deformatory trends as well. The temperature of resetting of argon in hornblende coincides with temperatures experienced during upper-greenschist to lower-amphibolite facies metamorphism. These late Pan-African ages are the first such ages reported for the Sirohi region and southern part of the Aravalli mountain range. They offer evidence for the extension of Pan-African amalgamation tectonics (evidence from southern India) into NW India.

The age of formation of the Erinpura augen gneiss magma is 880.5 ± 2.1 Ma, thus placing the Erinpura granitoids within the age limits of the Delhi orogeny (~ 900 - 800 Ma; Bhushan, 1995). Most deformation observed here would have been caused by compression during intrusion. The Erinpura granitoids are S-type granitoids due to their predominantly peraluminous nature, restricted SiO_2 -content, normative corundum and the presence of Al-rich muscovite and sillimanite in the mode. Weathered argillaceous metasedimentary material may also have been incorporated in this magma, while the presence of inherited cores suggests relatively lower temperatures of formation for these granitoids as compared to the Mt. Abu granitoids. The age of inheritance (1971 ± 23 Ma) in the Erinpura augen gneiss is taken as the age of the source component, which coincides with Aravalli SG formation.

The Sumerpur granitoids differ from the Erinpura granitoids in terms of macroscopic and microscopic texture (undeformed, rarely megaporphyritic) but conform geochemically to the Erinpura granitoid characteristics and may thus be related to the Erinpura granitoid suite. The Revdar Rd. granitoids that are similar in macroscopic appearance to Erinpura granitoids also conform geochemically, and may similarly belong to the Erinpura granite suite. A Revdar Rd. mylonite gneiss with the Erinpura granitoids' geochemical signature was dated at ~ 841 Ma, which does not conform to the age of the type-locality Erinpura augen gneiss dated here, but later intrusion within the same event cannot be ruled out because of the uncertainty in the age data (~ 21 Ma). The presence of garnet in one Revdar Rd. (Erinpura-type) sample implies generation of these granitoids at depth and/or entrainment from the source, similar to the S-type Erinpura granitoids.

The Ranakpur granitoids differ significantly from both the Erinpura and Mt. Abu intrusives due to their low SiO_2 -content and steep REE profiles (garnet present in the source magma); they are thought to have been generated under higher pressures from a more primitive source. The deeper pressure of generation is confirmed by the absence of a negative Eu-anomaly. The Ranakpur quartz syenite dated at 848.1 ± 7.1 Ma is younger by ~ 30 m.y. than the Erinpura augen gneiss. It is within the same time range as numerous other granitoids from this region as well as the Revdar Rd. granitoid dated in this study. The prevalence of 830-840 Ma ages may indicate that a major tectonic event occurred at this time. The Ranakpur quartz syenite may have been generated near a subduction or collision zone, where thickened crust allows for magma generation at depth. The deeply developed Nb-anomaly in the spider diagram also implies a larger subduction component to the magma.

The Swarupganj Rd. monzogranite is interpreted to have formed by high degrees of partial melting from a depleted crustal source and is dissimilar to other granitoids from this study. More sampling, geochemical and geochronological work needs to be done in order to characterize this intrusion.

The Kishengarh nepheline syenite gneiss is situated in the North Delhi Fold Belt and is the oldest sample dated within this study. The deformation in this sample is due to arc- or continental- collision during a Grenvillian-type orogeny related to the amalgamation of the Rodinia supercontinent (and peninsular India), dated by the highly reset zircons at ~990 Ma. This is considered a DARC (deformed alkaline rock and carbonatite) and represents a suture zone (Leelanandam et al., 2006). The primary age of formation of this DARC is older than 1365 ± 99 Ma, which is the age of xenocrystic titanites from the sample.

The granitoid rocks from this study area (Sirohi region) range widely in outcrop appearance, petrography and geochemistry. Granitoids from the Sirohi region dated in this study show a range of meaningful ages that represent geological events occurring at ~880 Ma, ~844 Ma, ~817 Ma, ~789 Ma, ~765 Ma and ~511 Ma. Granitoid magmatism (age of formation) in this region is predominantly Neoproterozoic, and the number of events associated with each granitoid intrusion as well as diverse tectonic settings implies a complexity in the South Delhi Fold Belt that is not matched by the conventional and simplified view of a progression from collision and orogeny during Grenvillian times (Rodinia formation), through late orogenic events, to anorogenic, within-plate (rift-related) alkaline magmatism during Rodinia dispersal. Instead, it is envisaged that convergence and subduction during the formation of Rodinia occurred at ~1 Ga (Kishengarh nepheline syenite deformation), with a transition to continental-continental collision at ~880-840 Ma (Erinpura and Ranakpur granitoids). This was then followed by far-field Mt. Abu and MIS magmatism, related to a renewed period of subduction at ~770 Ma. The last deformatory event to affect this region was that associated with the formation of Gondwana in the late Pan-African (~510 Ma).

ACKNOWLEDGEMENTS

I would like to thank the following people and institutions for their advice, support and understanding during this project:

- My parents, for understanding and supporting me.
- My supervisor, Prf. L. Ashwal, for having the patience and the faith to see me through.
- Prof. M. Pandit, for his enormous help in all aspects of this project.
- The staff at the Universiteit i Oslo Geoscience division, especially Prof. F. Corfu and Gunborg Bye Fjeld, for their willingness to help and their support during the three months of work.
- Bart Hendriks, for his invaluable guidance.
- The staff and my friends at Wits for all the craziness and fun amongst the learning.

CONTENTS

Declaration	
Abstract	
Acknowledgements	
List of Figures	
List of Tables	
<u>1. INTRODUCTION</u>	1
1.1 Regional Geology.....	1
1.2 Aim of the Study.....	7
<u>2. GEOLOGY OF THE STUDY AREA</u>	9
<u>3. ANALYTICAL METHODS</u>	14
3.1 Petrography.....	14
3.2 X-Ray Fluorescence (XRF) Spectrometry.....	15
3.3 LA-ICPMS (Laser Ablation Inductively-Coupled Plasma Mass-Spectrometry).....	16
3.4 U-Pb Zircon Geochronology.....	16
3.5 Ar-Ar Geochronology.....	18
<u>4. FIELD & PETROGRAPHIC STUDY</u>	20
4.1 Mt. Abu granitoids (and related rocks).....	25
4.2 Erinpura granitoids.....	32
4.2.1 Balda granitoid (late-stage Erinpura granite).....	36
4.3 Sumerpur granitoids (late-stage Erinpura granite).....	37
4.4 Ranakpur granitoids.....	38
4.5.1 Revdar Rd. granitoids (Mt. Abu type).....	41
4.5.2 Revdar Rd. granitoids (Erinpura type).....	43
4.6 Swarupganj Rd. granitoid.....	44
4.7 Kishengarh nepheline syenite.....	45
4.8 Mt. Abu dolerite dykes.....	46
4.9 Summary of Field and Petrographic Study.....	47
<u>5. GEOCHEMISTRY</u>	51
5.1 Major and trace element geochemistry.....	54
5.2 Maficity/molar Mg + Fe.....	75
5.3 REE diagrams.....	78
5.4 Spider diagrams.....	82
5.5 Summary of Geochemistry.....	85
<u>6. U-PB GEOCHRONOLOGY</u>	92
6.1 Older Samples (Erinpura, Revdar Rd. and Ranakpur).....	95
6.1.1 Erinpura augen gneiss (AA6-18).....	95
6.1.2 Revdar Rd. mylonitic gneiss (AA6-38).....	98

6.1.3 Ranakpur massive quartz syenite (AA6-2).....	100
6.2 Younger Group (Mt. Abu pluton).....	103
6.2.1 Mt. Abu granite with mafic mineral foliation (AA6-14B).....	103
6.2.2 Mt. Abu undeformed orange-pink granite (AA6-9).....	105
6.2.3 Mt. Abu augen gneiss (AA6-35).....	107
6.3 Kishengarh nepheline syenite-gneiss (AA6-52A).....	109
6.4 Discussion.....	114
6.4.1 Erinpura, Ranakpur and Revdar Rd. granitoids.....	114
6.4.2 Younger Group (Mt. Abu granitoids).....	117
6.4.3 Kishengarh nepheline syenite gneiss.....	119
6.4.4 Primary, metamorphic and inherited ages within the Erinpura and Ranakpur granitoids and Kishengarh nepheline syenite gneiss.....	121
<u>7. ⁴⁰AR/³⁹AR GEOCHRONOLOGY</u>	124
7.1 Mt. Abu orange-pink granite: AA6-9.....	124
7.2 Erinpura augen gneiss: AA6-18.....	126
7.3 Ranakpur quartz syenite: AA6-2.....	128
7.4 Kishengarh nepheline syenite: AA6-5.....	129
7.5 Interpretation.....	131
<u>8. SUMMARY COMPARISON OF MT. ABU TO SIMILAR GRANITOIDS FROM SEYCHELLES AND MALANI IGNEOUS SUITE (MIS)</u>	135
8.1 Summary comparison of Mt. Abu granitoids (and felsic dykes) to similar granitoids from Seychelles and MIS.....	135
8.2 Geochemical comparison of Mt. Abu and Erinpura granitoids (and felsic dykes) with those from the Seychelles and MIS.....	136
<u>9. DISCUSSION</u>	146
<u>10. CONCLUSIONS</u>	160
<u>11. REFERENCES</u>	164

Appendix A – Enlarged study area images

Appendix B – Petrography notes

Appendix C – Normative data

Appendix D – Major and trace elements (Mt. Abu dolerites, Seychelles and MIS granitoids)

Appendix E – Ar-Ar results tables

List of Figures

Figure 1.1. The regional geology of the Aravalli Craton showing location of Mt. Abu, adapted from Van Lente (2001).

Figure 2.1. Regional geology of the study area and accompanying legend. Sample sites are indicated as yellow dots within the Erinpura and MIS granitoids (after Geological Survey Map of India, 1998). Please see Appendix A for larger version of this map.

Figure 2.2. Topographical map showing the main Mt. Abu pluton in relation to the site of the Ranakpur granitoid samples.

Figure 2.3. Geological map of the Mt. Abu pluton and immediate surrounds. The black circles represent Mt. Abu felsic samples, the pale yellow circles Revdar Rd. samples, the dark grey circles are Swarupganj Rd. samples and the bright yellow circles represent various Erinpura granitoid samples. The type-locality Erinpura granite sample is not shown on this map as it outcrops further north (see Fig. 2.1). Please see Appendix A for larger version of this map.

Figure 4.1. Mt. Abu granitoids in the field, with a wide range of textures. A- lobate and somewhat diffuse contact between the K-feldspar rich type-granite on the left (AA6-15A) and the more porphyritic type (AA6-15B). B- subvertical slickenside lineations defined by fine-grained micas. C- Mt. Abu augen gneiss foliation (AA6-35). D- foliated and porphyritic granite with elongate mafic clusters.

Figure 4.2. Photomicrographs of magmatic textures in Mt. Abu samples. A- typical textural relation, with sericitized euhedral plagioclase and subhedral orthoclase surrounded by smaller recrystallized quartz and euhedral Fe-rich biotite between feldspars (AA6-27B; FOV=3 mm). B- a subhedral perthite phenocryst with an altered rim. Alteration is greatest along fractures within phenocryst (AA6-9; FOV=3 mm). C- a mafic cluster containing prismatic hornblende together with Fe-Ti oxides, which have fine-grained titanite rims. Quartz is granular-textured but becomes much finer-grained towards the boundaries between mafic clusters and feldspar grain (AA6-15A; FOV=3 mm). D- anhedral fluorite, with radiation damage from inclusions within the subhedral biotite that have made the fluorite purple (AA6-27A; FOV=1.5 mm). E- graphic texture between large microcline and quartz crystals, which are intergrown, as the blebs are optically continuous for both (AA6-8; FOV=3 mm). F- lobate myrmekite structures grown into the boundaries of an orthoclase phenocryst (AA6-8; FOV=1.5 mm).

Figure 4.3. Microphotographs of accessory minerals and textures in Mt. Abu samples. A- zircon with oscillatory zoning surrounding a core that seems to be disturbed (AA6-34; FOV=0.25 mm). B- radioactive long-prismatic zircon and what may be monazite (rhomb-shape) within a mafic cluster (AA6-9; FOV=1.5 mm). C- a reacted euhedral orthoclase phenocryst from a rhyolitic dyke. The core is somewhat altered and core grain boundary has been reacted to form myrmekite/graphic intergrowth. This reflects a change in magmatic conditions of the magma (AA6-11; FOV=1.5 mm).

Figure 4.4. Microphotographs of Fe-Ti oxide minerals in Mt. Abu samples. A- anhedral ilmenite, replaced by titanite rim (reflected light, AA6-8; FOV=0.9 mm). B- euhedral to subhedral titanomagnetite (reflected light, AA6-27A; FOV=1.5 mm).

Figure 4.5. Deformation microstructures in Mt. Abu samples. A- strained quartz with strain domains having different extinction angles and checkerboard grain boundaries (AA6-30A; FOV=1.5 mm). B- kinked deformed twinning within plagioclase that is non-parallel and terminates into points (AA6-8; not sub-parallel; FOV=3 mm). C- mafic (elongate biotite) and felsic minerals separated into bands due to strain partitioning around a more competent orthoclase phenocryst, with finer-grained recrystallized material formed around edges of orthoclase due to strain accommodation (AA6-36A; FOV=3 mm). D- a quartz phenocryst with undulose extinction and new subgrain formation on grain boundaries to accommodate strain (AA6-28; FOV=3 mm). E- gneissose texture with elongate biotite formation between recrystallized quartz and feldspar (AA6-35; FOV=3 mm). F- Carlsbad-twinning orthoclase

phenocryst with lobe-like myrmekitic extension into other twin, which may be related to ductile deformation of the feldspar and greater fluid content of magma. Groundmass is very fine-grained, with an alignment of platy muscovite (AA6-28; FOV=1.5 mm).

Figure 4.6. Mirpur granite and MIS dyke microphotographs. A- typical texture of the Mirpur granite where the feldspar is almost totally sericitized, while the quartz is inclusion-rich. Chlorite with radioactive haloes is the major mafic mineral, and is associated with skeletal to subhedral opaque minerals (AA6-21A; FOV=3 mm). B- subhedral to euhedral hematite and magnetite in irregular growth (reflected light, AA6-21A; FOV=0.9 mm). C- euhedral skeletal hematite with pink-purple ilmenite at either end (reflected light, AA6-51; FOV=0.9 mm).

Figure 4.7. Field photographs of Erinpura granitoid. A- highly strained augen gneiss, with augens somewhat flattened due to intensity of deformation (AA6-18). B- a porphyritic specimen, with large irregular rapakivi-textured phenocryst. Feldspars vary from euhedral to anhedral, with larger phenocrysts commonly anhedral (AA6-24).

Figure 4.8. Microphotographs of Erinpura samples. A- myrmekitic intergrowth along orthoclase phenocryst grain boundary that is related to deformation, as groundmass is very fine-grained and has a recrystallized flow-growth texture of felsic minerals and aligned biotite crystals (AA6-26; FOV=1.5 mm). B- primary hornblende in crossed-nicols, highly altered and sericitic, with primary magmatic zoning, then a zone of dissolution and regrowth (circular rim) and finally more growth-zoning into typical prismatic hornblende (replaced on edges by tremolite and chlorite). These events may have occurred in the magma chamber as conditions changed (AA6-22; FOV=0.9 mm). C- a biotite cluster which has undergone strain around the edges, as can be seen by the fine-grained recrystallization of the biotite to accommodate the strain and the lens-shape of the cluster (AA6-20; FOV=3 mm).

Figure 4.9. Alteration within the Erinpura samples. A- highly sericitized plagioclase feldspar, together with sutured quartz as well as biotite that has been almost completely altered to chlorite and Fe-oxides (AA6-22; FOV=3 mm). B- highly sericitized plagioclase phenocryst with a core altered to tremolite and chlorite (AA6-22; FOV=1.5 mm). C- coarse-grained blocky euhedral sillimanite within a biotite cluster (AA6-23; FOV=0.9 mm). D- highly fractured relict primary hornblende grain replaced in parts by chlorite (AA6-22; FOV=1.5 mm).

Figure 4.10. Microphotographs of accessory minerals in Erinpura granitoids. A- occurrence of monazite (high δ , somewhat wedge-shaped) within a biotite cluster (DB-1; FOV=0.25 mm). B- ilmenite with irregular growth blebs of hematite, which may be an exsolution feature (reflected light, AA6-26; FOV=1.5 mm).

Figure 4.11. Deformation microstructures in Erinpura samples. A- deformation twinning in a perthitic microcline (AA6-18; FOV=1.5 mm). B- somewhat lobate intergrowth of two feldspar grains, which may be due to recrystallization of the feldspar (AA6-18; FOV=1.5 mm). C- biotite cleavage being deformed/kinked into folds (AA6-20; reflected light, FOV=3 mm). D- strained quartz re-equilibrating by formation of subgrains around edges of larger quartz grains (AA6-18; FOV=3 mm). E- zone of high strain where all recrystallized felsic material is flattened in the direction of extension, while biotite has grown along edges of more competent orthoclase porphyroclasts and is also oriented with strain flow direction (AA6-20; FOV=3 mm). F- parallel elongate muscovite and biotite and blocky recrystallized quartz partitioned strongly into foliation bands (AA6-24B; FOV=3 mm).

Figure 4.12. The Balda sample, classified as the late-stage intrusion of the Erinpura granite. The image shows the magmatic texture of larger, subhedral tabular plagioclase crystal, grown together with subhedral quartz and K-feldspar with euhedral muscovite and phlogopite grown at grain boundaries (BL-1a; FOV=3 mm).

Figure 4.13. Field view of the massive, medium-grained Sumerpur granitoid. It has randomly oriented phenocrysts, such as this large euhedral plagioclase, which contains mafic biotite inclusions and has been embayed slightly on its upper edge, but otherwise does not seem to have been altered/dissolved by the magma (AA6-16).

Figure 4.14. Microphotographs of Sumerpur samples. A- sericitic plagioclase phenocryst with many fractures infilled by fine-grained quartz and muscovite. A corner is embayed due to impingement of new quartz/feldspar growth that surrounds phenocryst (AA6-17; FOV=3 mm). B- smaller tabular feldspars that have sericitized cores within a larger subhedral orthoclase grain, which shows sector twinning (AA6-17; FOV=3 mm). The smaller feldspars may be earlier, more Ca-rich and therefore more susceptible to alteration by fluid movement through fractures and cleavage planes within the larger subhedral feldspar.

Figure 4.15. Field outcrop images of Ranakpur intrusive. A- field view of the massive Ranakpur granitoid, showing slight variations in grain-size from medium- to fine- grained (AA6-2). B- ptygmatic isoclinal folding of boudinaged granitoid stringer between flowing bands of calc-silicate.

Figure 4.16. Microphotographs of Ranakpur samples. A- fracture infilled plagioclase with deformed twinning at edge of grain (AA6-2; FOV=1.5 mm). B- myrmekitic intergrowth extending into edge of larger perthite from groundmass (AA6-5; FOV=3 mm). C- euhedral Fe-Ti oxides associated with subhedral titanite and apatite, as well as platy biotite (AA6-7; FOV=3 mm). D- suturing of quartz and microcline indicating microstructural deformation (AA6-7; FOV=3 mm).

Figure 4.17. Microphotographs of Ranakpur granitoids and calc-silicate samples. A- euhedral ilmenite (pale pink) with exsolution lamellae of hematite (bright cross-hatching), rimmed by fine-grained titanite (AA6-2; reflected light, FOV=0.9 mm). B- typical texture of the calc-silicate, with subhedral clinopyroxene and prismatic phlogopite dominated by euhedral to subhedral to calcite/dolomite (AA6-1B, FOV=1.5 mm). C- molybdenite with its wavy habit and strong basal cleavage and bireflectance (AA6-1B; reflected light, FOV=0.9 mm). D- subhedral hematite disseminated within the sample (AA6- 1B; reflected light, FOV=0.9 mm).

Figure 4.18. Microphotographs of Revdar Rd. granitoids (Mt. Abu type). A- field view of phaneritic pink granite, similar to the Mt. Abu type-granite (AA6-48A). B- recrystallized sample with fine-grained quartzofeldspathic material surrounding larger microcline phenocryst. The mafic cluster is aligned parallel to the fine-grained material, and contains a wedge-shaped, altered crystal (to the right) which may be monazite, while the large altered/radiation damaged grain to the left (yellow rims) may be a zircon. These are associated with smaller rounded fine-grained titanite growths which are alterations of Fe-Ti oxides (AA6-42A; FOV=3 mm). C- polycrystalline quartz phenocryst within a fine-grained quartzofeldspathic groundmass (AA6-42A; FOV=3 mm). D- euhedral hematite with cross-hatched ilmenite exsolution (AA6-48A; reflected light, FOV=0.9 mm).

Figure 4.19. Microphotographs of Revdar Rd. granitoids (Erinpura type). A- view of a Revdar Rd. (Erinpura-type) gneiss with flattened augen structures and very fine, down to mm-scale, banding (AA6-38). B- polycrystalline quartz phenocryst that has recrystallized in a lenticular form due to deformation, surrounded by fine-grained quartzofeldspathic and mafic material (AA6-38; FOV=3 mm). C- a remnant orthoclase grain with very embayed margins into which poikilitic muscovite has grown (AA6-38; FOV=3 mm). D- a kinked muscovite grain with its cleavage deformed due to strain (AA6-38; FOV=3 mm).

Figure 4.20. Outcrop and microphotographic images of the Swarupganj Rd. granitoid. A- field view of Swarupganj monzogranite. B- anhedral hematite and magnetite intergrown (AA6-49; FOV=0.9 mm). C- fine-grained amphibolite, part of the Delhi Supergroup.

Figure 4.21. Outcrop images of the Kishengarh sample. A- stringers of the nepheline syenite within the surrounding schistose amphibolite. B- field view of foliated nepheline syenite, where foliations are well-defined by elongate mafic bands (AA6-52A).

Figure 4.22. Microphotographs of the Kishengarh nepheline syenite sample. A- magmatic texture with microcline (uneven twinning which may be deformation twinning) and subhedral nepheline (FOV=1.5 mm). B- subhedral hornblende intergrown with feldspar (FOV=3 mm). C- mafic cluster consisting of biotite and prismatic titanite (FOV=1.5 mm). All photomicrographs are of sample AA6-52A.

Figure 5.1 Ternary granitoid classification diagram utilizing modal proportions of plagioclase, orthoclase and quartz (after Streckeisen, 1976). A- A few Mt. Abu, Erinpura and Revdar Rd. granitoids do not plot in any field classified. Mt. Abu and Revdar Rd. felsic rocks plot as syenogranites to alkali-feldspar granites, while the majority of Erinpura granitoids are classified as syeno- to monzo-granites (including Sumerpur granites). Ranakpur and Sumerpur samples are scattered, while the Malani Igneous Suite dyke is highly alkalic in nature. B- The Kishengarh sample plots as a feldspathoid syenite, as expected.

Figure 5.2. Diagram of Streckeisen and Le Maitre (1979) that classifies granitoid and feldspathoid rocks according to their normative quartz, albite, anorthite, orthoclase and feldspathoid contents.

Figure 5.3. Aluminium saturation index (ASI) plot for all felsic rocks from this study. Mt. Abu samples are predominantly metaluminous, with a few peralkaline samples. Some Erinpura and Revdar Rd. samples are peraluminous as well (after Maniar & Piccoli, 1989).

Figure 5.4. Harker diagrams of the variations in major element oxides plotted against SiO₂ for all felsic rocks from this study. Mt. Abu and Revdar Rd. samples show good correlations for most samples.

Figure 5.5. Harker diagrams of alkalis and MgO versus silica (SiO₂). Mt. Abu (and most other granitoid samples) samples show scatter and no change with increasing silica, while Erinpura and Ranakpur samples have good correlations with MgO. Most samples from the study plot within the high-K sector of the calc-alkaline diagram of Le Maitre et al. (1989).

Figure 5.6. Harker diagrams of trace elements (in ppm) versus silica for all felsic samples from this study. Mt. Abu samples show negative (Eu) and positive (Rb, Th and U) correlations, but there is a lot of scatter within graphs. Other samples show indeterminate scatter.

Figure 5.7. Harker diagrams for compatible trace elements (in ppm) versus silica. Generally, all samples have good relationships between Ti and SiO₂, while for V, only Erinpura and Ranakpur samples show any correlation.

Figure 5.8. Harker diagrams for Ba and Sr with silica. The insets within each graph show the disparity between the Ranakpur granitoid abundances versus the rest of the samples in this study. Mt. Abu samples show moderate correlations for both trace elements.

Figure 5.9. Inter-element diagrams (in ppm) representing trace elements with similar atomic properties such as ionic radius and size of charge. All bivariate diagrams have a positive slope, indicating the good relationship between the two elements. However, Erinpura samples have a lot of scatter in the Ba-Sr graph, while Mt. Abu samples show a slight dip/kink in the Nb-Ta graph between 30-40 ppm Nb.

Figure 5.10. Inter-element diagrams (in ppm) showing positive correlations for Erinpura and Mt. Abu samples.

Figure 5.11. Inter-element diagrams of trace elements (in ppm) comparing the degree of correlation between the different granitoid suites. These various inter-element combinations are informative about magma conditions and processes.

Figure 5.12. Inter-element (in ppm) diagrams illustrating specific relationships between sample suites.

Figure 5.13. Inter-element diagrams of major elements (molar) versus maficity (molar Mg + Fe). The molar Mg + Fe is a differentiation index, much like SiO₂, but the relationship is not biased towards the (Mg + Fe) because these elements do not make up the majority of the rock. Most samples show good correlations with maficity, although Erinpura samples show a greater degree of scatter than the rest.

Figure 5.14. Inter-element diagrams for maficity versus trace elements (ppm). Mt. Abu samples show good correlations for some elements (notably the more compatible Cu, and Sr) while the more incompatible elements are more scattered, although their slope is negative. Samples from other rock suites do not show very good trends with maficity.

Figure 5.15. Inter-element diagrams for maficity versus the more compatible trace elements (in ppm) in felsic rocks. Erinpura and Ranakpur rocks show positive correlations, while Mt. Abu samples are usually scattered and with lower concentrations.

Figure 5.16. REE plots normalised to chondrites for the various rock suites. There are noticeable differences in REE diagram shape between the Mt. Abu, Erinpura and Ranakpur samples.

Figure 5.17. Spider diagram variation plots normalised to primitive mantle values for the various samples in this study. Elements in these plots are arranged from mobile and LIL on the left to less mobile and HFS on the right. Once again, there are discernable differences between the Mt. Abu, Erinpura and Ranakpur sample suites.

Figure 6.1. Zircons separated from the Erinpura augen gneiss. A, B and C show the different morphologies of zircon crystals analysed with A being long prismatic, B being zircon tips and C being short prismatic. All show the characteristic rounded-off crystal faces and are riddled with inclusions. Some also have a yellow-tint. D shows three abraded crystals dated that were suspected of having older cores, whose rims are a slightly different colour to the rims of the zircons.

Figure 6.2. U-Pb zircon concordia age diagram for the Erinpura augen gneiss, utilising two near concordant points (blue ellipses) while the two ellipses outlined in red are discordant and zircons from these analyses may contain inherited U or Pb.

Figure 6.3. BSE images of the Erinpura granite zircons, showing morphological features. A- well-shaped zircon fragment (BSE image) with very inhomogenous interior. B- BSE image of short prismatic zircon showing lighter core surrounded by a much darker rim of oscillatory zoning which is in turn surrounded by a lighter overgrowth. The zoning is disturbed and seems to fade away.

Figure 6.4. Monazite crystals separated from the Erinpura gneiss, some with characteristic half-moon morphology. The crystals are murky, with many fractures and reddish-orange alteration (fluid movement and metamorphism) streaks throughout. The monazite crystal to the far right is the most pristine, with a pale yellow colouring and very little alteration visible. All grains were extremely friable.

Figure 6.5. Erinpura gneiss zircon and monazite analyses. All zircon analyses are ellipses outlined in blue or red. The two red ellipses are those used to calculate an upper intercept age of inheritance for the zircons (one is near concordia, the other to the right, indicating a large inherited component). The monazites ellipses are outlined in green and are reversely discordant, falling above the concordia line. This is due to an excess of ^{206}Pb from the decay of ^{230}Th .

Figure 6.6. Zircons selected for age dating from the Revdar Rd. mylonite gneiss. A- Chosen long prismatic zircons, unabraded, showing a variety of internal colouration. B- long prismatic crystals abraded and separated according to clarity, with those on the left being less so.

Figure 6.7. Concordia diagram for the Revdar Rd. mylonitic gneiss. Ellipses outlined in blue were used to calculate the age, while the red outlined ellipse had an error on the age of ~ 100 Ma and was therefore unsuitable for use in calculating the age of the sample.

Figure 6.8. CL-images of zircons from the Revdar Rd. mylonite gneiss. A- darker-shaded core surrounded by bright material with a different crystallographic orientation to the outer edges of the zircon, which show magmatic zoning. B- Clearly showing a central relict core (transgressive across magmatic zoning). C- lobate-shaped zircon recrystallization/resorption in centre of grain. D- an irregular dark domain, probably recrystallization, transgressing into centre of grain as well as outer disturbed rim.

Figure 6.9. A- long prismatic zircons chosen for abrasion, all with a yellow tint and rounded-off edges. B- short prismatic zircons that have been abraded and divided according to clarity.

Figure 6.10. The U-Pb concordia age for the Ranakpur quartz syenite, where the ellipses used to calculate the age of crystallization are outlined in blue, while the ellipses outlined in red indicate analyses that are discordant to a large degree or plot above the line of concordia. The ellipses outlined in green denote the titanite analyses ages (recalculated using K-feldspar Pb).

Figure 6.11. CL-images of zircons from the Ranakpur quartz syenite. A- zircon with disturbed domains, probably due to recrystallization of zircon. B- long prismatic zircon with magmatic zoning, showing partial disturbance and uneven grain boundaries.

Figure 6.12. Titanite crystals separated from the Ranakpur quartz monzonite. A- Unabraded titanites separated according to colour. B- Abraded dark-coloured titanites that are relatively free of inclusions.

Figure 6.13. Zircons separated from the Mt. Abu foliated granite. A and B (short prismatic and long prismatic, respectively) contain some clear inclusions, but overall are quite transparent. C- Air abraded zircon tips, which have been abraded to reduce any alteration and fractures through grains and on rims.

Figure 6.14. CL-images of zircons from the Mt. Abu foliated granite. A- short prismatic zircon showing good magmatic zoning. B- short prismatic zircon with annealed fractures on the right side of grain which have disturbed the primary magmatic zoning.

Figure 6.15. The U-Pb concordia age for the Mt. Abu foliated granite. The three ellipses outlined in blue were used to calculate the age of crystallization while the two ellipses outlined in red are more discordant.

Figure 6.16. Air abraded prismatic crystals from the undeformed Mt. Abu granite; there are some variations in hue (a yellow tint). Most are clear and free of inclusions and fractures.

Figure 6.17. The U-Pb concordia age of the undeformed Mt. Abu granite. The four ellipses outlined in blue were used to calculate the crystallization age. The ellipse outlined in red increased the error on the crystallization age appreciably when combined with the others and was therefore not included in the age calculation.

Figure 6.18. Zircons imaged using CL from the undeformed orange-pink Mt. Abu granite. A- long prismatic zircon with featureless interior and thin bands of zoning on edges. B- long prismatic zircon with fracture running lengthwise through crystal. The fracture seems to be annealed, with remobilisation along it (lighter edges). C- long prismatic zircon with recrystallization along margins, shown by lighter-coloured material in lobate structures as well as disturbed magmatic zoning. This grain also has inclusions at prism-edges. D- short prismatic crystal with visible disturbance of the magmatic zoning and growth due to local recrystallization.

Figure 6.19. U-Pb concordia age for the deformed Mt. Abu augen gneiss. The two ellipses outlined in red were not used in the age calculation due to their greater degree of discordance.

Figure 6.20. Zircon tip fragments from the deformed Mt. Abu augen gneiss. Many have mineral inclusions (hornblende or biotite) while others have clear inclusions.

Figure 6.21. CL- and BSE- images illustrating the disturbed nature of zircons from the deformed Mt. Abu sample. A and B: zircon fragment showing faint fractures radiating out from a central core. This is made visible on the CL-image, which defines the dark, irregular inner core surrounded by a band of highly-luminescent material. This relict core has been overgrown and magmatic zoning is well-defined. C and D: zircon which is extremely fractured with a featureless interior (CL-image) which has been partially recrystallized (darker material in lobate forms).

Figure 6.22. Anhedral zircon fragments from the Kishengarh nepheline syenite. A- Unabraded zircon, most (especially larger crystals) with no distinct morphology, inclusion-riddled and murky. B- Abraded zircons chosen for analysis, with zircons to the left of the image being smaller and clearer with fewer inclusions, while those to the right of the image are larger and murkier

Figure 6.23. Various images of titanite separated from the Kishengarh nepheline syenite. A-inclusion-riddled titanite, many with distinct pale yellow cores surrounded by clear rims. B- A titanite with distinct core. C- Abraded titanite, many different hues/tones of colour. D- two groups of titanite, with LHS group much clearer and lighter in colour than the two grains to the right.

Figure 6.24. Concordia diagram age results for the Kishengarh nepheline syenite sample. A- U-Pb zircon concordia age for sample AA6-52A, utilising all four analyses. B- two near concordant zircon analyses (near the 1000 Ma mark on concordia) combined with the two titanite analyses (spread out above 1200 Ma on concordia) to give a minimum age for the inherited component within these zircons.

Figure 6.25. CL- and BSE- images of zircons from the Kishengarh sample. A- dissolution and fracturing throughout zircon. B- Very fractured zircon with disturbed domains (light and dark contrasts) as well as remobilization of elements around fractures. C- Concentration of highly-luminescent material around arcuate fractures within the zircon. D- This CL image shows what could be micro-veining on the edges of a zircon fragment and therefore high degrees of strain experienced during metamorphism.

Figure 6.26. Kishengarh zircons that show interrupted and disturbed magmatic zonation. A- highly deformed, patchy and irregular convoluted zoning. B- disturbed and uneven oscillatory zoning as well as irregular zones of homogenous zircon, probably recrystallized.

Figure 6.27. A visual summary of all samples dated in this study (errors on the age are included), excluding the Kishengarh nepheline syenite sample.

Figure 6.28. Combined previous work and age data from the current study for the Mt. Abu granitoid pluton. Uncertainties within previous work give the Mt. Abu pluton an age range in excess of 130 m.y. The U-Pb zircon age of Sivaraman & Raval (1995) of 777 Ma is without error uncertainties, as these were not published, hence the uncertainty in the age cannot be shown.

Figure 6.29. Combined previous work and age data from the current study for the Erinpura augen gneiss and the Ranakpur quartz syenite. The Erinpura and Ranakpur U-Pb zircon ages from this study are the ages of crystallization or formation of these samples.

Figure 6.30. A visual summary box diagram of all samples dated within the U-Pb zircon age range of the Kishengarh nepheline syenite of this study. The only other age dating done on this sample was by Crawford (1970). This Rb-Sr age is greater than the age of inheritance of the zircons in this study.

Figure 6.31. A visual summary box diagram of all samples dated in this study, including the ages of inheritance of both the Erinpura augen gneiss and Kishengarh nepheline syenite. All plots include the error on the ages.

Figure 7.1. Thin section images of mafic minerals within samples dated. A- a mafic cluster from the orange-pink Mt. Abu granite. Fine-grained green-blue hornblende and green-brown biotite are intergrown. Both mafic minerals have inclusions, but hornblende is larger, less altered and more well-formed than the biotite, making it easier to separate and provide a reliable age (AA6-14B, FOV=0.9 mm). B- a medium-grained biotite cluster from the Erinpura gneiss (AA6-18), with crystals that are subhedral to euhedral and are usually partially interstitial to the larger feldspars and quartz. The larger grains have few inclusions, are affected less so by alteration and are therefore useful in Ar-Ar-dating (AA6-18, FOV=3mm). C- disseminated biotite intergrown with subhedral titanite within the Ranakpur quartz syenite. The biotite is relatively inclusion-free, making it suitable for Ar-Ar age dating (AA6-2, FOV=2mm). D- large, well-formed hornblende from the Kishengarh nepheline syenite. However, it is inclusion-rich, as can be seen from the image. This makes it difficult to choose grains for Ar-Ar analysis, as inclusions skew the data and contribute to erratic values within the spectrum (AA6-52A, FOV=2mm).

Figure 7.2. The $^{40}\text{Ar}/^{39}\text{Ar}$ step-heating spectrum for the orange-pink Mt. Abu granite (AA6-9). The spectrum has a relatively flat plateau indicating little disturbance and Ar-loss from within the crystal structure of the hornblende. The horizontal blue bar indicates the steps used to calculate the age.

Figure 7.3. The age-heating spectrum for the Erinpura augen gneiss (AA6-18) is erratic, with many dips and increases within the middle part of the spectrum, where the majority of the Ar gas is released. The horizontal blue bar indicates the steps used to calculate the age. This sample has undergone post-magmatic alteration and metamorphic processes that have deformed the lattice-structure in the biotite and cause Ar-loss/gain.

Figure 7.4. The step-heating spectrum for the Ranakpur quartz syenite (AA6-2). It is disturbed and erratic, with large differences between successive steps and no true plateau.

Figure 7.5. The clearly disturbed spectrum of the Kishengarh nepheline syenite gneiss, with anomalously high ages at the beginning and end of heating and no true plateau in the middle of the spectrum. The horizontal blue bar indicates the steps used to calculate the age. The spectrum is saddle-shaped, a clear indicator of excess argon.

Figure 7.6. A- As can be seen the inverse isochron is generally level and yields a good age (stated in text). B- The inverse isochron for the Kishengarh nepheline syenite, showing steps 3-6, with a large jump in value to the Y-axis intercept. The Y-intercept on steps 3-6 is anomalously high, yielding a Y-intercept age anomalously high (older than that of the earth).

Figure 7.7. The Kishengarh nepheline syenite sample has a very low K/Ca ratio for most of the diffusion process because Ca is a major constituent of hornblende. However, since the ratio is >1 , this is not a problem for corrections due to interference from Ca-isotopes.

Figure 7.8. A visual box plot of all $^{40}\text{Ar}/^{39}\text{Ar}$ dates obtained in this study. The youngest sample, AA6-9, is the Mt. Abu massive granite, which is undeformed in hand specimen. However, the $^{40}\text{Ar}/^{39}\text{Ar}$ age is ~ 260 m.y. younger than that of the age of crystallization. This is evidence of a younger resetting by a tectono-metamorphic event. The $^{40}\text{Ar}/^{39}\text{Ar}$ age of the Erinpura augen gneiss (AA6-18) is within error of the Mt. Abu granite. This could imply that the event that reset the Mt. Abu granitoid was also experienced by the Erinpura augen gneiss. This event was not the cause for the deformation seen within the Erinpura augen gneiss, as a similar degree of deformation would have to be present within the Mt. Abu pluton as well. The Mt. Abu pluton, however, is variably deformed, with much of the pluton composed of undeformed massive to porphyritic varieties, which, through the Ar-Ar age dating, have been shown to have been affected by the ~ 510 Ma event, but not deformed by them. It has been concluded by De Wall & Pandit (2007) that the deformation within the Mt. Abu pluton is due to syntectonic intrusion. Thus, the ~ 510 Ma event is possibly a thermal/metamorphic expression of the Pan-African event experienced in other parts of India. The quartz syenite from Ranakpur yields a $^{40}\text{Ar}/^{39}\text{Ar}$ age of 789.8 ± 6.3 Ma, approximately 50 m.y. younger than the U-Pb zircon age calculated in this study. This could be the result of prolonged cooling of the intrusion or a younger resetting event. It has not been affected by the resetting event experienced by both the Mt. Abu and Erinpura granitoids, as evinced

by the older Ar-Ar age. The Kishengarh nepheline syenite has the oldest $^{40}\text{Ar}/^{39}\text{Ar}$ age calculated (944.2 ± 7.4 Ma), which is ~44 m.y. younger than the U-Pb zircon age obtained. This younger Ar-Ar age may be the result of prolonged cooling, or may also be related to a separate deformatory event that transformed the nepheline syenite into gneiss.

Figure 8.1. Ternary diagram for major mineral rock-classification, according to modal mineralogy proportions of K-feldspar, plagioclase and quartz (after Streckeisen, 1976).

Figure 8.2. Normative classification of the Mt. Abu, Erinpura, Seychelles and Malani Igneous Suite samples, according to Streckeisen and Le Maitre (1979).

Figure 8.3. Aluminium saturation index (ASI) plot for granitoids from Mt. Abu, Erinpura, MIS and Seychelles. Mt. Abu and Seychelles samples are predominantly metaluminous, with a few peralkaline samples, while MIS samples span all fields (after Maniar & Piccoli, 1989).

Figure 8.4. Harker diagrams of major elements (in wt %) versus silica (wt %) for Mt. Abu, Erinpura, MIS peraluminous, MIS peralkaline and Seychelles granitoids. Data for Seychelles granitoids are from Ashwal et al., 2002 and data for MIS samples are from Maheshwari et al., 2001, 2002).

Figure 8.5. Harker diagrams of major elements (in wt %) versus silica (wt %) for Mt. Abu, Erinpura, MIS peraluminous, MIS peralkaline and Seychelles granitoids.

Figure 8.6. Harker diagrams of incompatible trace elements (in ppm) versus silica for Mt. Abu, Erinpura, MIS peraluminous, MIS peralkaline and Seychelles granitoids. All are LILE, save for Zr, which is a HFSE.

Figure 8.7. Inter-element diagrams (in ppm) for Mt. Abu, Erinpura, MIS peraluminous, MIS peralkaline and Seychelles granitoids.

Figure 8.8. REE diagrams for Seychelles, Malani Igneous Suite peraluminous and Malani Igneous Suite peralkaline granitoids.

Figure 8.9. Spider diagrams for Seychelles, MIS peraluminous and MIS peralkaline granitoids and Seychelles and Mt. Abu dolerite dykes.

Figure 9.1. Proposed reconstruction (including Mt. Abu pluton) of part of the Rodinian supercontinent at ~750 Ma, with postulated subduction (eastward) along the western margin of India and Madagascar (after Ashwal et al., 2002).

List of Tables

Table 3.1- Analytical precision for major element analysis (obtained from the X-Ray Analytical Facilities, School of Geosciences, University of the Witwatersrand).

Table 4.1 Modal percentages for all felsic rocks from this study.

Table 5.1 Major and trace element data (this study).

Table 6.1 Samples utilized in U-Pb zircon (TIMS) age-dating.

Table 6.2 Results of ID-TIMS U-Pb zircon analysis.

1. INTRODUCTION

1.1 Regional Geology

The major late Mesoproterozoic-Neoproterozoic supercontinent, Rodinia, was postulated to have existed from ~1.3-1.0 Ga (Grenvillian-type orogenies) with dispersal from ~800 Ma to the amalgamation of the Gondwana supercontinent at ~550-500 Ma (Hoffmann, 1991; Moores, 1991; Trompette, 2000; Torsvik & Meert, 2003; Torsvik, 2003). However, major uncertainties exist in terms of latitudinal positioning of constituent land masses as well as the timing of formation and dispersal. This is due to the paucity of robust geochronological and palaeomagnetic data for many of its constituent terranes during this time period, which are vital in anchoring these geologic terranes both temporally and spatially (Torsvik et al., 2001b). Previous Rodinia models state that the Rodinia configuration is a static one where, once all constituent terranes amalgamated into the supercontinent, it remained largely unchanged until its breakup at ~750 Ma. Additionally, the position of India is unchanged from its placement in Rodinia through to Gondwana. However, other models propose a more dynamic Rodinia, where not all constituents were amalgamated by ~1 Ga and the subsequent configuration changed through time (Torsvik, 2003). Studies from the NW region of the Indian subcontinent that include robust geochronological data would help to ascertain the position of this region within the Rodinia framework.

The Aravalli Craton in Rajasthan on the NW Indian Shield (Fig. 1.1) has a complex geological history seen in the preservation of a continuous rock record from the Early Archaean, ~3.5 Ga to Late Proterozoic, ~0.75 Ma period. This region has undergone various regional tectonic episodes with accompanying dominantly felsic magmatism and metamorphism at ~3.0 Ga, ~1.8 Ga, ~1.1 Ga and 850-750 Ma (Deb & Sarkar, 1990; Bhushan, 1995; Sharma, 1999; Vijaya Rao et al., 2000); hence it is an ideal area in which to study tectonic and crustal evolution.

The structurally very deformed and complex Archaean Banded Gneissic Complex (~3.5 -2.5 Ga: Gopalan et al., 1990; Wiedenbeck & Goswami, 1994; Wiedenbeck et al., 1996; Roy and Kröner, 1996), forms the basement to the Proterozoic supracrustal sequences of the Aravalli and Delhi Supergroups (SG) and is considered the cratonic nucleus of the region (Ahmad & Tarney, 1994; Tobisch et al., 1994, Vijaya Rao et al., 2000). It consists of composite granitic gneisses of amphibolitic to granulitic grade together with subordinate amphibolite that is found enveloped within the gneisses (Tobisch et al., 1994, Sharma, 1999, Van Lente et al., 2009). Metasediments and mafic to ultramafic rocks also suggest a greenstone association (Sharma, 1999). They have also been intruded by several generations of granitic plutons that are of I- and S-type in origin (Tobisch et al., 1994; Roy & Kataria, 1999).

The Aravalli and Delhi Supergroups occur as linear belts that form the Aravalli Mtn. Range, a ~750 km-long NE-SW trending linear feature that runs through Rajasthan and northern Gujarat. These occur together with the basement Banded Gneissic Complex (BGC), with the Aravalli SG outcropping east of the Delhi SG and BGC (Sharma, 1999; Van Lente et al., 2009) (Fig. 1). The nature and timing (~2.5-1.9 Ga) of the contact between the Palaeoproterozoic Aravalli Supergroup and the stratigraphically older BGC is not well established due to scatter in the isotopic data (Sharma, 1999; Kaur et al., 2006). Some workers (e.g. Heron, 1953) consider the contact to be unconformable while others (e.g. Naha & Halyburton, 1974) consider it to be migmatized.

The Aravalli SG basal unit consists of mafic metavolcanics with intercalated quartzites and conglomerates followed by calcareous and argillaceous rocks as well as serpentinites that outcrop along the Rakhadev Lineament, which have been interpreted as a tectonic suture with the Delhi SG (Volpe & Macdougall, 1990; Ahmad & Tarney, 1994; Tobisch et al., 1994). These rocks are intruded by a host of syn- and late- to post-orogenic felsic and mafic plutons, some of which have been dated. They have experienced at least 3 major episodes of deformation (Ahmad & Tarney, 1994). Regional metamorphism ranges from lower greenschist- to upper amphibolite- facies grade (Gupta et al., 1989; Roy & Kataria, 1999).

A major part of the Aravalli mountain range is formed by the Meso-Neoproterozoic (~1.8-0.85 Ga, Sm-Nd-isotope dating, Rb-Sr-isochron dating: Kaur et al., 2006) Delhi SG, with characteristic associated extensive felsic magmatism (Pandit & Khatatneh, 1998; Sharma, 1999; Van Lente et al., 2009). It has a well-defined erosional unconformity with the BGC, although the nature of the contact with the Aravalli SG is contested, with some workers considering it to be a structural discordance or a tectonic suture that is the expression of a Proterozoic oceanic-basin closure (e.g. Sinha-Roy, 1988; Gupta et al., 1989; Sharma, 1999).

The majority of the Delhi SG consists of deep-water to platform-type sediments (Vijaya Rao et al., 2000). Gupta et al. (1989) classified the marine sediments into the Gogunda and Kumbhalgarh Groups, while the younger sediments were grouped into the Sirohi, Sindreth and Punagarh Groups. The Sirohi Group sediments (argillaceous mica-schists and phyllites with lesser marble and quartzite lenses) are postulated to have been deposited within geosynclinal troughs together with the Sindreth and Punagarh Groups. New precise age determinations using U-Pb zircon age dating by Van Lente et al. (2009) place the latter two Groups strictly within the Malani Igneous Suite. They consist of bimodal volcanics together with conglomerates, shale and quartzite (Roy & Kataria, 1999, Van Lente et al., 2009).

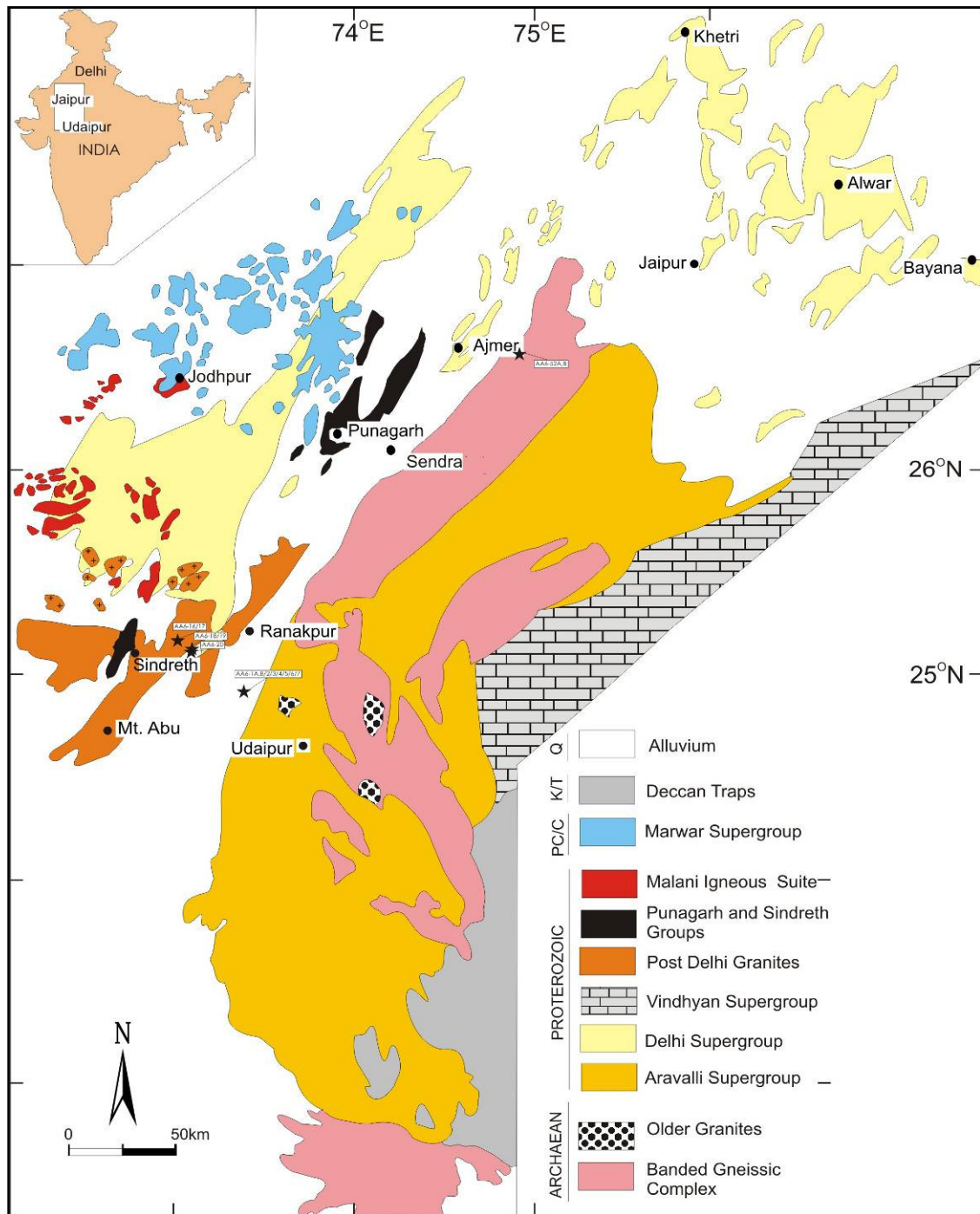


Figure 1.1. The regional geology of the Aravalli Craton showing location of Mt. Abu, adapted from Van Lente (2001).

These rocks are metamorphosed to the same grade as those in the Aravalli SG (Tobisch et al., 1994; Sharma, 1999). Both the Aravalli and Delhi Supergroups have experienced polyphase deformation as well as metamorphic recrystallization that reflect their complex tectonic history (Gupta et al., 1989; Wiedenbeck et al., 1996; Roy & Kataria, 1999).

The Delhi fold belt has traditionally been separated into an older northwestern component called the North Delhi Fold Belt or NDFB (1.7-1.5 Ga) consisting of the Bayana, Alwar and Khetri basins (Choudhary et al., 1984; Biju-Sekhar et al., 2003), whilst apparently younger rocks are found southwest of Ajmer in a basin

termed the South Delhi Fold Belt or SDFB (~850 Ma). The two components/basins are thought to have formed diachronously (Sinha-Roy, 1988) or to have been joined along a tectonic suture in the case of Volpe & Macdougall (1990). This has been based on poorly-constrained whole-rock Rb-Sr “errorchrons” of Choudhary et al. (1984) done on the numerous variably-deformed granitic plutons (assumed to be intrusive to the overlying sediments of the Delhi SG), as well as differences between volcanic/sediment ratios, base metal mineralization, sulphur and lead isotope ratios (Deb & Sarkar, 1990; Pandit & Khatatneh, 1998; Pandit et al., 2003).

Choudhary et al. (1984) dated the NDFB intrusives at 1.7-1.5 Ga (Rb-Sr), although these dates have large errors and are unreliable. NDFB granites such as the Ajitgarh and Khetri granites have been dated at 1450 Ma and 1480 ± 40 Ma, respectively (Crawford, 1970; Gopalan et al., 1979; Choudhary et al., 1984). More recently, ages of between 1.78 Ga to 1.71 Ga from granitoid plutons (EPMA chemical dating) were obtained by Biju-Sekhar et al. (2003) and Kaur et al. (2006). These granitoids are seen as the basement upon which the Delhi sediments in this area were deposited, and as such, may be considered the older limit of the age of the NDFB sediments. Zircons from this study also have rims dated at ~1.0-0.9 Ga, which is likely the expression of the widespread ~1 Ga magmatism in the SDFB. The older Rb-Sr ages are considered a thermal overprint of younger magmatism. The Kishengarh nepheline syenite, a highly deformed pluton at the northern tip of the NDFB, located just outside Ajmer, has also been dated at 1490 ± 15 Ma (Crawford, 1970) by Rb-Sr dating methods with a model-age obtained of 1910 Ma from a single sample (Roy and Dutt, 1995). Biotite from an inclusion was also dated at 970 Ma. In his book on the geology and tectonics of India, Balasubrahmanyam (2006, p. 89) mentions the age of the Kishengarh rocks as 1140 Ma.

Initially, the SDFB was so-defined because Choudhary et al. (1984) dated various granitoid plutons utilizing Rb-Sr whole-rock isochrons (data is unpublished) of the regionally extensive Erinpura granite to a $\sim 800 \pm 50$ Ma time span, implying that they were all formed by a single tectonic event. Granitoids dated by Deb et al. (2001) and Pandit et al. (2003) cluster around the ~1 Ga mark and may record a major magmatic event at this time, although the extent in this region is unknown due to the lack of precise geochronology.

Heron (1953) grouped all the variably deformed granitic (including granite, tonalite, diorite as well as banded gneisses and mylonites) intrusives from Ajmer in the north to Idar in the south as the syntectonic Erinpura granite, including Mt. Abu. In present usage, the Erinpura granite refers to a group of heterogeneous granitic plutons of $\sim 800 \pm 50$ Ma age that occur within and along the western part of the SDFB (Pandit & Khatatneh, 1998). The extensive Erinpura granite and equivalents are characterised by a syntectonic fabric that implies intrusion and deformation within the Delhi orogeny (Bhushan, 1995).

A diorite and metagabbro dated by Volpe & Macdougall (1990) from Ranakpur falls within the Erinpura-type age range at 835 ± 43 Ma and 838 ± 36 Ma (Sm-Nd isochron) while the Siwaya foliated granite, approximately 15 km south of Mt. Abu, is also within error of both the Erinpura and Ranakpur granitoids at $836 \pm 7/-5$ Ma (U-Pb zircon; Deb et al., 2001). This age of ~ 840 Ma is thought to represent the maximum age of the end of the Delhi orogeny (Deb et al., 2001). Intermediate felsic plutonic samples dated by Van Lente et al. (2009) give U-Pb zircon ages of 800 ± 2 Ma and 873 ± 3 Ma, which are interpreted as being part of the Erinpura magmatism. The Balda and Sumerpur granitoids are stated as the late-stage (mineralized and pegmatitic in places) fractionates of the Erinpura granite by Bhushan (1999). The type-locality Erinpura granite-gneiss has never been robustly dated, despite being the basis for correlation of a host of other granitoid plutons within the SDFB; hence a large component of this extensive felsic magmatism is not well-constrained.

To the west of Mt. Abu and the Aravalli-Delhi range lies the dominantly felsic MIS volcano-plutonic suite, one of the largest worldwide, with an estimated 51 000 km² areal extent (Bhushan, 2000). This suite consists of three distinct phases, the first of which are the predominantly rhyolitic and rhyodacitic volcanic flows (with minor basic volcanism), followed by peraluminous (Jalore-type locality) and peralkaline (Siwana-type locality) granitoid plutons (which are intrusive or overlie the Delhi SG metasediments). Felsic and mafic dykes crosscut the other phases of the suite (Roy, 2001, Gregory et al., 2008; Van Lente et al., 2009). Characteristically, this suite is relatively undeformed, unmetamorphosed and gently tilted and folded (Torsvik et al., 2001b; Ashwal et al., 2002). Age-dating of this suite varied from 779 ± 10 to 681 ± 20 Ma implying an extended period of magmatism of ~ 100 Ma (Rathore et al., 1999). New robust U-Pb zircon age dating by Gregory et al. (2008) on a rhyolitic tuff constrains the age of the first phase to 771 ± 5 Ma, while unpublished U-Pb zircon dates (Tucker unpubl.; mentioned in Torsvik et al., 2001b) for rhyolites (771 ± 2 and 751 ± 3 Ma) suggest a shorter time span for the magmatism in the MIS.

The Mt Abu pluton has traditionally been grouped together with the Erinpura granite, usually as the late-orogenic phase of magmatism because the Mt. Abu pluton contains variably deformed granitoids (Bhushan, 1995; Bhushan, 1999). De Wall & Pandit (2007) used AMS studies of the foliations within the Mt. Abu pluton as evidence of the syntectonic nature of the pluton and the possibility of it being related to the Sirohi orogeny. The Mt. Abu intrusive is also thought of as a composite pluton because the visibly undeformed pink and grey granites have been classified as part of the MIS while the granitic-gneiss has been classed as Erinpura-type magmatism on Geological Survey of India (1998) maps. Gupta et al. (1989) separates the Erinpura and Mt. Abu granites because Rb-Sr age dating (735 ± 15 Ma, Crawford & Compston, 1970) places the Mt. Abu pluton within the limits of the MIS as its plutonic equivalent.

The Neoproterozoic felsic magmatism within the Aravalli craton can be divided into four broad periods, which may or may not be continuous. Major granitoid plutonism occurs at ~1.7 Ga, ~1 Ga, ~900-800 Ma and ~750 Ma (Roy, 2001; Sharma, 2004), together with subordinate mafic to ultramafic extrusive (e.g. Phulad Ophiolite Suite and Punagarh and Sindreth mafics) and intrusive (e.g. gabbro-norite bodies SW of Mt. Abu) rocks. These may correspond to tectonic crust-forming events or extensional rifting and associated breakup of the crust.

The ~1.0 Ga magmatism, which is Grenvillian in age, involves both felsic plutonism coupled with mafic meta-volcanic magmatism (Sendra and Ranakpur granitoids and Phulad Ophiolite Suite). The data for these rocks suggest a convergent plate margin setting (Pandit et al., 2003). The ~900-800 Ma magmatic event, with the intrusion of the syn-orogenic Erinpura granite and equivalents, to the late-orogenic Mt. Abu granite has been theorised as being caused by the Delhi orogeny.

Bhushan (1995; 1999; 2000) and other workers (Rathore et al., 1999; Roy, 2001) favour a continuum of felsic magmatism between the Erinpura and Mt. Abu granites and the MIS, in effect a change from a tectonic compressive-deformatory environment to post-orogenic to one of extension and rifting due to a hotspot-related plume. Sharma (1999) considers the evolution of the Neoproterozoic magmatism to be related to 'ensialic orogenesis' involving extension and contraction over time of the mantle and crust above a plume. Sharma (2004) proposes intraplate rift-related extensional tectonics as the origin of the MIS, due to thermal build-up after consolidation of the Rodinia supercontinent at 1 Ga.

Gregory et al. (2009) and others (Volpe & Macdougall, 1990; Torsvik et al., 2001a & Ashwal et al., 2002) have argued for a convergent Andean-type arc setting with the MIS and related rocks from the Seychelles and northern Madagascar on the western margin of a Rodinia supercontinent whose constituent components were not assembled in a single orogenic event (the 1 Ga Grenvillian type-orogeny) but by discrete orogenies that occurred within the 1-0.7 Ga period. The mafic-ultramafic sequences of the Phulad Ophiolite Suite (~1 Ga; Volpe & Macdougall, 1990) and the Punagarh and Sindreth meta-volcanics (~764 Ma, U-Pb zircon age dating; Van Lente et al., 2009) are taken as evidence of ophiolitic assemblages that formed within or near Andean-type arcs. Granulites found southwest of Mt. Abu may also be related to this event, as similar rock-types are also found in northern Madagascar (Srikarni et al., 2004).

1.2 Aim of the Study

The focus of this study is the establishment of the geochronological position of the Mt. Abu granitoid pluton within the voluminous felsic magmatism of SW Rajasthan. The Mt. Abu pluton has been correlated by various authors with either the older Erinpura granite (850 ± 50 Ma; Rb-Sr, Choudhary et al., (1984) or the younger MIS (~ 771 Ma; U-Pb zircon, Gregory et al., 2008). Most authors consider these events as separate and belonging to two distinct 'cycles' (late-orogenic for the Erinpura granite and rift-related for the MIS), but some (mentioned above) favour a continuum between the Erinpura and the MIS magmatism, with the Mt. Abu pluton considered as the late-stage expression of the Erinpura magmatism. The Mt. Abu pluton has not been robustly dated (735 ± 15 , 800 ± 50 Ma, Rb-Sr: Crawford & Compston, 1970; Choudhary et al., 1984) or characterized well in terms of petrography and geochemistry. The geochronological, geochemical and petrographic characterization of the Mt. Abu pluton will be investigated. This is needed in order for comparisons to either felsic suite to be made and to determine if the Mt. Abu pluton formed within a single event. It is postulated here that the Mt. Abu pluton is unrelated to the Erinpura granite suite, but can be correlated geochronologically with the ~ 750 -770 Ma (U-Pb zircon: Tucker unpubl.; mentioned in Torsvik et al., 2001b; Gregory et al., 2008) MIS. The MIS felsics have been related to ~ 750 Ma (U-Pb zircon, Tucker et al., 2001) granitoids from the Seychelles.

It would also be of value to compare the Mt. Abu granitoid pluton to other felsic intrusives within the surrounding area and to establish the geochronological, geochemical and petrographic relationships between the different intrusives. The type-locality Erinpura granite outcrops ~ 60 km north of the pluton and is an ideal comparison for the Mt. Abu granitoids. Felsic intrusives that outcrop within the region also include the cryptic granitoids within the metasediments along Revdar Rd, immediately south of the Mt. Abu pluton, as well as the granitoids south of Ranakpur. These intrusives have not been dated.

The Mt. Abu granitoids are also variably deformed, which has given rise to the confusion regarding its stratigraphic position. The proposed U-Pb zircon age-dating and geochemical characterization will enable a comparison of the undeformed and augen gneiss variants within the pluton. Ar-Ar geochronology may also be able to clarify the timing of the metamorphism (and accompanying deformation) within the granitoids.

Questions to be answered in this study include: i) is the Mt. Abu pluton an intermediate linkage between the Erinpura granitoids and the MIS, or was it formed contemporaneously with the younger MIS felsic magmatism and can it be linked by petrography, geochemistry or geochronology to either suite; ii) is the Mt. Abu pluton related to other nearby granitoid plutons such as the Ranakpur, Revdar Rd. or Sumerpur granitoids? All are classified as Erinpura granitoids within the Sirohi region; iii) is the Mt. Abu pluton formed during a single intrusive event despite the variations in texture; iv) can the timing of the deformation be

constrained and v) if the Mt. Abu pluton is proven similar in age to the MIS, can it also be linked geochemically to the ~750 Ma granitoids from the Seychelles, interpreted to have formed in an arc-setting. Proposed U-Pb zircon and Ar-Ar geochronology as well as geochemical and petrographic characterization will enable a comparison of the Mt. Abu pluton with Seychelles and MIS samples.

2. GEOLOGY OF THE STUDY AREA

The area sampled is situated at the southern end of the Aravalli Mountain Range in the Sirohi-Mt. Abu region (Mamtani et al., 2000; De Wall et al., 2006). This mountain belt trends NNE for ± 700 km across Rajasthan and into northern Gujarat and is formed predominantly by the Delhi Supergroup (SG) rocks (Tobisch et al., 1994; Biju-Sekhar et al., 2001; Pandit et al., 2001, Van Lente, 2001). These Delhi SG rocks are intruded by granitoid plutons of varying composition and age (Bhushan, 1995; Bhushan, 1999).

The highest point in Rajasthan is situated on the Mt. Abu pluton, which rises to ~ 1640 m above sea level. It is correlated on most geological maps (e.g. Geological Survey of India, 1998; Fig. 2.1) as belonging to the Erinpura granite suite. The regionally extensive Erinpura granite (Fig. 2.1) is a heterogeneous suite of granitoids that intruded into the Delhi metasediments. The Erinpura granite is composed of various heterogeneous felsic plutons that are considered late- to post-tectonic in nature. As no evidence for deformation in the Erinpura granite was found it was concluded that the intrusions were unrelated to the Delhi orogeny (Choudhary et al., 1984; Roy & Kataria, 1999; Sharma, 1999). This is untrue, as the Erinpura granitoids are usually deformed to an augen gneiss texture (Sharma, 2004). The Rb-Sr isochron method was used to date various plutons, giving a range of intrusive ages from ~ 955 to ~ 740 Ma (Crawford and Compston, 1970; Crawford, 1975; Roy & Kataria, 1999). Part of the Mt. Abu pluton is augen gneiss, which is the reason for the correlation with the Erinpura granite.

Felsic intrusives within the area, such as the Ranakpur granitoids (also mapped as part of the Erinpura suite), outcrop ~ 60 km NE of the Mt. Abu pluton (Fig. 2.2), and are intruded into surrounding calc-silicate. The Sumerpur intrusion is thought of as a late stage fractionate of the Erinpura granite and outcrops just 10 km west of the type-locality Erinpura pluton. Other granitoids sampled (Fig. 2.1, Fig. 2.3) include those from the plains immediately south of the pluton, which are sediment-covered. These various granitoids are classed as late- to post-tectonic Erinpura granite on the basis of field-relations.

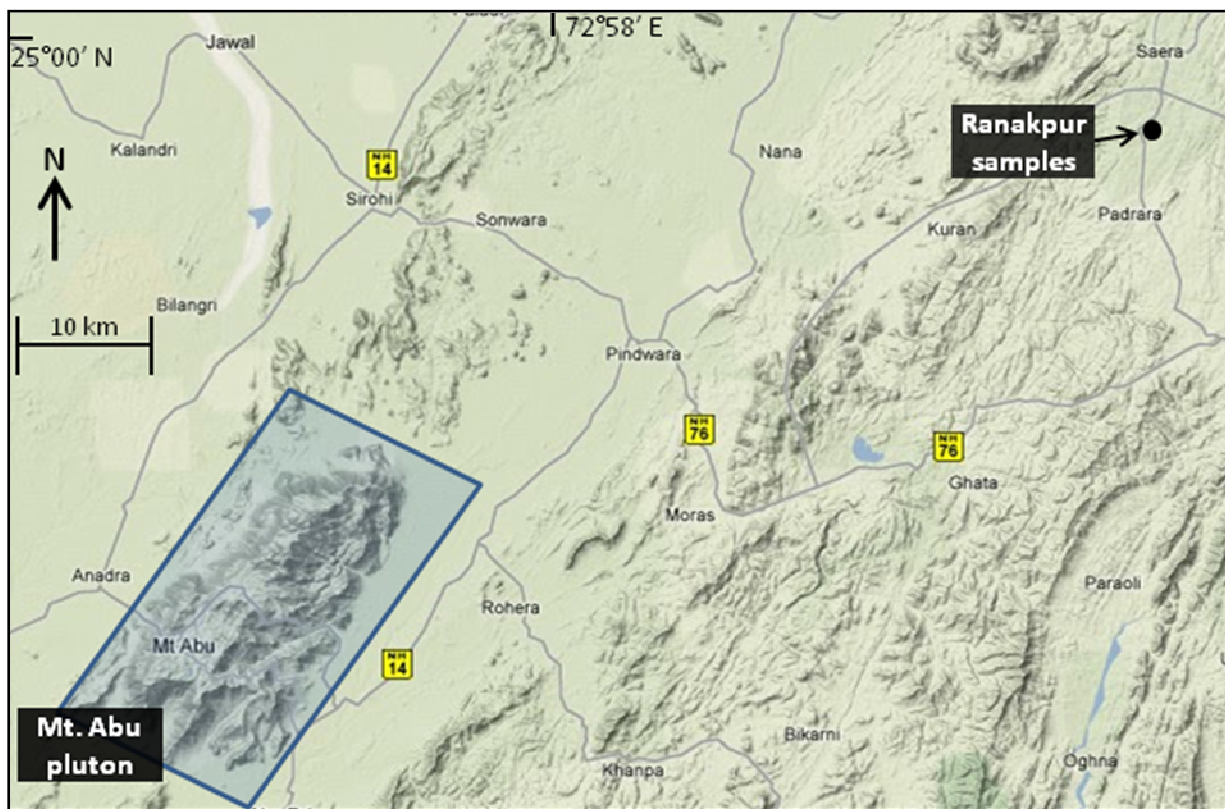


Figure 2.2. Topographical map showing the main Mt. Abu pluton in relation to the site of the Ranakpur granitoid samples.

The main focus of this study, the Mt. Abu granite massif (Fig. 2.3), has also traditionally been grouped together with these intrusions (Bhushan, 1995; Sharma, 1999; Wiedenbeck et al., 1996). However, it was suggested by Choudhary et al. (1984) that the Mt. Abu pluton is younger than the Erinpura Granite and ascribed the intrusion to a separate thermal event at 800 ± 50 Ma (Rb-Sr whole-rock isochron-dating). Gupta et al. (1989) also separated the Mt. Abu pluton and the Erinpura granite on the basis that the age obtained by Crawford and Compton (1970) of 735 ± 15 Ma placed the Mt. Abu pluton within the timespan of the Malani Igneous Suite (MIS). The pluton is heterogenous in composition and intruded by rhyolitic and mafic dykes (Bhushan, 1995; De Wall et al., 2006).

According to the published maps of the Geological Survey of India (1998), part of the massif is correlatable to pink undeformed Malani peraluminous granites (due to lack of deformation and mineralogical similarity), while the rest of the massif (with deformed gneissose fabric) is correlated to the older Erinpura Granite. De Wall & Pandit (2007), using AMS studies of the foliation and shears in the granitoids, concluded that the Mt. Abu pluton is syntectonic in nature and possible related to the Sirohi orogeny (~ 830 Ma; Sharma, 2007).

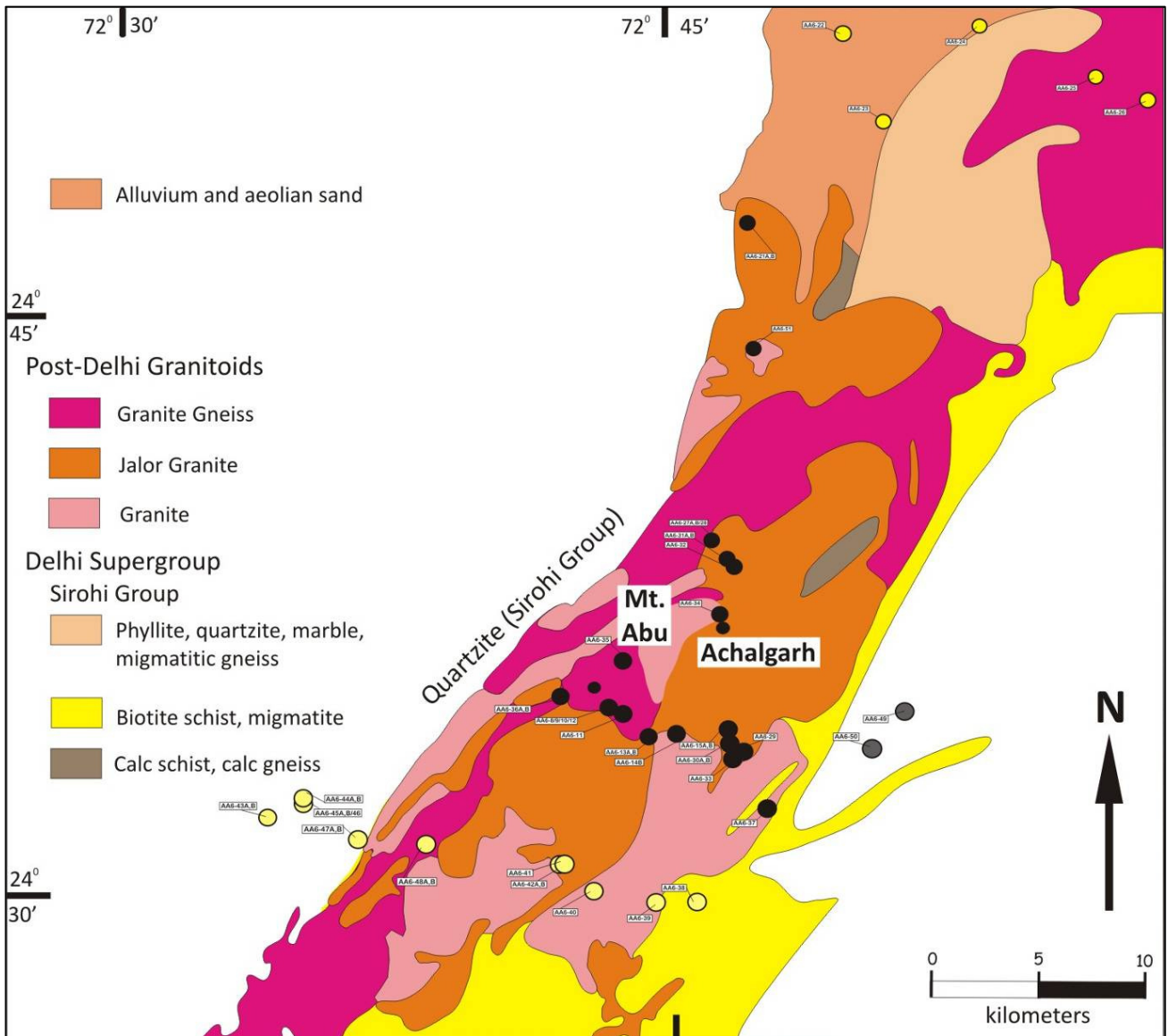


Figure 2.3. Geological map of the Mt. Abu pluton and immediate surrounds. The black circles represent Mt. Abu felsic samples, the pale yellow circles Revdar Rd. samples, the dark grey circles are Swarupganj Rd. samples and the bright yellow circles represent various Erinpura granitoid samples. The type-locality Erinpura granite sample is not shown on this map as it outcrops further north (see Fig. 2.1). Please see Appendix A for larger version of this map.

Age dating of these granitoids was done using the Rb-Sr ‘errorchron’ method (Crawford & Compston, 1970; Choudhary et al., 1984). As the pluton has undergone metamorphism, these ages are unreliable and thus poorly constrained (Roy & Kataria, 1999). Sivaraman and Raval (1995) also dated a single Mt. Abu granite sample at 770 Ma (U-Pb zircon) but no sample or analytical data were given (Pandit unpubl.) and as such, the quality of the data could not be established.

Bhushan (1999) describes the Mt. Abu granite as a composite pluton with variation from granite to quartz diorite. The intrusives are foliated at contacts and have a xenoblastic granular texture with K-feldspar

porphyroblasts. According to Bhushan (1999), these rocks have lower ($\text{Na}_2\text{O} + \text{K}_2\text{O}$), MgO and CaO when compared to the Erinpura granite.

Other work done within the study area includes a comparative study of the dolerite dykes that intrude the Mt. Abu pluton with those that intrude the Seychelles granitoids. Solanki (2005; Hons. Thesis unpubl.) conducted a geochemical and petrographic comparison between the dolerites intruding the Mt. Abu road granitoids and those that intrude the granitoids of the Seychelles. The study found that petrographically, the Mt. Abu dolerites were all partially to totally altered to upper-greenschist lower-amphibolite mineral assemblages while the Seychelles dolerites were relatively unaltered, containing primary plagioclase and clinopyroxene. Geochemically, however, trace element data show remarkably similar patterns for both areas (Mt. Abu and Seychelles) in terms of immobile elements that are unaffected by hydrothermal alteration. Major element data also showed good agreement between the two areas studied. When compared to another, unrelated set of data (Karoo basalts and dolerites), both the Mt. Abu and Seychelles show completely different mobile-immobile trace-element patterns to this dataset, supporting the supposition of the Mt. Abu and Seychelles dolerites being geochemically similar. This conclusion provides support for the current study's hypothesis of coevality between the two terranes/provinces.

3. ANALYTICAL METHODS

The analytical methods utilized in this study include transmitted and reflected light microscopy, X-Ray Fluorescence Spectrometry (XRF), Laser-Ablation Inductively Coupled Plasma Mass Spectrometry (LA-ICPMS), Isotope Dilution Thermal Ionization Mass Spectrometry (ID-TIMS) and $^{40}\text{Ar}/^{39}\text{Ar}$ step-heating. The microscope work was done in order to characterize the sample thin sections, such as modal proportions of major, minor and trace minerals contained in the rock sample. Thin section characterization may also provide some information on the crystallization sequence of minerals and magma conditions during formation and crystallization of the rock sample.

XRF spectrometry was used to analyze the major element oxide-concentrations of the rock samples. Major and minor elements were used in the classification of the rock samples, as well as in variation diagrams, which provided information on magmatic conditions and alteration of rock specimens. Trace elements, analyzed by LA-ICPMS, are particularly useful in discriminating between petrological processes (unlike major elements). They provide information out of proportion to their concentration in rock samples. This is due to their large number and their differential behaviour in various petrological processes such as partial melting, fractional crystallization and alteration.

The ID-TIMS method of U-Pb zircon age-dating is highly accurate, provided that the minerals being dated (zircon or other U-bearing minerals) had a relatively simple formational history, as this method requires dissolution of the entire crystal. This method provides accurate information on the age of formation of the rock, and may also provide ages for other significant modification events in the history of the crystallized rock, such as ages of metamorphism and/or deformation. The ^{40}Ar - ^{39}Ar spectrum age dating method is a useful tool in samples suspected of having undergone some post-crystallization metamorphic or deformatory event.

3.1 Petrography

All samples were characterized under a Leica transmitted and reflected light microscope. All microphotographs in Chapter 4 were taken in transmitted light, unless they are classed as 'reflected light' within the textbox below the microphotographs. The microscope was used for mineral and textural identification, as well as to see the effects of weathering and alteration within certain minerals. These characteristics help to constrain the type of conditions under which these samples formed. Reflected light microscopy was used to study the opaque minerals (oxides and sulfides) that the dykes contained and to ascertain the alteration/oxidation associated with the oxides. However, as only one thin section was made

of each sample, the modal analyses cannot be representative of rocks that are very coarse-grained or phenocrystic in nature. Therefore, the Streckeisen diagrams utilized in Chapter 5 serve best as guidelines to the rock types, and must be used in conjunction with other analytical methods to classify the rock type. Colours used to describe rock types and minerals are according to the Munsell rock-colour chart.

3.2 X-Ray Fluorescence (XRF) Spectrometry

This technique was used to calculate the major-element (SiO_2 , TiO_2 , Al_2O_3 , Fe_2O_3 , MnO , MgO , CaO , Na_2O , K_2O and P_2O_5) composition of each sample and was performed at the University of the Witwatersrand Analytical X-Ray Fluorescence Laboratory.

Samples were obtained from outcrops using a sledgehammer, as the granitoids were very hard and the freshest possible samples were needed for analytical purposes. Samples varied between 1.0-4.0 kg, depending on the coarseness of the grainsize and phenocrysts. This allowed for samples that were representative of the rock type. Samples were first prepared using a rock-splitter, then a jaw-crusher. The fragments were then milled to a talcum powder-like fineness in a 100 ml Sieb ring mill for approximately 90 seconds. All necessary precautions against contamination (cleaning with pure quartz, compressed air and then wiping down with acetone) were taken.

For major element analysis, 0.35 g of the powdered (oxidized) sample was mixed with 2.5 g borate glass flux and 0.02 g of sodium nitrate and was fused in a Pt-crucible at 1000°C for 5-10 minutes or until the sample was dissolved. This solution was then poured out onto a graphite plate and an aluminium plunger was then used to quench the melt into a flat round glass disk. This was then left to cool on an asbestos mat and all rough edges were filed off before the disk was put into the Philips PW2404 XRF spectrometer for silicate analysis. A rhodium X-Ray tube was used and run at 50 kV and 50 mA. Analytical precision for major elements is given in Table 3.1. The analysis is based on duplicate samples representing 5 calibrations. Calibration standards were primary International Reference Materials USGS series (USA) and NIM series (South Africa).

Table 3.1- Analytical precision for major element analysis (obtained from the X-Ray Analytical Facilities, School of Geosciences, University of the Witwatersrand).

Element	Standard deviation	Absolute % error	Relative Error - %	Standard Range %
Fe ₂ O ₃	0.09	-0.03	-3.7	0.09 - 26.65
MnO	0.01	-0.009	4.8	0.01 – 0.35
TiO ₂	0.07	-0.04	13.7	0.00 – 2.69
CaO	0.04	0.003	0.2	0.11 – 16.03
K ₂ O	0.07	0.005	-5.6	0.01 – 15.40
P ₂ O ₅	0.02	-0.02	14.2	0.01 – 1.40
SiO ₂	0.36	0.06	-0.09	34.40 – 76.31
Al ₂ O ₃	0.07	0.07	1.3	0.30 – 30.04
MgO	0.18	-0.05	-6.1	0.03 – 43.18
Na ₂ O	0.13	-0.05	-6.8	0.04 – 6.57
LOI	0.26	-0.21	7.1	
Total	0.58	-0.18	0.2	

The major elements were analyzed according to the methods of Norrish & Hutton (1969).

3.3 LA-ICPMS (Laser Ablation Inductively-Coupled Plasma Mass-Spectrometry)

Samples were prepared by being finely crushed in a Sieb mill, and then 50 mg was weighed into a digestion vessel. The samples were then dissolved within a MARS microwave digester by a combination of heat and high purity HF-HNO₃. The sample was then diluted and analyzed in the ICP-MS (a Perkin Elmer DRC-e). Trace elements were analysed against certified primary solution standards. International reference materials AGV-2, BCR-1 and BR-1 were analysed with every run. The analytical precision (agreement to accepted values of the standards) was better than 10% for all elements and in many cases better than 5%. Elements analyzed by LA-ICPMS were P, Sc, Ti, V, Cr, Co, Ni, Cu, Zn, Ga, As, Rb, Sr, Y, Zr, Nb, Ba, Cs, La, Ce, Pr, Nd, Sm, Eu, Gd, Tb, Dy, Ho, Er, Tm, Yb, Lu, Hf, Ta, W, Pb, Th and U).

3.4 U-Pb Zircon Geochronology

U-Pb zircon geochronology utilizing the ID-TIMS method was performed at the Universiteit i Oslo (Oslo, Norway) under the instruction of Prof. Fernando Corfu.

Sample preparation began with the rock being first cleaned of any debris in an ultrasonic cleaner, then rinsed off with water and alcohol and put in an oven to dry. The sample was then crushed into fragments in a jaw-crusher. Next, the samples were milled to a <0.5mm powder in a crush mill. Using the Wilfley table,

the heavy fraction was separated from the light fraction. Both fractions were then dried out in an oven. Next, all the magnetite was removed from the heavy fraction using non-magnetic freefall separation ranging from 0.5 A to 1.5 A, depending on the amount of magnetic material. The non-magnetic fraction was then put through the Franz magnetic separator at a magnetic amplitude (m) of 0.4 A.

Heavy liquid flotation separation using methyl iodide (CH_2I_2 ; $\rho = 3.32$) was performed on the 0.4 A non-magnetic residue. The heavy mineral fraction was then washed through with acetone and dried on a hot plate. If the amount of magnetic material was still substantial, then this fraction was put through the Franz Isodynamic magnetic separator at $m = 1.5$ A, and the non-magnetic fraction from this separation was then used for picking zircons. The magnetic fraction from the heavy liquid separation is usually where the titanite is found, while monazite, though rare, did occur in both magnetic and non-magnetic fractions.

Zircons were picked by hand using a binocular microscope and grouped according to: i) zircon tips, ii) fragments, iii) those with suspected cores, iv) those with any inclusions or fractures and v), whole zircon crystals. This last group was divided into long- and short-prismatic crystals. The zircons were separated in this way in order to minimize the effects of inheritance or lead loss (using the long prismatic crystals, which are less likely to contain cores or have lead loss versus fractured crystals). Zircons ranged from ~ 200 μm to 250 μm in length, so were relatively easy to discern and pick out. Selected groups of zircons were then air abraded with pyrite (for titanite and monazite, no pyrite was used) at ~ 80 -120 gas pressure for 2-4 hours, until the crystal rims (which are more likely to have been disturbed/reset) were removed. Abrasion also decreases the surface area of the crystal that common-Pb can contaminate (Corfu et al., 2003; Krogh, 1982). The zircons are then washed (with alcohol) into a petri dish which is placed in an ultrasonic cleaner to remove the pyrite. HNO_3 is added and the dish is put on a hot plate for ~ 10 minutes in order to remove the remaining pyrite from the zircons. The zircons are washed (distilled H_2O and alcohol) and then separated out under the microscope and pipetted into separate glass vials.

The zircons in the vials are then washed with a solution of HNO_3 and H_2O , then the liquid is evaporated on a hotplate for 20-30 minutes and further washed with H_2O and acetone. Next the zircons are weighed on a microbalance and put into a bomb/ savillex (in the case of titanite or monazite) together with 1 drop of HNO_3 and 12 drops of HF. The spike (a mixture of ^{202}Pb - ^{205}Pb - ^{235}U) is then added to each Teflon bomb/savillex (Krogh, 1982), which is then sealed and put into an oven at 184°C (or in the case of savillexes, on a hotplate) in order to dissolve the zircons. The columns (purify the sample using anion-exchange resin) are prepared by washing through with cycles of H_2O , 6N HCl and 8N HNO_3 . The bombs/savillexes are removed from the oven and evaporated on a hotplate. Then 10 drops of 3N HCl are added and the bombs are put back into the oven (savillexes on the hotplate).

The sample solution is then transferred to the clean columns (which were pre-conditioned with 16 drops of 3N HCl, then washed down with more of the HCl. The Pb and U elutions were captured by washing through the solution with 6N HCl and H₂O. These are captured in the original bomb/savillex. Two drops of H₃PO₄ are then added, and the solution is evaporated on a hotplate (Corfu, 2004). For titanite and monazite, this separation is carried out using a novel single stage HBr-HCl procedure with anion exchange resin. The samples are loaded onto Re-filaments together with a Si-gel, and onto a barrel. This barrel is then slotted into the MAT 262 mass spectrometer. Depending on the signal strength, measurements were either done using the Faraday cup collector, or using a secondary electron multiplier. Results were then plotted using Isoplot.

3.5. Ar-Ar Geochronology

The Ar-Ar age-dating was performed at the Norwegian Geological Survey under Dr. Bart Hendriks.

Mineral separates of the samples were made in order to isolate the mineral (either biotite or hornblende) of interest. Minerals were hand-picked using a binocular microscope and cleaned by rinsing in acetone and distilled water. Samples consisted of ~1 milligram of the mineral of interest, which were then packed in Al-foil and sealed into an Al-capsule with Cd-shielding. Irradiation of the sample packages was done in the 5C site of the McMaster Nuclear Reactor Facility, Hamilton, Canada.

Temperatures within the reactor were <50°C while the samples were being irradiated at 50 MWH with in a neutron flux measured at $4 \times 10^{13} \text{ n.cm}^{-2}.\text{s}^{-1}$. Interference from isotopes of Ca and K was measured by inclusion of CaF and K₂SO₄ salts in the irradiation (ratios of $^{36}\text{Ca}/^{37}\text{Ca} = 0.00030$, $^{39}\text{Ca}/^{37}\text{Ca} = 0.00070$ and $^{40}\text{Ca}/^{39}\text{K} = 0.027$ were used). The neutron fluence monitor standard used was the Tinto biotite of age 410.3 Ma (Rex and Guise, 1995) and the error in the J-value thus calculated was conservatively put at 1 % for all unknowns. Analysis of the irradiated samples was done at the $^{40}\text{Ar}/^{39}\text{Ar}$ Geochronology Laboratory at the Norwegian Geological Survey. Samples were degassed (in a step wise fashion) by a Merchantek MIR-10 CO₂ laser (operating in a continuous wave mode). A KBr cover slip was used for each sample while it was heated in the laser port for ~3 minutes. Gas from each step of heating went through an extraction line (two pairs of SAES AP-10 getters) for 11 minutes. These are mounted in isolated sections of the line, each with their own vacuum pump to ensure ultraclean vacuum conditions. This gas was then analyzed using a MAP 215-50 mass spectrometer. Background levels (measured after every third sample) in the CO₂ laser port were kept below 8×10^{-12} ccSTP for mass 40 and less than 3×10^{-14} ccSTP for mass 36. The dynamic blank measurements were done on mass 40 and were indicative of a stable background (1.0×10^{-13} ccSTP), while the background levels of masses 37, 38 and 39 were kept to the blank measurements levels.

The corrected data from the unknowns was then reduced with the IAAA (Interactive Ar-Ar analysis) software package; a programme based in part upon equations from Dalrymple et al. (1981) and McDougall & Harrison (1999), written by T. H. Torsvik and N. O. Arnaud. This programme takes into account corrections on interfering isotopes, mass discrimination error in blanks and decay of ^{37}Ar when doing data reduction.

4. FIELD & PETROGRAPHIC STUDY

Samples were grouped according to their location on the Geological Survey Map of Rajasthan (1998) into Mt. Abu, Erinpura, Sumerpur, Ranakpur, Revdar Rd. and Swarupganj Rd. granitoids as well as the isolated occurrence of the Kishengarh nepheline-syenite ~300 km NW of the Mt. Abu pluton, within the NDFB. Mt. Abu granitoids constitute the main pluton of interest, while Revdar Rd. granitoids stem from the southern terminus of the Mt. Abu pluton, are not well-exposed due to overlying sedimentary cover and vary in texture considerably. Exposure of granitoid bedrock to the east of the Mt. Abu pluton is also rare, and only one sample was collected along the Swarupganj Rd.

The Erinpura granitoids are found at various locations to the north and east of the Mt. Abu pluton, while Ranakpur granitoids are samples from a single pluton ~76 km NE of the Mt. Abu pluton. Sumerpur samples are located just south of Sumerpur town, ~70 NNE of the Mt. Abu pluton. Both Ranakpur and Sumerpur granitoids are classified as part of the Erinpura granite (Fig. 2.1). The red Mirpur granite, located ~20 km north of the Mt. Abu pluton, which is classified as part of the Erinpura granite, was also sampled. A felsic dyke sample, thought to be part of the Malani Igneous Suite (MIS), was also collected, ~5 km south of the Mirpur granite samples. Revdar Rd. and Swarupganj Rd. granitoids are not classified on the map of the Geological Survey of Rajasthan, but as they outcrop immediately to the south of the Mt. Abu pluton, they can be classed as either Mt. Abu or Erinpura granitoids. Modal percentage values can be found in Table 4.1. Visual estimation of modes was preferred, as the variance in grain size precluded point-counting as a viable method. Petrographic descriptions of each sample in this study can be found in Appendix B.

Table 4.1 Modal percentages for all felsic rocks from this study.

	Mt. Abu									
Sample	AA6/8	AA6/9	AA6/10	AA6/12	AA6/13A	AA6/13B	AA6/14B	AA6/15A	AA6/15B	AA6/27A
Lithology:	massive granite	massiv e granite	porphy. granite	foliated granite	foliated granite	foliated granite	foliated granite	massive granite	porphy. granite	porphy. granite
Quartz	20	20	31	51	20	56	25	30	30	55
K-feldspar	60.5	55	40	27	50	16.5	50	46.6	46.6	13
Plagioclase	6	2	17.5	14	10	11	6	10.4	10.4	7
Biotite/(Phlogopite)	10	5	8	6	6.5	11	12	3	3	4
Hornblende	tr.	15	1				tr.	7	7	
Actinolite/Tremolite										
Chlorite										
Muscovite					1					tr.
Titanite	1	1	1.5	tr.			tr.	1	2	tr.
Epidote										
Apatite	tr.	tr.	tr.	tr.	tr.	tr.	tr.	tr.		tr.
Zircon	tr.	tr.	tr.	tr.	tr.	5.5	tr.	tr.		tr.
Monazite				tr.			tr.			
Fluorite										tr.
Sillimanite										
Garnet										
Magnetite	1.5	1	tr.	tr.						1
Titanomagnetite					1.5	1.5	tr.	tr.	1	
Ilmenite	tr.	tr.			tr.	tr.				
Haematite										
Chalcopyrite										
Calcite				tr.	1			tr.	tr.	

	Mt. Abu									
Sample	AA6/27	AA6/28	AA6/29	AA6/33	AA6/34	AA6/35	AA6/36A	AA6/36B	AA6/37	AA6/11
Lithology:	foliated granite	foliated granite	porphy. granite	foliated granite	foliated granite	augen gneiss	augen gneiss	mylonitic gneiss	augen gneiss	rhyolite porph. dyke
Quartz	63	30	47	60	37	34	43	46	40	42
K-feldspar	27	54	41	34	52	40	40	45	37	34
Plagioclase	7	6	8	4	6	5	4	2	5	
Biotite/(Phlogopite)	7	9	4	3	4	15	10	2	1	25
Hornblende									15	
Actinolite/Tremolite										
Chlorite										
Muscovite						3	1	5		
Titanite	tr.	tr.	tr.	tr.	tr.	2	1	tr.	1	
Epidote					tr.					
Apatite	tr.	tr.	tr.		tr.	tr.	tr.	tr.	tr.	
Zircon	tr.	tr.	tr.		tr.	tr.	tr.	tr.	tr.	
Monazite										
Fluorite	tr.	tr.								
Sillimanite		tr.								
Garnet										
Magnetite	tr.									
Titanomagnetite		1	tr.		tr.	1	1	tr.	1	
Ilmenite										tr.
Haematite				tr.						
Chalcopyrite								tr.		
Calcite					tr.	tr.				

	Mt. Abu cont.					Sumerpur granitoids			
Sample	AA6/30B	AA6/31A	AA6/31B	AA6/30A	AA6/21A	AA6/16A	AA6/16 B	AA6/17 massive	
Lithology:	rhyolite porph. dyke	rhyolite porph. dyke	rhyolite dyke	foliated granite	massive granite	massive granite	massive granite	massive granite	granite
Quartz	48	47	84	21	35	33	30	22	
K-feldspar	35	45	7	60	50	34	33	51	
Plagioclase	7	1	2	10	10	15	25	20	
Biotite/(Phlogopite)	10	7	7	8	5	11	10	5	
Hornblende				tr.					
Actinolite/Tremolite									
Chlorite									tr.
Muscovite						6	2	1	
Titanite		tr.	tr.	1	tr.	1	2		
Epidote									
Apatite				tr.	tr.	tr.			
Zircon				tr.	tr.				
Monazite									
Fluorite									
Sillimanite									
Garnet									
Magnetite	tr.	1	tr.						
Titanomagnetite				tr.	tr.	2	tr.	tr.	
Ilmenite									
Haematite		tr.	tr.		tr.				
Chalcopyrite									
Calcite									
Erinpura granitoids									
Sample	AA6/18	AA6/19	AA6/20	AA6/22	AA6/23	AA6/24	AA6/25	AA6/26	BL1-A
Lithology:	augen gneiss	augen gneiss	porphy. granite	augen gneiss	granite gneiss	augen gneiss	porphy. granite	granite	biotite granite
Quartz	31	10	50	20	37	48	27	37	45
K-feldspar	31	72	26	16	10	13	48	50	20
Plagioclase	31	5	12	40	40	8	13	9	20
Biotite/(Phlogopite)	6	10	11	tr.	12	20	10	5	5
Hornblende				1					
Actinolite/Tremolite				tr.					
Chlorite				7		tr.			
Muscovite	tr.	1	1		1	10			10
Titanite			tr.	tr.	tr.				
Epidote									
Apatite	tr.		tr.				1		
Zircon	tr.	1	tr.				tr.		
Monazite									
Fluorite									
Sillimanite					tr.				
Garnet									
Magnetite	tr.	1	tr.	tr.				1	
Titanomagnetite			tr.			tr.	1	tr.	
Ilmenite									
Haematite					tr.				
Chalcopyrite									
Calcite				tr.					

	Erinpura granitoids		Ranakpur granitoids						
Sample	DB-1	SR-1	AA6/2	AA6/3A	AA6/3B	AA6/5	AA6/6	AA6/7	
Lithology:	porphy. granite	augen gneiss	grey granite	grey granite	grey granite	grey granite	grey granite	grey granite	
Quartz	40	15	32	11	11	15	25	26	
K-feldspar	30	62	15	65	65	60	55	57	
Plagioclase	11	13	32	10	10	17	6	4	
Biotite/(Phlogopite)	15	8	12	11	11	5	10	9	
Hornblende			4			2	tr.		
Actinolite/Tremolite									
Chlorite									
Muscovite	1								
Titanite				1.5	1.5	1	2	2	
Epidote									
Apatite		tr.	1						
Zircon	1		1	1	1				
Monazite		tr.							
Fluorite									
Sillimanite									
Garnet									
Magnetite			1		tr.		tr.	tr.	
Titanomagnetite	2	2		tr.					
Ilmenite			tr.		tr.		tr.	tr.	
Haematite	tr.			tr.					
Chalcopyrite	tr.		1						
Calcite									
	Revdar Rd. (Erinpura type)					Revdar Rd. (Abu type)			
Sample	AA6/38	AA6/47A	AA6/47B	AA6/45A micaceous	AA6/45 B	AA6/43B	AA6/44B pegmatite	AA6/39	AA6/40
Lithology:	granite gneiss	augen gneiss	augen gneiss	gneiss	granite gneiss	gneiss		augen gneiss	massive granite
Quartz	35	30	33	60	45	25	46	36	45
K-feldspar	45	3	65			62	47	58	52
Plagioclase		65		15	44			4	2
Biotite/(Phlogopite)	8				7				1
Hornblende									
Actinolite/Tremolite						10			
Chlorite	2			2	3	1			
Muscovite	10	1		22			7		
Titanite						2			tr.
Epidote									
Apatite									
Zircon									
Monazite									
Fluorite									
Sillimanite									
Garnet					tr.				
Magnetite	tr.	tr.	tr.		tr.	tr.			
Titanomagnetite	tr.			tr.				tr.	tr.
Ilmenite									
Haematite									
Chalcopyrite									
Calcite									

	Revdar Rd. (Abu type)			Revdar Rd. granitoid	Swarupganj granitoid	Kishengarh	MIS dyke
Sample Lithology:	AA6/42A porphy granite	AA6/42B porphy granite	AA6/48A foliated granite	AA6/48B aplitic dyke	AA6/49 foliated granite	AA6/52A nepheline syenite	AA6-51 rhyolite porph. dyke
Quartz (Nepheline)	40	35	41	45	40	(47)	23
K-feldspar	42	59	49	34	28		22
Plagioclase		2	5	18	28	40	
Biotite/(Phlogopite)	10	4	4	2	4	3	
Hornblende	4					7	
Actinolite/Tremolite							
Chlorite	tr.						30
Muscovite					tr.		
Titanite	2	tr.	tr.	tr.		3	
Epidote							
Apatite							
Zircon	1						tr.
Monazite							
Fluorite							
Sillimanite							
Garnet							
Magnetite							
Titanomagnetite	1	tr.					20
Ilmenite					tr.		5
Haematite	tr.		tr.	tr.	tr.		
Chalcopyrite							
Calcite							tr.

4.1 Mt. Abu granitoids (and related rocks)

These samples outcrop as massive, moderate orange-pink, undeformed and sub-equigranular granite to medium light-grey, variably deformed and porphyritic granite. Subvertical slickenside surfaces, which vary from single mm-width surfaces to zones (~10 cm width), run through all textural varieties within the Mt. Abu pluton. Weak foliation defined by elongate mafic clusters is common. Highly deformed samples are gneissic with well-defined augens and S-C fabric (Fig. 4.1 A-D). Contacts between texturally different granitoids vary from diffuse to gradational or sharp (especially between deformed augen-gneisses and other types). Most margins are diffuse and uneven to gradational (maximum ~30 cm gradational zone). Most granitoid types, excluding the massive, moderate orange-pink granite, show signs of deformation in the form of elongated mafic clusters, slickenside surfaces or augen gneiss foliation. Mafic enclaves with diffuse contacts are rare.

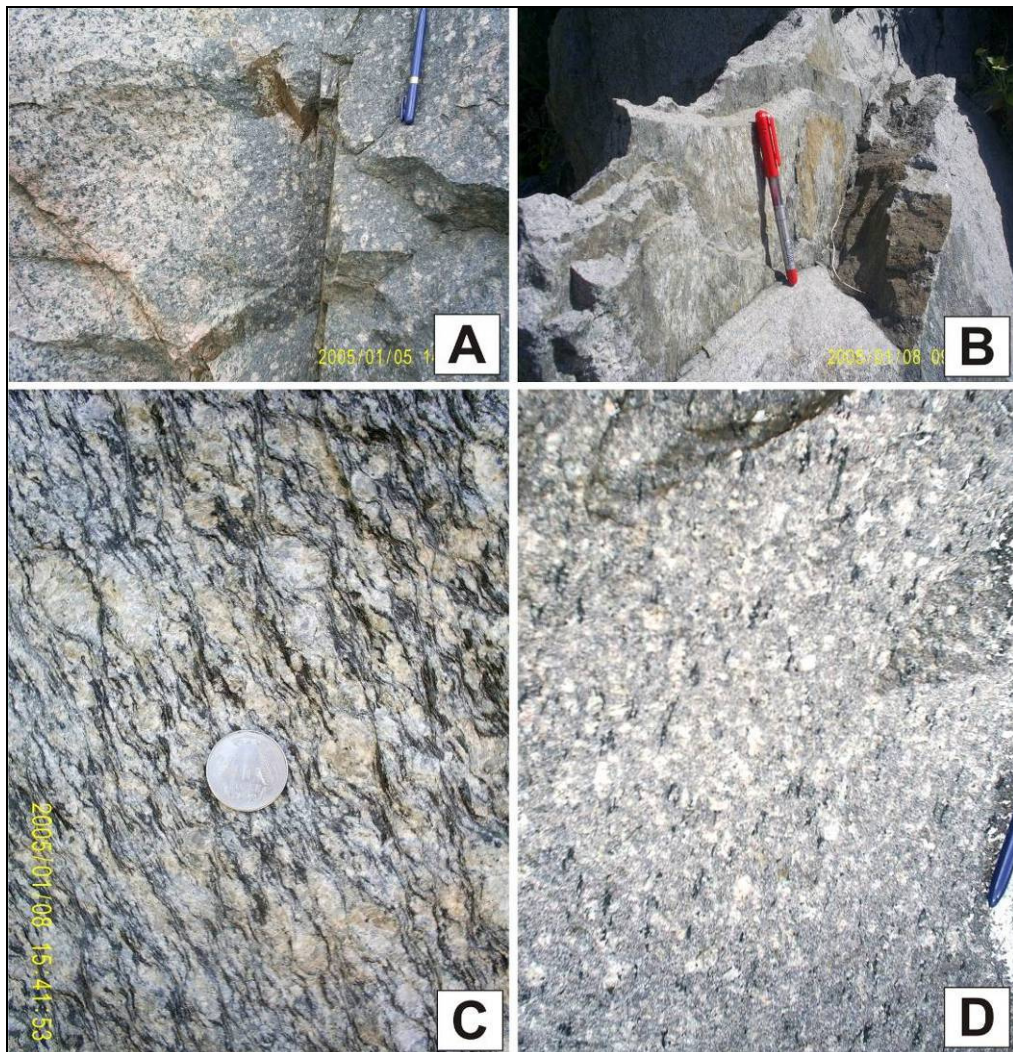


Figure 4.1. Mt. Abu granitoids in the field, with a wide range of textures. A- lobate and somewhat diffuse contact between the K-feldspar rich type-granite on the left (AA6-15A) and the more porphyritic type (AA6-15B). B- subvertical slickenside lineations defined by fine-grained micas. C- Mt. Abu augen gneiss foliation (AA6-35). D- foliated and porphyritic granite with elongate mafic clusters.

Augen and mafic foliation within Mt. Abu samples is generally oriented NNE to NE, with steep to subvertical dips of $>65^\circ$ to the SE. The shear zone on the north-western edge of the pluton trends $035^\circ/63^\circ$ SE, similar to the foliation trends seen in other granitoids from the pluton. Foliation on the shear plane in gneisses trends approximately E-W, with dips of $>80^\circ$. The general NNE to NE trend of the Mt. Abu granitoid, with the steep dip angles, is similar to granitoids south of Mt. Abu that outcrop along Revdar Rd.

The major felsic minerals are subhedral K-feldspar (between 0.3 mm-4 mm) where orthoclase is dominant over microcline, euhedral to subhedral plagioclase with the same diameter as K-feldspar and blocky to anhedral quartz (diameter <0.1 mm in fine-grained groundmass, up to 3 mm in phenocrysts). Usually, feldspar crystals are larger than quartz crystals, creating a sub-equigranular texture in massive phaneritic samples (Fig. 4.2 A, B).

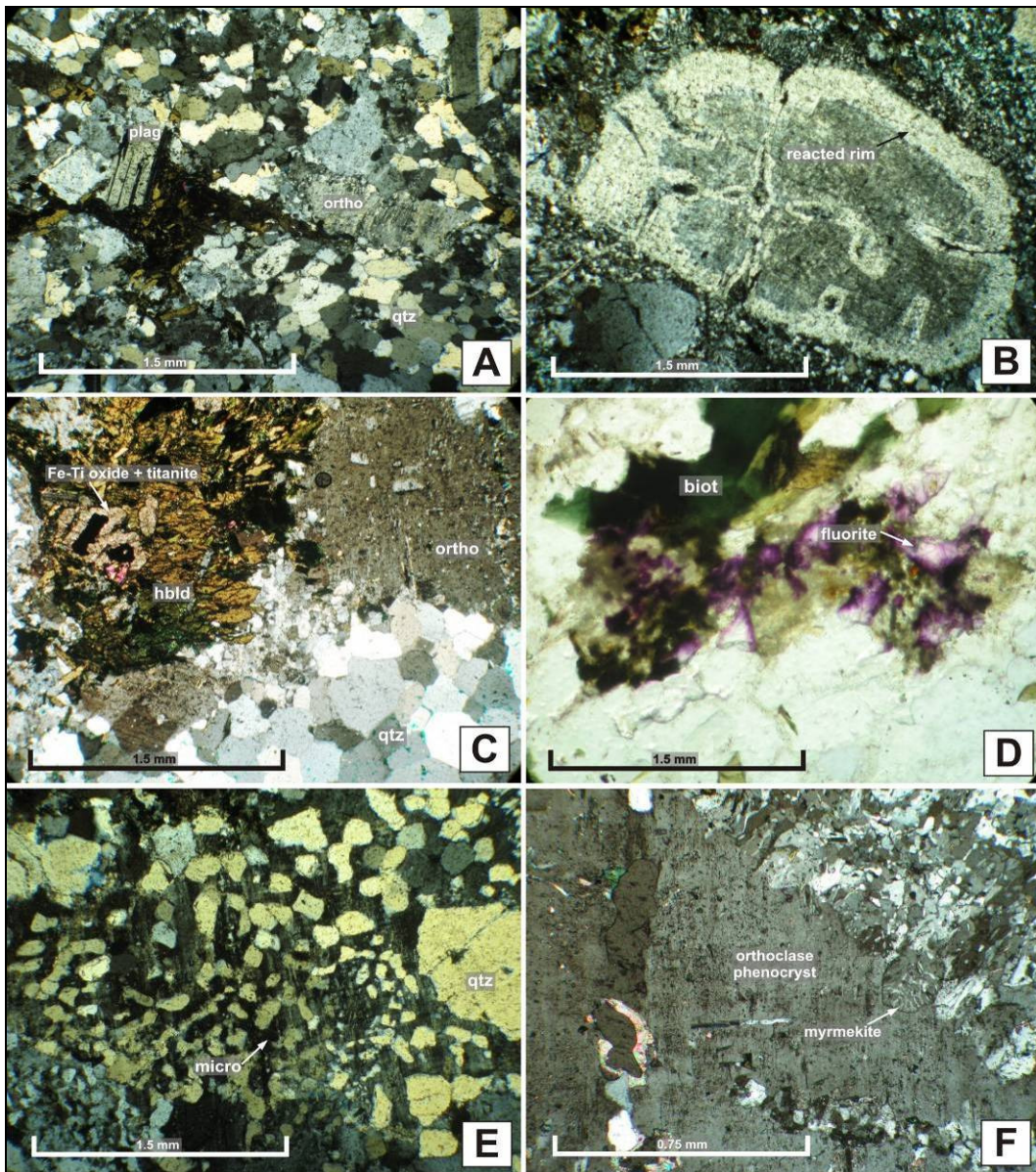
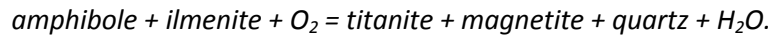


Figure 4.2. Photomicrographs of magmatic textures in Mt. Abu samples. A- typical textural relation, with sericitized euhedral plagioclase and subhedral orthoclase surrounded by smaller recrystallized quartz and euhedral Fe-rich biotite between feldspars (AA6-27B; FOV=3 mm). B- a subhedral perthite phenocryst with an altered rim. Alteration is greatest along fractures within phenocryst (AA6-9; FOV=3 mm). C- a mafic cluster containing prismatic hornblende together with Fe-Ti oxides, which have fine-grained titanite rims. Quartz is granular-textured but becomes much finer-grained towards the boundaries between mafic clusters and feldspar grain (AA6-15A; FOV=3 mm). D- anhedronal fluorite, with radiation damage from inclusions within the subhedral biotite that have made the fluorite purple (AA6-27A; FOV=1.5 mm). E- graphic texture between large microcline and quartz crystals, which are intergrown, as the blebs are optically continuous for both (AA6-8; FOV=3 mm). F- lobate myrmekite structures grown into the boundaries of an orthoclase phenocryst (AA6-8; FOV=1.5 mm).

The major mafic minerals are euhedral to subhedral yellowish-green to olive-brown biotite (<1.5 mm) that is inclusion-rich and subordinate subhedral, altered and fractured blue-green hornblende (<3 mm diameter). Biotite has opaque minerals and alteration to chlorite along cleavage planes, euhedral zircon and quartz blebs. Fine-grained recrystallization of biotite and muscovite exploit fractures within the hornblende, which contains quartz blebs and has Fe-staining along cleavage planes. Biotite and hornblende occur together in clusters with associated anhedronal, altered Fe-Ti oxides, predominantly titanomagnetite (Fig. 4.4 A-B). Clusters of mafic minerals are elongate when defining a foliation, with biotite commonly becoming extremely elongate in highly deformed (gneissic) samples.

Very fine-grained anhedral titanite (very high birefringence) is commonly found as alteration rims surrounding Fe-Ti oxides. Prismatic wedge-shaped titanite is also found in some samples. The fine-grained titanite rims surrounding the Fe-Ti oxides were formed by alteration involving fluid movement during the oxidizing reaction:



Other accessory minerals associated with mafic clusters are euhedral apatite (low birefringence, hexagonal prismatic habit), prismatic zircon (Fig. 4.3 A) and light yellow-green monoclinic monazite (Fig. 4.3 B: prismatic rhombic habit, high relief). Zircon usually has concentric oscillatory zoning, sometimes disturbed, but is most commonly featureless (no zoning visible, flat surface) under the light microscope.

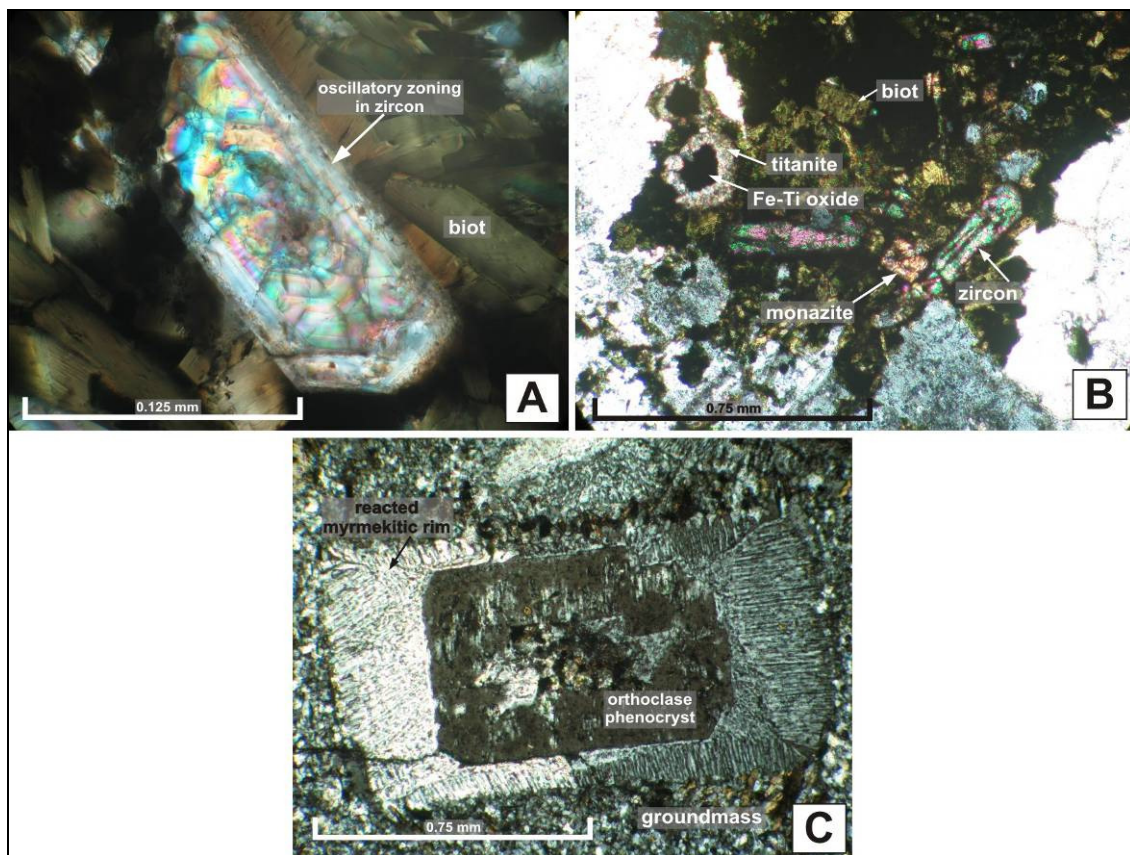


Figure 4.3. Microphotographs of accessory minerals and textures in Mt. Abu samples. A- zircon with oscillatory zoning surrounding a core that seems to be disturbed (AA6-34; FOV=0.25 mm). B- radioactive long-prismatic zircon and what may be monazite (rhomb-shape) within a mafic cluster (AA6-9; FOV=1.5 mm). C- a reacted euhedral orthoclase phenocryst from a rhyolitic dyke. The core is somewhat altered and core grain boundary has been reacted to form myrmekite/graphic intergrowth. This reflects a change in magmatic conditions of the magma (AA6-11; FOV=1.5 mm).

The latter two cause radioactive haloes in biotite. Rare fine-grained fluorite (Fig. 4.2 D) is bright purple from radiation-damage, and the anhedral, somewhat interstitial nature suggests that it is crystallized from a late-stage volatile-rich fluid. Fluorite in one sample is also euhedral and colourless, with radiation-damaged purple haloes around radioactive minerals contained within the crystal. The euhedral fluorite may have crystallized early in the magma evolution. However, most fluorite is anhedral and fine-grained, suggesting late-stage hydrothermal fluid growth.

Magmatic textures (Fig. 4.2 A, B, E, F) include granophyric intergrowth in large K-feldspar crystals, anhedral quartz blebs intergrown with large feldspar crystals as well as large phenocrysts of K-feldspar, plagioclase and quartz. Veins of recrystallized finer-grained quartz and biotite infill fractured orthoclase grains, which may be a late magmatic feature. Lobate myrmekitic structures have grown into the grain boundaries of larger K-feldspar phenocrysts as the local composition of magma changes at the grain boundary or due to rapid cooling. This may also be a deformation texture due to solid-state replacement of K-feldspar by plagioclase and quartz.

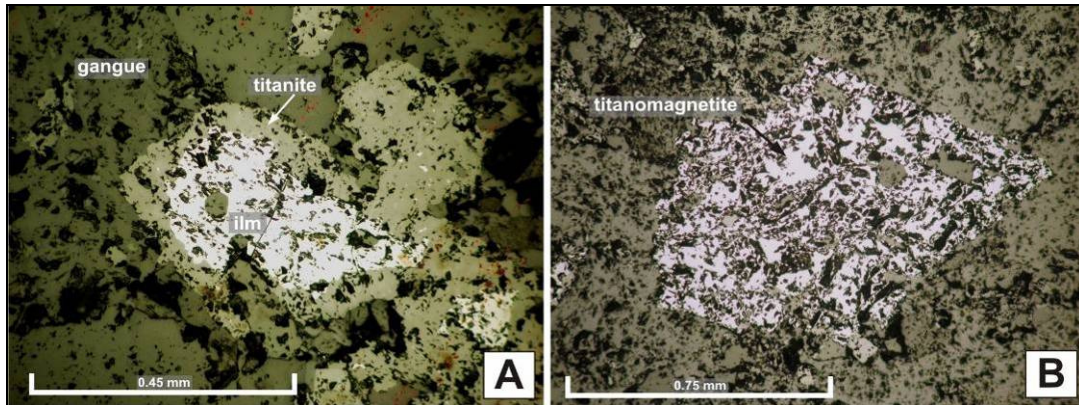


Figure 4.4. Microphotographs of Fe-Ti oxide minerals in Mt. Abu samples. A- anhedral ilmenite, replaced by titanite rim (reflected light, AA6-8; FOV=0.9 mm). B- euhedral to subhedral titanomagnetite (reflected light, AA6-27A; FOV=1.5 mm).

In porphyritic samples, the groundmass is recrystallized fine-grained blocky quartz, feldspar and euhedral mafic minerals (Fig. 4.3 C). The fine-grained nature of the groundmass gives them their distinctive medium light-grey colour as opposed to the massive moderate orange-pink granite. Phenocrysts commonly have embayed grain boundaries, while some have more reacted and altered cores. The rhyolitic porphyry dykes consist of subhedral to anhedral biotite, quartz and feldspars, while phenocrysts of orthoclase (<1.5 mm diameter) have myrmekitic/graphic intergrowth rims ~0.25 mm in diameter. The regular rims may be due to a change in the magma conditions. The groundmass is usually very fine-grained (<0.04 mm in diameter). Quartz phenocrysts are subhedral and smaller in size than feldspars.

Common to all thin sections are signs of deformation as well as alteration products such as sericite, chlorite and calcite/dolomite within plagioclase and biotite, which give the thin-sections a cloudy texture. Deformation microstructures include suturing of grain boundaries (grain boundary recrystallization) and undulatory extinction to subgrain formation in quartz. Kinked and deformed twins also occur in plagioclase (Fig. 4.5 A-B, D, F). Well-defined foliations comprising separate micaceous and quartzofeldspathic material, as well as strain separation around porphyroclasts, are indicators of a single (or multiple) deformation event that these samples have experienced (Fig. 4.5 C, E).

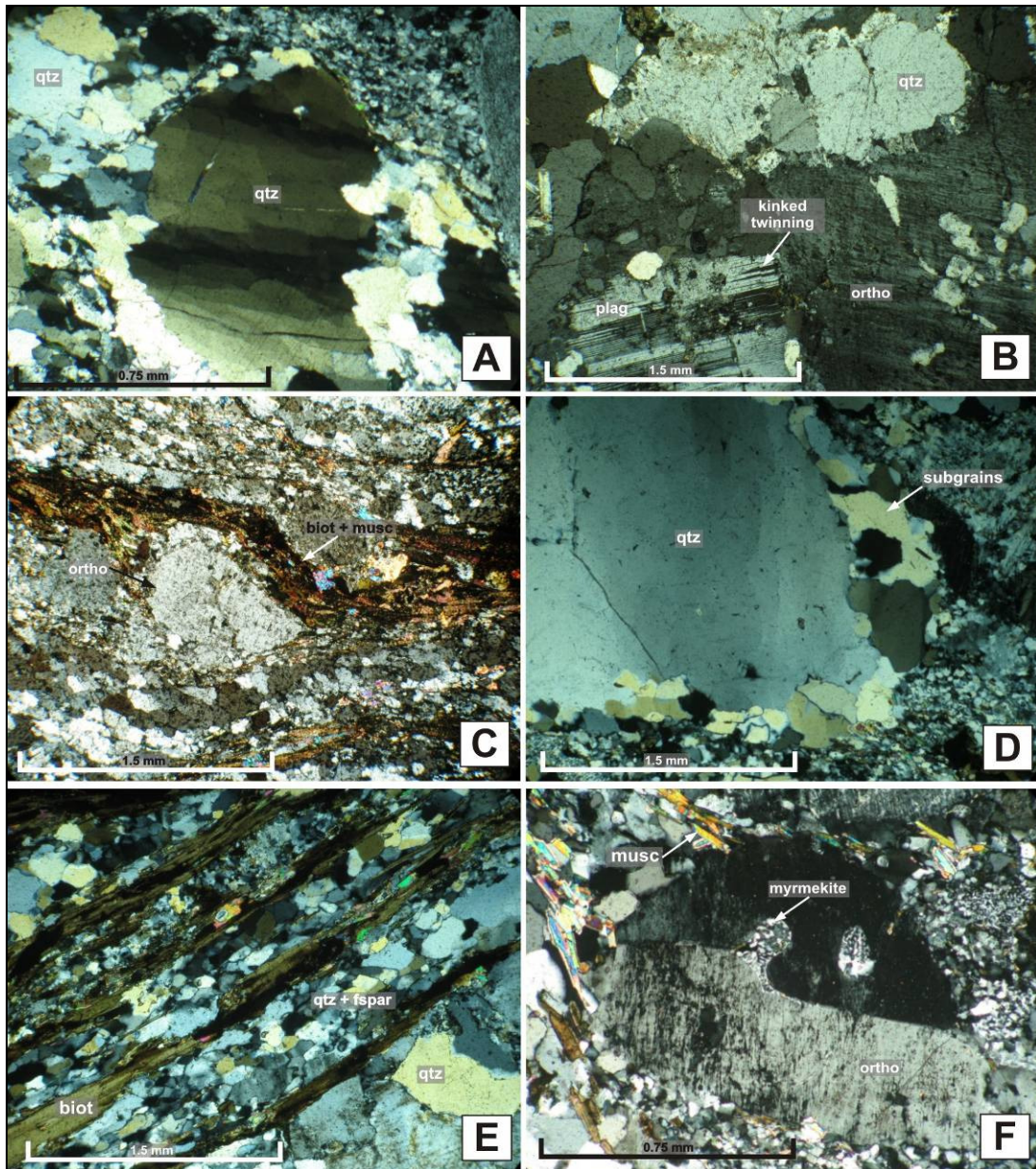


Figure 4.5. Deformation microstructures in Mt. Abu samples. A- strained quartz with strain domains having different extinction angles and checkerboard grain boundaries (AA6-30A; FOV=1.5 mm). B- kinked deformed twinning within plagioclase that is non-parallel and terminates into points (AA6-8; not sub-parallel; FOV=3 mm). C- mafic (elongate biotite) and felsic minerals separated into bands due to strain partitioning around a more competent orthoclase phenocryst, with finer-grained recrystallized material formed around edges of orthoclase due to strain accommodation (AA6-36A; FOV=3 mm). D- a quartz phenocryst with undulose extinction and new subgrain formation on grain boundaries to accommodate strain (AA6-28; FOV=3 mm). E- gneissose texture with elongate biotite formation between recrystallized quartz and feldspar (AA6-35; FOV=3 mm). F- Carlsbad-twinned orthoclase phenocryst with lobe-like myrmekitic extension into other twin, which may be related to ductile deformation of the feldspar and greater fluid content of magma. Groundmass is very fine-grained, with an alignment of platy muscovite (AA6-28; FOV=1.5 mm).

Orthoclase phenocrysts have reacted rims whose extinction differs from that of the cores, indicating a different composition (Fig. 4.1 B). Dissolution pockets within phenocrysts may also indicate hydrothermal alteration by a fluid phase through fractures in the crystal. Polycrystalline quartz forms elongate lenses in more deformed specimens.

Sample AA6-21A is classified as the subsolvus Mirpur Granite (i.e. the coexistence of two feldspar species, such as K-feldspar and plagioclase), and is thought to be similar to the MIS granitoids. The feldspars are light red in colour, with brilliant- to olive-green mafic minerals and clear subhedral quartz. The texture (Fig. 4.6) varies from phaneritic to somewhat porphyritic in nature (2-7 mm diameter), with larger feldspar grains. Orthoclase and microcline are almost totally sericitized and subhedral, while plagioclase is only partially sericitized and retains its prismatic tabular habit. Chlorite is the major mafic mineral and varies from single coarse-grains to fine-grained aggregates. It has associated subhedral titanite, grown along cleavage planes as well as subhedral to euhedral titanomagnetite. Other accessories found are zircon and apatite.

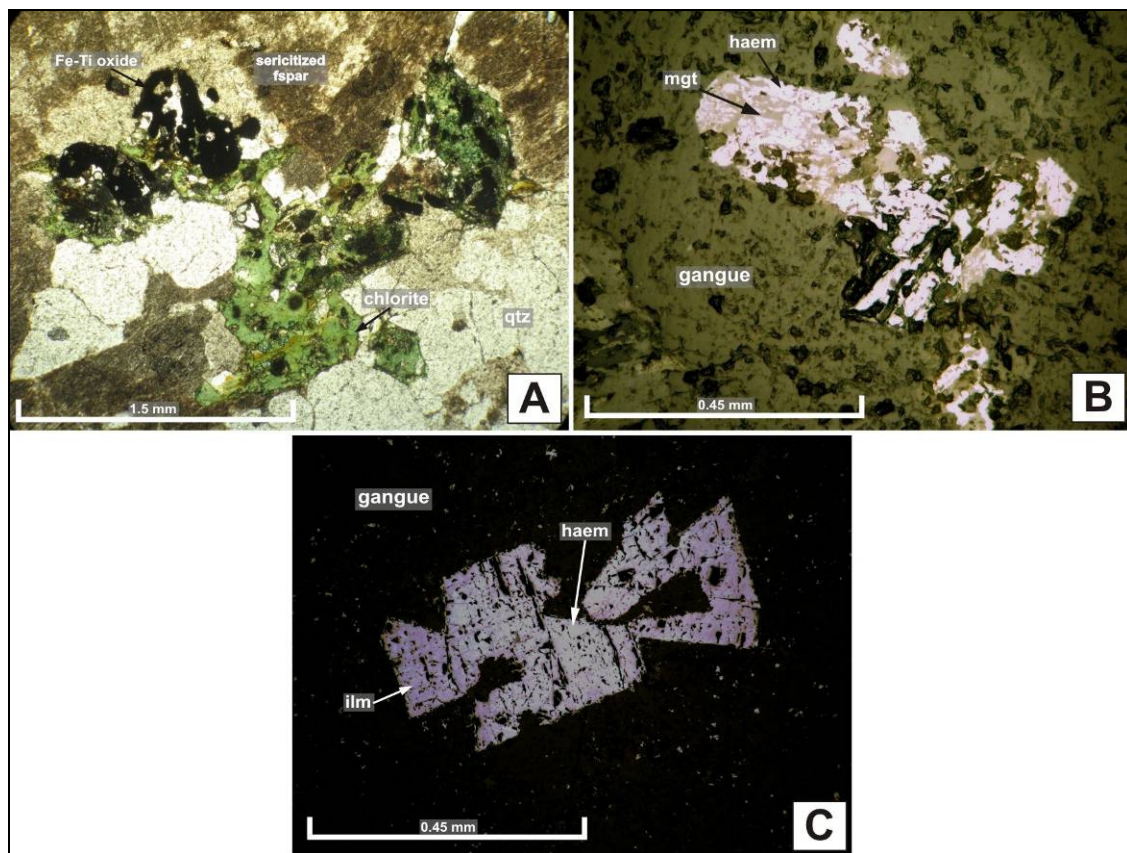


Figure 4.6. Mirpur granite and MIS dyke microphotographs. A- typical texture of the Mirpur granite where the feldspar is almost totally sericitized, while the quartz is inclusion-rich. Chlorite with radioactive haloes is the major mafic mineral, and is associated with skeletal to subhedral opaque minerals (AA6-21A; FOV=3 mm). B- subhedral to euhedral hematite and magnetite in irregular growth (reflected light, AA6-21A; FOV=0.9 mm). C- euhedral skeletal hematite with pink-purple ilmenite at either end (reflected light, AA6-51; FOV=0.9 mm).

Sample AA6-51 is a rhyolite porphyry dyke, possibly part of the Malani Igneous Suite. The phenocrysts are composed of euhedral to subhedral orange-pink orthoclase and microcline as well as subhedral quartz. The fine-grained groundmass (< 0.25 mm) contains subequal amounts of chlorite with radioactive haloes, opaque minerals and quartzofeldspathic material. Accessories include zircon and rare calcite. The opaque minerals, euhedral and blocky to tabular in habit, form straight trails that are subparallel to each other, with the spaces between filled by the other groundmass minerals.

4.2 Erinpura granitoids

The Erinpura light- to medium-grey granitoids vary texturally in outcrop from phaneritic granite to augen-gneiss (Fig. 4.7 A) with variable snowy-white to moderate pink feldspar phenocrysts to megacrysts (3-70 mm in length), which can range from euhedral tabular to anhedral within a single outcrop (Fig. 4.7 B). These granitoids are weathered and friable, with Fe-staining around grain boundaries is common. Gneissic samples define the type-locality granitoid and are the most common expression, with much Fe-staining due to weathering. Some samples also display rapakivi texture in hand specimen (Fig. 4.7 B). Quartz phenocrysts are subhedral and generally smaller (2-10 mm in length). These phenocrysts are separated by dark bands of micaceous minerals such as biotite and muscovite as well as fine-grained recrystallized quartz. A shear zone, located ~30 km NE of the main Mt. Abu samples in this study (Fig. 2.3; locality can be found in Appendix A) is the contact between the Erinpura granitoid and the surrounding Delhi Supergroup metasediments. Here, the Erinpura granitoid grades from augen gneiss to thinly-banded (<3 mm) mylonitic gneiss towards the tectonic contact.

In thin section, plagioclase, orthoclase and microcline are usually subequal, with a large amount of sericitization (Fig. 4.8 A-B). Within some plagioclase phenocrysts the sericitized cores have been altered to epidote, chlorite and tremolite/actinolite.

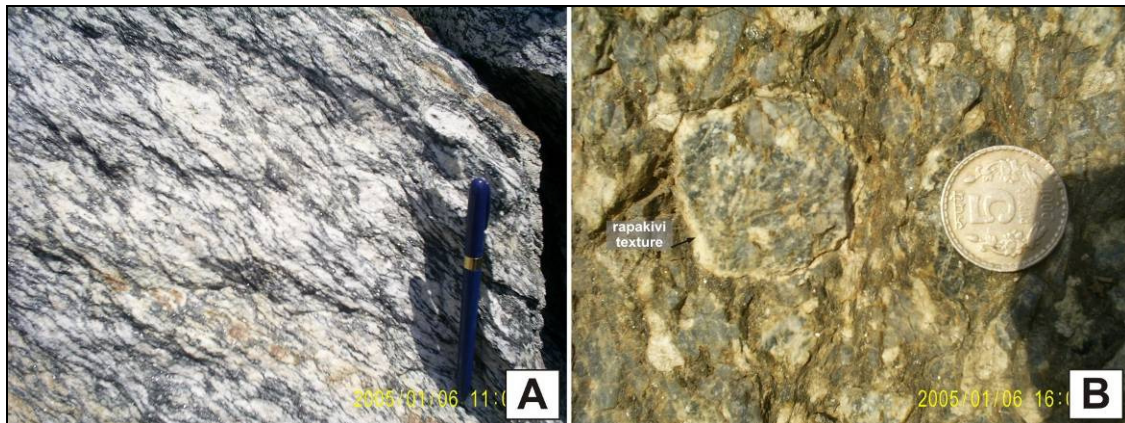


Figure 4.7. Field photographs of Erinpura granitoid. A- highly strained augen gneiss, with augens somewhat flattened due to intensity of deformation (AA6-18). B- a porphyritic specimen, with large irregular rapakivi-textured phenocryst. Feldspars vary from euhedral to anhedral, with larger phenocrysts commonly anhedral (AA6-24).

Feldspar phenocrysts are subhedral to euhedral, some with embayed margins due to dissolution and enclosing smaller anhedral quartz blebs and euhedral biotite. Most orthoclase is perthitic (Fig. 4.8 A), while some antiperthite (plagioclase with flame-like structures) is observed in one sample. Quartz is largely recrystallized, blocky and fine-grained and found between larger feldspar grains.

Biotite with acicular habit is the predominant mafic mineral, with subordinate muscovite usually found at the edges of biotite grains. One sample (Fig. 4.8 B) has magmatic hornblende with the relict prismatic habit and zoning visible, with alteration to chlorite and what may be tremolite. Titanite, Fe-Ti oxides, zircon, apatite and monazite are accessory minerals associated with the biotite clusters. Titanite may be fine-grained surrounding Fe-Ti oxides and a reaction rim, or prismatic and wedge-shaped (more commonly than in Mt. Abu granitoids). Zircon is subhedral, with corners rounded off, although oscillatory zoning can be seen in some crystals.

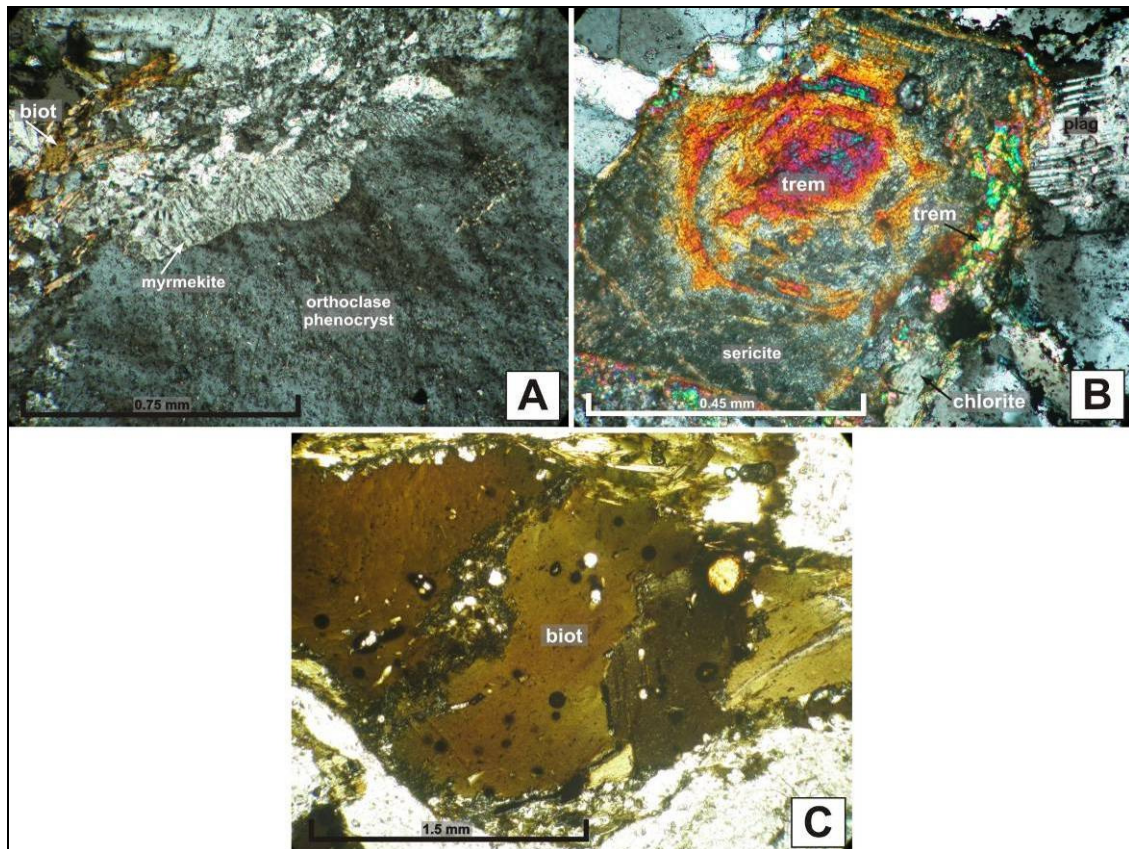


Figure 4.8. Microphotographs of Erinpura samples. A- myrmekitic intergrowth along orthoclase phenocryst grain boundary that is related to deformation, as groundmass is very fine-grained and has a recrystallized flow-growth texture of felsic minerals and aligned biotite crystals (AA6-26; FOV=1.5 mm). B- primary hornblende in crossed-nicols, highly altered and sericitic, with primary magmatic zoning, then a zone of dissolution and regrowth (circular rim) and finally more growth-zoning into typical prismatic hornblende (replaced on edges by tremolite and chlorite). These events may have occurred in the magma chamber as conditions changed (AA6-22; FOV=0.9 mm). C- a biotite cluster which has undergone strain around the edges, as can be seen by the fine-grained recrystallization of the biotite to accommodate the strain and the lens-shape of the cluster (AA6-20; FOV=3 mm).

Biotite (yellowish-green to olive-brown; varies from <1 mm to 2 mm in diameter) is found in clusters of 2-4 mm diameter as well as disseminated between boundaries of felsic minerals. It is usually euhedral, and can be elongate and highly deformed (kinked cleavage) with a semi-parallel orientation within deformed clusters and bands. In Figure 4.8 C, a cluster of biotite crystals has become lens-shaped due to the strain partitioning around the edges of the larger biotite and crystallization of fine-grained biotite.

Most Erinpura samples are altered due to the high degree of deformation that these rocks have experienced. This is shown in Fig. 4.9 A, B, D, where most plagioclase has become almost completely sericitized and some crystals have altered cores of tremolite and chlorite. Hornblende has also been partially replaced by chlorite while retaining its euhedral shape.

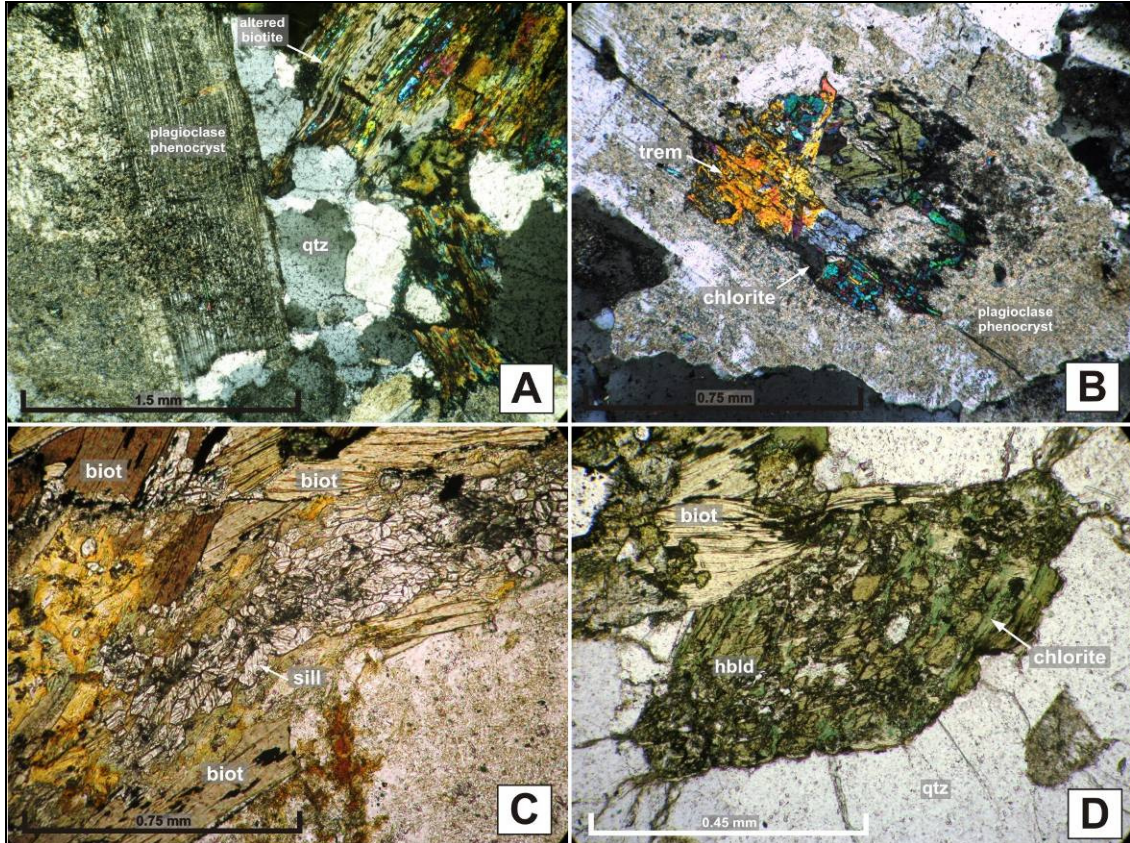


Figure 4.9. Alteration within the Erinpura samples. A- highly sericitized plagioclase feldspar, together with sutured quartz as well as biotite that has been almost completely altered to chlorite and Fe-oxides (AA6-22; FOV=3 mm). B- highly sericitized plagioclase phenocryst with a core altered to tremolite and chlorite (AA6-22; FOV=1.5 mm). C- coarse-grained blocky euhedral sillimanite within a biotite cluster (AA6-23; FOV=0.9 mm). D- highly fractured relict primary hornblende grain replaced in parts by chlorite (AA6-22; FOV=1.5 mm).

Ilmenite, hematite, muscovite, titanite, apatite, zircon and monazite (rare) are usually associated with the mafic biotite clusters (Fig. 4.10 A-B).

Deformation microstructures (Fig. 4.11 A-F) include undulatory extinction in quartz, subgrain formation and formation of small quartz grains on boundaries of larger ones in order to accommodate strain. Elongate quartz and biotite grains have also grown parallel to direction of strain. Deformation twins in microcline are also present, as are microfractures in feldspar that are infilled by recrystallized quartz and feldspar. Myrmekite is also a feature on K-feldspar grain boundaries.

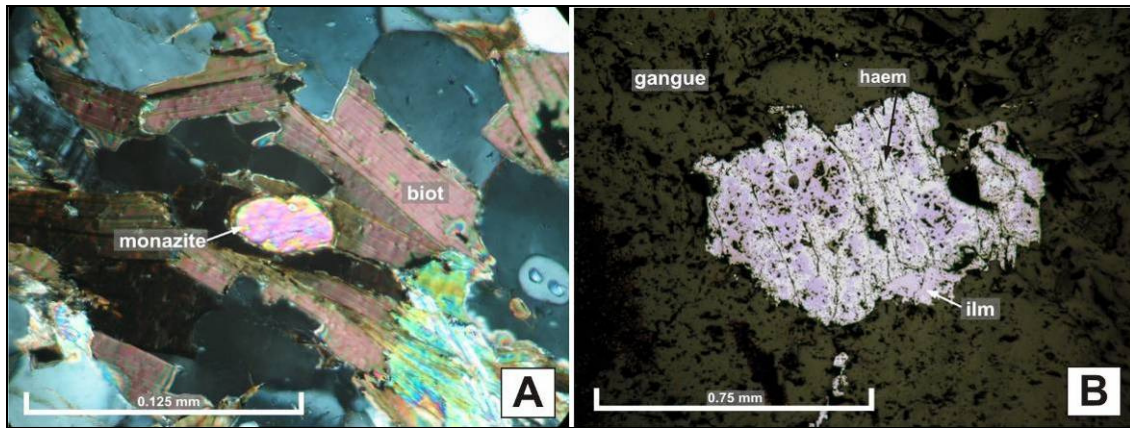


Figure 4.10. Microphotographs of accessory minerals in Erinpura granitoids. A- occurrence of monazite (high δ , somewhat wedge-shaped) within a biotite cluster (DB-1; FOV=0.25 mm). B- ilmenite with irregular growth blebs of hematite, which may be an exsolution feature (reflected light, AA6-26; FOV=1.5 mm).

Mylonitic solid-state deformation is suggested by very elongate muscovite defining a strong foliation and growth of blocky recrystallized quartz between, as well as very fine-grained recrystallized quartz and biotite grown around more competent feldspar porphyroclasts. Other deformation microstructures mentioned may also be submagmatic in nature.

Sample AA6-23, found ~5 km south of Sirohi town, is deformed and migmatitic in nature and contains an occurrence of coarse, euhedral blocky sillimanite associated with a mafic mineral cluster (Fig. 4.9 C). The euhedral habit of the sillimanite may indicate that it formed during a high temperature metamorphic event that affected the Erinpura granitoids.

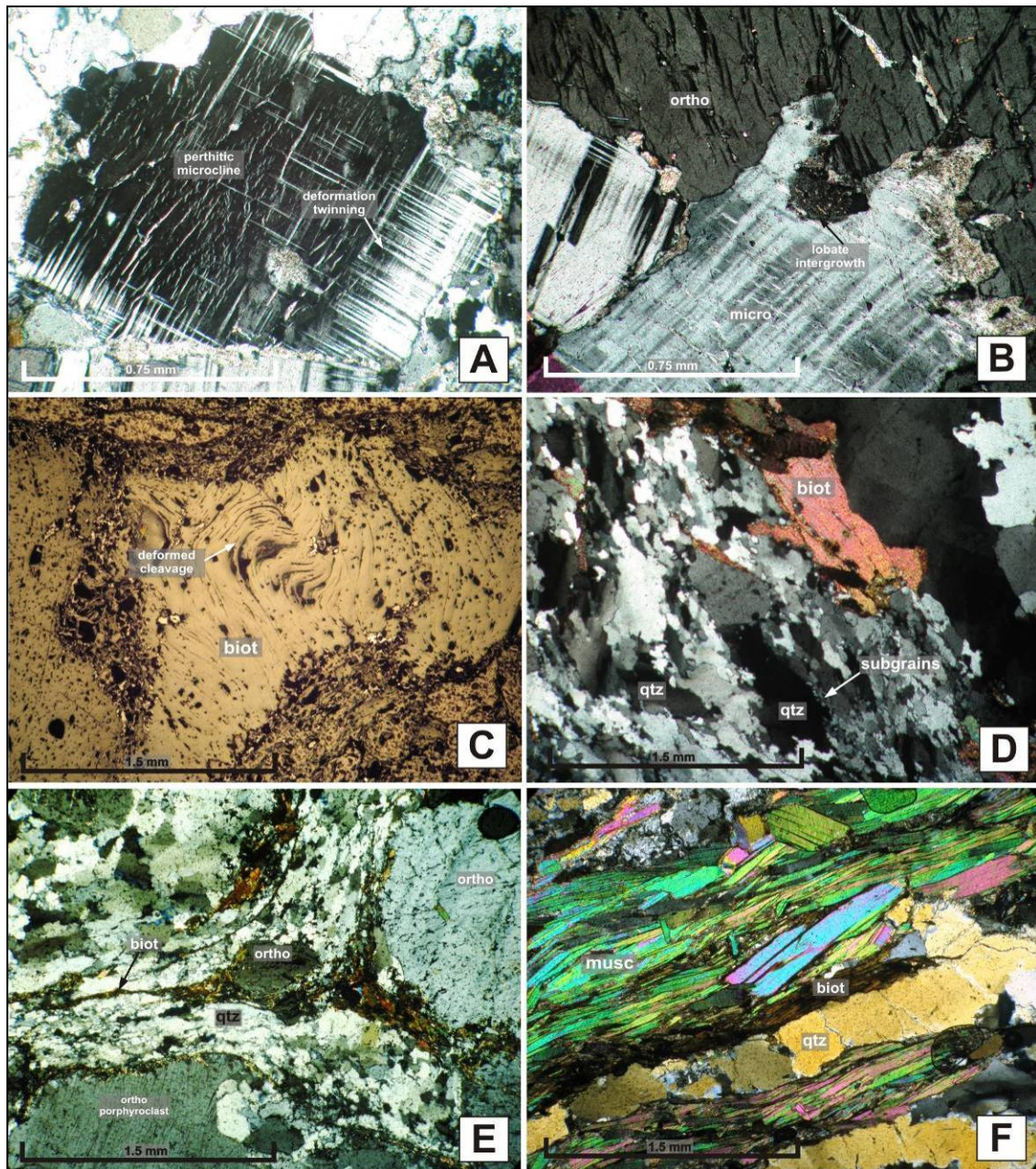


Figure 4.11. Deformation microstructures in Erinpura samples. A- deformation twinning in a perthitic microcline (AA6-18; FOV=1.5 mm). B- somewhat lobate intergrowth of two feldspar grains, which may be due to recrystallization of the feldspar (AA6-18; FOV=1.5 mm). C- biotite cleavage being deformed/kinked into folds (AA6-20; reflected light, FOV=3 mm). D- strained quartz re-equilibrating by formation of subgrains around edges of larger quartz grains (AA6-18; FOV=3 mm). E- zone of high strain where all recrystallized felsic material is flattened in the direction of extension, while biotite has grown along edges of more competent orthoclase porphyroclasts and is also oriented with strain flow direction (AA6-20; FOV=3 mm). F- parallel elongate muscovite and biotite and blocky recrystallized quartz partitioned strongly into foliation bands (AA6-24B; FOV=3 mm).

4.2.1 Balda granitoid (late-stage Erinpura granite)

This phaneritic granitoid is yellowish-grey, with light-coloured micas, few mafic minerals and no discernable deformatory fabric. It is considered a late-stage intrusive of the Erinpura granite suite.

In thin section this sample consists predominantly of quartz (~0.15 mm-7 mm), plagioclase, microcline, perthitic orthoclase (similar in diameter: 0.7-3 mm) and reddish-brown phlogopite. Feldspars are sericitic

and usually subhedral with interlocking grain boundaries throughout (Fig. 4.12). The micas (muscovite is associated with the phlogopite) are usually subhedral and <0.25 mm in diameter. Larger grains of feldspar and quartz are interspersed between smaller phlogopite, muscovite and quartz grains. Chlorite is found as a secondary alteration product of phlogopite. Pleochroic haloes in some mica indicate the presence of a radioactive mineral such as zircon.

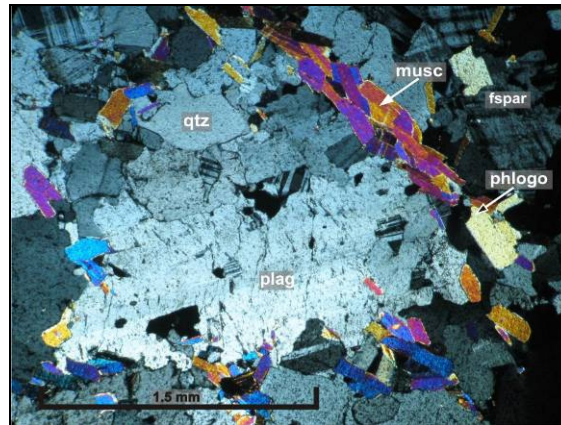


Figure 4.12. The Balda sample, classified as the late-stage intrusion of the Erinpura granite. The image shows the magmatic texture of larger, subhedral tabular plagioclase crystal, grown together with subhedral quartz and K-feldspar with euhedral muscovite and phlogopite grown at grain boundaries (BL-1a; FOV=3 mm).

4.3 Sumerpur granitoids (late-stage Erinpura granite)

These samples in outcrop are medium-grained (~1-2 mm) light-grey granitoids with rare megacrysts of snowy-white euhedral to subhedral tabular feldspar (>3 cm across) randomly scattered within the sub-equigranular rock (Fig. 4.13). Magmatic flow-banding is present in outcrop as well as mafic enclaves, which have diffuse contacts with the surrounding granite. The Sumerpur granite is massive and undeformed in outcrop, with cryptic contacts to the surrounding metasediments.



Figure 4.13. Field view of the massive, medium-grained Sumerpur granitoid. It has randomly oriented phenocrysts, such as this large euhedral plagioclase, which contains mafic biotite inclusions and has been embayed slightly on its upper edge, but otherwise does not seem to have been altered/dissolved by the magma (AA6-16).

In thin section, samples have a cloudy texture, which is caused by alteration of feldspars to sericite as well as fine-grained muscovite and biotite within fractures and on grain boundaries (Fig. 4.14 A). The dominant subhedral to euhedral orthoclase, microcline and plagioclase (~0.5-4 mm in diameter) are intergrown with blocky quartz (0.1-0.5 mm in diameter) in a sub-granular texture.

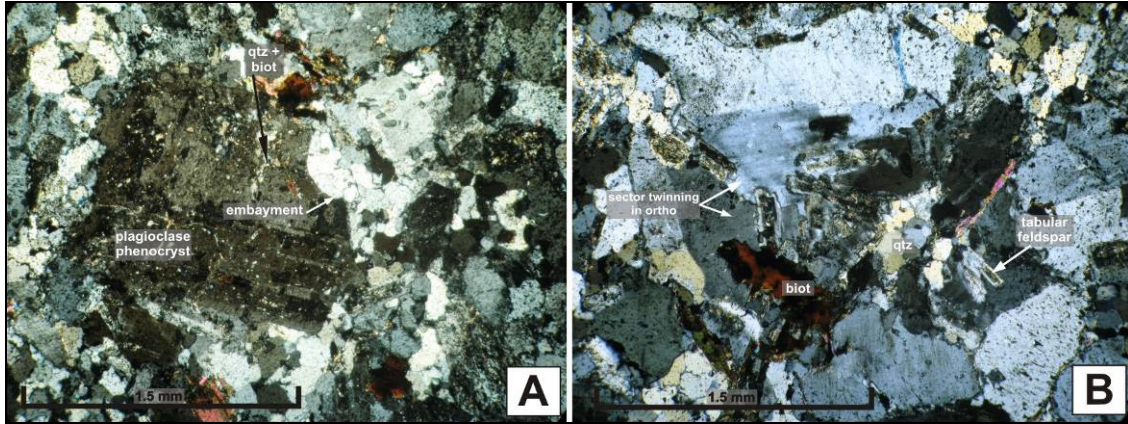


Figure 4.14. Microphotographs of Sumerpur samples. A- sericitic plagioclase phenocryst with many fractures infilled by fine-grained quartz and muscovite. A corner is embayed due to impingement of new quartz/feldspar growth that surrounds phenocryst (AA6-17; FOV=3 mm). B- smaller tabular feldspars that have sericitized cores within a larger subhedral orthoclase grain, which shows sector twinning (AA6-17; FOV=3 mm). The smaller feldspars may be earlier, more Ca-rich and therefore more susceptible to alteration by fluid movement through fractures and cleavage planes within the larger subhedral feldspar.

Small early-formed feldspar grains are tabular with wholly-sericitized cores and are found within larger feldspar phenocrysts that show faint primary magmatic zoning and sector twinning (Fig. 4.14 B). Subhedral to euhedral disseminated biotite (<0.5 mm) is the major mafic mineral and contains radioactive haloes as well as some alteration to chlorite. Muscovite is associated with the biotite as well as opaque titanomagnetite, occasionally with titanite rims present.

4.4 Ranakpur granitoids

In outcrop these light-grey to medium light-grey granitoids grade from massive to porphyritic and are deformed at contacts, with boudin-structures as well as ptygmatic isoclinal folding in granite veins within the surrounding less-competent calc-silicate of the Delhi Supergroup (Fig. 4.15 A-B). Granitoid samples are somewhat friable and fine yellow oxidation rims around crystals are visible in hand specimen.

In thin section, samples have a granular texture (Fig. 4.16 D) with subhedral feldspar grains being phenocrystic and having embayed margins (0.5-6 mm in diameter). Orthoclase dominates over plagioclase and subordinate microcline, while quartz is recrystallized. Smaller feldspar grains are found between larger ones together with subhedral to anhedral quartz and euhedral biotite (0.3-2.5 mm in diameter). Some

samples have subhedral hornblende (~1.5 mm) associated with biotite in clusters, while biotite is also disseminated throughout (Fig. 4.16 C).

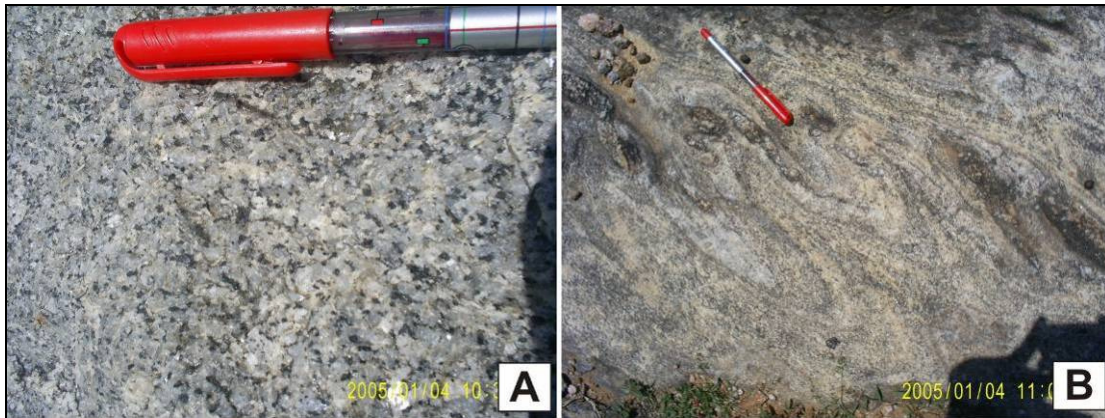


Figure 4.15. Field outcrop images of Ranakpur intrusive. A- field view of the massive Ranakpur granitoid, showing slight variations in grain-size from medium- to fine- grained (AA6-2). B- ptygmatic isoclinal folding of boudinaged granitoid stringer between flowing bands of calc-silicate.

Euhedral titanite as well as magnetite, hematite and ilmenite (some with titanite rims), apatite and zircon are usually associated with the mafic biotite and blue-green hornblende (Fig. 4.16 C, Fig. 4.17 A, B). Deformation microstructures (Fig. 4.16 A, D) include undulatory extinction, subgrains on boundaries, recrystallization of quartz and deformation twinning in plagioclase. Interfingering of grain boundaries between quartz and feldspars is also present. Myrmekite occurs between boundaries of adjacent feldspar grains (Fig. 4.16 B).

Biotite is euhedral, while hornblende is subhedral; both are found disseminated as well as on feldspar grain boundaries. Prismatic titanite is also found disseminated or together with biotite, apatite and prismatic zircons. Magnetite and ilmenite are the major Fe-oxides, sometimes with hematite exsolution, while Fe-sulphides are rare and are found at the cores of zoned opaque minerals, rimmed by magnetite and then ilmenite. This may reflect original reducing magma conditions, with progressive change to more oxidized conditions with ascent.

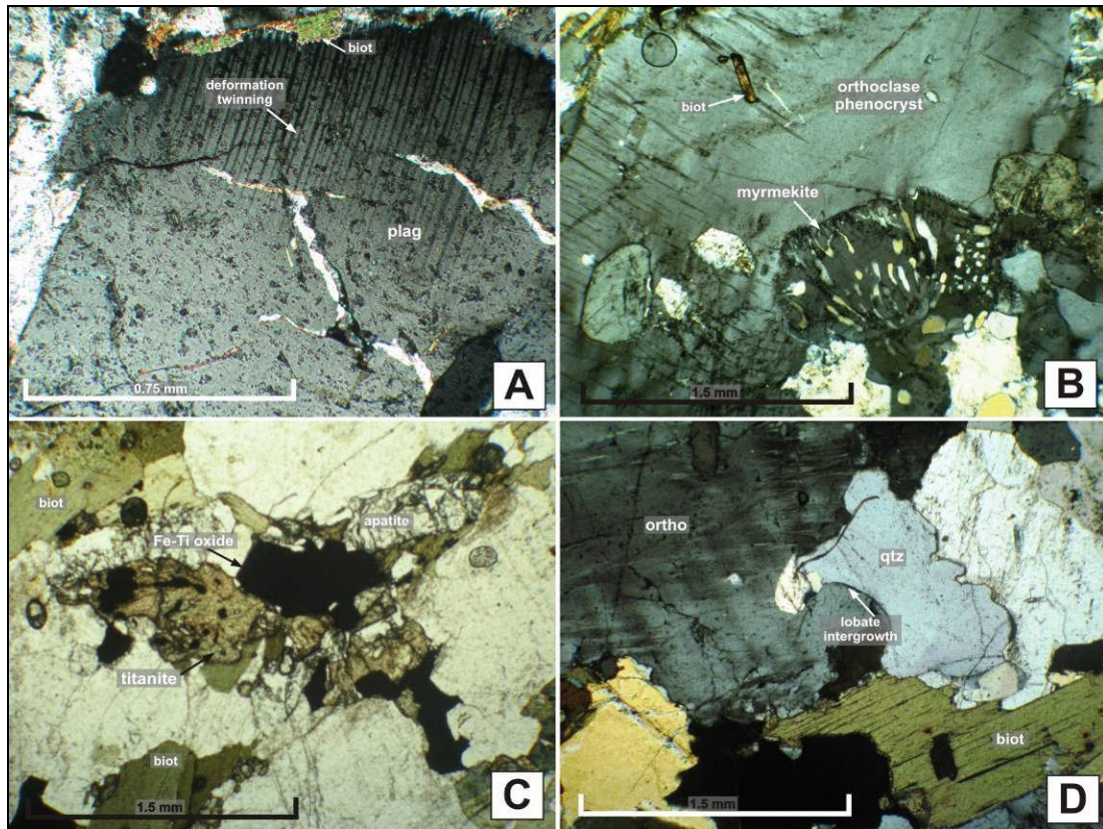


Figure 4.16. Microphotographs of Ranakpur samples. A- fracture infilled plagioclase with deformed twinning at edge of grain (AA6-2; FOV=1.5 mm). B- myrmekitic intergrowth extending into edge of larger perthite from groundmass (AA6-5; FOV=3 mm). C- euhedral Fe-Ti oxides associated with subhedral titanite and apatite, as well as platy biotite (AA6-7; FOV=3 mm). D- suturing of quartz and microcline indicating microstructural deformation (AA6-7; FOV=3 mm).

It is pertinent to describe the country rock here, as the mineral assemblage provides clues to the grade of metamorphism experienced. The calc-silicate is a clinopyroxene-phlogopite-talc marble. The marble is granular, with disseminated crystals of clinopyroxene, flaky talc and phlogopite (Fig. 4.17 B). Titanite is associated with clinopyroxene, while molybdenite with wavy habit and hematite are associated with the talc (Fig. 4.17 C, D). Coarse, curved, molybdenite laths show strong bireflectance and reflection pleochroism of light grey to dark brown-grey. These laths also have a strong basal cleavage, which shows the effects of deformation similar to kink-banding (Fig 4.17 C). The calc-silicate is quite weathered, with reddish-orange Fe-staining, and very friable.

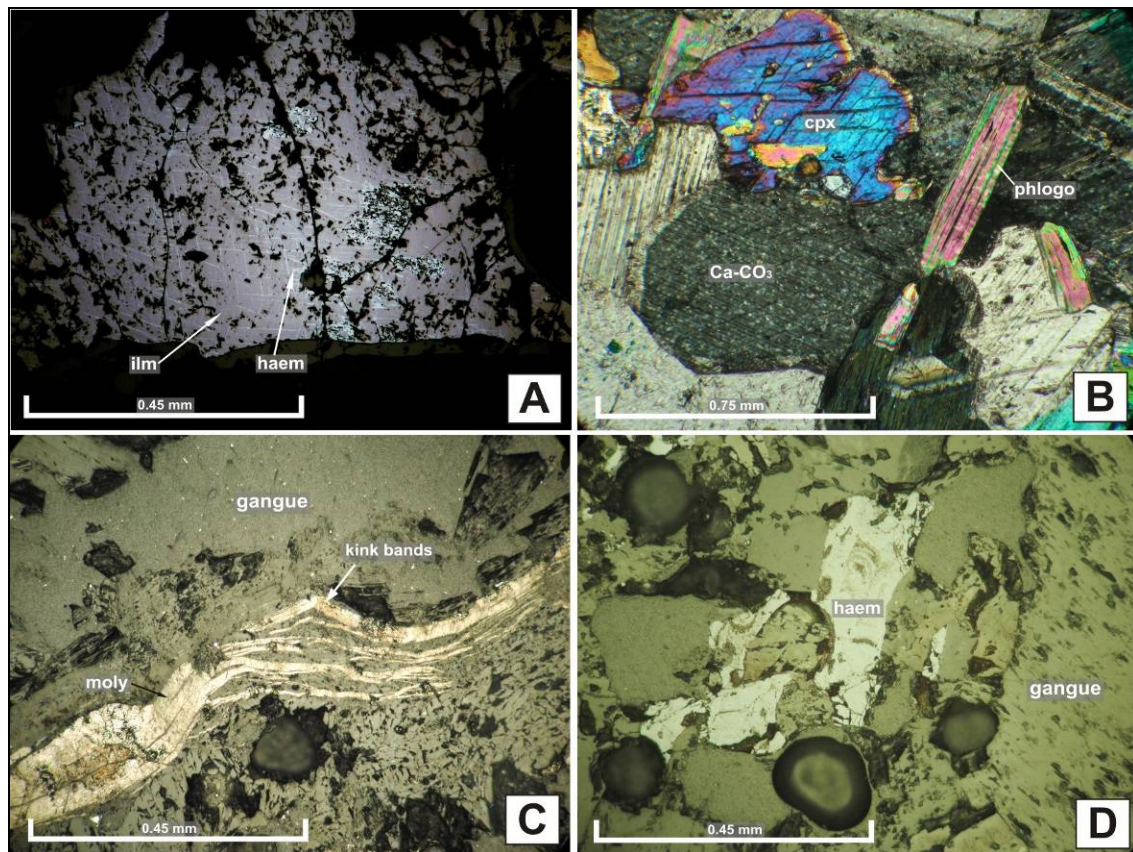


Figure 4.17. Microphotographs of Ranakpur granitoids and calc-silicate samples. A- euhedral ilmenite (pale pink) with exsolution lamellae of hematite (bright cross-hatching), rimmed by fine-grained titanite (AA6-2; reflected light, FOV=0.9 mm). B- typical texture of the calc-silicate, with subhedral clinopyroxene and prismatic phlogopite dominated by euhedral to subhedral to calcite/dolomite (AA6-1B, FOV=1.5 mm). C- molybdenite with its wavy habit and strong basal cleavage and birefractance (AA6-1B; reflected light, FOV=0.9 mm). D- subhedral hematite disseminated within the sample (AA6- 1B; reflected light, FOV=0.9 mm).

4.5.1 Revdar Rd. granitoids (Mt. Abu type)

These granitoids are found in river-cuttings, as outcrop is extremely scarce south of the main Mt. Abu pluton (Fig. 2.3). The result is that most specimens are extremely weathered and friable. Granitoid-gneiss foliation trends 035° - 040° , with dip to the SE of $>70^{\circ}$; similar to the main Mt. Abu trends further north. Metasediments found along this road include a subvertical Fe-stained quartzite as well as marble found in a quarry. Both metasediments are deformed, with the quartzite having elongate flattened grains and the tremolite-talc-marble being folded together with intrusive biotite-gneiss.

In hand specimen, these samples range from massive to foliated and porphyritic granite-gneiss. Most show signs of alteration in the form of pervasive yellow Fe-staining. The phaneritic orange-pink granite (Fig. 4.18 A) is dominated by subhedral to euhedral orthoclase, microcline and plagioclase (2-11 mm across), subhedral quartz (3-7 mm across) and mafic clusters of biotite. Biotite is also found accumulated at felsic grain boundaries. Some feldspars are quite fractured and infilled with fine-grained material.

Orthoclase and microcline phenocrysts, commonly glomeroporphyritic, are generally larger (0.5-1 cm) than quartz, perthitic, inclusion-rich and sericitized. Quartz phenocrysts are polycrystalline (Fig. 4.18 C). Equigranular recrystallized quartz grains and smaller, more euhedral feldspars (0.75-1 mm across) are found between larger grains.

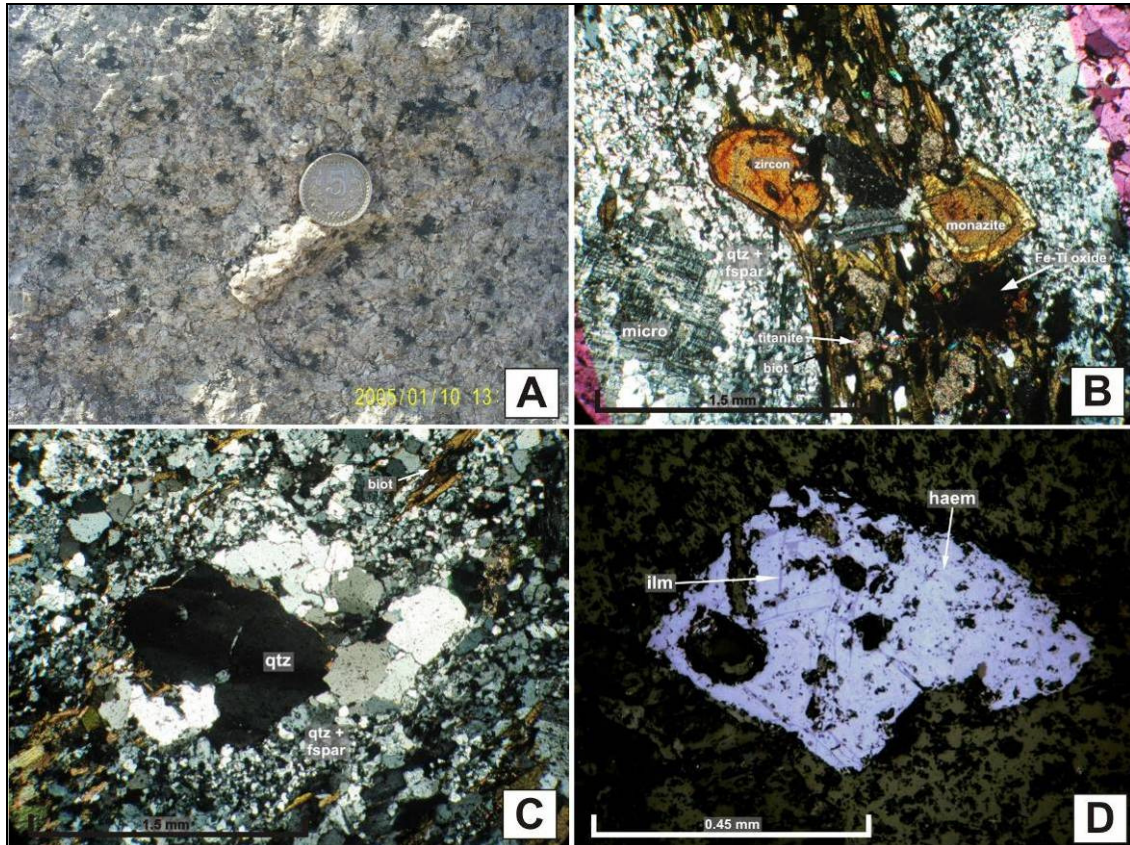


Figure 4.18. Microphotographs of Revdar Rd. granitoids (Mt. Abu type). A- field view of phaneritic pink granite, similar to the Mt. Abu type-granite (AA6-48A). B- recrystallized sample with fine-grained quartzofeldspathic material surrounding larger microcline phenocryst. The mafic cluster is aligned parallel to the fine-grained material, and contains a wedge-shaped, altered crystal (to the right) which may be monazite, while the large altered/radiation damaged grain to the left (yellow rims) may be zircon. These are associated with smaller rounded fine-grained titanite growths which are alterations of Fe-Ti oxides (AA6-42A; FOV=3 mm). C- polycrystalline quartz phenocryst within a fine-grained quartzofeldspathic groundmass (AA6-42A; FOV=3 mm). D- euhedral hematite with cross-hatched ilmenite exsolution (AA6-48A; reflected light, FOV=0.9 mm).

In foliated and gneissic specimens, biotite is clustered and oriented with long axes parallel (Fig. 4.18 C). Associated with biotite are opaque Fe-Ti oxides, euhedral titanite and moderate-yellow zoned zircon/monazite (Fig. 4.18 B, D). Quartz shows undulatory extinction and recrystallized subgrains on boundaries, while the groundmass is recrystallized to finer-grained quartz, feldspar and biotite, which have grown around more competent phenocrysts in some places (Fig. 4.18 B, C).

Hornblende is found either intergrown with biotite or disseminated. There is also much granophyric growth between quartz and K-feldspar in the groundmass, which is extremely fine-grained and recrystallized.

4.5.2 Revdar Rd. granitoids (Erinpura type)

These samples outcrop within riverbed cuttings along Revdar Rd., and commonly range from porphyritic granite-gneiss to mylonitic gneiss (Fig. 4.19 A), so have all undergone some deformation. Foliation trends vary within samples from $\sim 270^\circ/50^\circ$ S to 040° /subvertical, the latter of which is similar to other (Mt. Abu) granitoids within the study area. All samples have a preferential direction of growth, with the mylonitic gneiss having separate light (quartz, orthoclase and microcline) and dark bands (biotite, chlorite and muscovite) ~ 1 -5 mm in width. Quartz is recrystallized and fine-grained with <1 mm polycrystalline lenses/phenocrysts that are elongate in the direction of greatest extension, along the fabric (Figure 4.19 B). The feldspar is also very sericitized. Orthoclase and microcline phenocrysts are remnant, with most recrystallized into finer-grained aggregates. Muscovite is also strained along this fabric and shows kink banding (Figure 4.19 C, D), while biotite is disseminated and fine-grained in the groundmass.

The granite-gneiss and porphyritic granite display a preferential fabric along which feldspars are elongated (vary from 0.75 mm-2.5 cm length). Quartz is anhedral and smaller than the feldspars (<0.75 mm) as well as having undulatory extinction and subgrains between larger feldspars. Fe-staining is pervasive, and Fe-oxides are the major accessory found along streamers of Fe-staining between grains.

Garnet found in one sample is fractured, anhedral with embayed margins to quartz. This garnet probably formed by the breakdown of biotite, muscovite and quartz to garnet, K-feldspar and H_2O . The presence of garnet suggests high pressures and temperatures experienced by this rock post-crystallization.

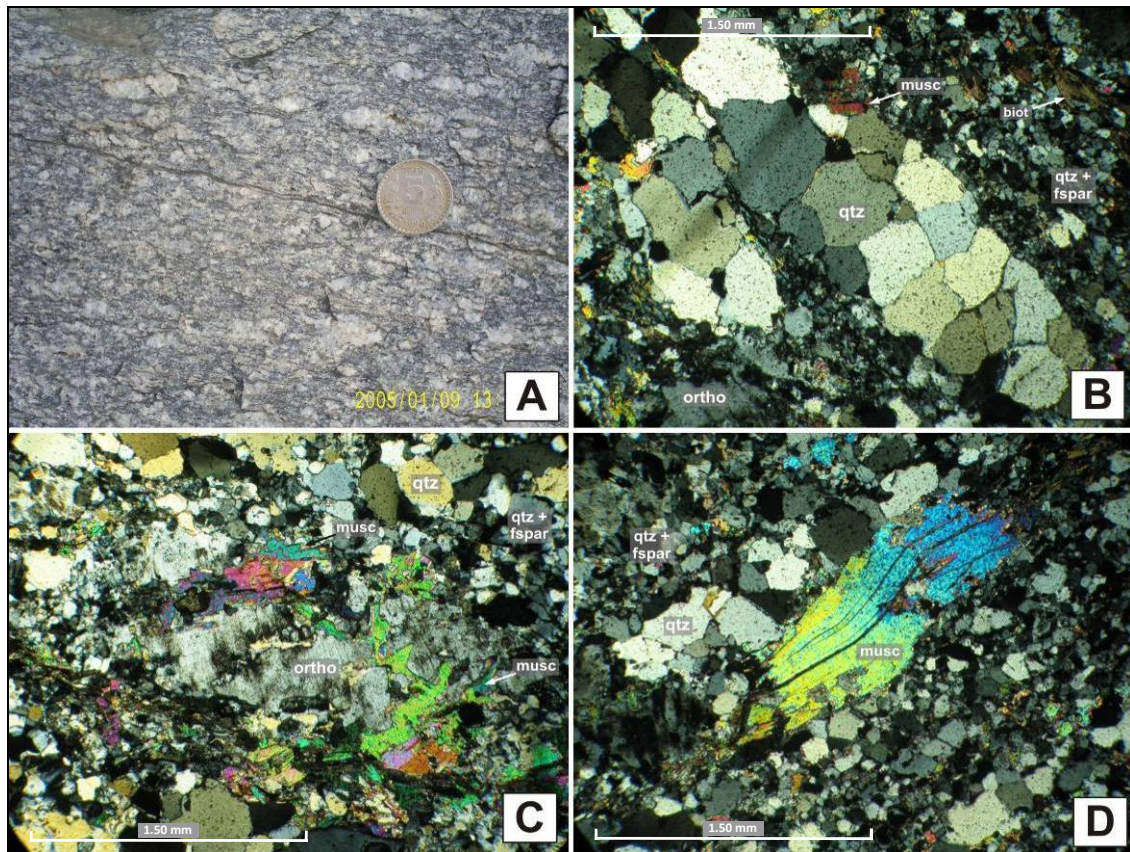


Figure 4.19. Microphotographs of Revdar Rd. granitoids (Erinapura type). A- view of a Revdar Rd. (Erinapura-type) gneiss with flattened augen structures and very fine, down to mm-scale, banding (AA6-38). B- polycrystalline quartz phenocryst that has recrystallized in a lenticular form due to deformation, surrounded by fine-grained quartzofeldspathic and mafic material (AA6-38; FOV=3 mm). C- a remnant orthoclase grain with very embayed margins into which poikilitic muscovite has grown (AA6-38; FOV=3 mm). D- a kinked muscovite grain with its cleavage deformed due to strain (AA6-38; FOV=3 mm).

4.6 Swarupganj Rd. granitoid

This is a foliated granite defined by platy biotite in elongated clusters (Fig. 4.20 A). Amphibolite (fine-grained, Fig. 4.20 C) from the Delhi SG outcrops a few hundred metres south of this granitoid. It is in contact with extremely weathered granite, from which no fresh sample could be obtained. Phaneritic subhedral plagioclase, orthoclase and quartz (1-4 mm in length) occur between biotite, while Fe-staining is pervasive throughout.

This sample has an equigranular cloudy texture with intergrown plagioclase and quartz as well as anhedral orthoclase, which range from 0.1-0.8 mm in length. Biotite is euhedral, <1 mm in length, and usually occurs between felsic grains. Anhedral hematite and magnetite (Fig. 4.20 B) are disseminated within the groundmass and very rare.

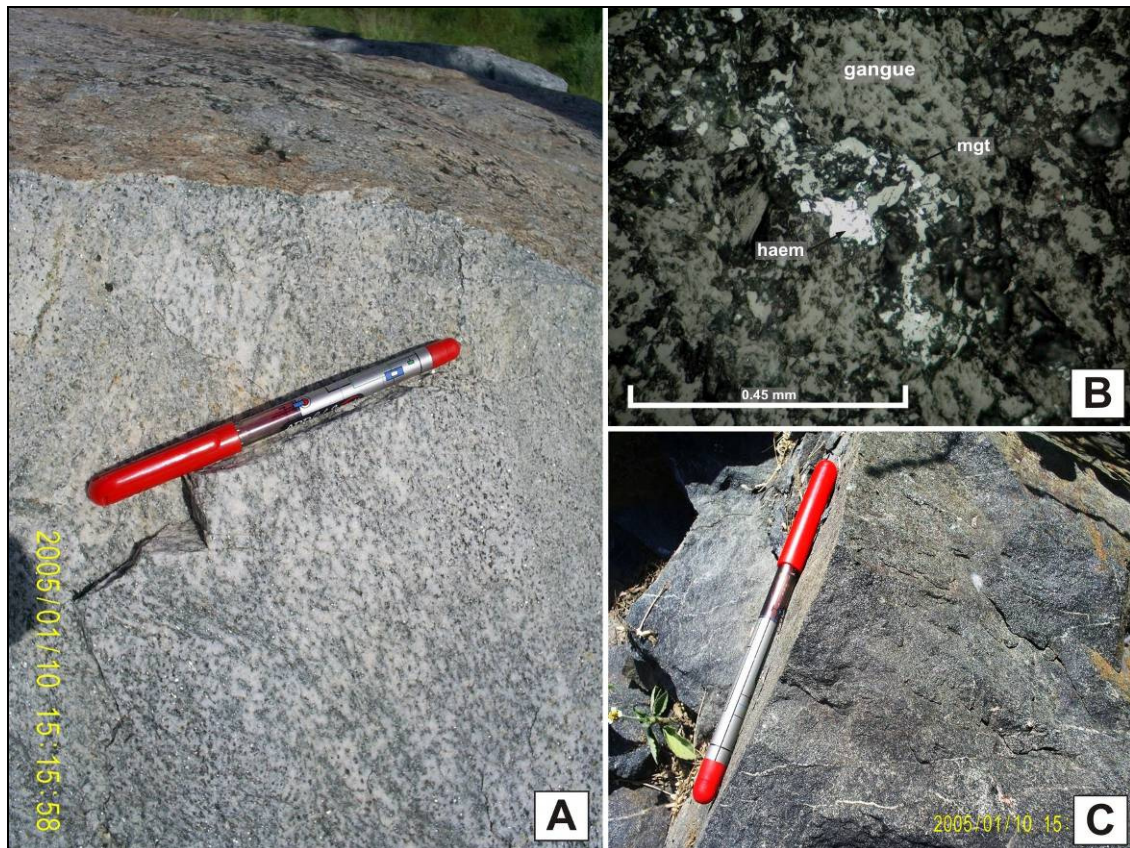


Figure 4.20. Outcrop and microphotographic images of the Swarupganj Rd. granitoid. A- field view of Swarupganj monzogranite. B- anhedral hematite and magnetite intergrown (AA6-49; FOV=0.9 mm). C- fine-grained amphibolite, part of the Delhi Supergroup.

4.7 Kishengarh nepheline syenite

This isolated and poorly-dated deformed syenite intrudes schistose amphibolite as can be seen in Fig. 4.21 A. The syenite is phaneritic with snowy-white microcline (\pm plagioclase) and nepheline as well as mafic minerals which form the foliation in this sample.

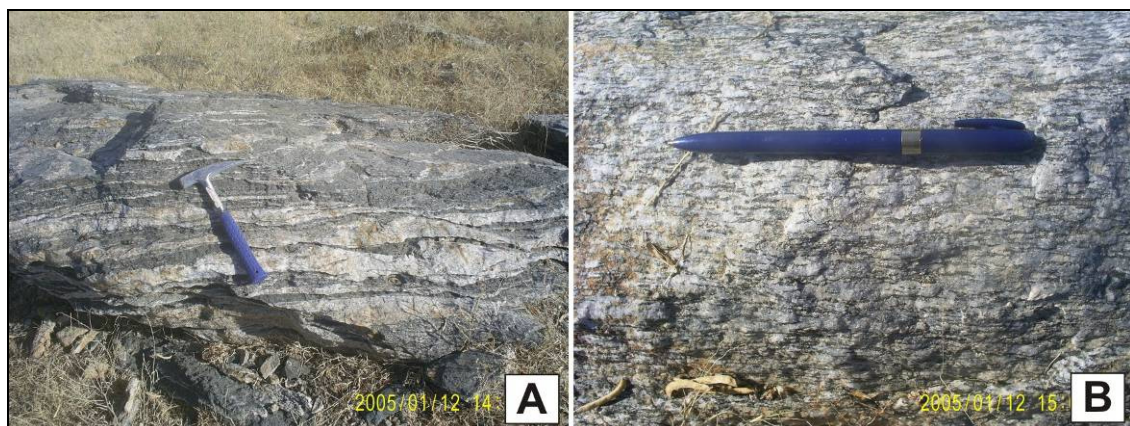


Figure 4.21. Outcrop images of the Kishengarh sample. A- stringers of the nepheline syenite within the surrounding schistose amphibolite. B- field view of foliated nepheline syenite, where foliations are well-defined by elongate mafic bands (AA6-52A).

In thin section (Fig. 4.22A-C), the texture is granoblastic (0-1.5 mm) and magmatic with slightly larger euhedral tabular microcline and subordinate plagioclase grown together with blocky to subhedral nepheline. However, microcline does show deformation twinning. Large hornblende grains (~2 mm length) are orientated randomly, while the foliation is defined by finer-grained hornblende and associated biotite and titanite.

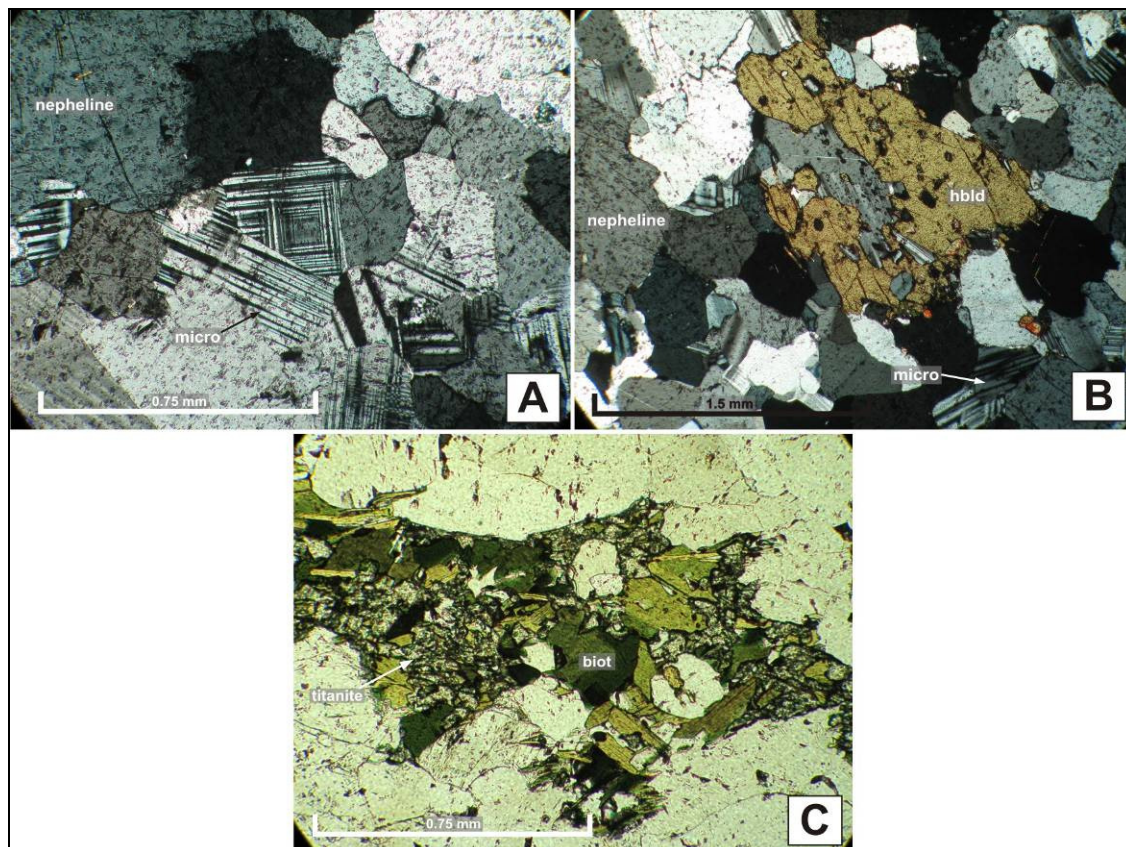


Figure 4.22. Microphotographs of the Kishengarh nepheline syenite sample. A- magmatic texture with microcline (uneven twinning which may be deformation twinning) and subhedral nepheline (FOV=1.5 mm). B- subhedral hornblende intergrown with feldspar (FOV=3 mm). C- mafic cluster consisting of biotite and prismatic titanite (FOV=1.5 mm). All photomicrographs are of sample AA6-52A.

4.8 Mt. Abu dolerite dykes

These dolerite dykes intrude the Mt. Abu granitoids, usually with sharp contacts, although occasional ‘interfingering’ and diffuse contacts are seen. Dykes vary from ~20 cm-7 m width and intrude subvertically. Many have a schistose fabric, indicative of shearing.

Magmatic texture is preserved only in embayed phenocrysts of remnant plagioclase, which are heavily sericitized or altered to euhedral epidote, with the mineral assemblage largely being hydrous in nature. Large crystals of secondary dark to light yellowish-green actinolite-to-hornblende are present, surrounded by finer-grained (≤ 0.4 mm) crystals of blocky plagioclase, acicular amphibole and brown biotite, titanite, epidote (after plagioclase), calcite, Fe-sulphides and Fe-Ti oxides. The amphiboles constitute 40-70 % of the

modal mineralogy, with biotite being the other major mafic mineral. The schistose texture samples are biotite dominant and found at dyke margins. Very elongate sub-parallel biotite, sometimes with well-developed crenulations cleavage, forms the pervasive fabric. Plagioclase, the other major mineral, is found as rare remnant phenocrysts or more usually blocky and recrystallized within the groundmass. Fine-grained titanite is an alteration product of the ilmenite and magnetite, although euhedral wedge-shaped crystals are also disseminated throughout. Pyrite is disseminated throughout the groundmass, occasionally with some associated chalcopyrite.

These dolerite dykes have been shown to be geochemically similar (trace- and immobile-elements) to Seychelles dolerites, although Seychelles dolerites are more pristine, with greater preservation of the igneous mineral assemblage (Solanki, 2005). However, Mt. Abu dolerites have experienced a greater degree of alteration and metamorphism compared to Seychelles dolerites, as evinced by the mineral assemblage, with the major secondary mineral being hornblende, so placing it within the upper-greenschist to lower-amphibolite facies (~400-600°C).

4.9 Summary of Field and Petrographic Study

Mt. Abu and Erinpura

- Mt. Abu and Erinpura samples are broadly similar in the sense that they are both granitoids, dominated by orthoclase, quartz and biotite.
- The feldspars are partially metasomatized in both Mt. Abu and Erinpura samples, with many Mt. Abu and most Erinpura felsic rocks not preserving the original mineral assemblages.
- All Mt. Abu granitoid types have subvertical slickenside shear planes running through them, as well as the formation of augen gneiss, S-C foliation and elongate mafic foliations within granitoids. These may indicate space constraints and synkinematic deformation, during intrusion. This has also been suggested by De Wall et al. (1996).
- Mt. Abu granitoids are also intruded by numerous metamorphosed dolerite dykes (now altered to greenschist to lower-amphibolite facies grade schists), which do not intrude the Erinpura samples. These may have acted as conduits for fluid movement during metamorphism.
- Erinpura samples have a more complex deformational and metamorphic history, are more weathered and friable, with greater Fe-staining around grains. Samples from widely spread outcrops share similarities in texture, colour and composition. The Sumerpur samples are the exception, being fresh, phaneritic and without visible deformation.
- Erinpura granitoids are usually gneissic or porphyritic with megacrystic phenocrysts (up to 12 cm diameter) that often display rapakivi texture. Mt. Abu granitoids vary widely in texture and colour

as well as being more pristine (less altered, magmatic texture preserved) than Erinpura samples. The rapakivi texture often seen in Erinpura phenocrysts may suggest a change in the magma composition during ascent (either through injection of a different magma, or contamination).

- The percentage of plagioclase is greater in Erinpura granitoids with hornblende being virtually absent, likely reflecting different source composition from Mt. Abu granitoids, and a more primitive composition.
- Alteration of Fe-Ti oxides to titanite is common to Mt. Abu granitoids, with rare euhedral, primary titanite more abundant within Erinpura granitoids. Zircon is found in greater abundance within Mt. Abu granitoids, which may reflect greater Zr-concentrations in this magma.
- Hornblende (blue-green) is found together with biotite (dominant) in Mt. Abu samples, while biotite dominates over chlorite (alteration) and muscovite in Erinpura samples. Relict primary hornblende found in Erinpura samples is altered almost entirely to tremolite and chlorite. The relict hornblende, possibly from a more primary /original magma, may suggest a more primitive magmatic origin for the Erinpura granitoids when compared with those of Mt. Abu.
- Zircon is prismatic in Mt. Abu granitoids unlike Erinpura zircons which are subhedral, having rounded edges. Zircons from both suites have defined oscillatory zoning visible under the light microscope, which is somewhat disturbed. Apatite is present as an accessory in both Mt. Abu and Erinpura granitoids. Rare fluorite is only found in Mt. Abu samples and reflects a more evolved granitoid composition and more shallow level of intrusion.
- The differing proportions of plagioclase and microcline to orthoclase in Mt. Abu and Erinpura granitoids, the presence of hornblende as well as differences in the habit of zircons within each suite, implies dissimilar formation and origins.

Sumerpur (vs. Erinpura)

- In outcrop the Sumerpur granitoids do not resemble the Erinpura granite as they are very light grey, undeformed and massive, although they contain rare megacrysts of plagioclase and K-feldspar. Faint magmatic banding is visible over some areas of the granitoid, which also contains mafic enclaves, some with diffuse boundaries to the granitoid.
- In thin section, Sumerpur granitoids are dominated by recrystallized granular quartz, orthoclase and plagioclase. The recrystallized quartz may imply a low degree of deformation experienced, or could be submagmatic in nature.
- Plagioclase forms a substantial percentage of the feldspar makeup, similar to Erinpura granitoids.
- Biotite with radioactive haloes is the major mafic mineral and is disseminated throughout the samples, together with muscovite, similar to Erinpura granitoids.

- Sumerpur samples do not show any strain deformation structures in thin section or outcrop, but are similar in modal mineralogy to Erinpura granitoids. This similarity may be due to the Sumerpur granitoids being a later stage intrusive of the Erinpura granite suite.

Ranakpur (vs. Erinpura)

- These medium-grey phaneritic granitoids are massive (some phenocrysts) in outcrop, with high-strain deformation of the granitoid near or at contacts with the surrounding calc-silicate. Alteration of the granitoid is reflected in Fe-staining at grain boundaries, as well as the friable nature.
- Granitoid deformation in outcrop is both extensional (boudinaged) and compressional (ptygmatic folds), suggesting multiple episodes of deformation. The clinopyroxene-talc marble has a granular texture with Fe-staining around grain boundaries due to alteration and fluid movement. Mineralogy in the calc-silicate suggests a medium-to-high grade of metamorphism.
- Orthoclase dominates over plagioclase and subordinate microcline, while quartz is recrystallized with interfingering on grain boundaries, subgrain formation and undulatory extinction.
- The modal mineralogy is somewhat similar to that of Erinpura granitoids, with the exception of the hornblende and Fe-sulphides presence. The sulphides may be a reflection of reduced source magma conditions, with a progressive change to more oxidized conditions during magma ascent.
- Texturally, these granitoids are also largely undeformed, save for at tectonized contacts, although alteration is pervasive.

Revdar Rd.

- These granitoids are similar in outcrop to both Mt. Abu orange-pink and foliated granitoids as well as Erinpura gneisses. They are very weathered, with very little outcrop and many boulders. River-cutting samples are very weathered and friable.
- The samples that are similar in outcrop to Mt. Abu granitoids follow the trend in thin section (texturally and mineralogically). This also applies to those similar to Erinpura samples.
- An Erinpura-type sample contains garnet, indicative of the high pressures experienced by this sample.
- Generally, those described as similar to Erinpura are gneissic to mylonitic in nature, while those described as similar to Mt. Abu are phaneritic pink massive granitoids. The gneissic samples could also belong to the Mt. Abu group; however, they are more altered and less pristine than the gneissic samples from Mt. Abu.

Swarupganj Rd.

- This foliated granitoid is composed of quartz and equal amounts of plagioclase and K-feldspar. These are interspersed with mafic biotite and muscovite, which form elongate clusters but are also

disseminated throughout the rock. Hematite with blebs of ilmenite is associated with the biotite, as is the accessory muscovite.

Kishengarh nepheline syenite

- This nepheline syenite is deformed with fine-grained hornblende, biotite and associated titanite forming the foliation within the nepheline syenite.
- The felsic rock intrudes schistose amphibolite. Magmatic texture is preserved, with tabular microcline and plagioclase and blocky nepheline, but microcline does show some deformation twinning, an indication of some deformation event that affected this sample. Larger hornblende crystals are oriented randomly throughout the sample.

5. GEOCHEMISTRY

Samples were analyzed by X-Ray Fluorescence (XRF) and Inductively Coupled Plasma Mass Spectrometry (ICP-MS) methods in order to measure major and trace element concentrations within the granitoids. The major elements measured are used to calculate normative mineralogy, which is then utilized in the classification of granitoids into different groups according to their normative quartz, orthoclase, albite and anorthite content. Normative mineralogy is anhydrous, so hydrous phases such as biotite and amphibole are not considered in the norm. Normative data can thus only be a guideline, and must be utilized in conjunction with petrographic analysis and classification. Major elements may also show trends, such as those of fractionation and differentiation within granitoid suites. Trace elements may be used to show changes in magma composition, be it from differentiation, partial melting, contamination or alteration. They may also be used to compare magma composition of the source rocks. The list of elements analyzed is: SiO₂, TiO₂, Al₂O₃, Fe₂O₃, MnO, MgO, CaO, Na₂O, K₂O, P₂O₅, P, Sc, V, Cr, Co, Ni, Cu, Zn, As, Rb, Sr, Y, Zr, Nb, Sb, Ba, La, Ce, Pr, Nd, Sm, Eu, Gd, Tb, Dy, Ho, Er, Tm, Yb, Lu, Hf, Ta, W, Pb, Th and U.

The petrographic analysis of the all felsic rocks from this study, including Mt. Abu felsic samples, indicated that most had undergone alteration and did not preserve primary mineral assemblages. The geochemical composition of these samples should not be considered primary, as most major and trace elements are highly mobile in aqueous solution. Potassium and sodium of the major elements are extremely mobile, which affects classification schemes based on major element concentrations. These elements (K and Na) are usually found enriched within altered felsic rocks and so skew any classification schemes that utilize normative minerals rich in Na and K (orthoclase and albite) towards the K-feldspar side of such diagrams. Trace elements are highly useful in petrogenetic studies, as they convey information out of all proportion to their abundance within the rock. They are more sensitive to changes in the magma caused by fractional crystallization, assimilation, differentiation or partial melting, and this results in larger variations as the process continues. However, as with the major elements, many trace elements are also highly mobile in aqueous solution, and thus any interpretation of trends in diagrams utilizing such elements must be interpreted cautiously. These elements usually have large ionic radii and low valencies of 1 or 2 (K, Rb, Cs, Sr and Ba). Their large size does not favour incorporation into a crystalline structure; during partial melting or alteration, these elements move into the liquid phase. The elemental data cannot be interpreted unambiguously; immobile trace element ratios are more useful indicators of primary magma composition, and magmatic processes.

Figure 5.1 is the Streckeisen (1976) ternary diagram for the classification of granitoid rocks. Rock samples are plotted according to their modal content of K-feldspar, plagioclase and quartz. This classification diagram and the modal proportions for samples here may only be used as a guideline. As most samples are

phenocrystic, a single thin section is not fully representative of the rock sample. Additionally, most samples are partially metasomatized and do not reflect primary igneous compositions. Most Mt. Abu felsic samples plot as syenogranites to alkali-feldspar granites, while a few plot as quartz-rich granitoids, which may indicate greater alteration than the other Mt. Abu samples. Both the Mirpur granite and the Malani Igneous Suite (MIS) dyke plot in these classes as well. Erinpura granitoids are less K-feldspar rich than Mt. Abu samples and plot as syeno- to monzo-granites (including Sumerpur samples), with a couple of less evolved granodiorite samples. Ranakpur samples plot towards the K-feldspar apex, although a lone sample plots as a granodiorite. This is also the least altered sample, which may point towards a truer granitoid classification of these Ranakpur granitoids. Most Revdar Rd. granitoids cluster with the Mt. Abu samples, although two samples are tonalitic in nature and more primitive. The Swarupganj Rd. granitoid plots as a monzogranite, together with a few Erinpura samples. As expected, the Kishengarh sample plots as a silica-undersaturated feldspathoid (nepheline)-bearing syenite.

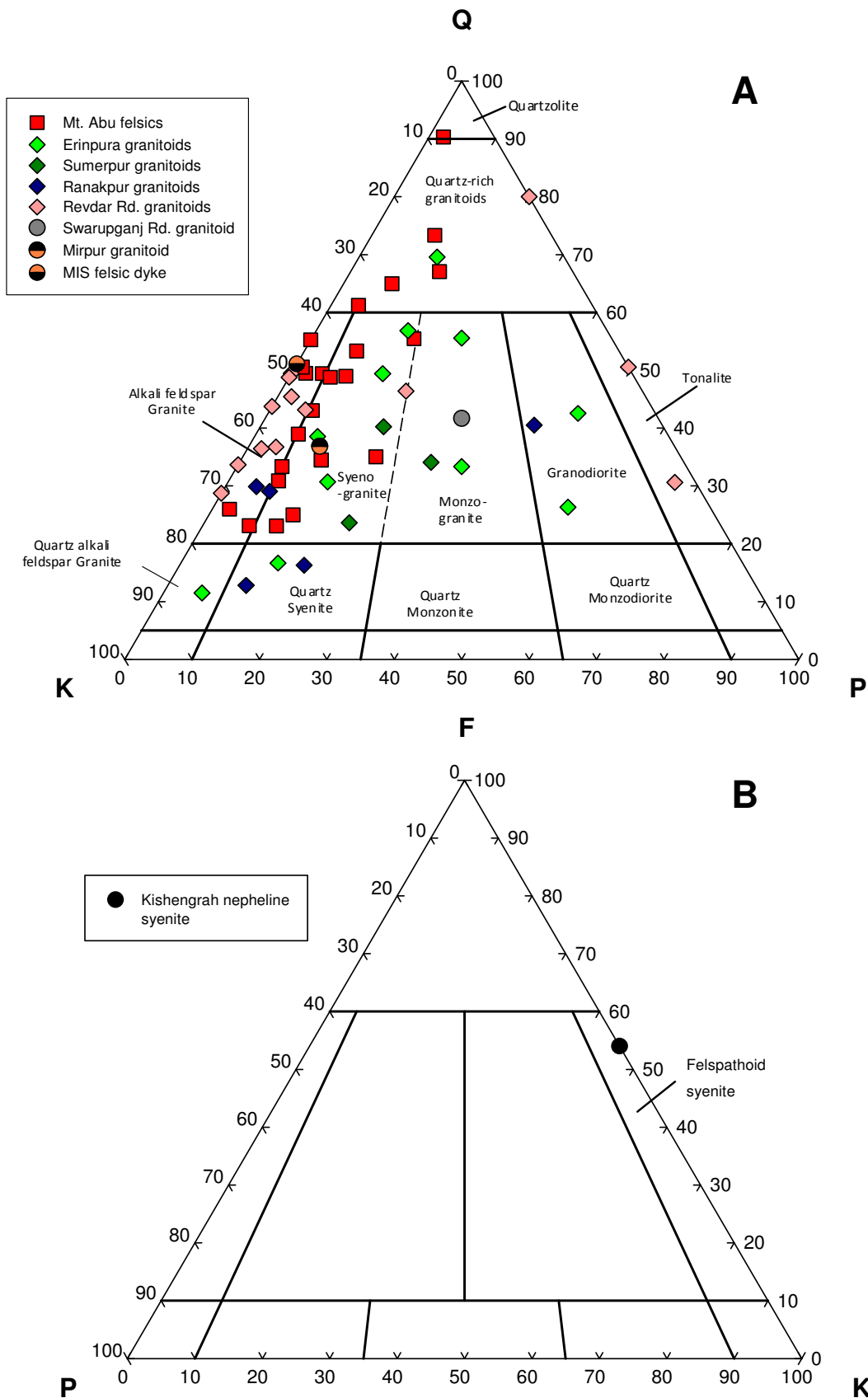


Figure 5.1 Ternary granitoid classification diagram utilizing modal proportions of plagioclase, orthoclase and quartz (after Streckeisen, 1976). A- A few Mt. Abu, Erinpura and Revdar Rd. granitoids do not plot in any field classified. Mt. Abu and Revdar Rd. felsic rocks plot as syenogranites to alkali-feldspar granites, while the majority of Erinpura granitoids are classified as syeno- to monzo-granites (including Sumerpur granites). Ranakpur and Sumerpur samples are scattered, while the Malani Igneous Suite dyke is highly alkalic in nature. B- The Kishengrah sample plots as a felspathoid syenite, as expected.

5.1 Major and trace element geochemistry

Mt. Abu granitoids and porphyry dykes range from 66.60-77.73 wt % SiO₂ (average SiO₂ = 72.84 ± 2.83 wt %). Major and trace element values can be found in Table 5.1. Major element compositions were utilized in the calculation of normative mineral compositions (anhydrous) which were then used to classify samples according to the Q' (F') - ANOR diagram of Streckeisen & Le Maitre (1979) in Fig. 5.2. The Q' (F') – ANOR diagram is useful, as it excludes Ab from the feldspar (x) axis, thus negating the need to allocate it to either K-feldspar or plagioclase. This axis is also a measure of differentiation or degree of evolution of samples, as those that are highly evolved/differentiated do not contain much An. The majority of samples collected from the Mt. Abu pluton cluster within the alkali feldspar granite and syenogranite fields, save for an augen gneiss, which plots in the alkali feldspar quartz syenite field. Both the Q'ANOR and the Streckeisen (1976) ternary diagram are in good agreement for the Mt. Abu samples. Geochemically, a third of Mt. Abu samples do not have any modal anorthite, which is as a result of their evolved/differentiated nature.

The Mt. Abu samples are subsolvus granitoids, as orthoclase, microcline and plagioclase are present, although the predominant feldspar is orthoclase. All samples have <10 % mafic minerals (biotite, hornblende and muscovite), normatively. Mt. Abu massive and porphyritic granitoids varieties are classified as metaluminous, while most foliated varieties and all rhyolite dykes are peralkaline in nature, and are usually enriched in terms of silica content as well (Fig. 5.2). The peralkaline samples also have most of the highest SiO₂ values and conversely, many of the lowest TiO₂, Fe₂O₃ and CaO values of the Mt. Abu granitoids. They also have the majority of the lowest P, Co, Sr and Eu values and the highest Ba, Pb and Th values (Table 5.1). These samples could be the result of the greatest fractionation within the pluton, as they are the most depleted in the major elements (Ca, Fe and Ti) that are removed through differentiation and removal of calcic high temperature plagioclase, early Mg-Fe silicates and Fe-Ti- oxides (Wolhuter, 1971; Middlemost, 1997), as well as in trace elements (Sr and Eu) that usually partition into earlier crystallized phases such as plagioclase. They are also most probably the late-stage intrusives, which would explain their fine-grained (in the case of the dykes) and foliated (the granites) nature. The higher concentrations of Ba, Th and Pb in these samples may be attributed to their being the most differentiated and therefore enriched in K-feldspar, into which Ba partitions preferentially. K-feldspar is also a major reservoir of radiogenic Th and Pb (Hall, 1996; Middlemost, 1997; Best, 2003).

Erinpura granitoids plot within the monzogranite field (mineral classification according to the anhydrous CIPW norm) and are clearly distinct from the Mt. Abu felsic samples. SiO₂ ranges from 66.47-74.3 wt % (average SiO₂ = 71.05 ± 2.33 wt %). A few samples are more K-feldspar rich and plot with the Mt. Abu felsic samples. Erinpura granite gneisses are subsolvus granitoids, with subequal amounts of plagioclase and orthoclase and usually <10 wt % mafic minerals (normatively, although modally, most samples contain

more than 10 % biotite or hornblende). Samples also have subequal weight percentages of magnetite and ilmenite (normatively), as compared to the Mt. Abu samples, where the majority (barring three) are magnetite-dominant. Approximately half the samples cluster along the metaluminous-peraluminous border, with the rest being highly peraluminous. Almost all have normative corundum in their norms, indicative of excess Al in their chemical compositions. They are also more plagioclase-rich. There is no discernable difference in major or trace element compositions between the metaluminous or peraluminous samples.

The three Sumerpur samples form part of the Erinpura suite of granites. They average 73.14 ± 2.34 wt % SiO_2 , are metaluminous and scatter from monzogranite to alkali feldspar granite in Fig. 5.2. As these originate from a single, homogenous-seeming outcrop, the range in normative values is unexpected and is caused by widely differing An-values. These samples have subequal orthoclase and plagioclase in the norm, with <10 wt % mafic minerals. They are also subsolvus, with orthoclase and microcline as well as plagioclase present in thin section.

The Ranakpur granitoids range in SiO_2 content from 64.28-66.14 wt %, with an average $\text{SiO}_2=65.4 \pm 0.82$ wt %, the lowest values in this study. These samples were taken in order to discern any change in composition across the intrusive for those samples proximal to the calc-silicate metasedimentary 'raft', to those further east of it. Two sub parallel W-E lines were sampled. Samples from the line further north have a slightly higher SiO_2 content than the three samples further south. However, this difference is statistically insignificant. The lines are ~75 m apart. Ranakpur samples are subsolvus (plagioclase, orthoclase and microcline) and metaluminous in nature. These samples are classified normatively as quartz syenites, with plagioclase > orthoclase and <10 wt % mafic minerals, in contrast to modal proportions of ~10-15 wt %. Ranakpur samples do not correlate well between modal and normative rock classification diagrams, which may be due to their variable degrees of alteration. These rocks have greater abundances of Al_2O_3 (>16 wt %), TiO_2 (>0.48 wt %), CaO (>2.44 wt %), Na_2O (>4.2 wt %), MgO (>0.77 wt %) and P_2O_5 (>0.19 wt %) than that of the Mt. Abu samples. The lower SiO_2 - and greater Mg#, CaO- and TiO_2 - content are an indication of a less-evolved composition than the Mt. Abu samples (Pankhurst et al., 2000; Christiansen et al., 2007), as CaO in felsic rocks is found in abundance in early magmas where it partitions strongly into early crystallized, high temperature plagioclase, while TiO_2 is found in greater abundance in early-formed Fe-Ti oxides (Zhong et al., 2007).

The Revdar Rd. granitoids are somewhat problematic, as five samples do not plot within the Q'ANOR diagram's fields. These gneisses are described in outcrop as friable with very weathered surfaces. The anomalous quartz (silica) enrichment may be attributed to remobilization during metamorphism and weathering. The majority plot as alkali feldspar granites, within the field of Mt. Abu samples. Outliers are

towards the less potassic end of the diagram. SiO_2 ranges from 66.67-78.23 wt % with an average SiO_2 of 72.18 ± 5.98 wt %. Most are subsolvus (modally and normatively), with orthoclase and microcline being predominant over plagioclase and <10 % mafic minerals. Samples are generally metaluminous, with four samples being highly peraluminous, and one weakly peralkaline. Five granitoids are also corundum-normative. Samples generally follow the trend of decreasing major element oxides with increasing SiO_2 (wt %), and have good correlations with MnO and P_2O_5 .

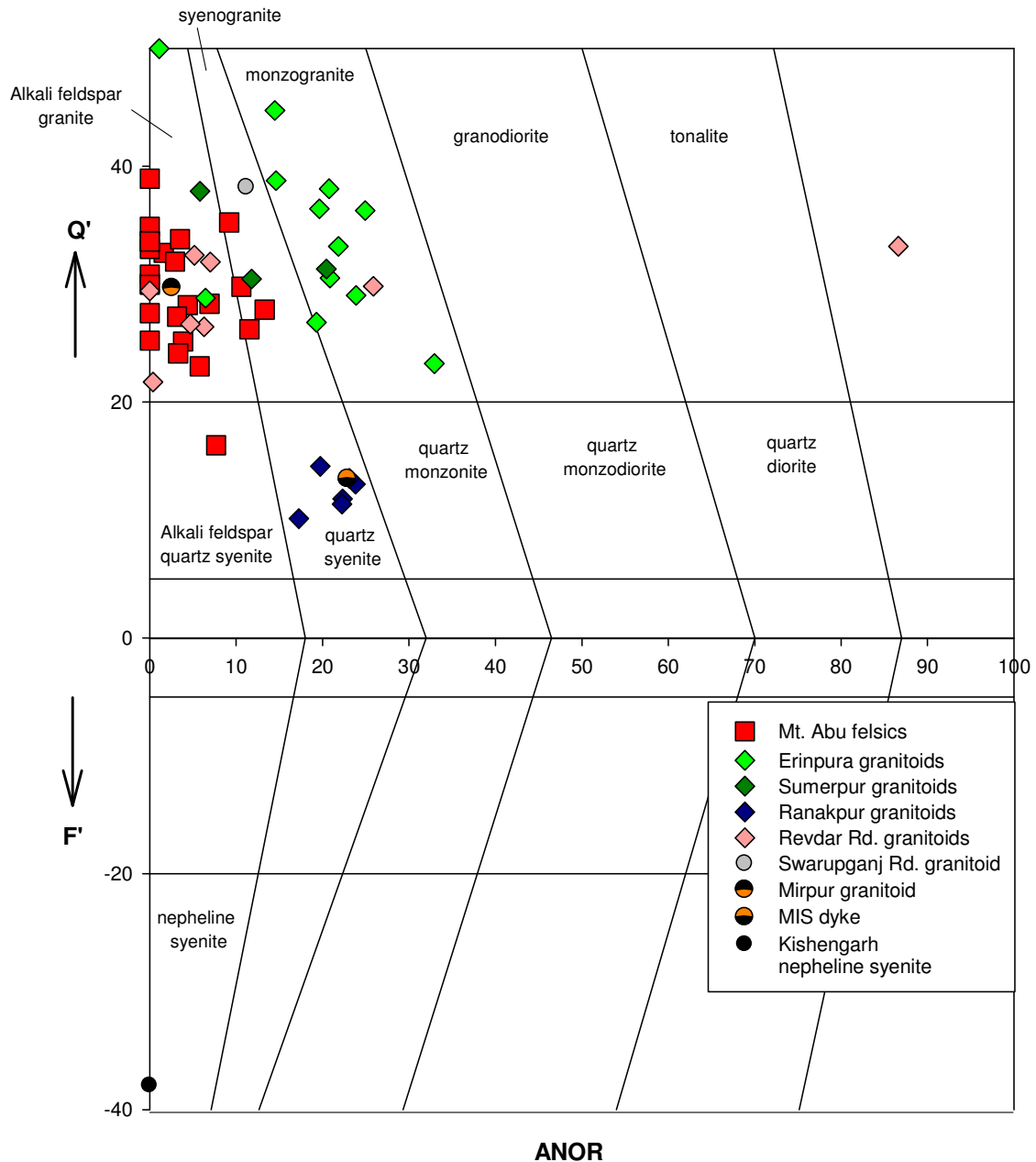


Figure 5.2. Diagram of Streckeisen and Le Maitre (1979) that classifies granitoid and felspathoid rocks according to their normative quartz, albite, anorthite, orthoclase and felspathoid contents. $Q' = [Q/(Q + Ab + An + Or)]$, $F' = [Ne + Lc + Kp]/(Ne + Lc + Kp + Or + Ab + An)$ and $ANOR = 100 An / (Or + An)$.

The Swarupganj Rd. granodiorite gneiss is very silicic ($\text{SiO}_2=78.04$ wt %) and subsolvus, with more plagioclase than orthoclase and plots within the metaluminous field. The Kishengarh nepheline syenite is

silica-undersaturated ($\text{SiO}_2=54.92$ wt %) and peralkaline in nature. The modal and normative rock classification is in agreement; a classification of nepheline syenite for this sample.

For Mt. Abu samples, most major elements have the typical granitic inverse relationship - when plotted against SiO_2 in Fig. 5.4. CaO decreases with increasing differentiation, as Ca is less compatible than Na in more evolved Si-rich magmas, so most is taken up by early-formed Ca-rich high temperature feldspars, and the Ca-content of plagioclase decreases with differentiation (Blatt & Tracey, 1995). Total Fe-content decreases as Fe partitions into earlier formed Mg-Fe silicates and oxides, which are removed from the magma (Christiansen et al., 2007). The steady decrease in TiO_2 and Fe_2O_3 signify that fractional crystallization and removal of early plagioclase and Fe-Ti oxides occurred (Cobbing, 2000; Villaros et al., 2009). The negative trend in P_2O_5 can be explained by early crystallization of apatite from the P-saturated magma (Christiansen, 2007; White, 2007). K_2O has a slight negative trend, while Na_2O and MgO are relatively constant with increasing SiO_2 (Fig. 5.5). However, there is a lot of scatter in these graphs, which is probably due to later hydrothermal alteration, as the alkalis Na and K are very mobile (Middlemost, 1997; Best, 2003). Mt. Abu samples plot within the high-K calc-alkaline to shoshonitic sectors of the diagram of Le Maitre et al. (1989) and are thus anomalously enriched in K_2O (Liégeois et al., 1998; Clemens & Roberts, 1993). This is confirmed in the SiO_2 vs. MALI ($\text{K}_2\text{O}+\text{Na}_2\text{O}-\text{CaO}$) diagram of Frost et al. (2001). The MgO content is constant, probably because it has reached its steady state concentration earlier in the evolution of the magma (Wiebe et al., 1997). The Mg# of Mt. Abu samples are also some of the lowest from this study's group of granitoids, which may reflect the degree of evolution or differentiation of the Mt. Abu granitoids magma when compared to the Erinpura or Ranakpur samples (Liégeois et al., 1998). The variability in the Mg# may be due to changes in the oxidation conditions of the magma chamber, and the abundance of Fe-Ti oxides crystallizing out. TiO_2 decreases as well (Fig. 5.4), probably due to early crystallization of Fe-Ti oxides from the magma, as Ti partitions preferentially into the crystal structure of ilmenite and magnetite (Zhong et al., 2007), not the melt.

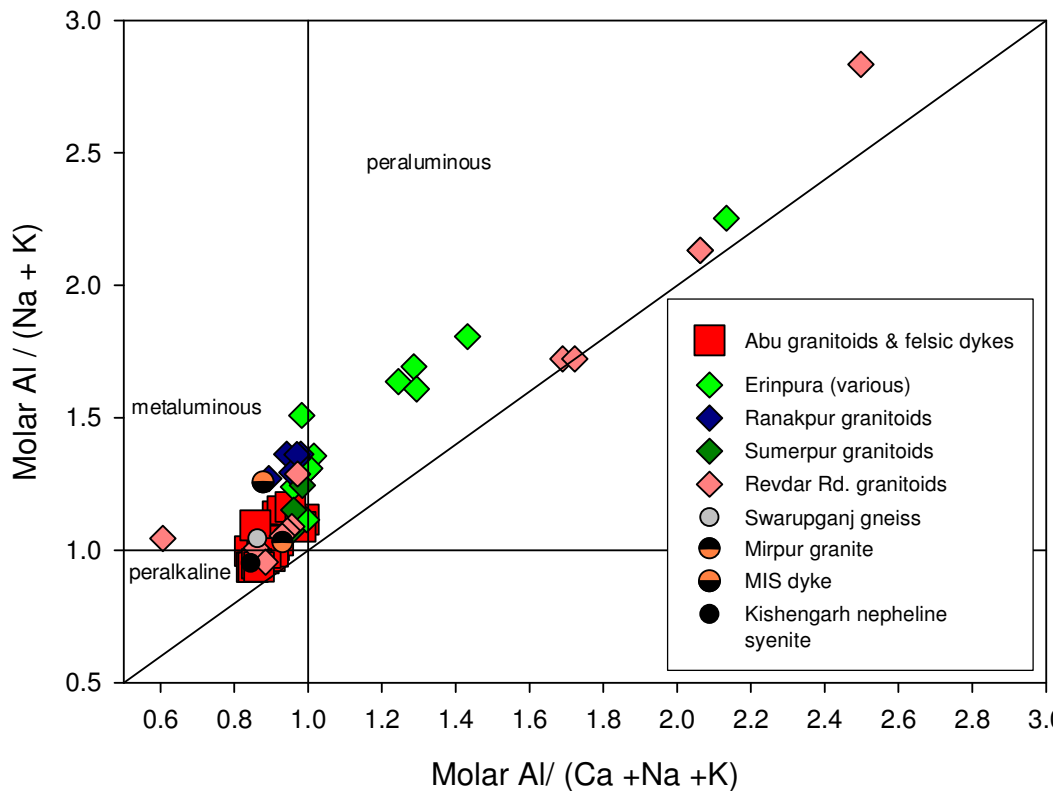


Figure 5.3. Aluminium saturation index (ASI) plot for all felsic rocks from this study. Mt. Abu samples are predominantly metaluminous, with a few peralkaline samples. Some Erinpura and Revdar Rd. samples are peraluminous as well (after Maniar & Piccoli, 1989).

In contrast, Erinpura granitoids have weaker linear relationships between SiO_2 and P_2O_5 , CaO , Na_2O and K_2O . MgO is the exception, while Fe_2O_3 and Al_2O_3 also have steeper gradients (weaker correlation) than the Mt. Abu rocks. The Erinpura samples also show more scatter than those from Mt. Abu, contributing the weakness of the relationships between SiO_2 and the other major elements. The weaker correlations between these major elements oxides and SiO_2 , which is an index of differentiation and fractionation, shows that the compositions of these rock samples may have been modified by other processes than fractional crystallization, such as partial melting and source compositions, entrainment from the source and magma mixing. Erinpura samples plot within the high-K calc-alkaline sector of the diagram of Le Maitre et al. (1989), similar to Mt. Abu granitoids. They are also calc-alkalic to alkali-calcic in nature according to the SiO_2 vs. MALI diagram, signifying their calc-alkaline nature. The higher P_2O_5 contents of these granitoids when compared to Mt. Abu samples may be as a result of the peraluminous nature of the magma, as a larger A/CNK value means that more P is able to dissolve in the magma. The removal of early Ca-rich plagioclase also inhibits large amounts of apatite crystallization, which can also increase the contents of P_2O_5 in the magma (Villaseca et al., 2008).

The Sumerpur samples usually plot within the Erinpura and Mt. Abu groupings for all major elements and are usually scattered.

The major element Harker diagrams show clearly that the Ranakpur samples form a population distinct from most other samples within this study. They have good correlations between SiO_2 and Fe_2O_3 , MgO , TiO_2 , MnO and CaO , while P_2O_5 , K_2O and Al_2O_3 are generally scattered, with no trend. The slope of most trends is steeper than that for Mt. Abu samples, resulting in generally weaker correlations between SiO_2 and other major elements. Ranakpur samples plot horizontally on the SiO_2 vs. Na_2O diagram and are alkaline in nature, according to the SiO_2 vs. MAFI diagram.

Revdar Rd. samples follow the granitic trend for all major element plots excluding K_2O , Na_2O and MgO , for which samples scatter widely. Most trace elements also show variable scatter but are usually within the Mt. Abu and Erinpura fields.

The single Swarupganj Rd. sample plots together with the main trend of Mt. Abu samples save for K_2O , Na_2O , MgO and CaO , where it plots as an outlier. The Kishengarh nepheline syenite is rich in the alkali elements K_2O and Na_2O , but otherwise plots as an outlier with mid-range abundances (in this study) of other major elements.

Most of the trace elements in the Mt. Abu rocks do not have good correlations with SiO_2 . Mt. Abu samples are enriched in most incompatible trace elements compared to Erinpura granitoids. This may be caused by a smaller degree of partial melting, which would noticeably increase the concentration of incompatible trace elements (Roberts & Clemens, 1993; Winter, 2001). This might explain the scatter and the weak positive or negative trends within the Mt. Abu samples (Fig. 5.6). An enriched source may also be responsible for the higher concentrations of incompatible elements and may suggest a large crustal input for the magma (Roberts & Clemens, 1993). Eu has a fair negative correlation with SiO_2 in Mt. Abu samples, expected because more plagioclase removal as differentiation proceeds.

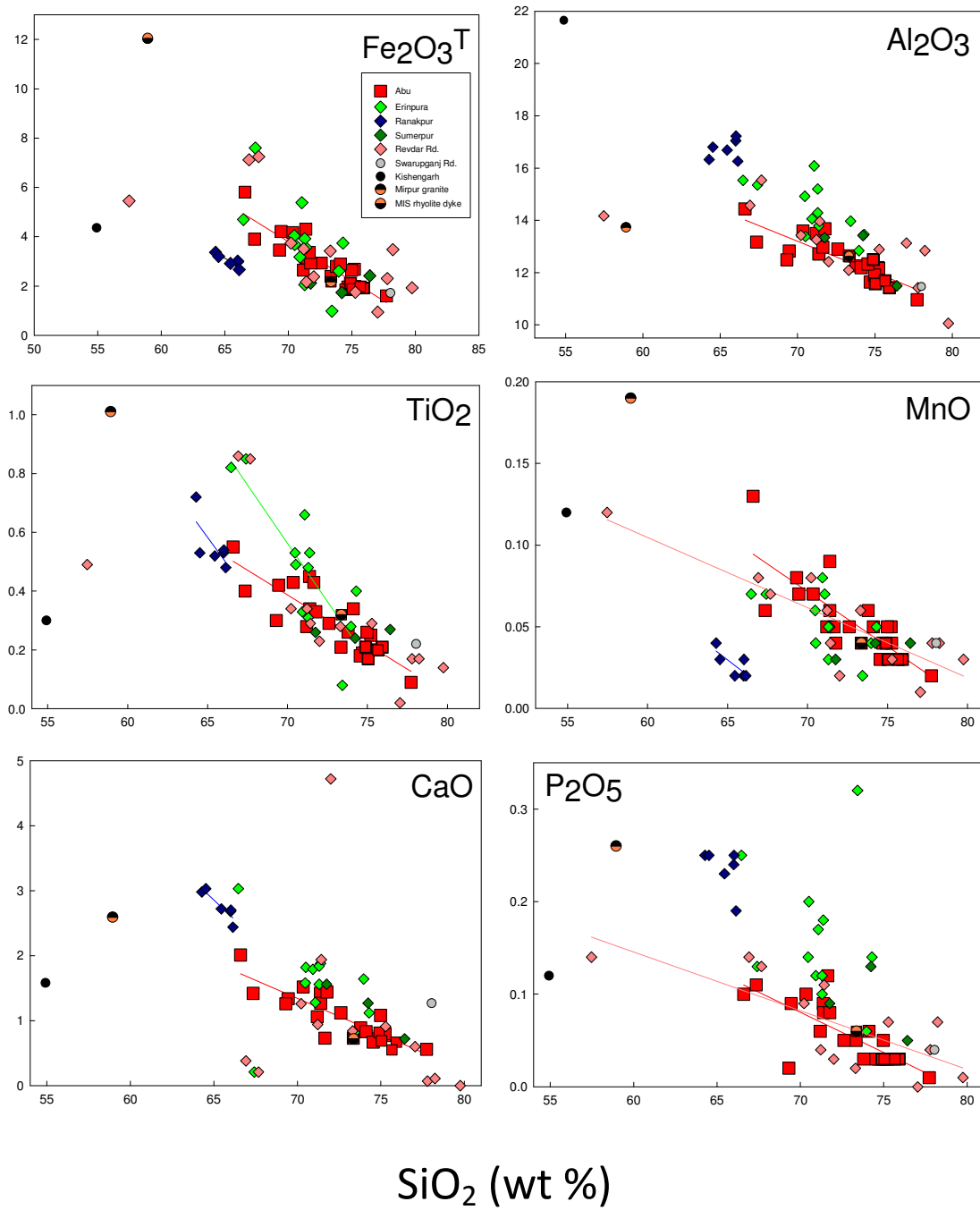


Figure 5.4. Harker diagrams of the variations in major element oxides plotted against SiO₂ for all felsic rocks from this study. Mt. Abu and Revdar Rd. samples show good correlations for most samples.

Table 5.1 Major and trace element data (this study).

Abu granitoids												
Sample:	AA6/8	AA6/9	AA6/10	AA6/12	AA6/13A	AA6/13B	AA6/14B	AA6/15A	AA6/15B	AA6/27A	AA6/27B	AA6/28
Lithology:	massive granite	massive granite	porphyritic granite	foliated granite	Foliated Granite	foliated granite	foliated granite	massive granite	porphyritic granite	porphyritic granite	foliated granite	foliated porphy. granite
SiO ₂	71.38	75.21	72.60	69.45	69.31	73.35	73.79	67.35	70.35	75.25	74.69	71.19
TiO ₂	0.45	0.25	0.29	0.42	0.30	0.21	0.26	0.40	0.43	0.20	0.19	0.28
Al ₂ O ₃	12.71	12.19	12.90	12.82	12.49	12.64	12.26	13.17	13.59	12.16	11.64	13.50
Fe ₂ O ₃ ^T	4.31	2.68	2.93	4.21	3.46	2.39	2.80	3.90	4.17	1.98	1.96	2.65
Fe ₂ O ₃ *	0.65	0.40	0.44	0.63	0.52	0.36	0.42	0.59	0.63	0.30	0.29	0.40
FeO*	3.30	2.05	2.24	3.22	2.65	1.83	2.14	2.98	3.19	1.51	1.50	2.03
MnO	0.09	0.05	0.05	0.07	0.08	0.04	0.06	0.06	0.07	0.04	0.04	0.05
MgO	0.31	0.17	0.09	0.30	0.00	0.22	0.16	0.08	0.09	0.19	0.19	0.28
CaO	1.42	0.77	1.12	1.34	1.26	0.73	0.89	1.42	1.52	0.80	0.72	1.06
Na ₂ O	3.37	3.15	3.75	3.55	3.93	3.88	3.78	3.41	3.37	3.51	3.72	3.80
K ₂ O	5.29	5.31	5.67	5.93	5.61	6.15	5.68	6.16	5.82	5.70	5.83	6.22
P ₂ O ₅	0.09	0.03	0.05	0.09	0.02	0.05	0.03	0.11	0.10	0.03	0.03	0.06
LOI	0.76	0.82	0.58	0.67	3.90	1.26	0.77	2.46	0.43	0.74	0.56	0.88
TOTAL	100.18	100.63	100.03	98.85	100.36	100.92	100.48	98.52	99.94	100.60	99.57	99.97
Mg # [†]	0.144	0.129	0.067	0.142	0.000	0.177	0.117	0.046	0.048	0.183	0.184	0.198
P	292.58	276.57	246.00	71.65	142.45	46.08	68.75	556.78	572.00	55.30	50.84	193.77
Sc	8.26	7.69	3.91	3.94	2.45	1.36	2.32	5.60	9.09	2.88	3.51	5.00
V	8.58	9.34	6.83	4.61	1.09	3.98	4.11	6.77	7.64	4.00	4.39	7.38
Cr	435.22	449.03	3.92	368.70	1.23	495.57	468.68	1.71	3.43	413.16	404.29	424.48
Co	2.27	2.23	2.76	1.10	1.25	1.08	1.12	2.88	3.10	1.20	1.10	1.92
Ni	7.10	6.60	4.04	4.52	2.93	6.19	6.10	3.94	4.48	4.88	4.80	5.59
Cu	9.15	7.05	7.99	9.35	13.43	4.46	6.45	6.59	6.33	3.88	5.46	6.44
Zn	116.08	93.61	80.32	41.51	143.27	84.06	101.11	83.84	82.41	56.67	54.71	63.64
As	0.33	0.33	0.24	0.32	0.39	0.31	0.31	0.26	0.18	0.56	0.39	0.57
Rb	191.60	257.71	383.97	241.25	383.68	334.30	255.00	291.47	326.18	403.23	397.33	357.39
Sr	82.27	68.28	42.91	51.35	24.29	23.19	35.87	65.69	60.96	20.21	21.86	43.90
Y	100.38	90.27	120.39	126.64	147.83	147.00	132.13	73.86	79.05	95.30	110.83	95.13
Zr	271.19	272.40	303.94	241.94	457.26	293.22	249.80	272.31	340.85	205.20	242.78	179.46
Nb	42.81	40.34	59.78	35.97	82.74	53.03	62.33	43.82	40.20	29.58	31.92	40.08
Sb	0.06	0.08	0.00	0.06	0.00	0.06	0.06	0.00	0.00	0.06	0.06	0.07
Ba	456.51	527.00	195.52	244.74	119.47	64.92	138.08	471.49	507.36	109.19	94.02	382.57
La	95.16	119.84	104.18	107.37	133.63	99.53	127.23	74.39	69.48	100.38	101.37	68.45
Ce	208.91	248.60	281.37	235.94	351.24	219.88	274.44	187.80	185.90	211.92	219.49	148.52
Pr	26.11	28.29	27.44	27.45	37.47	27.52	33.74	19.93	19.33	24.62	25.20	17.32
Nd	100.14	104.49	95.42	99.79	134.43	103.96	128.21	79.04	76.04	87.45	89.99	65.08
Sm	20.15	19.54	19.88	20.82	28.42	23.32	25.52	15.06	15.26	16.79	18.17	14.31
Eu	2.24	2.51	1.41	1.11	1.39	0.84	1.44	2.11	2.06	0.74	0.66	1.46
Gd	20.71	20.25	21.44	22.07	29.37	24.99	26.82	15.63	15.81	17.28	19.20	15.29
Tb	3.13	2.99	3.31	3.61	4.33	4.30	4.17	2.25	2.35	2.72	3.09	2.63
Dy	18.00	16.67	19.62	21.64	24.66	26.00	24.23	12.69	13.27	16.21	18.68	16.67
Ho	3.57	3.30	4.00	4.48	4.93	5.38	4.89	2.49	2.62	3.34	3.86	3.47
Er	9.89	9.17	11.37	12.71	14.18	15.00	13.67	6.83	7.30	9.73	11.21	10.14
Tm	1.49	1.38	1.77	2.00	2.24	2.33	2.08	1.03	1.11	1.55	1.76	1.69
Yb	9.13	8.28	10.84	12.01	13.62	13.66	12.56	6.31	6.76	9.56	10.72	10.70
Lu	1.36	1.21	1.61	1.72	2.03	1.91	1.82	0.94	1.02	1.39	1.57	1.57
Hf	8.04	7.96	9.76	9.24	15.17	11.48	9.59	7.53	9.22	7.90	9.50	7.86
Ta	3.14	2.83	4.43	3.41	5.52	4.11	4.72	2.80	2.71	2.89	3.00	9.53
W	2.71	2.38	4.30	2.24	2.97	2.46	3.74	1.88	1.95	6.90	2.72	9.57
Pb	50.10	50.01	58.14	54.99	69.97	64.33	58.05	54.29	54.32	63.97	65.89	53.33
Th	39.38	36.41	43.11	55.76	48.79	52.39	44.27	31.73	27.70	69.43	66.69	35.44
U	4.66	4.69	6.91	8.36	5.77	7.73	8.09	4.94	3.49	7.10	7.20	12.62
Eu* anomaly	0.33	0.38	0.20	0.15	0.14	0.10	0.16	0.41	0.39	0.13	0.11	0.29
La/Sm	2.73	3.55	3.03	2.99	2.72	2.47	2.89	2.86	2.64	3.46	3.23	2.77
Gd/Lu	1.70	1.86	1.48	1.42	1.61	1.46	1.63	1.84	1.73	1.38	1.36	1.08
Ce/Sm	2.36	2.89	3.22	2.58	2.81	2.14	2.44	2.83	2.77	2.87	2.75	2.36
La/Lu	5.77	8.12	5.32	5.13	5.40	4.29	5.74	6.49	5.63	5.95	5.32	3.58
Ce* anomaly	0.99	1.00	1.24	1.03	1.18	1.00	0.99	1.16	1.20	1.00	1.02	1.02
Tm* anomaly	1.04	1.04	1.05	1.07	1.06	1.07	1.05	1.04	1.04	1.06	1.06	1.07
(Ba)N	101.67	117.37	43.54	54.51	26.61	14.46	30.75	105.01	113.00	24.32	20.94	85.20
(Ba/La)N	0.48	0.44	0.19	0.23	0.09	0.06	0.11	0.63	0.73	0.11	0.09	0.56

^TTotal

*Calculated with FeO as 0.85 of total Fe.

[†]Mg/(Mg + Fe)

porphy: porphyritic.

Eu* anomaly: [Eu/Eu*]_N

Ce* anomaly: [Ce/Ce*]_N

Abu cont.												
Sample: Lithology:	AA6/29 porphyritic granite	AA6/30A foliated porphy. granite	AA6/33 foliated granite	AA6/34 foliated granite	AA6/35 augen Gneiss	AA6/36A augen gneiss	AA6/36B mylonitic gneiss	AA6/37 augen gneiss	AA6/11 rhyolite porph. dyke	AA6/30B rhyolite porph. dyke	AA6/31A rhyolite porph. dyke	AA6/31B rhyolite dyke
SiO ₂	74.98	71.39	77.73	74.11	71.77	71.65	74.54	66.60	74.89	75.93	75.04	75.66
TiO ₂	0.26	0.34	0.09	0.34	0.33	0.43	0.18	0.55	0.21	0.21	0.17	0.20
Al ₂ O ₃	11.91	12.72	10.96	12.19	13.68	12.97	12.33	14.44	12.50	11.42	11.57	11.69
Fe ₂ O ₃ ^T	2.64	3.17	1.60	2.89	2.93	3.37	1.85	5.81	2.12	1.92	1.89	1.97
Fe ₂ O ₃ *	0.40	0.48	0.24	0.43	0.44	0.51	0.28	0.87	0.32	0.29	0.28	0.30
FeO*	2.02	2.42	1.22	2.21	2.24	2.58	1.41	4.44	1.62	1.47	1.45	1.51
MnO	0.05	0.06	0.02	0.05	0.04	0.05	0.03	0.13	0.04	0.03	0.03	0.03
MgO	0.25	0.29	0.00	0.30	0.18	0.47	0.17	0.33	0.19	0.25	0.21	0.21
CaO	1.08	1.27	0.56	0.83	1.44	0.73	0.67	2.01	0.82	0.67	0.69	0.55
Na ₂ O	3.51	3.42	3.58	3.13	3.50	3.25	4.00	3.78	3.73	3.71	3.60	4.01
K ₂ O	5.26	6.09	4.91	6.11	5.54	6.07	5.38	6.45	6.00	5.64	5.79	5.44
P ₂ O ₅	0.05	0.08	0.01	0.06	0.08	0.12	0.03	0.10	0.03	0.03	0.03	0.03
LOI	0.76	0.79	0.46	0.76	0.89	0.96	0.99	0.44	0.53	0.68	0.96	0.61
TOTAL	100.75	99.62	99.92	100.77	100.38	100.07	100.17	100.64	101.06	100.49	99.98	100.40
Mg # ^a	0.181	0.176	0.000	0.195	0.125	0.245	0.176	0.117	0.173	0.233	0.206	0.199
P	147.25	259.59	65.80	190.22	493.80	462.50	59.90	389.41	47.74	49.42	50.27	45.34
Sc	4.41	5.53	2.98	4.18	6.32	6.20	1.52	8.05	1.43	2.47	1.82	2.80
V	7.08	9.19	0.38	9.18	15.12	19.84	4.43	6.75	3.20	3.88	6.17	4.44
Cr	470.28	242.98	1.10	178.07	5.64	432.93	56.09	364.50	362.34	46.27	47.07	42.46
Co	1.70	2.42	1.09	2.36	4.28	4.48	1.41	2.31	1.27	1.70	1.89	1.73
Ni	6.35	6.30	2.85	5.43	5.95	7.43	5.49	5.55	4.76	5.40	7.54	5.87
Cu	5.36	4.73	3.34	15.76	5.58	7.20	3.40	7.80	6.57	3.73	4.52	3.95
Zn	67.04	89.29	49.72	66.16	43.38	50.38	61.20	147.39	92.83	34.63	33.61	38.13
As	0.41	0.74	0.36	0.25	0.22	0.25	0.31	0.51	0.34	0.28	0.26	0.30
Rb	367.29	410.93	603.91	425.07	395.74	402.61	476.16	197.80	284.70	532.16	537.69	522.75
Sr	32.73	54.95	6.61	47.88	66.47	71.24	19.96	60.81	51.44	14.18	18.14	12.22
Y	110.59	102.48	129.28	79.58	63.54	59.14	101.71	105.32	138.90	84.90	73.51	104.55
Zr	203.21	250.64	254.77	293.48	192.66	200.76	216.63	195.29	390.62	269.14	204.50	268.08
Nb	33.30	35.77	49.27	43.00	19.37	19.72	36.96	73.81	64.52	30.41	32.54	31.24
Sb	0.05	0.11	0.00	0.08	0.00	0.10	0.12	0.06	0.08	0.08	0.11	0.08
Ba	207.62	422.32	14.46	196.06	426.54	425.95	60.68	423.47	73.83	18.94	53.46	17.76
La	98.15	80.01	162.22	101.34	56.31	53.72	74.23	111.05	133.86	115.32	86.16	121.49
Ce	204.58	197.19	370.05	269.48	133.08	159.33	176.23	270.90	296.23	256.30	202.43	261.80
Pr	24.29	21.52	34.28	25.16	13.98	14.45	18.83	33.37	34.67	25.73	19.15	27.73
Nd	88.74	80.70	103.00	92.53	52.10	53.62	68.77	135.65	127.38	87.21	66.16	94.92
Sm	18.07	16.61	19.93	16.67	10.39	11.04	14.31	27.70	25.14	15.04	11.98	17.02
Eu	1.14	1.83	0.20	0.81	1.17	1.17	0.60	3.44	0.73	0.21	0.31	0.21
Gd	19.04	17.63	22.08	18.24	10.96	11.90	15.82	27.98	26.60	16.29	13.23	18.56
Tb	3.06	2.83	3.30	2.53	1.70	1.78	2.65	4.04	4.14	2.40	1.98	2.87
Dy	18.64	17.23	19.68	14.53	10.07	10.50	16.80	22.63	24.44	14.07	12.01	17.14
Ho	3.86	3.51	4.04	2.82	2.03	2.09	3.58	4.30	5.04	2.86	2.45	3.50
Er	11.19	10.02	11.67	7.83	5.78	5.92	10.49	11.68	14.23	8.32	7.15	10.09
Tm	1.79	1.60	1.86	1.17	0.91	0.91	1.72	1.69	2.21	1.30	1.17	1.59
Yb	11.07	9.75	11.54	7.03	5.69	5.64	10.56	10.44	13.41	7.99	7.18	9.76
Lu	1.61	1.44	1.71	1.03	0.84	0.83	1.58	1.61	1.96	1.17	1.05	1.43
Hf	7.87	8.17	10.16	9.55	5.73	6.22	8.84	5.45	13.92	9.98	8.29	10.31
Ta	3.18	3.22	3.29	3.07	1.99	1.80	3.38	3.81	5.24	3.17	3.46	3.32
W	2.89	5.48	3.69	2.78	3.32	4.87	4.37	3.89	4.18	5.91	3.84	4.67
Pb	47.41	60.73	72.12	74.99	44.75	53.10	66.41	50.86	76.26	81.36	60.97	78.03
Th	59.57	40.86	76.47	58.22	37.64	42.85	64.17	28.22	59.99	96.71	67.70	100.92
U	13.03	5.27	11.43	7.14	5.67	4.96	11.30	3.25	12.13	10.93	12.68	13.29
Eu*												
anomaly	0.18	0.32	0.03	0.14	0.33	0.30	0.12	0.37	0.08	0.04	0.07	0.04
La/Sm	3.14	2.79	4.71	3.52	3.14	2.82	3.00	2.32	3.08	4.44	4.16	4.13
Gd/Lu	1.31	1.36	1.44	1.97	1.45	1.60	1.12	1.93	1.51	1.54	1.40	1.44
Ce/Sm	2.57	2.70	4.22	3.67	2.91	3.28	2.80	2.22	2.68	3.87	3.84	3.50
La/Lu	5.01	4.56	7.81	8.09	5.50	5.35	3.88	5.66	5.61	8.09	6.74	6.99
Ce*												
anomaly	0.99	1.13	1.14	1.26	1.12	1.36	1.11	1.06	1.03	1.09	1.16	1.05
Tm*												
anomaly	1.06	1.06	1.06	1.04	1.05	1.04	1.08	1.01	1.06	1.05	1.07	1.06
(Ba)N	46.24	94.06	3.22	43.67	95.00	94.87	13.51	94.31	16.44	4.22	11.91	3.96
(Ba/La)N	0.21	0.52	0.01	0.19	0.75	0.79	0.08	0.38	0.05	0.02	0.06	0.01

^TTotal
*Calculated with FeO as 0.85 of total Fe.
^aMg/(Mg + Fe)
porphy, porphyritic.
Eu* anomaly: [Eu/Eu*]_N
Ce* anomaly: [Ce/Ce*]_N

Abu cont.	Mirpur		MIS dyke		Kishengarh		Ranakpur granitoids					
Sample: Lithology:	AA6/21A massive granite	AA6/51 rhyolite porph. dyke	Sample: Lithology:	AA6/52A nepheline syenite	Sample: Lithology:	AA6/2 grey granite	AA6/3A grey granite	AA6/3B grey granite	AA6/5 grey granite	AA6/6 grey granite	AA6/7 grey granite	
SiO ₂	73.36	58.94	SiO ₂	54.92	SiO ₂	64.28	66.00	66.02	64.52	66.14	65.45	
TiO ₂	0.32	1.01	TiO ₂	0.30	TiO ₂	0.72	0.53	0.54	0.53	0.48	0.52	
Al ₂ O ₃	12.61	13.71	Al ₂ O ₃	21.63	Al ₂ O ₃	16.33	17.05	17.22	16.80	16.26	16.69	
Fe ₂ O ₃ ^T	2.17	12.04	Fe ₂ O ₃ ^T	4.36	Fe ₂ O ₃ ^T	3.37	2.99	3.01	3.20	2.67	2.92	
Fe ₂ O ₃ [*]	0.33	1.81	Fe ₂ O ₃ [*]	0.65	Fe ₂ O ₃ [*]	0.51	0.45	0.45	0.48	0.40	0.44	
FeO*	1.66	9.21	FeO*	3.33	FeO*	2.58	2.29	2.30	2.45	2.04	2.23	
MnO	0.04	0.19	MnO	0.12	MnO	0.04	0.02	0.03	0.03	0.02	0.02	
MgO	0.36	0.80	MgO	0.61	MgO	1.29	0.92	0.97	1.00	0.77	0.81	
CaO	0.72	2.59	CaO	1.58	CaO	2.98	2.68	2.70	3.03	2.44	2.72	
Na ₂ O	3.58	3.93	Na ₂ O	9.45	Na ₂ O	4.21	4.34	4.38	4.21	4.24	4.27	
K ₂ O	5.87	4.10	K ₂ O	6.65	K ₂ O	5.48	4.97	5.16	4.99	5.17	4.84	
P ₂ O ₅	0.06	0.26	P ₂ O ₅	0.12	P ₂ O ₅	0.25	0.24	0.25	0.25	0.19	0.23	
LOI	0.94	2.99	LOI	0.72	LOI	1.14	0.32	0.41	0.55	0.80	0.91	
TOTAL	100.03	100.56	TOTAL	100.46	TOTAL	100.09	100.06	100.69	99.11	99.18	99.38	
Mg # [‡]	0.279	0.134	Mg # [‡]	0.246	Mg # [‡]	0.471	0.418	0.429	0.421	0.402	0.393	
P	178.72	1076.82	P	468.88	P	976.67	1187.00	1180.29	1330.44	1087.32	1265.99	
Sc	4.36	24.28	Sc	0.61	Sc	3.12	3.97	4.45	4.38	2.29	3.10	
V	11.95	1.79	V	7.53	V	46.68	43.28	42.63	48.64	38.39	42.46	
Cr	452.69	1016.02	Cr	442.41	Cr	447.00	12.71	12.73	12.82	7.93	11.73	
Co	2.54	3.36	Co	3.97	Co	7.00	6.94	6.80	8.46	6.12	8.08	
Ni	6.37	4.36	Ni	5.41	Ni	12.92	9.98	9.98	10.51	8.10	9.79	
Cu	5.12	8.96	Cu	6.01	Cu	8.29	5.23	4.59	7.31	6.52	7.54	
Zn	24.82	50.1	Zn	56.57	Zn	45.78	53.62	51.19	57.53	41.05	51.98	
As	0.42	0.71	As	0.14	As	0.35	0.23	0.25	0.30	0.20	0.25	
Rb	440.85	203.76	Rb	93.65	Rb	104.65	151.82	174.57	177.27	86.53	134.53	
Sr	32.75	108.75	Sr	105.55	Sr	1259.99	1441.69	1607.68	1867.99	1180.78	1543.99	
Y	69.61	112.10	Y	9.66	Y	13.04	14.75	15.51	14.00	10.12	11.55	
Zr	245.66	2178.92	Zr	91.88	Zr	273.49	271.67	227.90	245.27	252.50	237.76	
Nb	15.41	56.34	Nb	62.09	Nb	9.89	12.28	12.76	11.05	8.11	10.03	
Sb	0.11	0.32	Sb	0.09	Sb	0.06	0.00	0.00	0.00	0.00	0.00	
Ba	136.15	747.72	Ba	775.15	Ba	4705.36	4849.54	5161.04	5946.09	4197.43	5341.25	
La	52.35	73.36	La	19.93	La	171.77	174.07	182.11	237.58	127.35	162.28	
Ce	131.26	192.11	Ce	39.20	Ce	358.71	389.84	397.43	447.73	298.57	402.37	
Pr	13.55	23.25	Pr	3.56	Pr	31.83	30.40	31.79	37.20	23.89	28.84	
Nd	47.93	97.88	Nd	11.67	Nd	103.30	89.70	92.42	105.42	71.12	84.54	
Sm	9.82	21.55	Sm	2.49	Sm	14.63	14.59	15.14	16.63	11.59	13.72	
Eu	0.59	5.32	Eu	0.90	Eu	4.38	4.42	4.53	5.16	3.63	4.50	
Gd	10.58	21.94	Gd	2.22	Gd	11.70	11.71	12.11	13.45	9.19	11.32	
Tb	1.75	3.34	Tb	0.31	Tb	0.88	0.91	0.93	1.00	0.68	0.80	
Dy	10.97	19.85	Dy	1.84	Dy	3.01	3.17	3.27	3.26	2.28	2.64	
Ho	2.29	4.19	Ho	0.39	Ho	0.43	0.46	0.49	0.45	0.32	0.37	
Er	6.68	12.07	Er	1.19	Er	1.42	1.51	1.59	1.51	1.06	1.23	
Tm	1.10	1.92	Tm	0.20	Tm	0.15	0.17	0.17	0.15	0.11	0.12	
Yb	6.77	12.53	Yb	1.43	Yb	0.89	1.03	1.06	0.89	0.66	0.75	
Lu	1.00	2.00	Lu	0.24	Lu	0.12	0.14	0.15	0.13	0.09	0.10	
Hf	8.14	42.26	Hf	2.13	Hf	6.06	5.81	4.78	4.87	5.34	4.90	
Ta	2.22	3.34	Ta	3.35	Ta	0.63	0.74	0.77	0.65	0.47	0.56	
W	4.81	4.00	W	1.30	W	1.53	0.02	0.02	0.03	0.03	0.03	
Pb	29.26	24.73	Pb	6.46	Pb	91.45	93.16	97.58	94.76	67.09	89.98	
Th	59.79	13.10	Th	3.70	Th	50.83	48.52	55.71	62.45	37.24	49.59	
U	15.07	2.50	U	0.47	U	2.22	2.10	2.21	2.49	1.59	2.00	
Eu* anomaly	0.17	0.73			Eu* anomaly	0.98	0.99	0.98	1.01	1.02	1.06	
La/Sm	3.09	1.97			La/Sm	6.80	6.91	6.96	8.27	6.36	6.85	
Gd/Lu	1.17	1.22			Gd/Lu	10.46	9.15	9.00	11.89	11.65	12.00	
Ce/Sm	3.04	2.03			Ce/Sm	5.57	6.07	5.97	6.12	5.85	6.67	
La/Lu	4.29	3.01			La/Lu	113.57	100.64	100.11	155.45	119.46	127.30	
Ce* anomaly	1.16	1.11			Ce* anomaly	1.10	1.20	1.17	1.04	1.23	1.32	
Tm* anomaly	1.08	1.03			Tm* anomaly	0.84	0.86	0.86	0.80	0.82	0.80	
(Ba)N	30.32	166.53			(Ba)N	1047.97	1080.07	1149.45	1324.30	934.84	1189.59	
(Ba/La)N	0.26	1.01			(Ba/La)N	2.72	2.77	2.82	2.49	3.27	3.27	

^TTotal

*Calculated with FeO as 0.85 of total Fe.

[‡]Mg/(Mg + Fe)

porphy, porphyritic.

Eu* anomaly: [Eu/Eu*]_N

Ce* anomaly: [Ce/Ce*]_N

Sumerpur granitoids				Erinpura granitoids								
Sample: Lithology:	AA6/16A massive granite	AA6/16B massive granite	AA6/17 massive granite		Sample: Lithology:	AA6/18 augen gneiss	AA6/19 augen gneiss	AA6/20 porphy. granite	AA6/22 augen gneiss	AA6/23 granite gneiss	AA6/24 augen gneiss	AA6/24 augen gneiss
SiO ₂	76.42	71.75	74.23		SiO ₂	73.97	70.51	71.38	70.93	67.41	70.47	71.30
TiO ₂	0.27	0.26	0.24		TiO ₂	0.28	0.49	0.53	0.33	0.85	0.53	0.48
Al ₂ O ₃	11.49	13.34	13.42		Al ₂ O ₃	12.84	13.38	13.79	14.06	15.35	14.92	15.20
Fe ₂ O ₃ ^T	2.42	2.12	1.74		Fe ₂ O ₃ ^T	2.61	3.69	3.56	3.18	7.60	4.04	3.92
Fe ₂ O ₃ [*]	0.36	0.32	0.26		Fe ₂ O ₃ [*]	0.39	0.55	0.53	0.48	1.14	0.61	0.59
FeO [*]	1.85	1.62	1.33		FeO [*]	2.00	2.82	2.72	2.43	5.81	3.09	3.00
MnO	0.04	0.03	0.04		MnO	0.04	0.04	0.05	0.08	0.07	0.06	0.05
MgO	0.23	0.55	0.52		MgO	0.25	0.45	0.70	1.01	2.40	1.03	0.76
CaO	0.72	1.56	1.27		CaO	1.64	1.82	1.88	1.79	0.21	1.58	1.56
Na ₂ O	2.87	3.48	3.23		Na ₂ O	3.43	2.96	2.97	3.66	2.01	2.43	2.53
K ₂ O	5.53	4.61	5.86		K ₂ O	3.91	4.62	5.18	4.36	3.24	4.73	4.45
P ₂ O ₅	0.05	0.09	0.13		P ₂ O ₅	0.06	0.20	0.18	0.12	0.13	0.14	0.12
LOI	0.88	0.55	0.67		LOI	1.33	0.49	0.79	1.63	0.71	1.39	1.30
TOTAL	100.92	98.34	101.35		TOTAL	100.36	98.65	101.01	101.15	99.98	101.32	101.67
Mg # ^a	0.181	0.377	0.410		Mg # ^a	0.182	0.221	0.314	0.425	0.424	0.373	0.311
P	201.91	330.69	527.63		P	355.61	1026.06	693.64	438.67	910.57	631.80	530.36
Sc	2.89	3.17	3.57		Sc	5.50	7.17	6.27	3.96	11.82	7.39	6.26
V	13.38	19.50	14.71		V	19.60	26.62	25.14	37.52	81.52	47.85	46.81
Cr	238.81	257.55	364.18		Cr	6.90	7.55	270.20	423.32	54.15	25.87	391.49
Co	1.65	2.62	2.59		Co	4.24	6.31	4.82	5.80	14.14	8.19	7.41
Ni	3.80	5.19	5.69		Ni	5.79	5.81	6.01	9.32	25.21	14.23	14.89
Cu	2.40	2.67	3.18		Cu	3.66	7.85	7.40	4.68	17.00	7.82	15.05
Zn	18.57	22.30	19.94		Zn	38.83	64.40	52.46	33.80	93.07	46.58	40.70
As	2.21	0.60	0.43		As	0.45	0.36	0.51	0.54	0.22	0.77	1.01
Rb	274.59	135.16	219.78		Rb	190.62	302.06	239.72	174.53	210.61	163.73	112.09
Sr	19.04	42.31	51.69		Sr	49.37	106.90	97.27	157.00	96.37	72.55	58.58
Y	39.23	27.54	23.67		Y	20.14	35.11	37.12	17.01	30.23	24.54	25.38
Zr	200.31	134.63	120.03		Zr	171.24	322.07	300.96	131.70	218.01	113.98	138.17
Nb	12.31	13.05	12.40		Nb	9.93	21.22	17.79	11.66	22.82	13.53	11.83
Sb	0.38	0.15	0.21		Sb	0.00	0.00	0.06	0.32	0.00	0.00	0.15
Ba	242.82	248.06	370.44		Ba	370.75	564.06	528.00	260.39	523.90	608.91	454.90
La	58.84	33.09	30.02		La	35.03	61.73	80.24	15.87	62.45	35.51	30.24
Ce	123.69	72.05	66.95		Ce	98.85	143.36	187.53	43.50	147.04	93.21	84.36
Pr	14.28	8.05	7.17		Pr	8.82	13.91	18.91	3.51	14.80	8.50	7.56
Nd	51.02	28.73	25.50		Nd	32.69	50.12	67.22	12.67	54.82	31.49	28.31
Sm	9.50	5.72	5.30		Sm	6.66	9.14	11.60	2.73	10.64	6.49	5.73
Eu	0.57	0.59	0.65		Eu	0.81	1.32	1.30	0.63	1.23	1.30	1.10
Gd	9.71	5.91	5.25		Gd	6.68	9.36	11.41	2.84	10.80	6.38	5.82
Tb	1.36	0.88	0.78		Tb	0.86	1.21	1.41	0.42	1.36	0.84	0.80
Dy	7.26	4.92	4.29		Dy	4.16	6.25	7.15	2.59	6.29	4.40	4.53
Ho	1.37	0.96	0.82		Ho	0.72	1.14	1.30	0.55	1.01	0.81	0.92
Er	3.83	2.71	2.29		Er	1.79	3.05	3.54	1.65	2.56	2.20	2.69
Tm	0.58	0.43	0.35		Tm	0.23	0.41	0.48	0.29	0.33	0.32	0.43
Yb	3.45	2.62	2.16		Yb	1.36	2.39	2.79	1.94	2.01	1.93	2.64
Lu	0.51	0.40	0.32		Lu	0.20	0.35	0.41	0.31	0.30	0.29	0.39
Hf	6.81	4.24	3.86		Hf	5.05	8.48	8.70	4.09	5.96	3.13	4.07
Ta	1.54	1.49	1.48		Ta	0.81	1.33	1.38	1.73	1.64	1.10	1.03
W	5.82	2.28	2.63		W	0.97	1.42	1.78	1.66	1.06	3.19	4.01
Pb	39.02	30.96	42.35		Pb	27.85	47.56	49.21	32.78	50.74	32.73	34.63
Th	54.71	24.16	17.94		Th	14.12	43.52	66.31	15.01	32.67	19.96	18.68
U	7.12	3.20	5.56		U	2.56	5.83	9.88	3.85	5.27	2.31	2.33
Eu* anomaly	0.18	0.30	0.37		Eu* anomaly	0.36	0.43	0.34	0.68	0.34	0.57	0.60
La/Sm	3.58	3.35	3.28		La/Sm	3.05	3.91	4.00	3.36	3.40	3.05	3.17
Gd/Lu	2.13	1.65	1.83		Gd/Lu	3.66	2.99	3.08	1.01	4.06	1.64	2.46
Ce/Sm	2.96	2.86	2.87		Ce/Sm	3.37	3.57	3.67	3.62	3.14	3.35	3.26
La/Lu	9.53	6.84	7.72		La/Lu	14.20	14.57	16.05	4.19	17.35	6.31	10.12
Ce* anomaly	1.00	1.04	1.07		Ce* anomaly	1.32	1.14	1.13	1.35	1.13	1.31	1.26
Tm* anomaly	1.05	1.06	1.03		Tm* anomaly	0.97	1.00	1.00	1.05	0.97	1.05	1.02
(Ba)N	54.08	55.25	82.50		(Ba)N	82.57	125.63	117.60	57.99	116.68	135.61	101.31
(Ba/La)N	0.41	0.74	1.23		(Ba/La)N	1.05	0.91	0.65	1.63	0.83	2.00	1.27

^TTotal

*Calculated with FeO as 0.85 of total Fe.

^aMg/(Mg + Fe)

porphy, porphyritic.

Eu* anomaly: [Eu/Eu*]_N

Ce* anomaly: [Ce/Ce*]_N

Erinpura cont.						Revdar Rd. (Erinpura type)						
Sample: Lithology:	AA6/25 porphy. granite	AA6/26 granite	BL1-A biotite granite	DB-1 porphy. granite	SR-1 augen gneiss		Sample: Lithology:	AA6/38 granite gneiss	AA6/47A augen gneiss	AA6/47B augen gneiss	AA6/45A micaceous gneiss	AA6/45B granite gneiss
SiO ₂	66.47	71.30	73.43	71.07	74.30		SiO ₂	71.43	77.79	79.75	67.67	66.92
TiO ₂	0.82	0.31	0.08	0.66	0.40		TiO ₂	0.29	0.17	0.14	0.85	0.86
Al ₂ O ₃	15.53	14.29	13.97	16.08	13.46		Al ₂ O ₃	13.96	11.42	10.06	15.54	14.57
Fe ₂ O ₃ ^T	4.70	2.06	0.98	5.38	3.74		Fe ₂ O ₃ ^T	2.17	2.31	1.93	7.25	7.12
Fe ₂ O ₃ *	0.71	0.31	0.15	0.81	0.56		Fe ₂ O ₃ *	0.33	0.35	0.29	1.09	1.07
FeO*	3.59	1.58	0.75	4.11	2.86		FeO*	1.66	1.77	1.48	5.55	5.45
MnO	0.07	0.03	0.02	0.07	0.05		MnO	0.04	0.04	0.03	0.07	0.08
MgO	1.16	0.64	0.16	1.09	0.68		MgO	0.35	0.29	0.01	2.37	2.65
CaO	3.03	1.84	0.82	1.28	1.12		CaO	1.94	0.07	0.00	0.21	0.38
Na ₂ O	3.27	3.69	4.44	2.03	2.06		Na ₂ O	3.95	0.05	0.05	0.87	1.02
K ₂ O	4.54	5.05	4.83	5.14	4.60		K ₂ O	4.01	6.05	5.32	3.15	3.20
P ₂ O ₅	0.25	0.10	0.32	0.17	0.14		P ₂ O ₅	0.11	0.04	0.01	0.13	0.14
LOI	0.88	0.79	1.03	-4.02	0.74		LOI	2.21	1.69	1.15	3.06	3.42
TOTAL	100.72	100.10	100.08	98.95	101.29		TOTAL	100.46	99.92	98.45	101.17	100.36
Mg # ³	0.365	0.420	0.276	0.321	0.298		Mg # ³	0.273	0.226	0.012	0.812	0.831
P	1012.61	351.06	1371.46	691.37	613.62		P	482.12	86.78	106.61	595.571	536.721
Sc	7.34	3.18	3.59	8.09	6.44		Sc	3.52	2.99	3.55	10.019	7.055
V	53.43	11.24	3.29	53.59	29.64		V	16.75	17.50	10.27	93.866	97.193
Cr	361.98	431.63	1294.08	662.59	588.07		Cr	463.03	81.88	102.39	571.991	506.436
Co	8.75	3.24	1.26	12.33	7.25		Co	3.88	2.66	2.43	19.021	16.714
Ni	9.67	8.13	5.50	28.37	11.52		Ni	4.30	5.34	7.55	39.742	37.943
Cu	11.86	4.48	2.90	32.47	13.86		Cu	4.00	10.24	4.26	5.683	5.937
Zn	54.29	31.69	5.61	76.34	41.25		Zn	38.20	22.40	20.77	55.800	52.602
As	0.32	0.24	0.23	0.26	2.40		As	0.08	0.13	0.09	0.804	0.201
Rb	133.05	162.19	571.67	184.45	266.21		Rb	294.49	427.88	458.72	91.974	105.683
Sr	147.47	214.74	26.54	82.05	52.25		Sr	74.57	10.72	11.66	35.628	27.432
Y	18.90	15.63	11.41	21.87	28.82		Y	18.28	13.96	21.88	14.635	16.981
Zr	167.01	187.85	43.18	130.94	124.17		Zr	166.91	102.74	122.14	232.889	279.851
Nb	15.58	8.02	26.82	16.60	12.53		Nb	13.88	15.56	16.23	19.416	18.303
Sb	0.05	0.05	0.12	0.00	0.00		Sb	0.00	0.09	0.00		0.112
Ba	707.36	603.84	199.88	456.48	476.53		Ba	385.07	289.62	307.81	290.404	88.741
La	67.00	87.11	2.26	41.37	38.61		La	32.98	34.60	60.26	45.891	38.597
Ce	162.04	181.07	6.60	97.80	91.49		Ce	86.56	152.49	207.13	105.020	94.485
Pr	14.48	17.53	0.78	9.88	9.27		Pr	7.52	9.13	15.17	10.794	9.257
Nd	50.47	59.59	2.58	36.81	33.49		Nd	27.10	31.60	47.61	39.189	34.463
Sm	7.56	9.11	1.34	7.11	6.85		Sm	4.76	5.64	9.40	7.220	6.155
Eu	1.57	1.20	0.15	1.06	0.97		Eu	0.72	0.31	0.37	1.021	0.601
Gd	7.67	8.63	1.31	6.98	6.84		Gd	4.60	5.99	8.76	6.820	6.378
Tb	0.83	0.94	0.37	0.89	0.93		Tb	0.56	0.60	0.91	0.786	0.773
Dy	4.04	4.11	2.35	4.35	4.95		Dy	2.98	2.81	4.11	3.502	3.806
Ho	0.70	0.60	0.34	0.72	0.88		Ho	0.56	0.54	0.72	0.532	0.648
Er	1.86	1.41	0.76	1.85	2.32		Er	1.59	1.62	2.19	1.310	1.688
Tm	0.23	0.14	0.12	0.25	0.33		Tm	0.23	0.27	0.35	0.155	0.219
Yb	1.25	0.79	0.73	1.62	2.03		Yb	1.48	1.96	2.81	0.995	1.283
Lu	0.16	0.12	0.08	0.23	0.29		Lu	0.21	0.26	0.34	0.132	0.193
Hf	4.28	5.46	2.74	3.53	3.50		Hf	4.41	3.79	4.38	6.270	8.030
Ta	1.14	0.45	9.09	1.29	1.13		Ta	2.43	1.78	1.67	1.426	1.414
W	1.55	1.72	29.99	1.40	3.89		W	0.58	2.12	0.55	0.611	2.246
Pb	27.10	65.98	5.14	53.12	30.81		Pb	31.11	250.37	157.90	11.621	6.019
Th	12.32	62.36	10.69	22.60	26.16		Th	24.13	12.59	25.54	18.733	16.380
U	1.54	3.73	5.35	4.66	2.59		U	2.15	6.54	5.87	2.954	3.264
Eu* anomaly	0.61	0.40	0.35	0.45	0.42		Eu* anomaly	0.46	0.16	0.12	0.43	0.29
La/Sm	5.13	5.53	0.98	3.37	3.26		La/Sm	4.01	3.55	3.71	3.68	3.63
Gd/Lu	5.25	8.16	1.74	3.31	2.64		Gd/Lu	2.43	2.55	2.85	5.74	3.68
Ce/Sm	4.87	4.52	1.12	3.13	3.04		Ce/Sm	4.14	6.15	5.01	3.31	3.49
La/Lu	33.90	60.90	2.23	14.51	11.02		La/Lu	12.92	10.89	14.49	28.60	16.46
Ce* anomaly	1.20	1.06	1.19	1.13	1.13		Ce* anomaly	1.28	2.03	1.61	1.10	1.17
Tm* anomaly	0.99	0.82	1.05	0.95	0.99		Tm* anomaly	1.00	0.98	0.92	0.89	0.97
(Ba)N	157.54	134.49	44.52	101.67	106.13		(Ba)N	0.22	0.23	0.23	85.27	64.68
(Ba/La)N	1.05	0.69	8.78	1.10	1.23		(Ba/La)N	0.00	0.00	0.00	0.83	0.75

^TTotal

*Calculated with FeO as 0.85 of total Fe.

³Mg/(Mg + Fe)

porphy. porphyritic.

Eu* anomaly: [Eu/Eu*]_N

Ce* anomaly: [Ce/Ce*]_N

Revdar Rd. (Abu type)						Revdar Rd. granitoid			Swarupganj granitoid		
Sample: Lithology:	AA6/39 augen gneiss	AA6/40 massive granite	AA6/42A porphy granite	AA6/42B porphy granite	AA6/48A foliated granite		Sample: Lithology:	AA6/48B aplitic dyke		Sample: Lithology:	AA6/49 foliated granite
SiO ₂	75.28	71.22	70.22	72.00	73.31		SiO ₂	77.04		SiO ₂	78.04
TiO ₂	0.29	0.34	0.34	0.23	0.28		TiO ₂	0.02		TiO ₂	0.22
Al ₂ O ₃	12.89	13.26	13.43	12.42	12.09		Al ₂ O ₃	13.13		Al ₂ O ₃	11.45
Fe ₂ O ₃ ^T	1.75	3.51	3.74	2.38	3.42		Fe ₂ O ₃ ^T	0.94		Fe ₂ O ₃ ^T	1.72
Fe ₂ O ₃ *	0.26	0.53	0.56	0.36	0.51		Fe ₂ O ₃ *	0.14		Fe ₂ O ₃ *	0.26
FeO*	1.34	2.68	2.86	1.82	2.62		FeO*	0.72		FeO*	1.32
MnO	0.03	0.06	0.08	0.02	0.06		MnO	0.01		MnO	0.04
MgO	0.33	0.20	0.36	0.26	0.07		MgO	0.00		MgO	0.58
CaO	0.91	0.94	1.26	4.72	0.84		CaO	0.60		CaO	1.27
Na ₂ O	2.98	3.49	3.65	4.00	3.74		Na ₂ O	5.48		Na ₂ O	5.62
K ₂ O	6.40	6.10	6.77	4.91	4.92		K ₂ O	4.38		K ₂ O	1.59
P ₂ O ₅	0.07	0.04	0.09	0.03	0.02		P ₂ O ₅	0.00		P ₂ O ₅	0.04
LOI	0.69	1.06	1.66	0.73	0.77		LOI	0.44		LOI	0.52
TOTAL	101.62	100.22	101.60	101.70	99.52		TOTAL	102.04		TOTAL	101.09
Mg # ³	0.305	0.117	0.183	0.203	0.046		Mg # ³	0.000		Mg # ³	0.440
P	120.83	119.33	217.00	23.64	136.50		P	72.67		P	93.48
Sc	6.53	2.37	5.83	0.54	3.39		Sc	1.04		Sc	3.12
V	6.02	4.14	3.95	0.28	1.30		V	0.66		V	27.20
Cr	113.12	112.59	204.75	22.70	130.83		Cr	69.65		Cr	88.19
Co	1.82	1.29	1.80	0.95	1.35		Co	1.04		Co	2.99
Ni	5.32	5.05	5.28	2.93	2.87		Ni	2.87		Ni	9.87
Cu	4.23	6.60	5.17	2.46	6.08		Cu	4.36		Cu	3.54
Zn	43.65	81.43	94.68	111.05	108.39		Zn	37.51		Zn	13.64
As	0.51	0.39	0.30	0.20	0.33		As	0.20		As	0.12
Rb	373.43	367.11	304.28	495.83	402.76		Rb	572.13		Rb	27.62
Sr	17.13	41.01	46.53	14.03	30.08		Sr	9.59		Sr	34.62
Y	82.54	117.42	124.39	211.16	247.05		Y	150.13		Y	9.95
Zr	265.69	333.74	259.37	518.28	519.11		Zr	115.21		Zr	66.95
Nb	22.50	63.31	54.36	81.61	85.82		Nb	69.17		Nb	2.41
Sb	0.10	0.10	0.08	0.00	0.00		Sb	0.00		Sb	0.08
Ba	61.69	151.32	257.59	16.29	163.34		Ba	15.98		Ba	308.68
La	127.50	136.05	120.44	77.09	107.37		La	13.74		La	3.12
Ce	283.64	314.51	298.81	175.96	292.74		Ce	41.64		Ce	9.66
Pr	31.80	36.31	32.32	23.10	31.79		Pr	4.78		Pr	1.19
Nd	113.69	139.54	123.09	84.46	113.43		Nd	19.14		Nd	5.15
Sm	20.94	26.75	23.97	23.18	29.26		Sm	6.49		Sm	1.51
Eu	0.52	1.71	2.28	0.33	1.34		Eu	0.13		Eu	0.39
Gd	21.74	27.86	25.67	25.04	31.79		Gd	7.94		Gd	1.40
Tb	3.03	4.02	3.94	4.58	5.49		Tb	1.89		Tb	0.24
Dy	16.67	22.54	23.05	29.52	34.92		Dy	14.68		Dy	1.57
Ho	3.10	4.37	4.69	6.14	7.18		Ho	3.51		Ho	0.35
Er	8.40	12.02	13.20	17.54	20.20		Er	11.76		Er	1.07
Tm	1.23	1.77	2.03	2.76	3.08		Tm	2.29		Tm	0.18
Yb	7.37	10.69	12.30	16.80	18.93		Yb	16.64		Yb	1.25
Lu	1.07	1.58	1.81	2.27	2.66		Lu	2.54		Lu	0.20
Hf	9.20	10.39	8.65	19.25	14.98		Hf	9.93		Hf	2.49
Ta	2.20	4.01	3.79	5.94	5.53		Ta	12.32		Ta	0.25
W	4.37	3.34	3.78	2.36	2.26		W	8.73		W	2.12
Pb	50.36	55.42	63.23	66.50	59.54		Pb	74.14		Pb	5.74
Th	71.64	49.66	39.25	54.91	48.14		Th	35.05		Th	0.95
U	7.69	5.89	3.80	11.73	7.44		U	7.58		U	0.28
Eu* anomaly	0.07	0.19	0.27	0.04	0.13		Eu* anomaly	0.05		Eu* anomaly	0.80
La/Sm	3.52	2.94	2.91	1.93	2.12		La/Sm	1.23		La/Sm	1.20
Gd/Lu	2.26	1.96	1.58	1.23	1.33		Gd/Lu	0.35		Gd/Lu	0.78
Ce/Sm	3.08	2.67	2.83	1.73	2.27		Ce/Sm	1.46		Ce/Sm	1.46
La/Lu	9.82	7.10	5.48	2.80	3.33		La/Lu	0.45		La/Lu	1.29
Ce* anomaly	1.05	1.06	1.13	1.00	1.20		Ce* anomaly	1.23		Ce* anomaly	1.20
Tm* anomaly	1.03	1.03	1.05	1.06	1.04		Tm* anomaly	1.06		Tm* anomaly	1.04
(Ba)N	0.21	0.23	0.24	0.23	0.00		(Ba)N	0.23		(Ba)N	68.75
(Ba/La)N	0.00	0.00	0.00	0.00	0.00		(Ba/La)N	0.01		(Ba/La)N	9.81

^TTotal

*Calculated with FeO as 0.85 of total Fe.

³Mg/(Mg + Fe)

porphy, porphyritic.

Eu* anomaly: [Eu/Eu*]_N

Ce* anomaly: [Ce/Ce*]_N

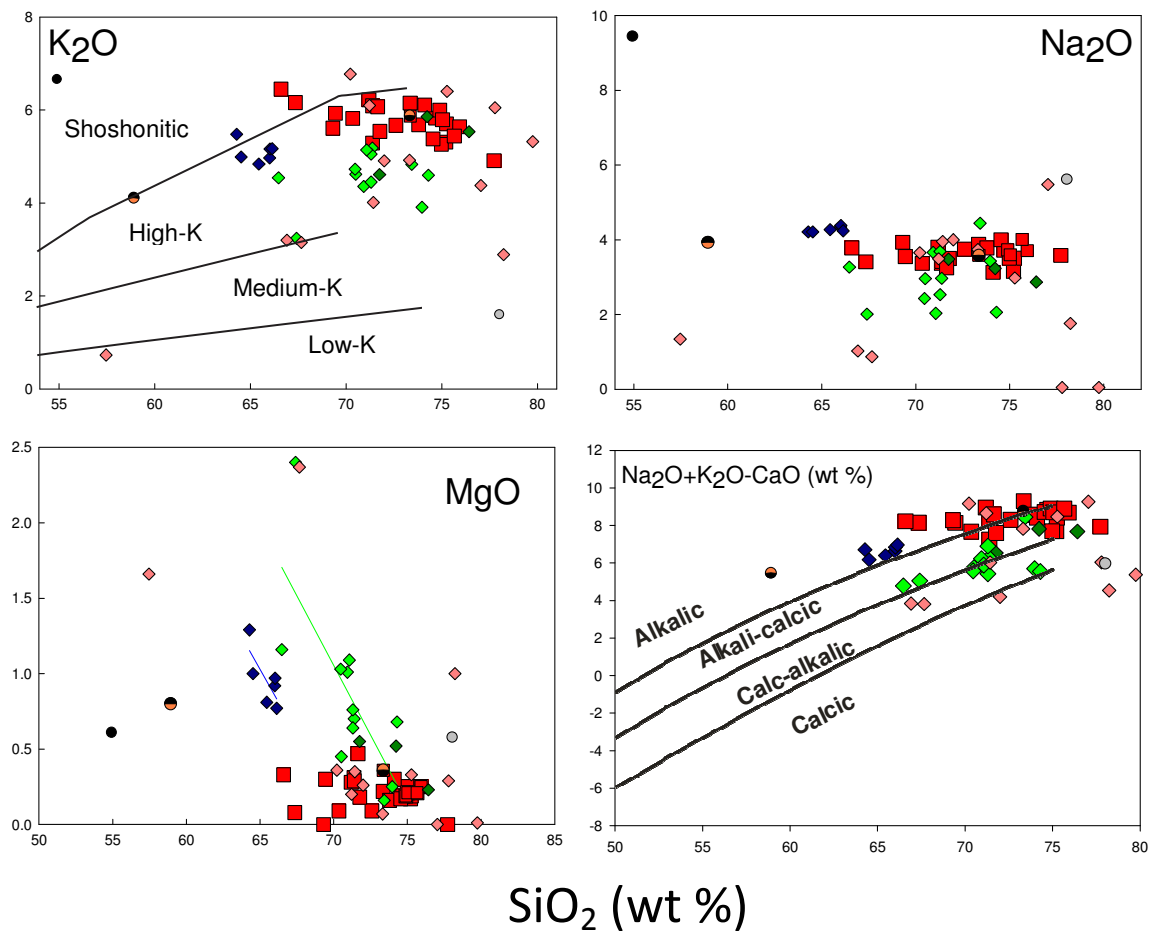


Figure 5.5. Harker diagrams of alkalis and MgO versus silica (SiO_2), as well as the MALI ($\text{Na}_2\text{O}+\text{K}_2\text{O}-\text{CaO}$) vs. SiO_2 of Frost et al. (2001). Mt. Abu (and most other granitoid samples) samples show scatter and no change with increasing silica, while Erinpura and Ranakpur samples have good correlations with MgO. Most samples from the study plot within the high-K sector of the calc-alkaline diagram of Le Maitre et al. (1989). In the Frost et al. (2001) diagram, Mt. Abu samples are alkali-calcic to alkalic in nature, while Erinpura and Revdar. Rd samples are less alkaline in nature. Ranakpur granitoids are the only wholly alkalic samples in the study.

This is less true for Erinpura, Ranakpur and Revdar Rd. samples, as they do not show the more evolved relationship of the Mt. Abu samples. Rb shows the best positive relationship with SiO_2 , expected of an incompatible large ion lithophile element (LILE) with an ionic radius that allows it to partition more readily into the melt phase than earlier formed crystals (Villaseca et al., 1998). However, this is not a tight linear trend, but contains much scatter, which could be attributed to remobilization of Rb (highly mobile during hydrothermal alteration and chemical weathering; Rollinson, 1993). Th and U are high field strength elements (HFSE) with a large ionic radius, which makes it difficult for these elements to substitute into crystal structures due to the need for coupled substitution to balance out the charges (White, 2007). They show generally positive trends, as they are also concentrated within successive melt fractions, being incompatible in most mineral structures, excluding zircon, monazite and titanite, which are found most abundantly in felsic rocks (Mahood & Hildreth, 1983; Rollinson, 1993). Vanadium, similar to MgO and Ni, which are also compatible, generally does not change with silica content, indicating that it may have reached its steady state concentration in the magma.

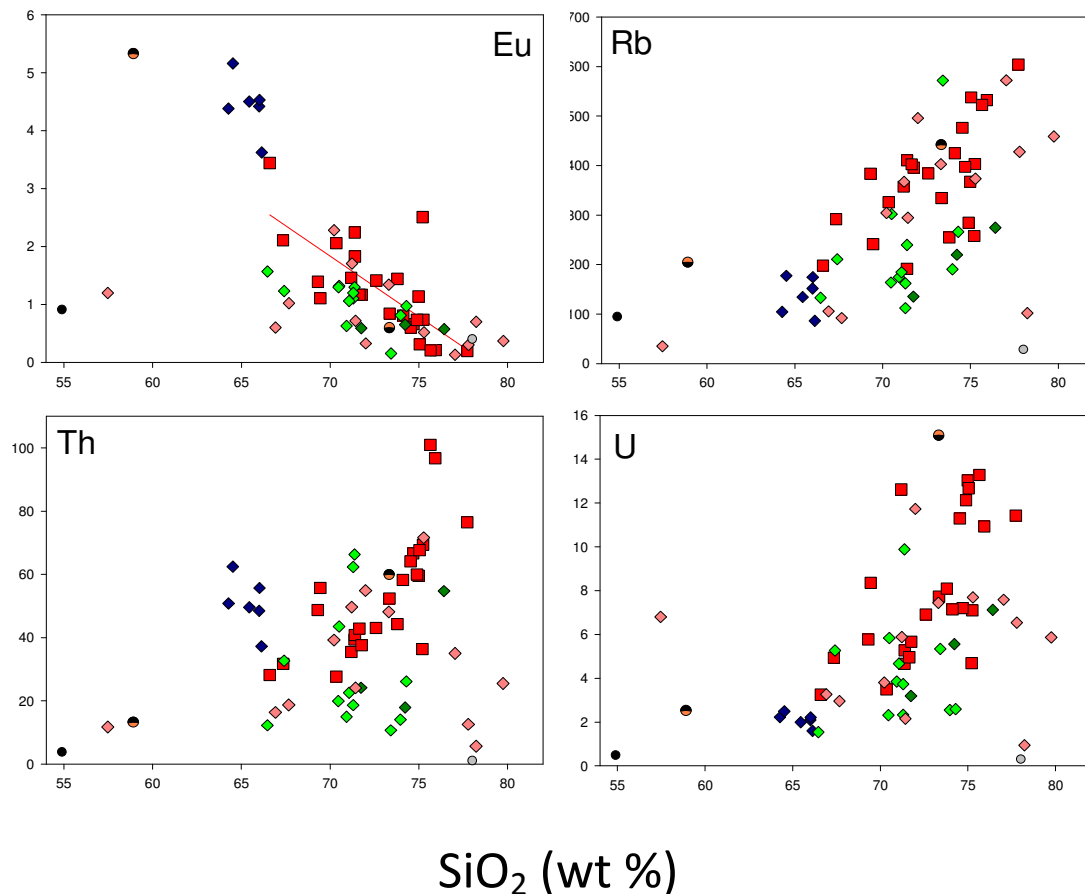


Figure 5.6. Harker diagrams of trace elements (in ppm) versus silica for all felsic samples from this study. Mt. Abu samples show negative (Eu) and positive (Rb, Th and U) correlations, but there is a lot of scatter within graphs. Other samples show indeterminate scatter.

In Erinpura samples, most trace elements are not well correlated with SiO_2 , save for V and Ti (Fig. 5.7). The trends of decreasing V and Ti with silica are caused by uptake of these elements into the magnetite structure during early crystallization of magnetite from the magma (Hall, 1996; Christiansen et al., 2007). In Sumerpur samples, only Rb and U show good positive correlations with increasing SiO_2 .

Ranakpur samples have strong negative linear correlations between SiO_2 and V, Cu, and Ni, which are all elements usually found in more mafic ferromagnesian and early-formed minerals (Thorpe et al., 1984; Wiebe et al., 1997). Ni, V, Co, P and Ti are enriched while Rb, U, Ta, W, Y and Tb-Lu are all depleted when compared to Mt. Abu samples. Other elements such as the highly incompatible Ba (>4000 ppm) and Sr (>1000 ppm) are extremely enriched over all samples. The Rb-depletion and Sr-enrichment is contrary to what is expected of felsic rocks. These samples could have a more primitive composition, with Sr not being partitioned strongly into plagioclase due to little plagioclase in the source residuum, or the Ranakpur magma entrained/retained some of its restite (Middlemost, 1997). Both are possible, as Rb also increases with increasing Sr (Fig. 5.11), indicating that the Ranakpur magma was quite undifferentiated. A strong

positive relationship between P_2O_5 and Th (unlike either Mt. Abu or Erinpura samples) may also be indicative of the presence of monazite in the magma.

Revdar Rd. samples do not display good correlations between SiO_2 and most trace elements with the exception of Rb (good negative correlations) Eu and Sr (weak negative correlation). The weak correlation may be due to these granitoids originating from different sample suites, or having different source compositions and conditions of emplacement. Alternately, the large variations may be due to metamorphic and thermal fluid activity, as many samples are foliated or gneissic in nature.

The Swarupganj Rd. sample usually plots towards the bottom of all trace element and inter-element diagrams with very low abundances, save for when it is an outlier such as in the V, Ni and Rb plots. The Kishengarh nepheline syenite also plots with low abundances of trace elements, especially incompatible Rb, Th and U. It has the highest Ba-content of all rocks in this study, which may be due to the presence of hornblende contained in this sample. The high B and moderate Sr content may also indicate a lower degree of fractionation compared to the Mt. Abu samples in this study.

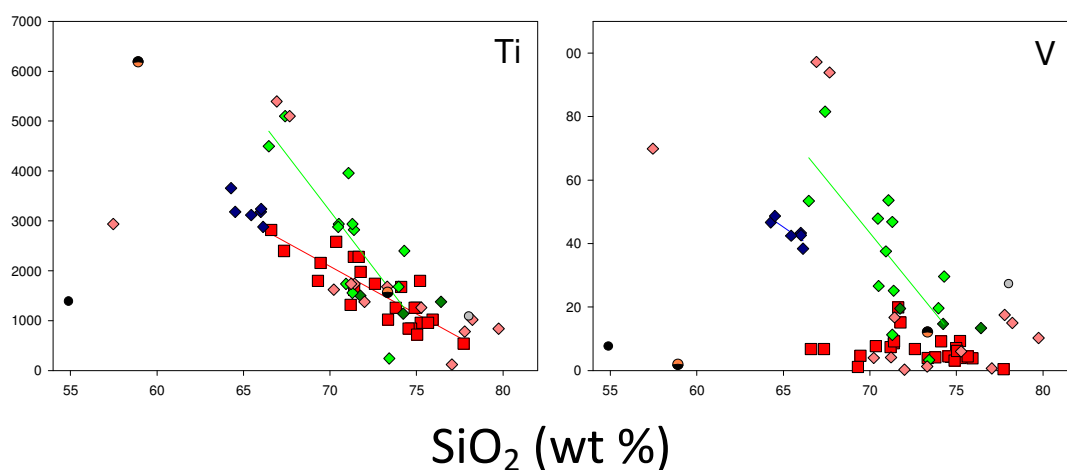


Figure 5.7 .Harker diagrams for compatible trace elements (in ppm) versus silica. Generally, all samples have good relationships between Ti and SiO_2 , while for V, only Erinpura and Ranakpur samples show any correlation.

Ba and Sr in Mt. Abu samples decrease slightly with increasing SiO_2 (Fig. 5.8). This is an indication of feldspar and biotite being removed from the magma (Liew et al., 1989), as both substitute very easily for Ca in plagioclase (Sr) and K in biotite and K-feldspar (Ba and Sr). Both behave compatibly in the silicic magma due to feldspar formation and removal. This might indicate open-system behaviour in the magma system, with recharge or crystallization of components from an earlier magma of the system, or magma mixing where co-crystallizing components are removed from the system. However, both show scatter, implying disturbance, possibly by thermal metamorphic fluids, as Ba, and to a lesser extent, Sr, are very mobile in aqueous solutions.

The elements in Fig. 5.9 all show good direct relationships with each other, as most pairs are similar in behaviour and ionic charge and radius. Zr and Hf for all samples have linear relationships. They are both HFSE with the same ionic charge, and so both partition preferentially into the mineral zircon (Watson & Harrison, 1983). All samples share a V-Co association. The likeliest phases for V and Co to partition into are Fe-Ti oxides such as magnetite and ilmenite (substituting for Fe in the octahedral site), which are present as accessories in all Mt. Abu samples (Wiebe et al., 1997; Christiansen et al., 2007).

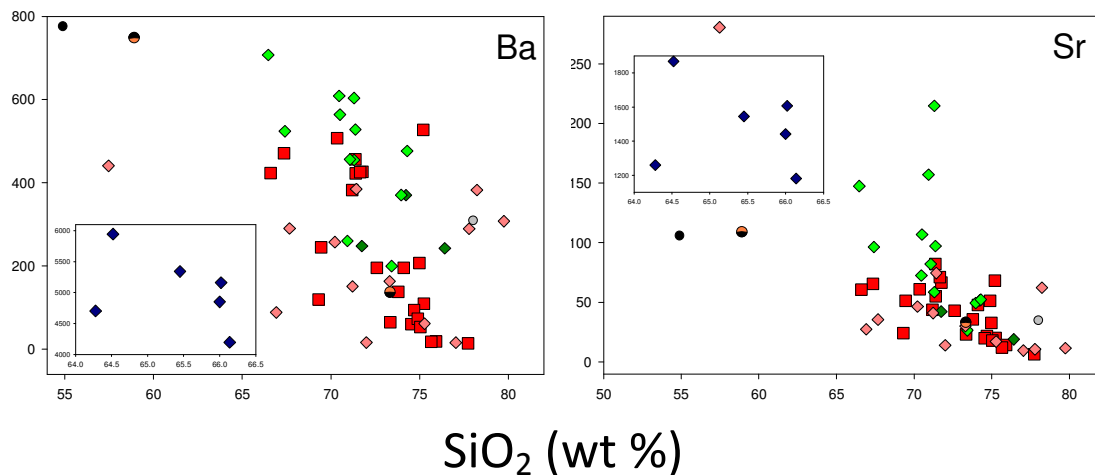


Figure 5.8. Harker diagrams for Ba and Sr with silica. The insets within each graph show the disparity between the Ranakpur granitoid abundances versus the rest of the samples in this study. Mt. Abu samples show moderate correlations for both trace elements.

Ba and Sr are partitioned into the feldspars, and so are related by their behaviour. Nb and Ta are HFSE with the same ionic charge, so are closely linked in behaviour (Eby, 1990). The diagram of Nb vs. Ta has an inflection at ~30-40 ppm Ta, where Ta concentrations are clustered tightly, then decrease slightly with increasing Nb (anomalous behaviour), then increasing together with Nb. This may reflect a change in conditions within the magma whereby Ta was taken up less preferentially than Nb, hence the almost level values in the middle of the graph for Mt. Abu. Scandium is preferentially partitioned into hornblende and ilmenite (Rollinson, 1993; Best, 2003; Christiansen et al., 2007), so it is reasonable that it should be correlated with Ti, as Ti partitions strongly into ilmenite as well. Since Ti is found in the Fe-Ti oxides and titanite, this is where the Zn should also be found, because they have a linear relationship with each other.

Zr, Pb and Th are strongly correlated in the Erinapura samples (Fig. 5.10), as Th and Pb partition particularly strongly into zircon (White, 2007). However, in the Mt. Abu samples, Th and Zr do not show any correlation with each other. For Erinapura samples, La (and other light rare earth elements) and Zr are closely correlated which could be indicative of La partitioning strongly into zircon, or that the same process of enrichment has affected both these immobile elements. Sumerpur samples usually fall within the Erinapura samples field, although as the sample size is small, relationships cannot be determined easily.

In the Ranakpur samples, Nb is strongly correlated with Ta and Y, which are both incompatible and immobile elements (Winter, 2001). Nb and Ta are depleted when compared to the Mt. Abu samples, as well as when compared to Ba or other LIL highly incompatible elements. As both Nb and Ta and highly incompatible as well, this depletion is commonly representative of magmas generated at subduction zones (White, 2007). Rb, Ba and Pb are also correlated with Th. The HFS nature of Pb and Th, and the LILE nature of Rb and Ba, ensure that these elements are highly incompatible in crystal structures and are partitioned preferentially into the melt. Rb, Ba and Sr also share a linear, direct relationship (with the greatest concentrations of Rb and Ba from all samples), although the range of Rb-concentrations is several orders of magnitude lower than that of Sr, while U also increases with Rb-content.

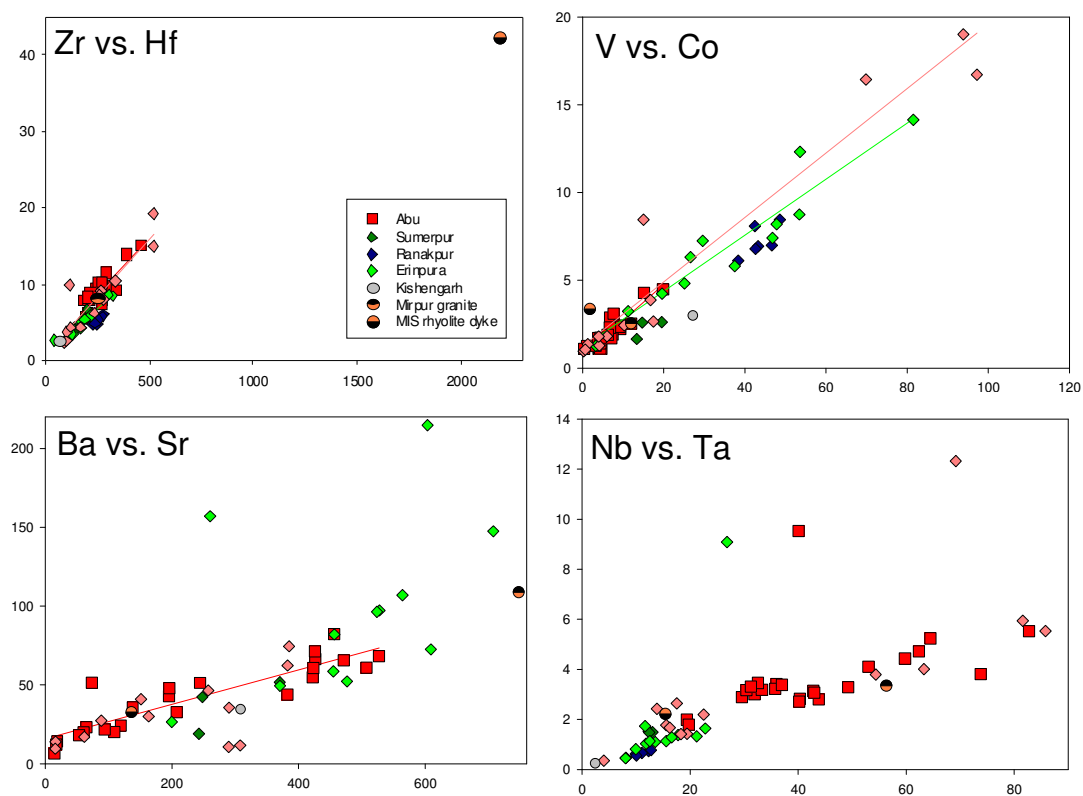


Figure 5.9. Inter-element diagrams (in ppm) representing trace elements with similar atomic properties such as ionic radius and size of charge. All bivariate diagrams have a positive slope, indicating the good relationship between the two elements. However, Erinpura samples have a lot of scatter in the Ba-Sr graph, while Mt. Abu samples show a slight dip/kink in the Nb-Ta graph between 30-40 ppm Nb.

As both are radioactive and incompatible in crystal structures, they partition preferentially into the more differentiated, felsic melt and are so concentrated. Ranakpur samples have the lowest abundances of all the rock samples in terms of these radioactive elements, which may be an indication of their more primitive nature.

Revdar Rd. samples show positive relationships for Zr-Hf, V-Co and Nb-Y. As with other samples, it can be inferred that the Hf partitions favourably into the zircon crystal structure, giving rise to such a good

relationship. Vanadium, as well, is known to enter the Fe-Ti oxides, especially magnetite, as a substitute for Fe, and so Co is also expected to reside in this crystal structure (Wiebe et al., 1997). Nb and Y form a close association, as Nb, being incompatible, is likely to be associated with the rare earth elements (REEs), and Y is similar in behaviour to the REEs. These samples also show a similar slope to that of Mt. Abu samples in the Nb-Ta association.

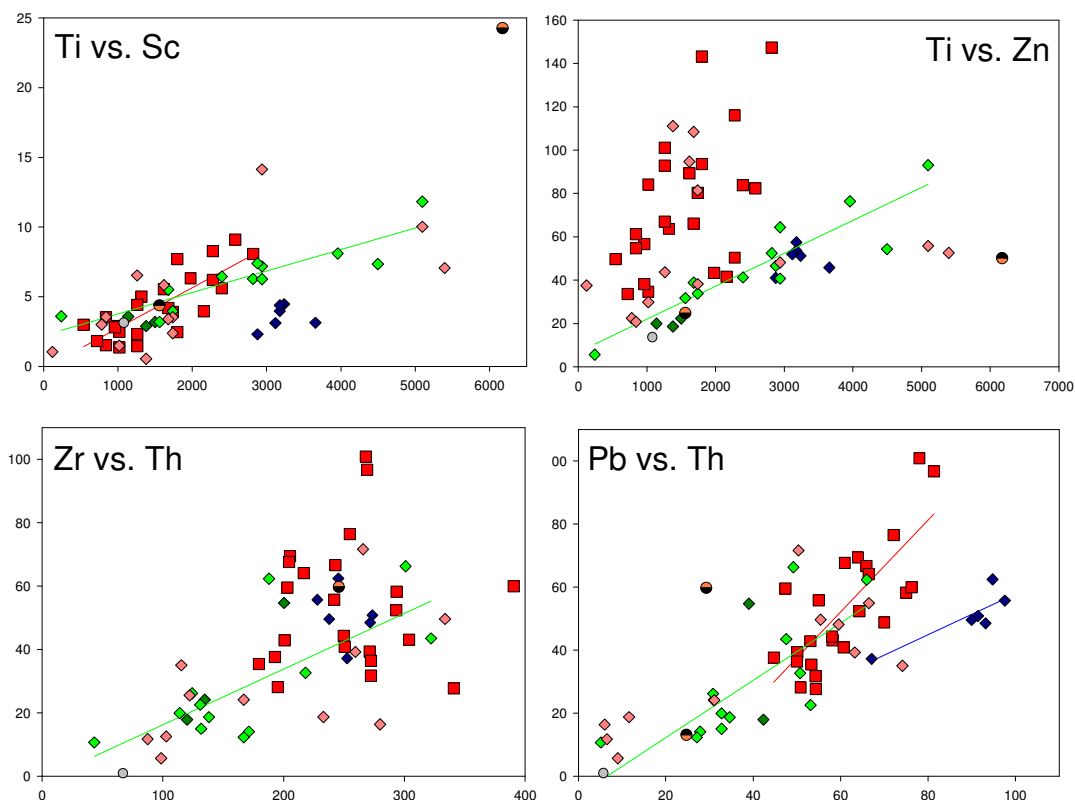


Figure 5.10. Inter-element diagrams (in ppm) showing positive correlations for Erinpura and Mt. Abu samples.

The CaO-Sr graph (Fig. 5.12) is used to trace plagioclase feldspar differentiation/evolution, as plagioclase becomes less Ca-rich the more the magma is differentiated (Blatt & Tracey, 1995). Sr also decreases with magma evolution, as, with its relatively low ionic charge and radius, it is more compatible in early crystallizing feldspars than e.g. Rb, which is concentrated into the melt (Villaseca et al., 2008). This relationship is true of the Mt. Abu and Sumerpur samples (and somewhat true of the Erinpura samples, although there is much scatter), as the trend is positive, although some scatter is visible, indicating other processes at work affecting the Sr and Ca concentrations within the system. For the Ranakpur samples, there is no correlation between the two, as CaO does not increase with Sr content, making it unlikely that the Sr has partitioned into early plagioclase.

The steeper gradient of the Erinpura samples on the La vs. La/Yb graph in Fig. 5.12 compared to Mt. Abu samples may indicate a smaller degree of partial melting, different source compositions or differing degrees of modification/evolution (White, 2007). The former is less likely, as Mt. Abu has the greatest enrichment in

REEs from the granitoids in this study. The steeper gradient of $(La/Yb)_N$ in Erinpura samples may be due to a greater retention of ferromagnesian clinopyroxene, hornblende and accessory minerals such as zircon in the source (Rollinson, 1993).

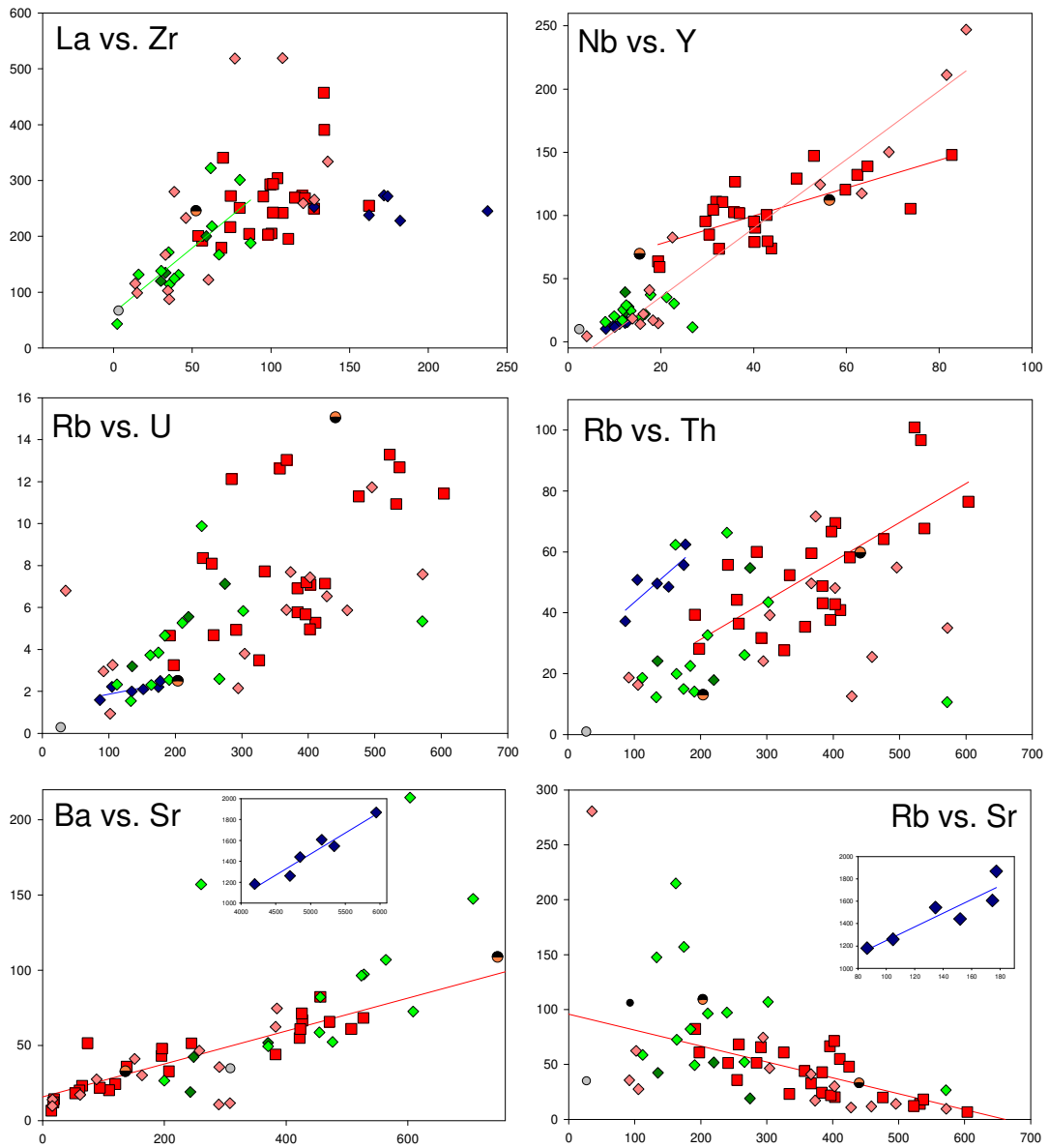


Figure 5.11. Inter-element diagrams of trace elements (in ppm) comparing the degree of correlation between the different granitoid suites. These various inter-element combinations are informative about magma conditions and processes.

These partition the heavy rare earth elements (HREEs) preferentially, thus resulting in a greater $(La/Yb)_N$ slope for the Erinpura granitoids and enrichment of La over Yb. Mt. Abu granitoids may originate from a more evolved source with less ferromagnesian minerals (or with a greater crustal component) where all REEs are highly-enriched. Ranakpur and Sumerpur samples have a similar slope to that of the Erinpura granitoids while Revdar Rd. samples are divided, with some plotting within the Mt. Abu samples field, and a

few within the Erinpura field, which may be an indication of the division between the Revdar Rd. samples in terms of sample suites.

The Fe_2O_3 vs. Ti graph in Fig. 5.12 illustrates that most of the titanium in the system has been locked into the most common Fe-containing minerals, the Fe-Ti oxides, ilmenite and magnetite (and their alteration products such as titanite), present in all granitoids from this study.

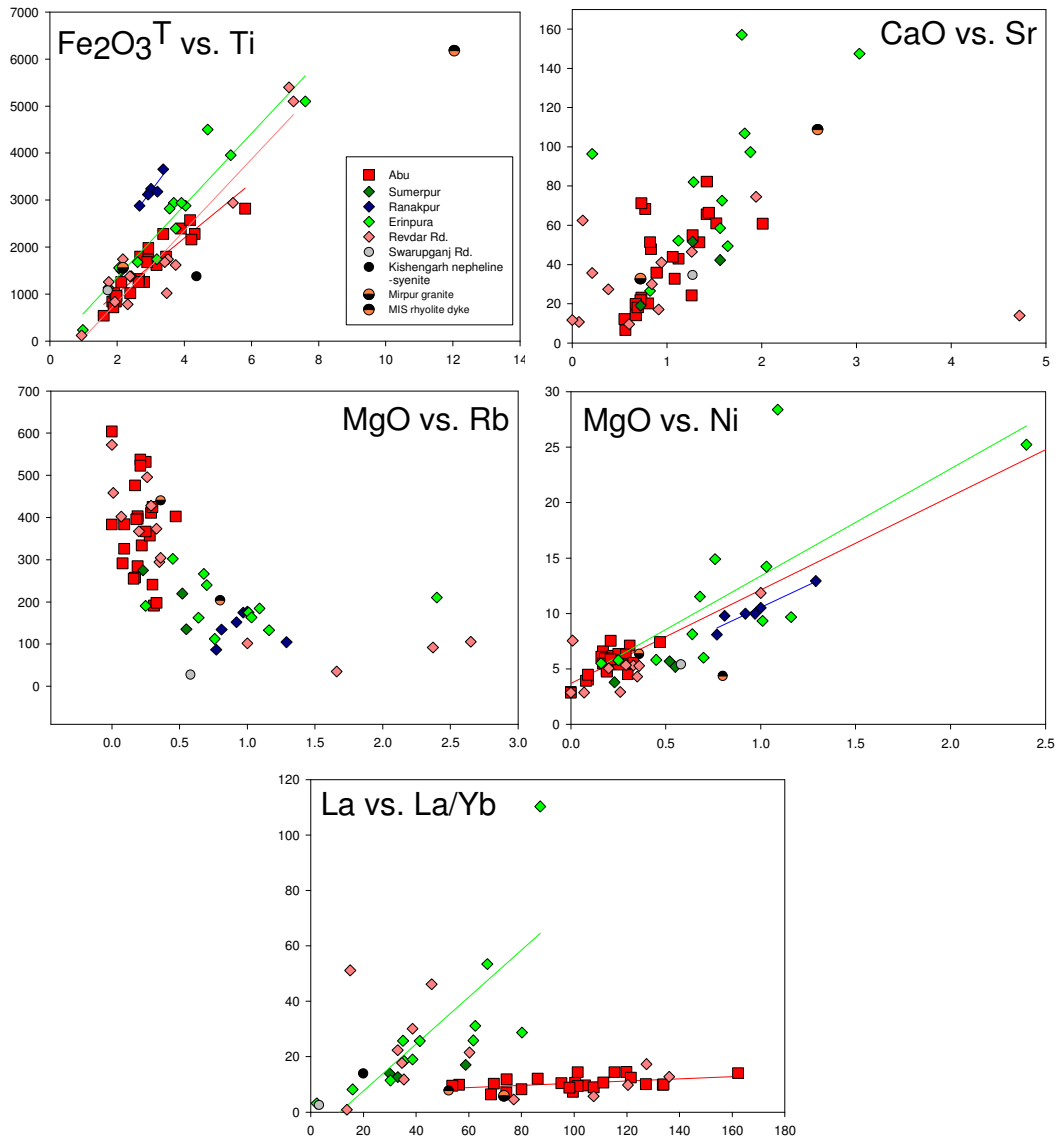


Figure 5.12. Inter-element (in ppm) diagrams illustrating specific relationships between sample suites.

In Mt. Abu samples, the MgO versus Rb graph in Fig. 5.12 illustrates that MgO, a compatible element, is constant while Rb increases. The lack of change (MgO should decrease in a fractionating magma) implies that fractional crystallization was not a major process in this magma (Martin & Moyen, 2002). This is not strictly true for Erinpura, Sumerpur or Revdar Rd. samples, as the slope of the MgO vs. Rb graph is shallower compared to Mt. Abu samples, and the relationship is linear. This suggests that MgO has not yet reached its steady-state concentration in the Erinpura samples (so it has not been through as many

crystallization episodes and represents a less evolved composition) or that the magma entrained a larger mafic component than that of Mt. Abu. Ranakpur samples show much scatter and the lowest concentrations of Rb, making it less likely that MgO has reached any saturation/steady state concentration point. They also show a strong positive correlation between MgO and Ni, indicating that Ni has preferentially partitioned into the crystal structure of Mg-rich early silicates and so its concentration steadily decreases in the increasingly felsic magma.

5.2 Maficity/molar Mg + Fe

For the Mt. Abu samples, the major elements Ca, P, Mn and Ti all show the expected positive trend versus maficity in Fig. 5.13, which is another measure of differentiation (total Fe- and Mg-content in atomic Fe +Mg) , where the weighting is more even compared to plots where SiO₂ is used. The good relationships shown between these major elements and molar Mg + Fe (and SiO₂) indicate that both are important for the geochemical evolution of the Mt. Abu magma. Al-content is less affected by molar Mg+Fe than by silica-content, while P₂O₅ shows a better relationship to maficity than to SiO₂, which is likely, given that P goes into apatite, which starts to crystallize relatively early in the evolution of the felsic magma, when the more mafic Mg and Fe are also found in greater concentrations. This changes as fractional crystallization proceeds, and SiO₂ becomes more concentrated, but as most apatite formation has already occurred, the P-content is not affected as much by increasing Si.

Mt. Abu samples are unlike those of Villaros et al. (2009), as they do not show positive correlations between refractory elements (Zr, Hf, LREE) and the maficity index, while element concentrations (Rb, Ba, Sr, Eu) in reactant, easily dissolved minerals have good correlations with maficity. These trends indicate that it is unlikely that Mt. Abu granitoids have entrained refractory minerals from the source. The high Zr-content in Mt. Abu samples thus may be due to a source rich in Zr.

The Erinpura samples show a shallow positive linear trend between the molar Mg + Fe ratio and Al, a shallow negative linear trend for Na and a strong positive correlation with Ti. P has a scattered, positive trend, excluding the outlier, BL-1A while Ca and K are scattered, with no discernable trend.

Ranakpur samples also have uniformly good correlations for most major elements and maficity with the exception of Al, which has the highest concentration in the middle. This may be due to a phase rich in Al crystallizing out of a magma that is enriched in Al, causing a drop in Al after crystallization (Rollinson, 1993).

Revdar Rd. samples generally follow the Mt. Abu samples trend, and do not have good correlations for Al and Ca.

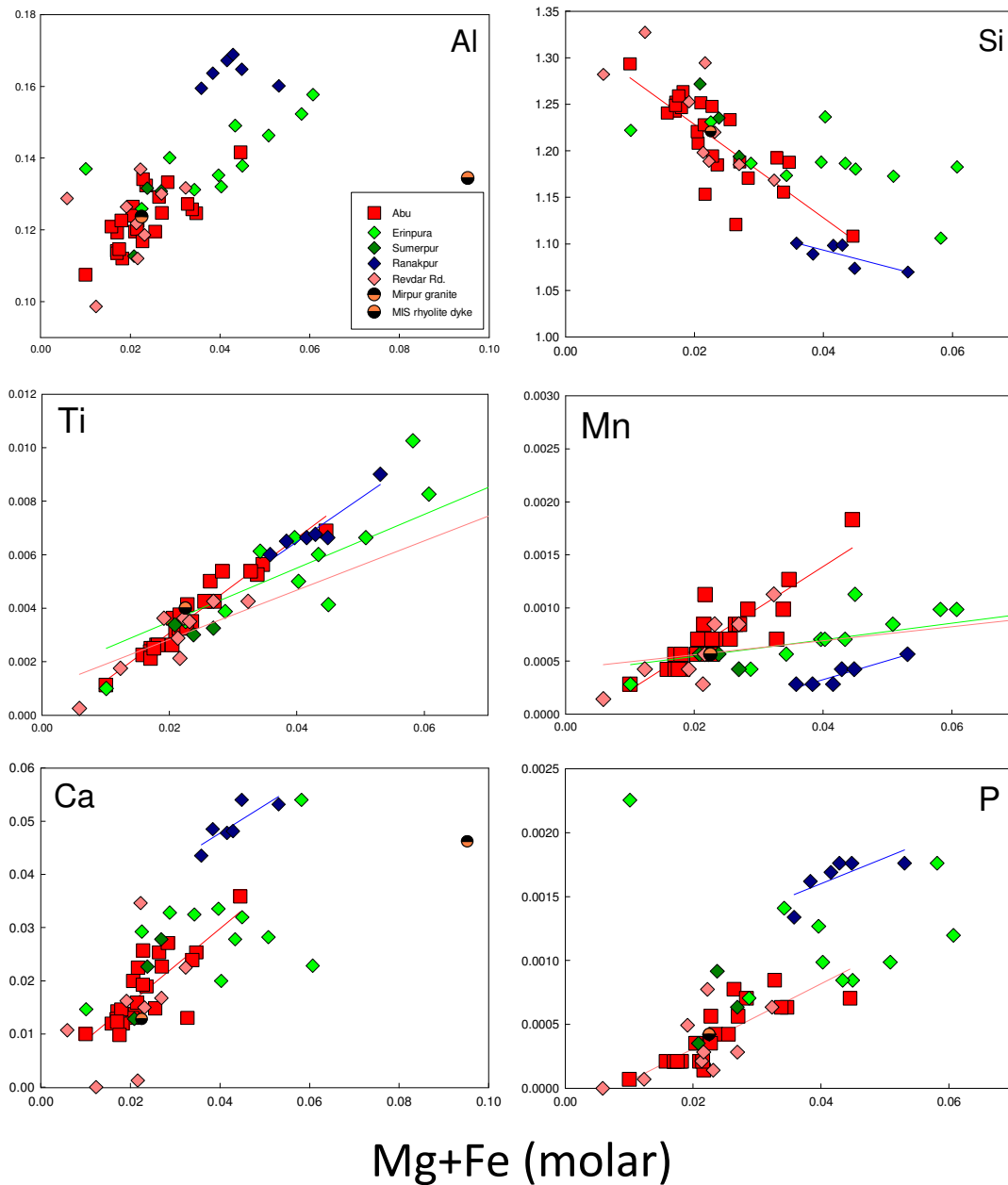


Figure 5.13. Inter-element diagrams of major elements (molar) versus maficity (molar Mg + Fe). The molar Mg + Fe is a differentiation index, much like SiO_2 , but the relationship is not biased towards the (Mg + Fe) because these elements do not make up the majority of the rock. Most samples show good correlations with maficity, although Erinpura samples show a greater degree of scatter than the rest.

Most trace elements in Mt. Abu samples do not show a good correlation with maficity (or with SiO_2) except for Eu, Sr and Cu in Fig. 5.14. The LREEs, Zr and Hf, which are concentrated into accessory phases, do not show linear negative or positive relationships with either silica or maficity. Mt. Abu samples have some evidence of xenocrystic zircon cores (Chapter 6). This may imply a source magma that was oversaturated in Zr, causing zircon crystallization. Separation of the Mt. Abu magma occurred, with some entrainment of xenocrystic zircon, as the temperature of the partial melt may not have been high enough ($\sim 900^\circ\text{C}$) to melt all the entrained zircon. However, the relative amount of entrained zircon would have been small, as seen

by the lack of any positive trend of Zr with increasing maficity. The high zircon concentrations may thus be the result of a small degree of partial melt, as well as an enrichment of Zr in the source magma.

Eu has the greatest correlation, but there is still scatter in all these graphs. The elements Rb, Th and U define somewhat negative trends with maficity in Fig. 5.14, but are not strongly correlatable. The weak correlations may be due to differing source compositions as well as the fact that most trace elements will have gone into accessory phases/minerals within the granitoid magma. Remobilization due to metamorphism may also be a factor here, especially in the more mobile LILE.

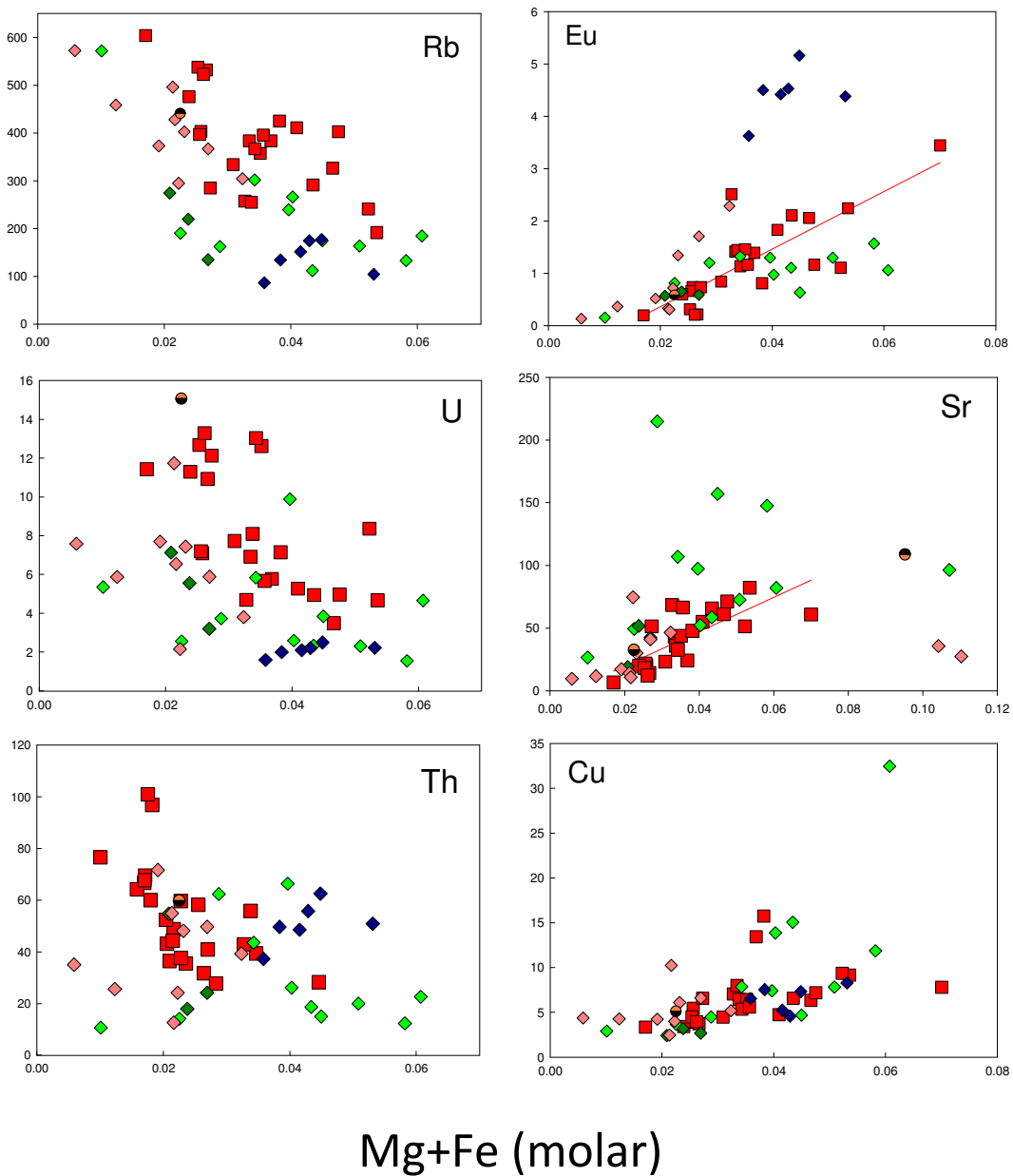


Figure 5.14. Inter-element diagrams for maficity versus trace elements (ppm). Mt. Abu samples show good correlations for some elements (notably the more compatible Cu, and Sr) while the more incompatible elements are more scattered, although their slope is negative. Samples from other rock suites do not show very good trends with maficity.

Erinpura and Ranakpur samples have strong correlations with the more compatible elements (Fig. 5.15: V, Co, Ni and Zn) that also partition into ferromagnesian minerals or Fe-Ti oxides (which have a high molar Mg + Fe). Mt. Abu and most Revdar Rd. samples have lower values of these elements, which may indicate they are more differentiated than the former. The higher values of Zn and the scatter in Mt. Abu and Revdar Rd. samples may be an indication of this element's mobility during metamorphism.

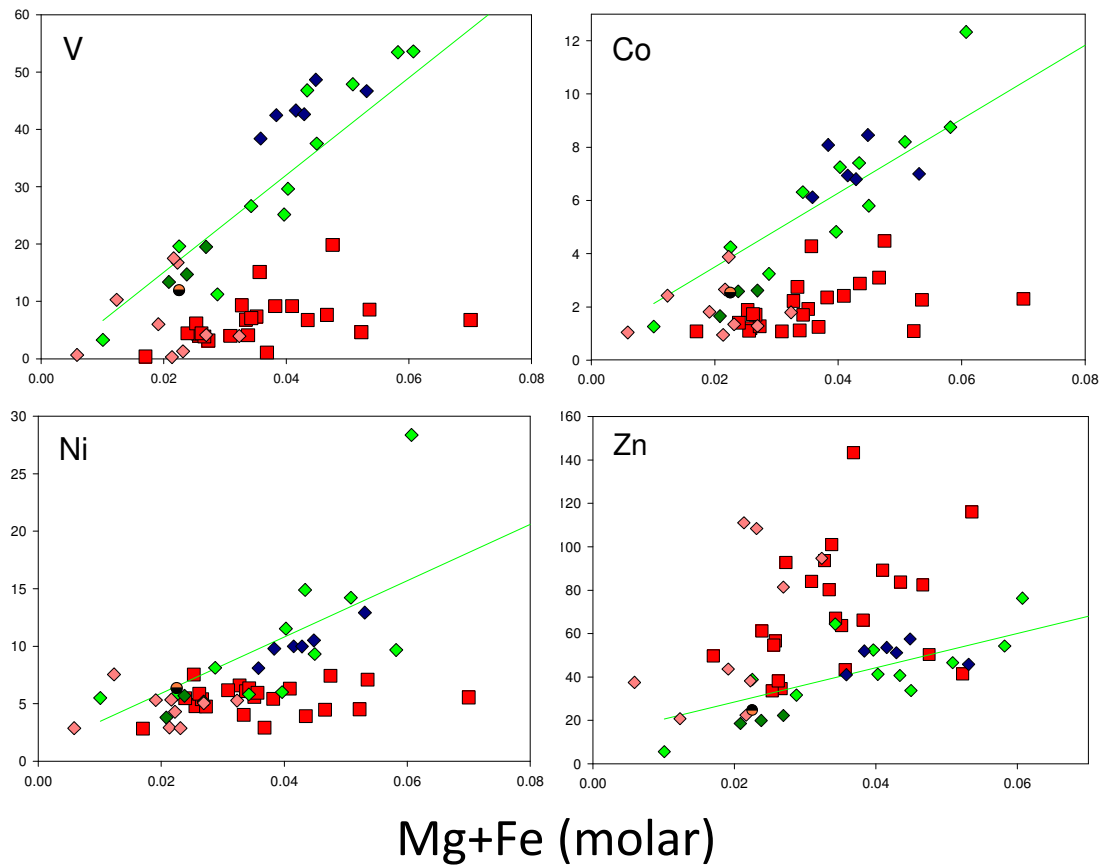


Figure 5.15. Inter-element diagrams for maficity versus the more compatible trace elements (in ppm) in felsic rocks. Erinpura and Ranakpur rocks show positive correlations, while Mt. Abu samples are usually scattered and with lower concentrations.

5.3 REE diagrams

Rare earth elements contain a large amount of information in proportion to their abundances within rocks. Being immobile, they provide information on source composition as well as the solid residue in the source magma. In the REE diagram, the degree of compatibility increases from left to right, so that certain shapes in the REE diagram can be interpreted as being caused by retention of certain minerals in the magma or in the source.

The REE plots for the Mt. Abu granitoids differ noticeably from those of the Erinpura, Sumerpur, Ranakpur and Swarupganj Rd. granitoids in Fig. 5.16. All samples have been normalised to the chondritic meteorite values of Anders & Grevesse (1989). The average slope or $(La/Lu)_N$ of the Mt. Abu granitoids and rhyolite dykes is shallower at 5.84, when compared to 14.6 and 119.42 for the Erinpura and Ranakpur samples,

respectively. The Sumerpur and Revdar Rd. samples have a slope between the Mt. Abu and Erinpura samples ($(La/Lu)_N=8.03$ and $(La/Lu)_N=7.47$, respectively) although Revdar Rd. samples can be split into two sections on the basis of the REE diagram. The Ranakpur samples have the greatest LREE enrichment as well as the greatest HREE depletion. The Swarupganj Rd. sample has the lowest abundances of REEs and may therefore be the most primitive of the samples from this study. It may also have a depleted source area compared to other samples.

Mt. Abu granitoids and rhyolite dykes have a shallow negative slope from LREE to HREE, and all REEs are highly enriched over chondritic meteorites (120.5-363.7 ppm La). They display well-developed negative Eu-anomalies (average $Eu/Eu^*=0.20$) and weakly developed Ce-anomalies which hover just above or below 1 (the majority being positive). The positive Ce-anomalies may be caused by the presence of apatite saturation or the presence of monazite, as Ce is readily taken up by apatite (or monazite) in its crystal structure (Hall, 1996; Best, 2003) while Zr and Ce have similar due to similar size and ionic charge, especially when Ce is present as Ce^{4+} , its oxidised state. Slight Tm-anomalies (positive) are also present, which may be due to the presence of magnetite. However, both are very small in magnitude and are considered insignificant. The relatively flat HREE slope is an indication of the absence of garnet in the source of these rocks and mid- to shallow- levels of melting in the crust (Villaseca et al., 2008). The REE pattern/shape, with enrichment in both LREE and HREE with well-developed Eu-anomaly and a shallow $(La/Lu)_N$ slope, is characteristic of the late stage differentiates of felsic magmatism. The most well-developed Eu-anomalies can be correlated with the pink to greyish-pink foliated granites and the rhyolitic dykes, which also have some of the highest Ba and Th values and are elements that are found in the greatest concentration in evolved magmas/late stage fractionates.

The Mirpur granite sample is similar in both LREE and HREE shape to Mt. Abu felsic samples. This is also true for all previous geochemical plots of the Mirpur granite, as it plots squarely within the field of Mt. Abu samples. The MIS felsic dyke, however, usually plots much further afield of Mt. Abu samples due in part to the lower silica content, but also due to the major differences in abundance of major and trace elements within the dyke. The REE plot differs in shape to that of the Mt. Abu samples, and the Eu-anomaly is one of the shallowest of all samples, barring the Ranakpur sample set. Both the LREE and HREE slopes are shallower than those of most Mt. Abu samples.

Erinpura granitoids have an average $(La/Lu)_N$ slope of 14.6, considerably steeper than that of the Mt. Abu samples as well as having overall lower REE enrichment. The average HREE slope of $(Gd/Lu)_N=3$ is steeper than that of the Mt. Abu samples as well. The negative Eu-anomaly is well-developed but on average, smaller in magnitude than Mt. Abu samples, while these samples also show weak positive Ce- and negative Tm- anomalies. The overall lower total REE abundances indicate a less evolved, more primitive magma of

origin for these granitoids. The relatively steeper HREE slope precludes us from stating that there is a genetic relationship between the two suites, as, if the Erinpura granite was related to the Mt. Abu granitoids, it is expected to have a similar but less enriched slope between La to Lu and LREE and HREE. The steeper gradient of the HREE slope may also indicate different mineral residua (such as hornblende) left behind in the source or a different compositional source material to that of the Mt. Abu samples. This may also be the reason for the crude negative slope versus silica for LREEs, which changes to a horizontal line for the HREEs, which are well-separated from Mt. Abu samples on these diagrams. Erinpura LREE values do plot within the lower end of the Mt. Abu sample field. However, the HREE slope is not as steep as other samples within the study, and this may be due to an absence of garnet in the source, which would tend to indicate mid-crustal levels of generation/melting (Villaseca et al., 2008).

The Erinpura samples form a fairly tight group even though samples are not sourced from a single site/pluton but are spatially distant from each other. This cohesion is an indication of the high probability of these samples being part of the same pluton/intrusive suite. This is true save for two samples, BL-1A and AA6-22. Sample AA6-22 is a porphyritic grey granite and has a less evolved pattern (lower enrichment of all REE, with a level slope for the HREE) than the rest of the Erinpura samples, with a smaller Eu-anomaly as well as slope of $(La/Lu)_N=4.19$. This sample, being porphyritic with very little evidence of deformation, is atypical of Erinpura-style granitoids, which are usually texturally granite-gneiss. The REE plot confirms that this sample likely should not be classified as part of the Erinpura granite. Sample BL-1A, the Balda Granite sample, has a radically different REE pattern, with the lowest levels of enrichment of any of the granitoids. The Eu-anomaly is well-developed, but there is very little separation between LREE and HREE with $(La/Lu)_N=2.23$. The REE also do not show the typical systematic and incremental felsic granitoid trend of enrichment from HREE to LREE (this sample has a slight negative LREE slope). This granite is classified as the youngest and most evolved member of the Erinpura granite suite, so it is expected to show the greatest amount of REE enrichment, but the opposite is true, which makes it doubtful that it is an evolutionary relation of the Erinpura granite. However, as only one sample is available, firm conclusions concerning the genetic relationship between the two cannot be made.

Sumerpur granitoids have a $(La/Lu)_N$ slope of 8.03, shallower than the Erinpura granitoids slope. The degree of enrichment of the REEs is similar to Erinpura samples, but their HREE slopes follow the trend of the Mt. Abu samples. The ratios of LREE to HREE and the LREE- vs. HREE-slopes are slightly higher than those of the Mt. Abu samples, but much lower than the values for the Erinpura samples. The Eu-anomaly with a magnitude of 0.28 also fits this trend. These samples also have the weak positive Ce- and Tm- anomalies common to the Erinpura and Mt. Abu samples.

Ranakpur samples have the steepest slope of all the samples in the study, with $(La/Lu)_N=119.42$, as well as having a steeper HREE than LREE slope. These samples have little or no Eu-anomaly, indicative of a very primitive magma of deeper origin, where plagioclase has not been crystallized due to its instability at deeper levels (Winter, 2001). The steep HREE slope and high enrichment of LREEs relative to HREEs is also an indication of garnet in the source, as garnet partitions the HREE very strongly into its crystal structure (Rollinson, 1993; Hanson, 1978). This magma was generated under high pressure conditions, where garnet is stable. These samples also have a visible Er-anomaly, which is possibly an analytical artefact.

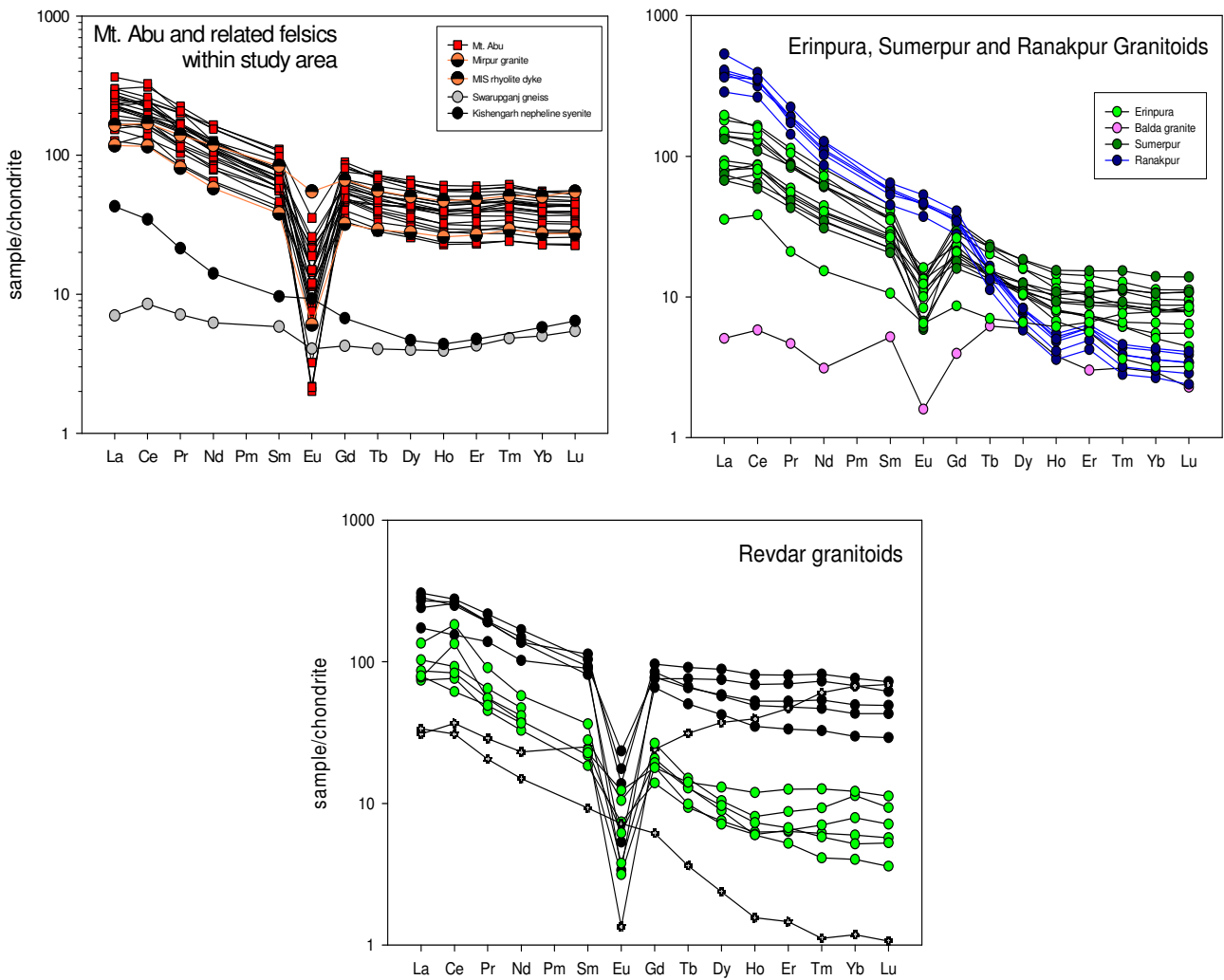


Figure 5.16. REE plots normalised to chondrites for the various rock suites. There are noticeable differences in REE diagram shape between the Mt. Abu, Erinpura and Ranakpur samples.

Revdar Rd samples can be divided into three subsets based on their REE plots, one of which follows the trend of the Mt. Abu samples, with elevated LREE and HREE concentrations and a relatively flat HREE slope as well as well-developed Eu-anomalies. The second subset loosely follows the Erinpura REE plots (greater slope between La-Lu, and overall lower total-REE enrichment) although the MREEs seem to be more depleted in comparison to the HREEs, and the HREE section of the graph is concave-upward in shape. This

could be caused by hornblende, titanite or apatite left behind in the source, because these minerals strongly partition the middle REEs (Hanson, 1978).

The last subset consists of two anomalous samples, one of which is an aplitic dyke in sharp contact with its coarse-grained granitic host rock. The REE plot is anomalous in a silica-rich rock, with a steeply increasing slope from Gd to Lu (HREE), and a La/Lu ratio of <1 , indicating enrichment of HREEs over LREEs. The Eu-anomaly is well-developed, with the weak Ce- and Tm- anomalies also present. This sample is fairly enriched over chondrites, so it has undergone fractionation, but minerals left behind in the source that strongly partition LREEs, thus enriching the residual melt in HREEs, such as plagioclase, monazite and allanite have likely caused this atypical REE trend. The second anomalous sample is a pegmatite, and has a steeply negative overall $(La/Lu)_N$ slope, with very low levels of enrichment of REEs, approaching zero in the HREEs. A Eu-anomaly is also absent, suggesting no plagioclase was retained in the source or that this is a cumulate containing a large amount of plagioclase.

The Swarupganj Rd. sample has a shallow positive slope $(La/Lu)_N=1.29$, and while all REEs are enriched over chondrites, this enrichment is slight, and the LREEs are only weakly enriched over the HREEs. This sample does have a slight negative Eu-anomaly, indicating that there has been fractionation of plagioclase, although to a lesser degree than other samples in the study. The shape of the REE pattern shows that the middle rare earth elements (MREEs) are depleted compared to the HREEs. This could be caused by hornblende being left behind in the source (Best, 2003) as well.

The Kishengarh nepheline syenite has low to moderate enrichment of REEs over chondrites, and a positive $(La/Lu)_N$ of 6.66. It has a slight positive Eu-anomaly, confirming the presence of plagioclase feldspar within the sample. This positive Eu-anomaly may also indicate its relatively primitive, less evolved character contrasted to the other felsic granitoids in this study. The MREEs are also depleted compared to the HREEs, similar to the Swarupganj Rd. granitoid and may also be caused by hornblende retention in the source.

5.4 Spider diagrams

All samples have been normalised to the primitive mantle values of White (2007) and elements are generally arranged in order of increasing compatibility in terms of mineral/melt relations, with mobile elements placed at the left of the diagram while the immobile elements (placed at the right of the diagram) increase in compatibility from left to right (Fig. 5.17).

In general, Mt. Abu granitoids are uniform in pattern and highly-enriched over the primitive mantle values (White, 2007) in terms of the LIL elements. Elemental concentrations decrease from LILEs (Ba) to Y with a gentle gradient. However, the slope is not smooth, as there are several well-developed negative anomalies. The depletions in Ba and Sr (both LIL elements that should be concentrated into the most felsic rocks) are due to K-feldspar and plagioclase removal from the melt, as both Ba and Sr partition strongly into these minerals (Winter 2001), having similar charge and ionic size to Ca and K, for which they substitute. These anomalies may also be caused by retention of the feldspars in the source during partial melting (Rollinson, 1993). The high concentrations of Rb, U and Th are expected, as these incompatible elements are usually found enriched in felsic melts (Roberts & Clemens, 1993). Rb is a LIL element that is also mobile, and hence is more likely to be enriched in rocks that are felsic and that have also undergone metamorphism and fluid movement, as these will cause preferential enrichment of mobile elements. The P and Ti depletions are due to early apatite and Fe-Ti oxides (respectively) crystallization and removal. The slight Nb-depletion is a typical crustal signature (and may be indicative of crustal involvement in the magma), as well as being a subduction zone signature when there is decoupling of Zr and Hf (enrichment) from Nb and Ta (depletion) (Roberts & Clemens, 1993; White, 2007). This is due to the fact that although all are similar in degree of incompatibility (and should therefore behave in a similar manner), in samples, Nb and Ta, being more incompatible and immobile in aqueous solutions, are left behind in the slab, while the Zr and Hf move up and enrich the crustal wedge. Nb and Ta can also be affected by crystallization of ilmenite and titanite from the magma (Winter, 2001).

Erinpura and Sumerpur granitoids are similar in overall spider-diagram shape, although Sumerpur granitoids have a steeper incompatible to compatible slope than the Mt. Abu granitoids, i.e. LILE levels of enrichment are similar; but the more compatible elements to the right of the graph are depleted in comparison to the Mt. Abu spider diagram. The Erinpura and Sumerpur samples have a more pronounced Nb-anomaly than Mt. Abu samples and conversely smaller Ba, Sr, P and Ti anomalies. The well-developed Nb-anomaly could indicate greater input/influence from a subduction zone and a volcanic arc origin (Roberts & Clemens, 1993; White, 2007). The smaller Ba and Sr anomalies signify less feldspar removal, which may be a consequence of these samples being more primitive and less fractionated than the Mt. Abu samples. The smaller P and Ti anomalies also imply lesser formation and separation of early apatite and ilmenite/magnetite/titanite in the early magma or that the source composition differs from that of the Mt. Abu samples. The Balda granite sample (BL-1A), assumed to be the youngest stage derivative of the Erinpura granite, has a slope from LIL elements to Y that is similar to the Erinpura samples, but the actual shape of the spider diagram differs markedly from the Erinpura samples. The moderate Ba-, Sr- and Ti-anomalies are still present, but P is enriched relative to its neighbours Zr and Nd, creating a positive anomaly. Pb is also depleted, while Rb forms a well-developed positive anomaly. The LREE La and Ce (and Nd) are depleted compared to Nb, with the result being that there is no Nb-anomaly present in this sample.

Ranakpur granitoids show the greatest slope from La to Y, or from more incompatible - to more compatible- trace elements. They also have a pronounced Nb-anomaly, similar to Erinpura samples in magnitude. Rb is relatively depleted in contrast to Ba, which is opposite to all other granitoid samples, and Sr is only weakly depleted. These confirm that plagioclase and K-feldspar have not been crystallized out and removed in great proportions from this magma. The weak negative anomalies in P and Ti, similar to Erinpura sample, are also indicative of less early removal of apatite and Fe-Ti oxides from the melt.

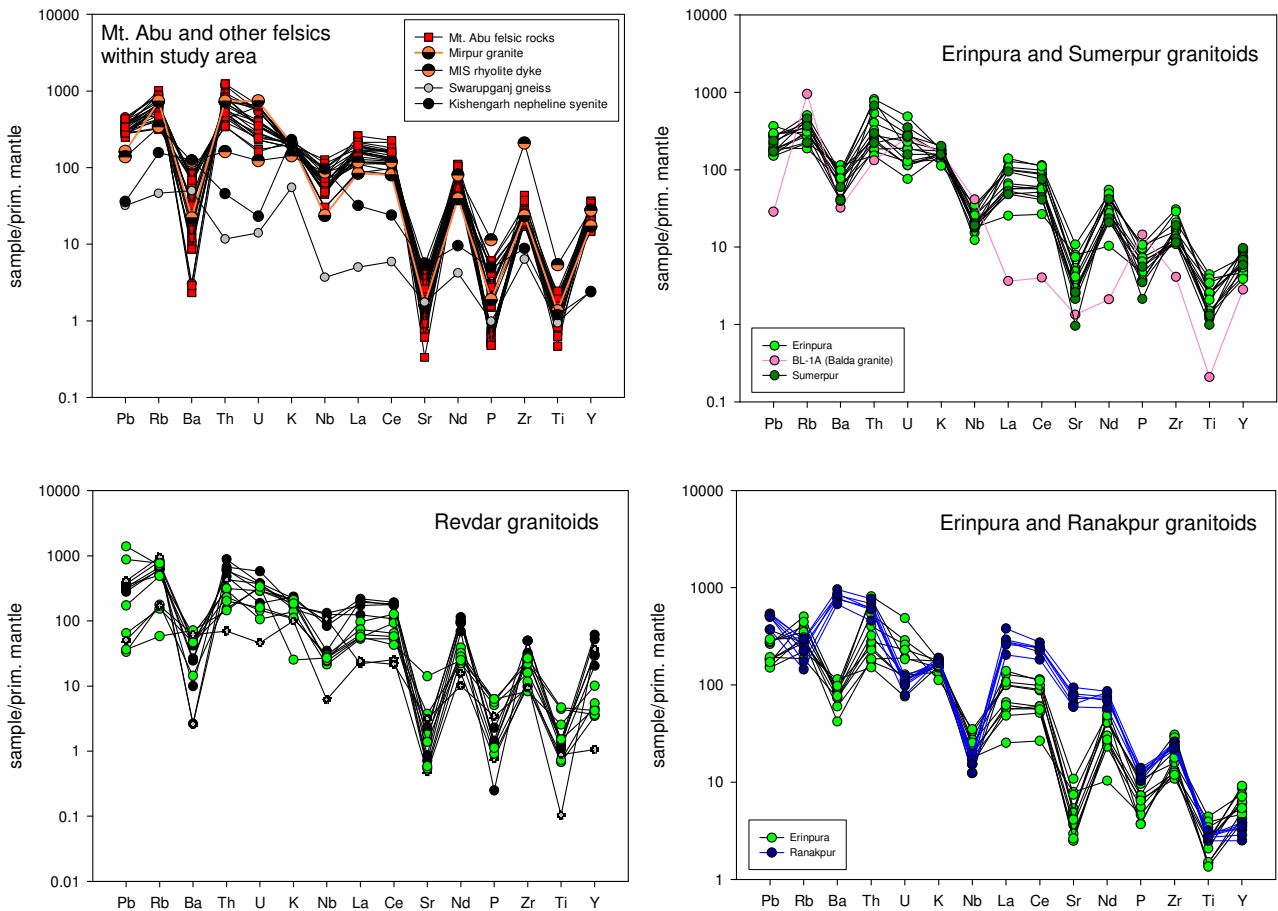


Figure 5.17. Spider diagram variation plots normalised to primitive mantle values for the various samples in this study. Elements in these plots are arranged from mobile and LIL on the left to less mobile and HFS on the right. Once again, there are discernable differences between the Mt. Abu, Erinpura and Ranakpur sample suites.

Revdar Rd. granitoids have been divided, on the basis of their REE plots, into three groupings. However, on the spider diagrams, these groupings are more subtle due to the fact that spider diagrams contain many different types of trace elements from LILE to HFSE to REE to immobile and mobile elements. Samples with Erinpura-like REE plots conform here to the Erinpura-type spider diagram, with lower levels of the more compatible (right side of the graph) elements and a more develop Nb-anomaly when compared to the samples labelled as more Mt. Abu-like.

These samples also follow the Mt. Abu trends in the shape and slope of their plots as well as relative depletion or enrichment of elements. The sample with the positive REE slope (La<Lu) has lower levels of the more compatible elements to the right of the spider diagram, but well-developed Sr, P and Ti anomalies. A slight positive Nb-anomaly is present, as Nb is enriched relative to the LREE. The pegmatite sample follows the general shape of Mt. Abu and Erinpura samples, although at lower levels of enrichment.

The Swarupganj Rd. granitoid and Kishengarh nepheline syenite have similar spider diagram shapes, although the nepheline syenite has a greater abundance of all elements, comparatively. Both are depleted in all elements in the spider diagram when compared to other samples. However, the Sr, P and Ti anomalies are present, which indicates Sr-removal from both magmas, possibly by plagioclase removal as well as early apatite and Fe-Ti oxide crystallization and removal. There is no negative Ba-anomaly, and K forms a positive anomaly. These make it likely that K-feldspar (microcline in the case of Kishengarh) has not been removed from either magma. The REEs and the radioactive elements are depleted, which may indicate less differentiation and partial melting of these samples.

5.5 Summary of Geochemistry

Mt. Abu granitoids

Mt. Abu granitoids and rhyolite dykes have a fairly restricted range in composition (66.60-77.73 wt % SiO₂) and are classified as alkali-feldspar granites, monzogranites or quartz-rich granitoids (excluding sample AA6-37, an augen gneiss classified as a alkali feldspar quartz syenite). There is good agreement between the modal and normative rock classification schemes. Both schemes suggest that Mt. Abu felsic rocks are more evolved than the other granitoids from this study. Most foliated varieties and all rhyolite dykes are peralkaline in nature, and are usually the most enriched in terms of silica content. These samples also have the most-well-developed Eu anomalies and usually the highest incompatible- and radioactive-element concentrations (Ba, Th, Pb) of the Mt. Abu samples. Conversely, they are usually the most depleted in terms of Fe₂O₃, TiO₂, CaO, Sr, Eu, P and Co when compared to other Mt. Abu samples. In the case of the rhyolite dykes, this may be taken as evidence of their highly differentiated nature (greater degree of fractionation and removal of early Fe-Ti oxides, Fe-rich silicates and Ca-rich plagioclase) within the pluton. The dykes are the late-stage fractionates of the magma, explaining their enrichment in the most radioactive and incompatible elements. This is also presumed to be the case for the foliated granitoids, as they also have most of the lowest relatively compatible element values (P, Co, Sr and Eu). The large amount of scatter within the diagrams of silica versus the above-mentioned elements may also be indicative of remobilization due to hydrothermal fluids released during emplacement or a later metamorphic event, as these elements

are highly mobile in aqueous solution. The presence of fluorite as an accessory in a few samples is another indicator of this later hydrothermal fluid movement event.

Mt. Abu samples have good negative linear correlations between SiO_2 (wt %) and most major-element oxides. Due to the restricted composition of the Mt. Abu samples and the lack of more mafic samples, these trends cannot be wholly dependent on fractional crystallization, but partial melting and/or magma mixing must also play a major role in the genesis and evolution of the magma. MgO , Na_2O and K_2O are generally level for all Mt. Abu samples, which may indicate a uniform enrichment of the source rocks of these samples, as well as there being a single source that contributed to these felsic rocks. The high-K calc-alkaline to shoshonitic nature of the Mt. Abu granitoids suggest source rocks anomalously enriched in K and other incompatible elements (Roberts & Clemens, 1993), borne out by the predominantly alkali-calcic nature of these felsic samples in the MALI diagram. This indicates a large crustal input for the Mt. Abu magma. Many HFS- and incompatible- elements (Zr, Nb, Ta, Y and REEs) show scatter but are enriched over other suites within this study. This enrichment may also be due to partial melting of an enriched source region.

The elements Sr, Ba and Eu decrease with greater SiO_2 -content due to a preference for earlier-crystallized Ca-plagioclase, biotite and K-feldspar, which are left behind in the source during partial melting. The correlation between CaO and Sr provides good evidence of this.

The maficity index (molar $\text{Mg}/(\text{Mg} + \text{Fe})$) trends for major- and trace-elements are usually the reciprocal of the SiO_2 trends for Mt. Abu samples. Unlike the Villaros et al. (2009) study, here the Mt. Abu samples are not positively correlated with refractory HFSEs, and instead of scatter expected amongst the elements in reactive minerals involved in melting (Rb, Sr, Eu, Ba), fairly good negative correlations are found. Since there is no good correlation between maficity and refractory elements in the Mt. Abu samples, this is taken as evidence of there being few refractory minerals (such as zircon, Fe-oxides and garnet) entrained from the source, unlike in the S-type granites of Villaros et al. (2009). This implies that the Mt. Abu granitoids are not S-type in nature.

The REE profiles are typical of crustally-derived felsic rocks where partial melting has enriched LREEs over HREEs (Bagas et al., 2010). The LREE slope is noticeably steeper than that of the HREEs, although when compared to Erinpura and Ranakpur samples, Mt. Abu samples are shallower. The relatively flat HREE slopes indicate a lack of garnet in the source, implying mid-to-shallow levels of melting (Villaseca et al, 2008). Well developed Eu-anomalies (ranging from $\text{Eu}/\text{Eu}^*=0.04-0.39$) also confirm early plagioclase removal and residuum in the source (Atherton & Sanderson, 1985). Weakly positive Ce-anomalies may be due to the presence of monazite in these samples, as it is preferentially partitioned into this mineral, or due

to the assimilation of weathered sedimentary-material, although there is no evidence for this. The Nb-depletion in the spider diagram is a typical crustal and subduction zone signature (White, 2007).

Erinpura granitoids

The Erinpura granitoids in the Streckeisen (1976) diagram plot across from plagioclase-rich to K-feldspar dominant granitoids. This diversity may be explained by their megacrystic nature and varying degrees of alteration; thus, the modal classification should only be used as a guideline. They are classed as monzogranites normatively, although two samples are more K-feldspar rich. They also have a lower average content and compositional range of SiO₂ (wt %) than the Mt. Abu felsic rocks. Similar to the Mt. Abu samples, these Erinpura granitoids are subsolvus, although they contain >10 % mafic minerals modally.

The majority of Erinpura granitoids plot along the metaluminous-peraluminous boundary, while the rest are strongly peraluminous. Normatively, all samples (excluding sample AA6-26) contain corundum, indicating Al-enrichment relative to Mt. Abu samples. Both the peraluminous nature and normative corundum are unlike Mt. Abu granitoids, and suggest S-type granitoid affinities.

For the majority of major element oxides, Erinpura granitoids have weaker correlations and are less linear compared to Mt. Abu samples, with the exception of MgO. The decreasing MgO with differentiation indexes SiO₂ and Rb may be due to these samples having not yet reached their steady-state saturation/concentration with respect to MgO. Since MgO-saturation is commonly reached early on in a magma's history, this implies that the Erinpura granitoids are less evolved than the Mt. Abu felsic rocks, although the silica content is similar. The weakness of the SiO₂-major oxide relationships may be due in part to processes other than fractional crystallization acting upon the magma (partial melting, magma mixing and entrainment of refractory and restite minerals) as well as a source composition that differs from the Mt. Abu felsic rocks. The Erinpura samples fall only within the high-K portion of the SiO₂-K₂O diagram, indicating that the source is likely enriched in K, although not to the degree that it is in Mt. Abu samples.

Erinpura samples display somewhat stronger relationships between the maficity index and major elements such as Al, Ti, Mn (positive trends) and Na (negative trend). Transition elements V, Co, Ni and Zn are all positively correlated with regards to maficity. These relationships may be indicative of a higher mafic component in the Erinpura magmas, or a greater proportion of restite (Fe-Ti oxides, mafic minerals) entrained (as these transition elements are compatible to only moderately incompatible), similar to the S-type granites of Villaros et al. (2009).

The average slope ((La/Lu)_N=19.89) of the REE diagrams for the Erinpura samples is steeper than that of the Mt. Abu samples as well as having lower overall REE-enrichment. The lower degree of enrichment may be

attributed to larger degrees of partial melting or a less evolved magma than that of Mt. Abu. The negative Eu-anomaly is well-developed, but on average smaller than those of the Mt. Abu samples. The HREE slope is much steeper than that of the Mt. Abu samples, and also slightly concave up, which indicates retention of hornblende in the source, unlike those of the Mt. Abu samples. It is therefore likely that the source of the Erinpura samples is different to that of the Mt. Abu samples. The Balda granite (BL-1a) is described as being the youngest phase of the Erinpura granite, but this is unlikely, as the REE profile is radically different and depleted in all REEs. It is also anomalously enriched in P, with no negative Nb-anomaly. This indicates that it is P-saturated, and there has been no previous removal of apatite. It has not been included within the Erinpura granitoids in this study. The shape of the spider diagram for Erinpura granitoids is similar to Mt. Abu, but with greater negative Nb-, and smaller Zr-, Ti- and P- anomalies. The lower Ba, Sr, P and Ti values may be attributed to lesser feldspar, Fe-Ti oxide and apatite removal, while the larger Nb-anomaly indicates a greater arc/crustal component.

Sumerpur granitoids

Sumerpur granitoids plot as syeno-to monzo-granites modally, similar to Erinpura samples. Normatively, their erratic An-content is reflected, as the three samples plot in three different areas of the diagram. These samples scatter within the Erinpura and Mt. Abu felsic samples, and are metaluminous in nature. They are usually also scattered within the Erinpura and Mt. Abu fields for all major and trace elements and only Rb and U are positively correlated with respect to SiO₂. In general, however, Sumerpur samples follow Erinpura trends in Harker diagrams. The REE plots follow the Erinpura trend, with the same degree of enrichment but a ((La/Lu)_N= 8.03) slope that is intermediate between that of the Erinpura and Mt. Abu samples. The main difference is that the Sumerpur samples have a flatter HREE slope than that of Erinpura samples. Eu anomalies are also similar to Erinpura and Mt. Abu samples. Sumerpur samples have similar shapes to the Erinpura granitoids in the spider diagrams as well. The major and trace element analysis, and modal data, point to these undeformed granitoids being related to the Erinpura deformed granitoids. The immobile REEs, in particular, show a similar pattern to the Erinpura granitoids. These may be late-stage intrusives of the Erinpura granite suite.

Ranakpur granitoids

Ranakpur granitoids scatter within the modal diagram of Streckeisen (1976), similar to Erinpura granitoids. Ranakpur granitoids have a very restricted range in composition, as well as being the least felsic from all the samples in this study. Conversely, they have the highest average Al₂O₃, TiO₂, MgO, CaO, Na₂O and P₂O₅ values of all samples in this study, which is indicative of their less fractionated/evolved character. Normatively, these subsolvus, metaluminous granitoids are quartz syenites, indicating a high K-feldspar component.

In major element Harker diagrams, these samples form a population distinct from all other granitoids in this study, and have weaker correlations than for the Mt. Abu samples, with the exception of MgO. These granitoids also plot within the high-K to shoshonitic sector of the SiO₂-K₂O diagram, reflecting an enriched source, although enrichment due to alteration cannot be ruled out, due to the weathered nature of most samples. The difference in Harker diagrams reflects a difference in source composition from all other granitoids in this study.

The elements Ba, Sr and Eu have the most elevated values of all samples in this study, while Rb is depleted relative to Sr. The high values of the above, together with the relatively high values for the more compatible elements (and conversely low Rb and U values), suggests a lesser degree of early plagioclase crystallization and removal as well as separation of the restite. This magma is thus more primitive in nature compared to the Mt. Abu and Erinpura granitoids. This may also be the reason for the poor relationship between CaO and Sr. The depletion in radioactive Rb and U, as well as the enrichment in more compatible elements such as Ca, Sr, V and Ni (which have good positive correlations with maficity), indicate that these samples are less evolved than those of Mt. Abu.

With regards to the maficity index, Ranakpur samples have uniformly good correlations for the major elements, excepting Al, which has a bell-shape. This may be due to initial high Al-concentration within the magma, which then saturates and crystallizes out a phase rich in Al. Ranakpur granitoids have good positive relationships between maficity and the more compatible elements, similar to Erinpura granitoids.

Ranakpur samples have REE diagram shapes that are distinct from all others within this study, implying a very different source region. They are enriched in LREEs above all other felsic samples and this, coupled with the large negative HREE gradient, gives them the steepest overall (La/Lu)_N slope. The steep HREE slope is an indication of garnet retention in the source (which may also be the Al-rich component crystallized out), and consequently higher pressures and lower depths of generation. The Eu-anomaly is very weak, another indication of less plagioclase in the source.

The spider diagram shows positive anomalies for Ba, and the deepest negative Nb-anomalies of all in this study, while the LREE La and Ce are highly enriched. The well-developed Nb-anomalies offer strong evidence of a subduction origin for these granitoids Ba is enriched over Rb and Sr, indicating very little early K-feldspar or biotite removal.

Revdar Rd. granitoids

Modally, the majority of Revdar Rd. granitoids are alkali-feldspar granites, although three samples do not contain any k-feldspar and plot accordingly. The modal and normative granitoid classification schemes are

in agreement for these granitoids. However, five samples also do not plot within any field of the Q'-ANOR diagram. This anomalous behaviour may be due to alteration within the samples. Samples are metaluminous in nature, while others are strongly peraluminous (with normative corundum), and one is weakly peralkaline. The majority of granitoids are subsolvus as well.

With regards to major elements, Revdar Rd. samples show the usual granitic trend of decrease as SiO₂ increases, although the goodness of correlation varies. The majority of samples fall within the high-K field of the SiO₂-K₂O diagram, similar to all other granitoids from this study area. Trace element concentrations are usually variable and no trends can be discerned, with the exception of Rb (weakly positively correlated) Eu and Sr (weakly negatively correlated).

Revdar Rd. granitoids show a division, some plotting on the Erinpura-slope and others on Mt. Abu-slope of the La vs. (La/Yb)_N graph. This separation may indicate a distinction between granitoid-suite types in this area. The relationship between MgO and Rb is quite linear in these samples, which could indicate that the magma has not evolved sufficiently in order to reach a steady-state concentration of MgO. The correlation with the maficity index is most similar to Mt. Abu felsic samples.

Revdar Rd. samples can be divided into three groups based on REE patterns. The distinction in the La vs. (La/Yb) diagram is here confirmed. The first major grouping is similar in shape and REE-concentrations to Mt. Abu samples, while the other major grouping is similar to Erinpura granitoids, with the characteristic steeper HREE-slope and lower LREE abundances. This division is borne out in the trace element concentrations as well. Abu- type samples have greater abundances (sometimes by more than an order of magnitude) of HFS and REEs. Erinpura-type samples are enriched in V and Co. The third group is anomalous samples, which have the lowest LREE abundances. The samples in this group have either a positive or negative overall (La/Lu)_N slope and their shapes do not conform to any of the other samples within this study. In terms of spider diagrams, Revdar Rd. samples generally follow their designations from the REE diagrams, although the difference is more subtle due to the greater variety of trace elements utilized.

Swarupganj Rd. granitoid

Modally, the Swarupganj Rd. granitoid is a monzogranite, while the geochemical classification places it within the syenogranites field due to a higher orthoclase component. In major element vs. silica diagrams, it usually plots within the Mt. Abu field, but in trace elements it usually plots towards the bottom of graphs (generally low abundances) with the exception of V, Ni and Rb. In the REE plot, it has the lowest abundances of all REEs (enriched less than 10x over chondrites), with a slight enrichment of LREEs over HREEs. The shape is concave-up in the MREEs, indicating hornblende as well as plagioclase left behind in the source (a slight negative Eu-anomaly is also present) and a very different source magma to any other

granitoids within the area. In the spider diagrams, there is no negative Ba anomaly, while K is enriched, indicating K-feldspar is retained within the sample and has not been crystallized out. The depletion in the REEs may indicate that this sample's magma has not undergone much partial melting or fractional crystallization and is therefore relatively unevolved.

Kishengarh nepheline syenite

This sample is classified as a nepheline syenite under both modal and normative granite nomenclature schemes, as it contains nepheline and is silica-undersaturated. The abundance of alkali elements in this sample classifies it as peralkaline. Rocks that are peralkaline in nature, particularly felspathoids, are usually formed in extensional environments such as continental rifts and ocean islands, but also in supra-subduction positions within subduction zones. High Ba and moderate Sr values suggest less microcline and plagioclase feldspar fractionation occurred from this magma. The REE diagram shows that it is moderately enriched over chondrites, and has a positive $(La/Lu)_N$ slope. The positive Eu-anomaly indicates plagioclase retention in the samples and implies lesser fractionation of the magma. The depletion of MREEs in comparison to HREEs is indicative of hornblende also retained in the source. The spider diagram also suggests lesser differentiation when compared to other samples in the study.

6. U-PB GEOCHRONOLOGY

U-Pb dating on zircons is the most robust method of age-dating available (Corfu et al.; 2003; Allègre, 2008; Faure & Mensing, 2005; Dickin, 2005). Zircons preserve and record the sometimes complex magmatic and metamorphic history of samples, which are vital clues to understanding the genesis of a rock sample. They are so widely used in geochronology because they can survive most magmatic, metamorphic and erosional processes that destroy/completely reset other, less robust, minerals (Corfu et al., 2003). Macroscopically, qualities such as clarity, amount and type of inclusions, fractures and external morphology are observed using a binocular microscope. Cathodoluminescence (CL) and backscatter-electron (BSE) imaging of zircons have been invaluable in identifying certain features of zircons such as magmatic and metamorphic zoning, fracturing and annealing, inclusions, cores and disturbances within single crystals (Corfu et al., 2003).

Seven samples from the study area were dated (Table 6.1) using U-Pb zircon (TIMS) age dating. The U-Pb zircon geochronological results have been divided into three overall groups, based on age (all error ellipses are to 2σ). Results are shown in Table 6.2. All zircons are between 80 μm and 250 μm in diameter. The three Mt. Abu samples, which the results show are similar in age, constitute the younger group. The Erinpura, Revdar Rd. and Ranakpur granitoids have been grouped together because they are between ~70-110 m. y. older than the Mt. Abu granites. The Kishengarh nepheline-syenite dated is distinctly older than either of the former groupings.

Table 6.1 Samples utilized in U-Pb zircon (TIMS) age-dating.

SAMPLE DATED	FELSIC SUITE	DESCRIPTION
AA6-18	Erinpura	Augen gneiss
AA6-2	Ranakpur	Massive granitoid
AA6-38	Revdar Rd.	Mylonitic gneiss
AA6-14B	Mt. Abu	Massive orange-pink granite
AA6-9	Mt. Abu	Foliated granite
AA6-35	Mt. Abu	Augen gneiss
AA6-52A	Kishengarh	Nepheline syenite gneiss

Table 6.2 Results of ID-TIMS U-Pb zircon analysis.

Type Rock	Fraction Analysed	Properties	Weight	Pb(t)	U	Th/U	Pbc	Pb	²⁰⁶ Pb/ ²⁰⁴ Pb	²⁰⁷ Pb/ ²³⁵ U	2σ	²⁰⁶ Pb/ ²³⁸ U	2σ
									(common)				
Abu (zircon)	AA6/14B	Z1	1	79	579	0.67	0.00	1.5	3042	1.10483	0.00630	0.12407	0.00064
	AA6/14B	Z 10 GR	12	47	337	0.70	0.17	4.1	7647	1.11256	0.00511	0.12473	0.00056
	AA6/14B	Z 19 GR	8	58	424	0.69	0.19	3.6	7326	1.09409	0.00266	0.12301	0.00026
Abu (zircon)	AA6/9	Z 19 GR	22	14	101	0.75	0.02	2.5	6985	1.11548	0.00431	0.12490	0.00044
	AA6/9	Z 8 GR	12	49	357	0.72	0.19	4.3	7697	1.10572	0.00382	0.12372	0.00037
	AA6/9	Z 7 GR	12	9	69	0.81	0.02	2.2	2849	1.08012	0.00471	0.12072	0.00045
	AA6/9	Z 37 GR	36	18	127	0.75	0.20	9.2	3871	1.10922	0.00281	0.12438	0.00027
Abu (zircon)	AA6/35	Z 8 GR	12	39	291	0.60	0.37	6.5	4180	1.10815	0.00415	0.12425	0.00043
	AA6/35	Z 27 GR	22	43	318	0.59	0.19	6.3	8766	1.12221	0.00474	0.12567	0.00048
	AA6/35	Z 13 GR	5	56	425	0.52	0.00	1.8	9307	1.10355	0.00273	0.12380	0.00027
Erinpura (zircon)	AA6/18	Z 1 GR	2	118	843	0.21	0.00	1.9	8001	1.34853	0.03547	0.14325	0.00375
	AA6/18	Z 15 GR	3	83	589	0.27	0.00	1.9	8257	1.34659	0.00402	0.14277	0.00038
Erinpura (monazite)	AA6/18	M 1 GR	1	5520	4618	24.41	0.92	3.0	15537	1.45910	0.00857	0.15833	0.00089
	AA6/18	M 4 GR	1	3107	1988	34.05	3.35	5.4	3538	1.41885	0.00571	0.15331	0.00061
	AA6/18	M 1 GR	1	821	920	20.28	7.04	9.2	876	1.24386	0.00918	0.13693	0.00082
Ranakpur (zircon)	AA6/2	Z 5 GR	5	48	318	0.55	0.05	2.3	6221	1.31359	0.01546	0.14145	0.00166
	AA6/2	Z 1 GR	1	106	674	0.85	0.00	1.4	4010	1.26876	0.00693	0.13711	0.00071
	AA6/2	Z 8 GR	2	163	1035	0.80	0.31	2.6	6803	1.28041	0.00715	0.13823	0.00073
	AA6/2	Z 3 GR	1	58	333	1.36	0.00	1.0	2791	1.24804	0.01149	0.13563	0.00140
Ranakpur (titanite*)	AA6/2	T 8 GR	70	48	97	8.71	4.82	339.6	186	1.23709	0.01053	0.13476	0.00047
	AA6/2	T 6 GR	92	59	118	9.01	5.48	506.7	198	1.22853	0.01646	0.13420	0.00089
Revdar Rd. (zircon)	AA6/38	Z 4 GR	1	25	161	0.71	0.37	2.4	588	1.24108	0.01338	0.13541	0.00072
	AA6/38	Z 8 GR	8	18	139	0.47	0.95	9.8	867	1.08792	0.00589	0.11887	0.00048
	AA6/38	Z 3 GR	1	326	2115	0.78	10.28	12.5	1427	1.22542	0.00519	0.13285	0.00038
	AA6/38	Z 2 GR	1	32	224	0.92	0.00	1.5	1219	1.13707	0.00796	0.12440	0.00062
Kishengarh (zircon)	AA6/52A	Z 1 GR	1	9	48	0.88	0.00	1.1	475	1.59598	0.02461	0.16026	0.00147
	AA6/52A	Z 14 GR	2	22	103	1.41	0.16	2.3	914	1.61336	0.01232	0.16238	0.00080
	AA6/52A	Z SBH-ANH 2GR	1	11	63	0.70	0.00	1.0	664	1.58973	0.01520	0.15983	0.00080
	AA6/52A	Z SB-AN 4GR	1	2	8	3.06	0.00	1.0	98	1.54784	0.10108	0.15563	0.00162
Kishengarh (titanite)	AA6/52A	TIT BR 2GR	40	10	14	5.10	2.73	117.2	88	2.79259	0.07149	0.23320	0.00117
	AA6/52A	TIT PBR 6GR	18	8	14	3.55	2.53	50.0	85	2.45689	0.06751	0.21278	0.00114

Type Rock	Fraction Analysed	Properties	rho	²⁰⁷ Pb/ ²⁰⁶ Pb	2σ	²⁰⁶ Pb/ ²³⁸ U (age, Ma)	2σ	²⁰⁷ Pb/ ²³⁵ U (age, Ma)	2σ	²⁰⁷ Pb/ ²⁰⁶ Pb (age, Ma)	2σ	Discordancy
Abu (zircon)	AA6/14B	Z1	0.89	0.06458	0.00017	754.0	3.7	755.7	3.0	760.8	5.4	1.0
	AA6/14B	Z 10 GR	0.87	0.06469	0.00015	757.7	3.2	759.4	2.5	764.4	4.9	0.9
	AA6/14B	Z 19 GR	0.92	0.06451	0.00006	747.9	1.5	750.5	1.3	758.3	2.0	1.5
Abu (zircon)	AA6/9	Z 19 GR	0.88	0.06477	0.00012	758.7	2.5	760.8	2.1	766.9	3.8	1.1
	AA6/9	Z 8 GR	0.90	0.06482	0.00010	752.0	2.1	756.1	1.8	768.4	3.2	2.3
	AA6/9	Z 7 GR	0.74	0.06489	0.00019	734.7	2.6	743.7	2.3	770.8	6.2	4.9
	AA6/9	Z 37 GR	0.91	0.06468	0.00007	755.7	1.5	757.8	1.4	763.9	2.3	1.1
Abu (zircon)	AA6/35	Z 8 GR	0.82	0.06469	0.00014	755.0	2.5	757.3	2.0	764.1	4.6	1.3
	AA6/35	Z 27 GR	0.96	0.06477	0.00008	763.1	2.7	764.0	2.3	766.7	2.5	0.5
	AA6/35	Z 13 GR	0.90	0.06465	0.00007	752.4	1.5	755.1	1.3	763.0	2.2	1.5
Erinpura (zircon)	AA6/18	Z 1 GR	0.99	0.06827	0.00023	863.0	21.1	866.9	15.2	876.9	6.9	1.7
	AA6/18	Z 15 GR	0.93	0.06840	0.00008	860.3	2.1	866.1	1.7	880.8	2.3	2.5
Erinpura (monazite)	AA6/18	M 1 GR	0.98	0.06684	0.00008	947.5	4.9	913.6	3.5	832.7	2.6	-14.8
	AA6/18	M 4 GR	0.79	0.06712	0.00017	919.5	3.4	896.9	2.4	841.6	5.3	-9.9
	AA6/18	M 1 GR	0.67	0.06588	0.00037	827.3	4.6	820.6	4.2	802.7	11.6	-3.3
Ranakpur (zircon)	AA6/2	Z 5 GR	0.98	0.06735	0.00015	852.8	9.3	851.7	6.8	848.8	4.6	-0.5
	AA6/2	Z 1 GR	0.89	0.06712	0.00017	828.3	4.0	831.8	3.1	841.4	5.3	1.7
	AA6/2	Z 8 GR	0.96	0.06718	0.00010	834.6	4.1	837.0	3.2	843.4	3.1	1.1
	AA6/2	Z 3 GR	0.82	0.06674	0.00039	819.9	7.9	822.5	5.2	829.6	12.2	1.2
Ranakpur (titanite*)	AA6/2	T 8 GR	0.62	0.06658	0.00046	815.0	2.7	817.6	4.8	824.6	14.4	1.2
	AA6/2	T 6 GR	0.59	0.06639	0.00072	811.8	5.0	813.7	7.5	818.8	22.5	0.9
Revdar Rd. (zircon)	AA6/38	Z 4 GR	0.48	0.06647	0.00063	818.6	4.1	819.4	6.0	821.4	19.6	0.4
	AA6/38	Z 8 GR	0.63	0.06638	0.00028	724.0	2.8	747.5	2.9	818.4	8.8	12.2
	AA6/38	Z 3 GR	0.76	0.06690	0.00019	804.1	2.2	812.3	2.4	834.6	5.8	3.9
	AA6/38	Z 2 GR	0.64	0.06629	0.00036	755.8	3.6	771.1	3.8	815.6	11.2	7.8
Kishengarh (zircon)	AA6/52A	Z 1 GR	0.65	0.07223	0.00085	958.2	8.2	968.6	9.6	992.4	23.7	3.7
	AA6/52A	Z 14 GR	0.70	0.07206	0.00039	970.0	4.4	975.4	4.8	987.6	11.1	1.9
	AA6/52A	Z SBH-ANH 2GR	0.60	0.07214	0.00055	955.8	4.4	966.2	5.9	989.8	15.5	3.7
	AA6/52A	Z SB-AN 4GR	0.53	0.07213	0.00436	932.5	9.0	949.6	39.5	989.7		6.2
Kishengarh (titanite)	AA6/52A	TIT BR 2GR	0.05	0.08685	0.00224	1351.3	6.6	1353.6	19.4	1357.2	49.0	0.5
	AA6/52A	TIT PBR 6GR	0.06	0.08374	0.00232	1243.6	6.5	1259.4	20.1	1286.6	53.0	3.7

*titanite recalculated using initial Pb from K-feldspar: ²⁰⁶Pb/²⁰⁴Pb = 17.755 (± 0.2%), ²⁰⁷Pb/²⁰⁴Pb = 15.735 (± 0.3%)

6.1 Older Samples (Erinpura, Revdar Rd. and Ranakpur)

These three samples are all are classed as Erinpura granite in much of the literature as well as on the Geological Survey of India, District Resource Map of the Sirohi District (1998). The Jawai dam, type-Erinpura augen gneiss and the Ranakpur quartz monzonite are ~60 km north and northwest, respectively, of Mt. Abu, while the Revdar Rd. mylonite is less than 10 km southwest of the granitoids sampled from the main Mt. Abu pluton.

6.1.1 Erinpura augen gneiss (AA6-18)

This is a sample of the type-locality Erinpura granite. It was chosen as a comparison to the Mt. Abu granitoids, which are stratigraphically equivalent on many geological maps of the region. The sample is an augen gneiss with well-defined light and dark bands. Zircons separated from this sample have a purplish hue and very few were free of inclusions or fractures (Fig. 6.1 A-C). The majority of zircons are prismatic, with slightly rounded-off face edges, similar to the Ranakpur sample (AA6-2). Older cores were suspected in some crystals (Fig. 6.1 D) as these had a faint outline within the crystal visible under the binocular microscope. Zircons were divided into groups based on morphology (as for all samples dated), with six analyses being completed.

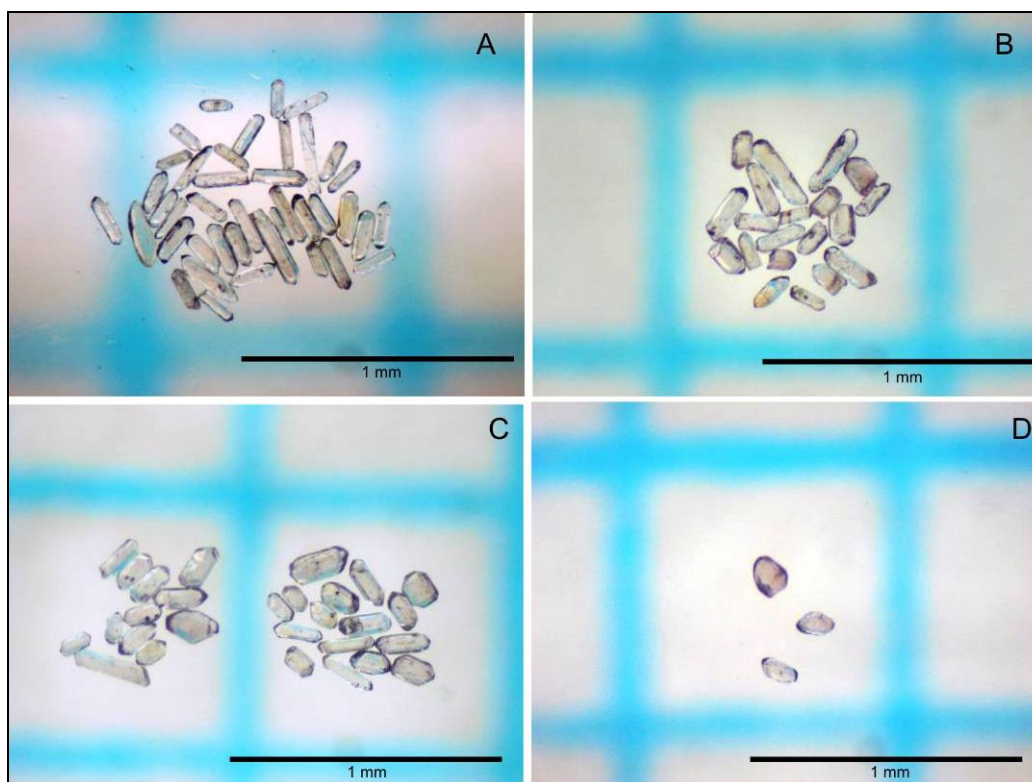


Figure 6.1. Zircons separated from the Erinpura augen gneiss. A, B and C show the different morphologies of zircon crystals analyzed with A being long prismatic, B being zircon tips and C being short prismatic. All show the characteristic rounded-off crystal faces and are riddled with inclusions. Some also have a yellow-tint. D shows three abraded crystals dated that were suspected of having older cores, whose rims are a slightly different colour to the rims of the zircons.

The first run of analyses showed a large degree of inheritance, with two error ellipses (consisting each of one single large zircon crystal) plotting very far to the right, off concordia (Fig. 6.2), although the error on their ages was minimal.

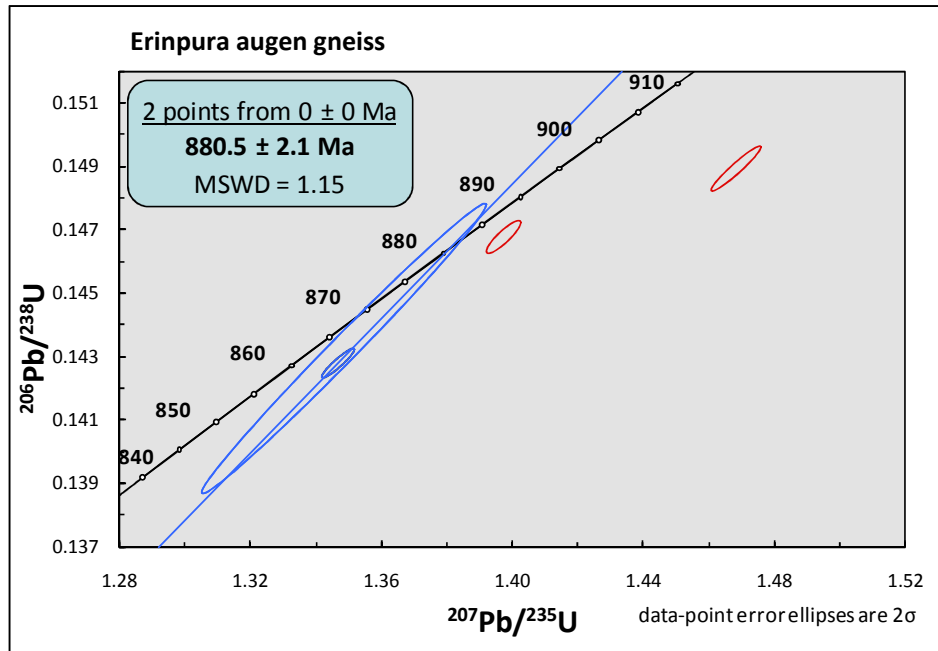


Figure 6.2. U-Pb zircon concordia age diagram for the Erinpura augen gneiss, utilising two near concordant points (blue ellipses) while the two ellipses outlined in red are discordant and zircons from these analyses may contain inherited U or Pb.

The remaining two analyses were (relatively) much closer to concordia as well as being younger in age. In order to reduce the effect of inheritance, only long-prismatic (LP) crystals (two groups, each with >10 zircons) were selected for the next analyses because these grains are less likely to contain cores (Corfu et al., 2003). This had the effect of reducing the size of the error ellipse, as well as bringing the analyses closer to concordia. Thus, the best two-point geochron generated gave a best-fit age of 880.5 ± 2.1 Ma when anchored at 0 Ma. The anchoring at 0 Ma was done to minimise effects of inheritance.

When ages were calculated using one point close to concordia and one from the assumed inherited component (highly discordant ellipse), the age of crystallization (lower intercept) of the sample is 875.3 ± 3.7 Ma, with an upper intercept of 1971 ± 23 Ma. This is assumed to be the possible age of the xenocrystic cores inherited from the source magma.

The backscatter-electron images of zircons from this sample do not unequivocally show relict cores, although one zircon fragment (Fig. 6.3 A) does show inhomogeneous dark and light domains and no magmatic zoning, which could be an indication of metasomatization within this sample. The zircon in Figure 6.3 (B) has what looks to be a light, U-rich core with a definite dark zone of oscillatory zoning surrounded by

a lighter outer-rim. Many zircons imaged show rim overgrowths, and what could be taken as a core. However, other zircons imaged displayed magmatic zoning, which increased the possibility of obtaining a meaningful age, and indicates zircon crystallization within the magma that these rocks formed from, and not inherited xenocrystic zircons.

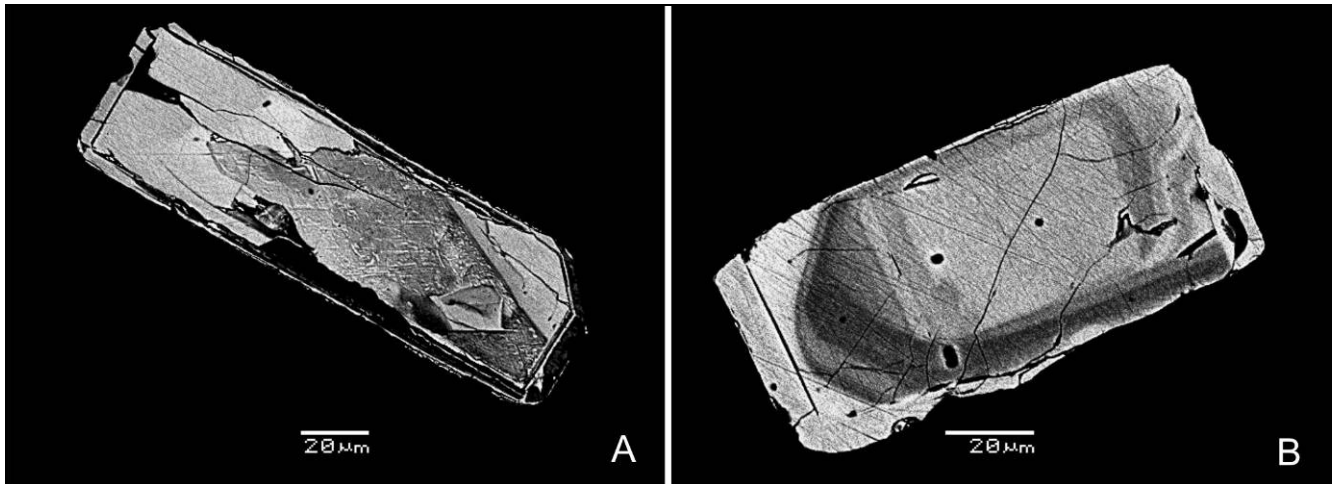


Figure 6.3. BSE images of the Erinpura granite zircons, showing morphological features. A- well-shaped zircon fragment (BSE image) with very inhomogenous interior. B- BSE image of short prismatic zircon showing lighter core surrounded by a much darker rim of oscillatory zoning which is in turn surrounded by a lighter overgrowth. The zoning is disturbed and seems to fade away.

Pale yellow monazite from the Erinpura sample (Fig. 6.4) was also separated, although the quality of the crystals was poor as most were murky and shot through with reddish-orange streaks, which are signs of alteration. The grains were also very friable as well as being opaque (or murky). Three analyses were done (two groups of smaller crystals and one consisting of a large, relatively clear crystal) with ages varying from ~800-842 Ma. These ages are not reliable, however, as all plot above the line of concordia due to excess ^{206}Pb (Fig. 6.5). Thus, only $^{207}\text{Pb}/^{235}\text{U}$ ages that are relatively near concordia should be utilised in interpretation.

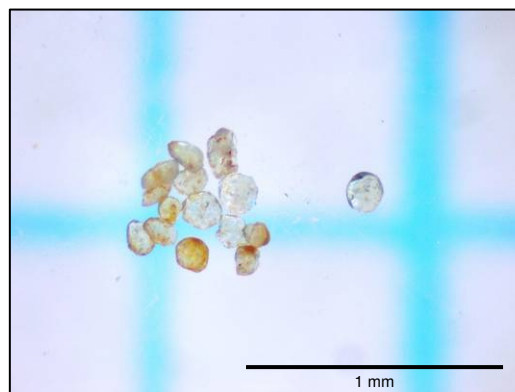


Figure 6.4. Monazite crystals separated from the Erinpura gneiss, some with characteristic half-moon morphology. The crystals are murky, with many fractures and reddish-orange alteration (fluid movement and metamorphism) streaks throughout. The monazite crystal to the far right is the most pristine, with a pale yellow colouring and very little alteration visible. All grains were extremely friable.

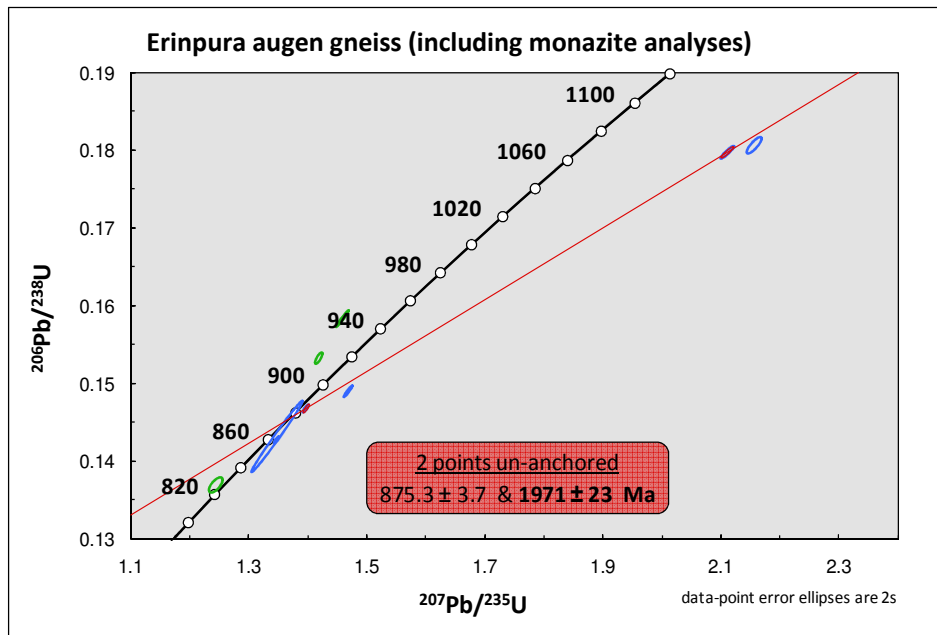


Figure 6.5. Erinpura gneiss zircon and monazite analyses. All zircon analyses are ellipses outlined in blue or red. The two red ellipses are those used to calculate an upper intercept age of inheritance for the zircons (one is near concordia, the other to the right, indicating a large inherited component). The monazites ellipses are outlined in green and are reversely discordant, falling above the concordia line. This is due to an excess of ^{206}Pb from the decay of ^{230}Th .

One monazite grain ellipse close to concordia (and therefore likely to be more reliable) gives a $^{235}\text{U}/^{207}\text{Pb}$ age of 820.6 ± 4.2 Ma (Table 6.1). The other monazites plot too far above concordia (reverse discordancy caused by excess ^{206}Pb from the decay of ^{230}Th) and are therefore not a true indicator of the age of the monazite crystals. The monazite is likely younger than the zircon, because although there is ambiguity in the data, none of the monazite ages are older than that of the zircons. It is also common for monazite to form during cooling after crystallization or metamorphism (Foster et al., 2002).

An upper intercept age of 1971 ± 23 Ma (Fig. 6.5) for a geochron between two analyses, one near to concordia and one from further off-concordia is the assumed age of the inherited component from the zircons.

6.1.2 Revdar Rd. mylonitic gneiss (AA6-38)

This sample was found in a riverbed cutting, south of the main Mt. Abu pluton, within the biotite schist and migmatite of the Sirohi Group (according to the 1998 Geological Survey of India, District Resource Map, Sirohi District).

It is a highly deformed mylonitic gneiss with alternating bands/laminations of ~ 2 mm thickness and augens of white feldspar. Zircon mineral separation techniques yielded very few zircons (~ 50 in total) with most of them being of poor quality (Fig. 6.6 B). Prismatic crystals were riddled with inclusions as well as striations

and most were not suitable for use in age-dating. Those picked were sorted into i) LP and ii) crystal tips and fragments. Each subset was then divided and used for dating. However, since the zircons were not prismatic and clear, the age data obtained was not as tightly constrained as other samples dated (Fig. 6.6 A-B).

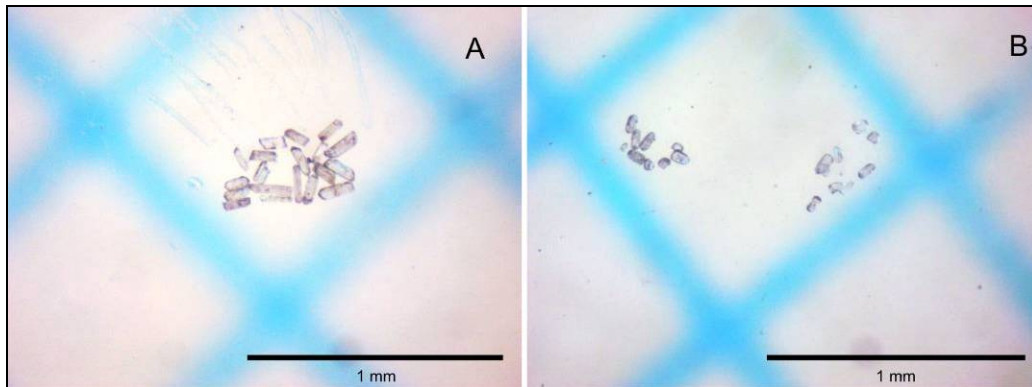


Figure 6.6. Zircons selected for age dating from the Revdar Rd. mylonite gneiss. A- Chosen long prismatic zircons, unabraded, showing a variety of internal colouration. B- long prismatic crystals abraded and separated according to clarity, with those on the left being less so.

Four initial analyses were performed. A second LP zircon analysis was done (in order to more accurately date the sample), but was discarded due to the large error ellipse. The zircons yielded a best age of 841 ± 21 Ma when anchored at 200 Ma (Fig. 6.7). The need to anchor the age indicates that this sample

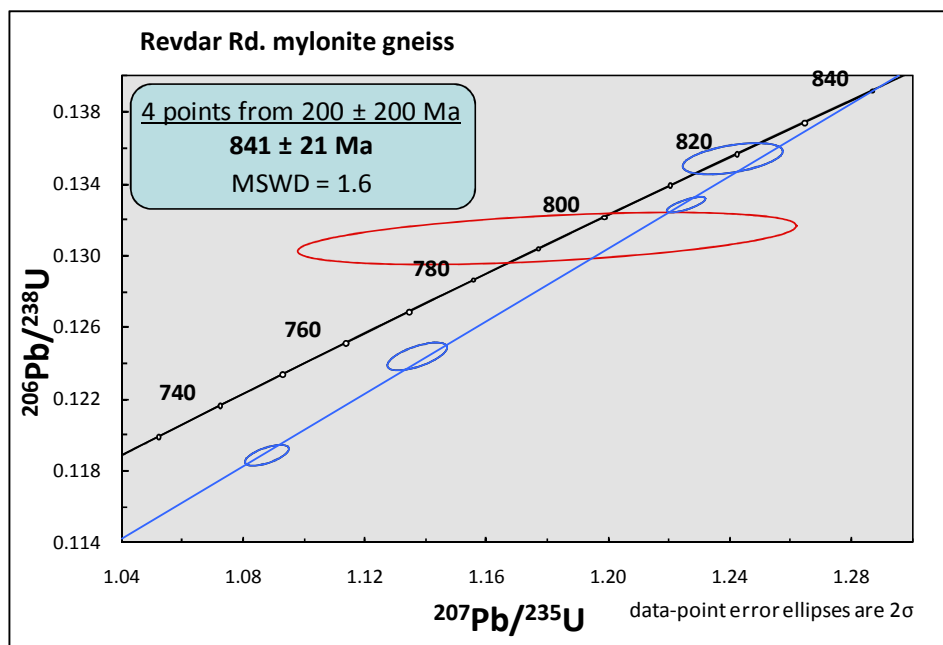


Figure 6.7. Concordia diagram for the Revdar Rd. mylonitic gneiss. Ellipses outlined in blue were used to calculate the age, while the red outlined ellipse had an error on the age of ~ 100 Ma and was therefore unsuitable for use in calculating the age of the sample.

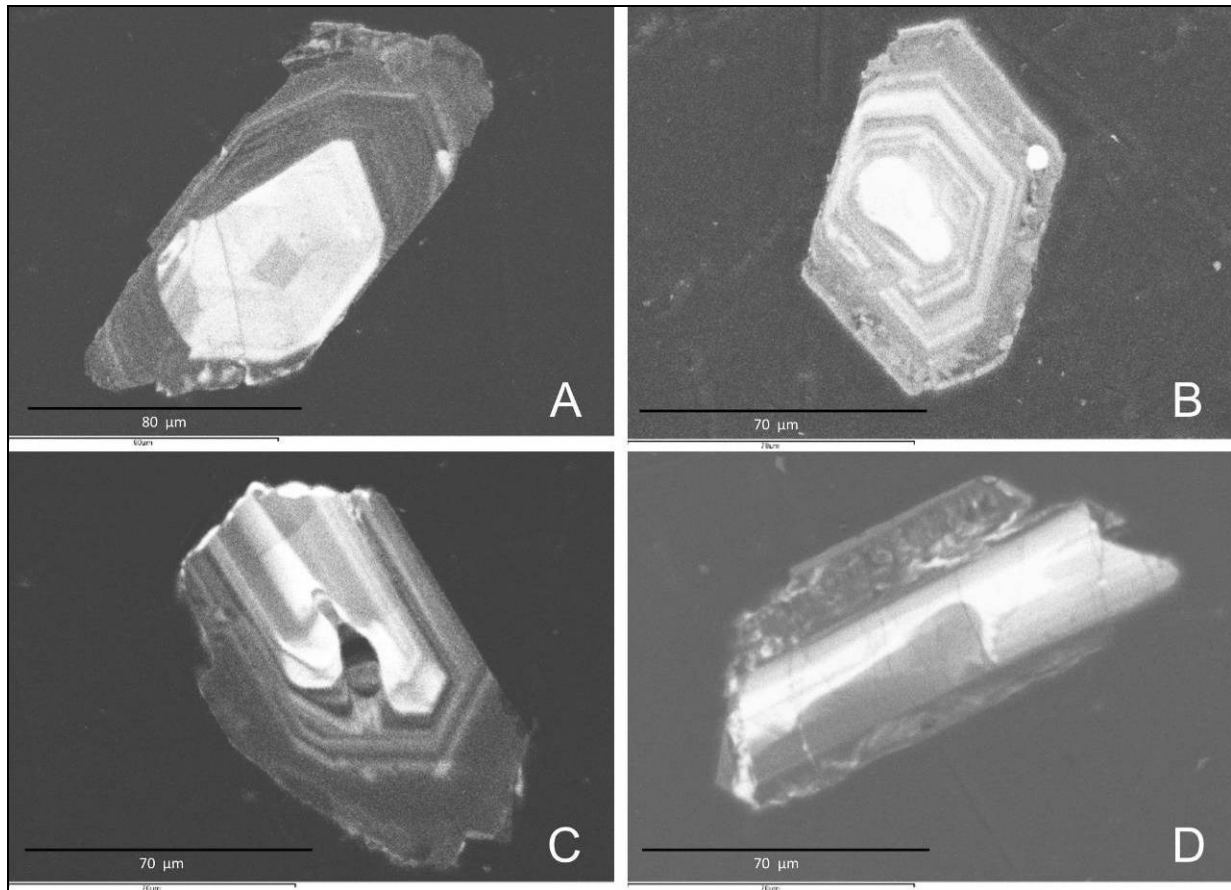


Figure 6.8. CL-images of zircons from the Revdar Rd. mylonite gneiss. A- darker-shaded core surrounded by bright material with a different crystallographic orientation to the outer edges of the zircon, which show magmatic zoning. B- Clearly showing a central relict core (transgressive across magmatic zoning). C- lobate-shaped zircon recrystallization/resorption in centre of grain. D- an irregular dark domain, probably recrystallization, transgressing into centre of grain as well as outer disturbed rim.

underwent a later metamorphic event that has reset the U and Pb in the zircons. CL images of zircons show (variously) younger rim-overgrowths (Fig. 6.8 A, C, D), relict cores (Fig. 6.8 B) and recrystallization of zircon material (Fig. 6.8 C, D: lobate growth of zircon into centre of zircon). These are all indicative of the zircons undergoing intense metamorphism and deformation post crystallization (Corfu et al., 2003).

6.1.3 Ranakpur massive quartz syenite (AA6-2)

This sample contained an abundance of long prismatic crystals, ideal for minimising the chance of choosing crystals with inherited cores. The zircon crystals are yellow-hued and retain their prismatic habit, although the slightly rounded-off crystal edges (Fig. 6.9) are indicative of some post-crystallization modification (dissolution).

The zircons were divided into long-prismatic (LP), short-prismatic (SP), as well as zircon tips subsets (Fig. 6.9 A-B). The least-inclusion-riddled and clearest LP and SP zircons were chosen for analysis because there was no visible evidence of cores in either subset.

Six analyses were performed and one (consisting of LP crystals) was discarded as it fell above the concordia line. Another analysis utilising crystals from the same group of LP zircons was done, which plotted on concordia. An analysis consisting of a group of 11 SP zircons was discarded because it fell much further off concordia than the rest. This was probably due to an inherited component as there is a greater chance of cryptic cores in crystals with this short, stubby morphology (Corfu et al., 2003).

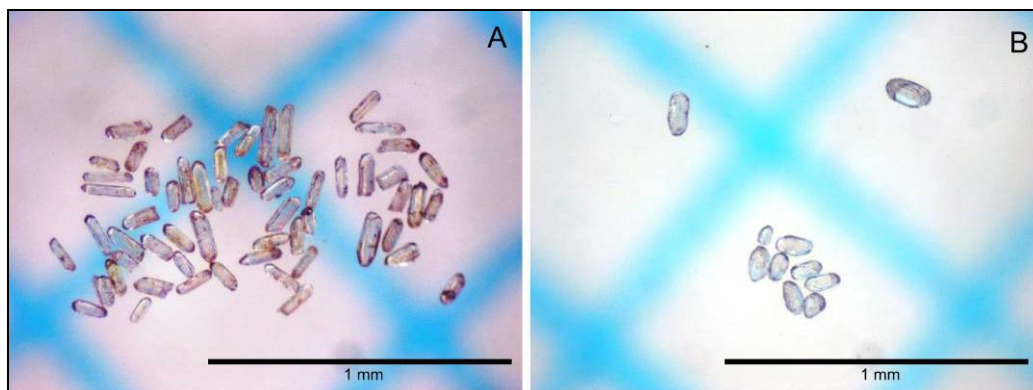


Figure 6.9. A- long prismatic zircons chosen for abrasion, all with a yellow tint and rounded-off edges. B- short prismatic zircons that have been abraded and divided according to clarity.

The four analyses deemed acceptable yielded an age of 848.1 ± 7.1 Ma (MSWD = 0.72), with a lower intercept age of 370 ± 260 Ma (Fig. 6.10), which may indicate a post-magmatic metamorphic event.

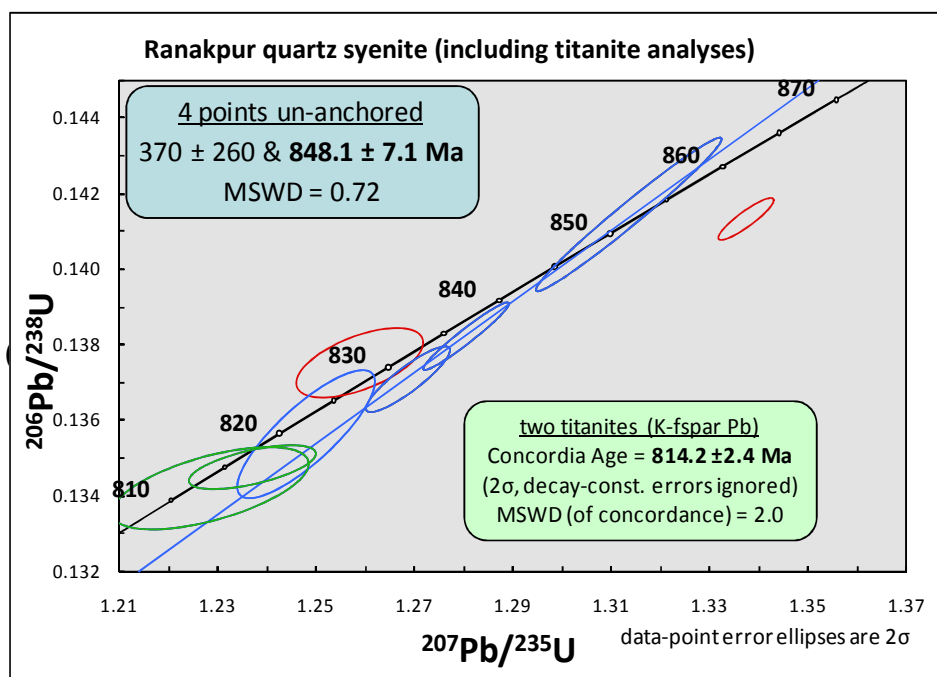


Figure 6.10. The U-Pb concordia age for the Ranakpur quartz syenite, where the ellipses used to calculate the age of crystallization are outlined in blue, while the ellipses outlined in red indicate analyses that are discordant to a large degree or plot above the line of concordia. The ellipses outlined in green denote the titanite analyses ages (recalculated using K-feldspar Pb).

The CL images show magmatic zoning that has been highly disturbed (Fig.6.11A-B) as well as uneven rims that might be due to zircon dissolution or new growth due to metamorphism (Corfu et al., 2003; Hoskin & Schaltegger, 2003). Some fractures are also present. These could account for some of the discrepancies within the age data, as having been the cause of Pb-loss (Bowring & Schmitz, 2003; Corfu et al., 2003; Dickin, 2005).

Titanite is prevalent (Fig. 6.12 A-B), with grains varying from a light- to dark-amber. The darker the hue, the greater the levels of U for measurement, as a comparison of the two analyses shows. The analysis with fewer darker crystals contains a greater amount of U than the analysis with more lighter-coloured titanite. None of the grains have a distinct prismatic shape, but those chosen were free of inclusions and/or fractures.

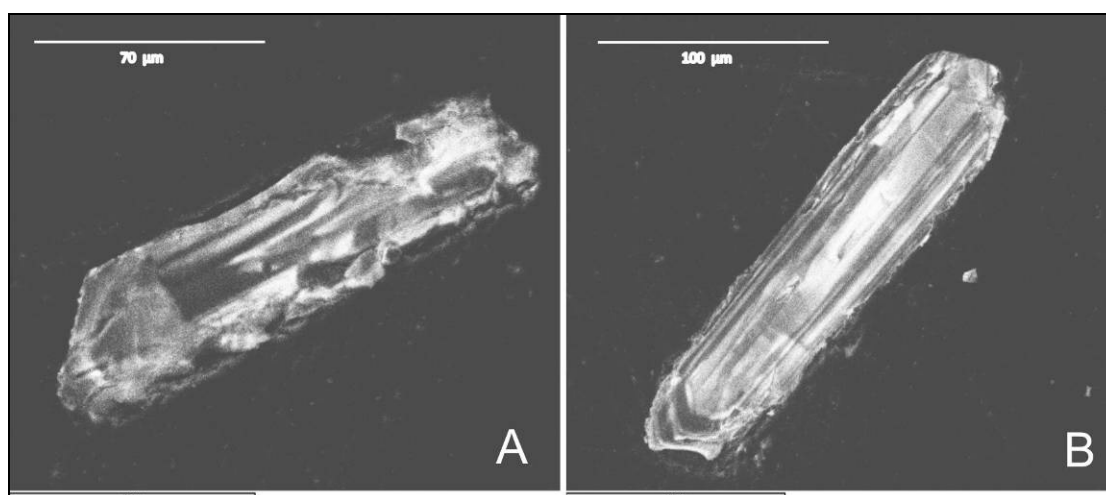


Figure 6.11. CL-images of zircons from the Ranakpur quartz syenite. A- zircon with disturbed domains, probably due to recrystallization of zircon. B- long prismatic zircon with magmatic zoning, showing partial disturbance and uneven grain boundaries.

Four analyses were run, which were divided into groups of lighter (comparatively less U) and darker grains. All were troublesome analyses, with no reduction of the error on the data although the number of measurements was increased. Hence, the error-ellipse for each analysis was correspondingly large. The large error on each analysis was not due to low U-content, as the lowest U-value was 97 ppm, high enough to give reliable data. However, the common Pb content in three analyses was found to be quite high (>300 ppm for all three) and may have been the cause of the inaccuracy in the age data. The ratio of radiogenic to common Pb is very important as well, as the smaller this ratio, the less sensitive is the analysis to common Pb (Bowring & Schmitz, 2003; Dickin, 2005). The inaccuracy in the ages (large error-ellipses) was decreased by using the initial-Pb readings calculated from K-feldspar grains of the same sample and substituting this common-Pb value for that in Stacey and Kramer's (1975) model. The K-feldspar likely incorporated the same initial-Pb as the titanite at formation. The difference is discernable, with both titanite points shifting to the left (towards concordia), resulting in a more accurate age.

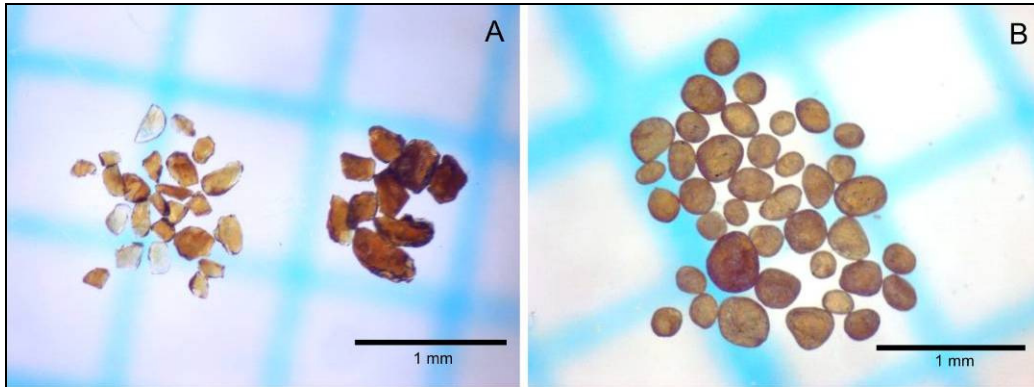


Figure 6.12. Titanite crystals separated from the Ranakpur quartz monzonite. A- Unabraded titanites separated according to colour. B- Abraded dark-coloured titanites that are relatively free of inclusions.

When the points are plotted, the titanites give an age of 814.2 ± 2.4 Ma, which is significantly younger than the zircons.

6.2 Younger Group (Mt. Abu pluton)

This group constitutes the three Mt. Abu samples dated in this study, which are all located within the main Mt. Abu pluton. This is a composite pluton, so the granitoids range from undeformed with no visible strain/deformation, to augen-gneiss in hand specimen.

Zircons in Mt. Abu samples show a common range in morphologies from stubby short prismatic to acicular and long prismatic crystals, with many zircon fragments consisting of the prism part of the zircons and tips, which are the terminal pyramids of zircons. Since there is little evidence in either CL-images or U-Pb concordia diagrams of inherited cores from older, more refractory zircon, this is interpreted as the source material having a composition that was undersaturated in zircon (i.e. little zircon crystallization occurred) or that zircon crystallized in the source was dissolute and recrystallized in the Mt. Abu magma (Corfu et al., 2003).

6.2.1 Mt. Abu granite with mafic mineral foliation (AA6-14B)

This sample is part of the main Mt. Abu pluton, and is a coarse-grained granite with elongated mafic clusters that define a foliation. In contrast, the type-granite of the Mt. Abu locality (sample AA6-9) is seemingly undeformed phaneritic pale-pink granite. These rock types are juxtaposed within the pluton, with contacts that are usually gradational or somewhat diffuse.

Zircons from this sample are prismatic, with sharp, well-defined faces. They contain a fair number of mafic and clear gas/liquid inclusions, which are problematic in zircons chosen for dating (Corfu et al., 2003) (Fig. 6.13 A-B). Zircons had to be abraded down very well to reduce the number of inclusions (Fig. 6.13 C). Zircons from this sample were also very clear and transparent. These were divided into whole crystals, tips and fragments subsets as well as those with suspected cores. Five analyses were run, and the results obtained reflected the relatively pristine nature of the zircons.

Two analyses were discarded due to their greater discordance, which was possibly caused by the amount of common Pb as well as analytical error. These analyses, the whole crystals group and the fragments group, could also have been affected by Pb-loss as can be seen by the analyses falling below the line of concordia (Dickin, 2005; Bowring & Schmitz, 2003).

An age of 763.2 ± 2.7 Ma was calculated for this sample (when anchored at 250 Ma) a best-fit age (Fig. 6.15). The CL images of SP-zircons from this sample reveal well-defined magmatic zoning (Fig. 6.14 A), while there is no evidence for cores, even in stubby crystals. However, as can be seen in Figure 6.14 (B) there is evidence of fracturing and what looks like annealing (fractures healed by new growth after a metamorphic event). These fractures also disturb the magmatic zoning, where, in the bottom-right of the zircon, the zoning has become diffuse and wavy. The fracturing may be the cause of the Pb-loss (Corfu et al., 2003).

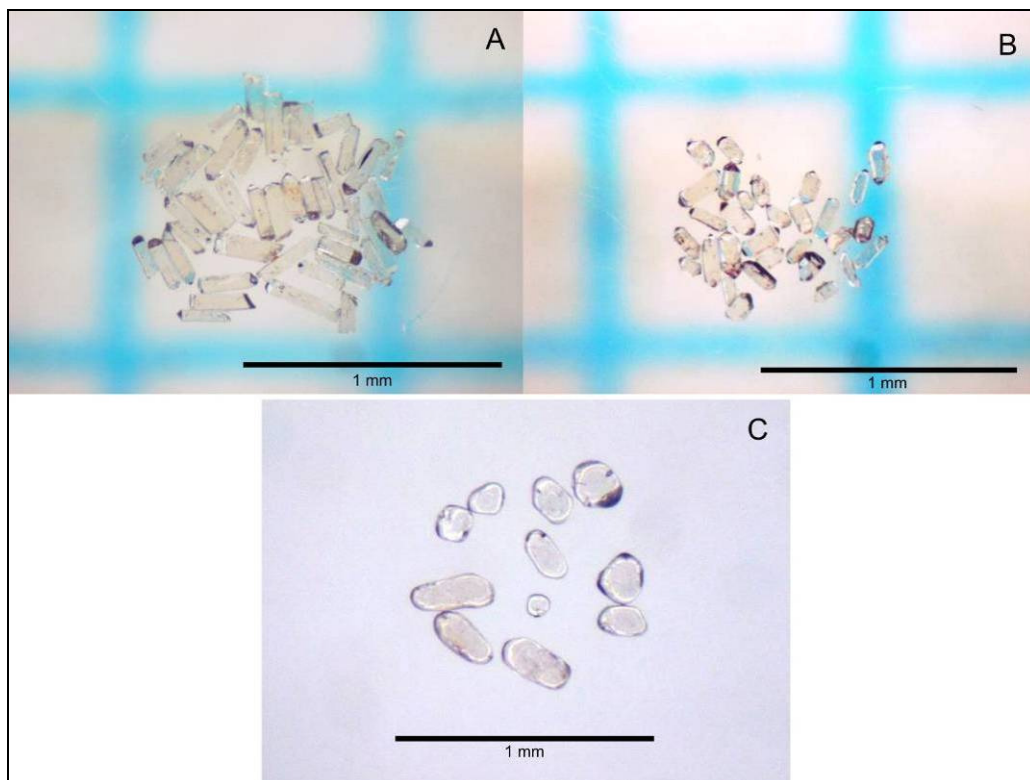


Figure 6.13. Zircons separated from the Mt. Abu foliated granite. A and B (short prismatic and long prismatic, respectively) contain some clear inclusions, but overall are quite transparent. C- Air abraded zircon tips, which have been abraded to reduce any alteration and fractures through grains and on rims.

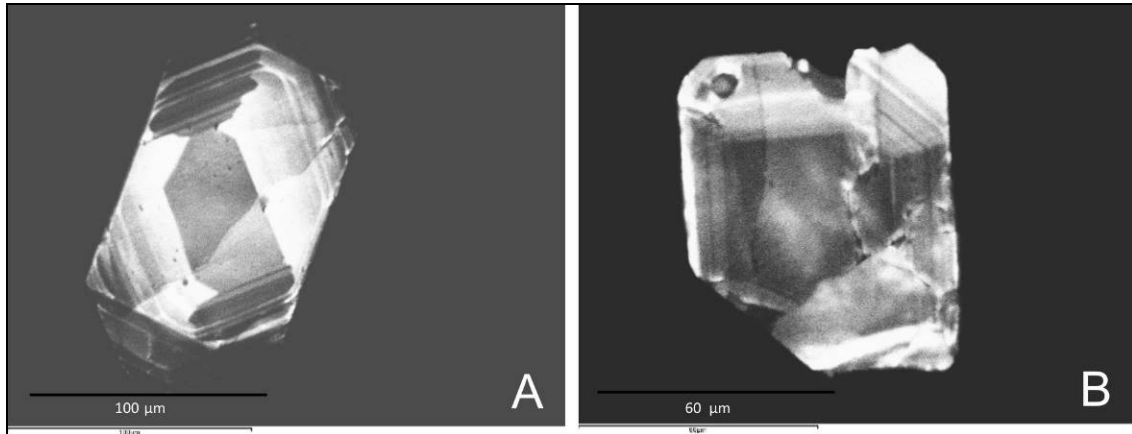


Figure 6.14. CL-images of zircons from the Mt. Abu foliated granite. A- short prismatic zircon showing good magmatic zoning. B- short prismatic zircon with annealed fractures on the right side of grain which have disturbed the primary magmatic zoning.

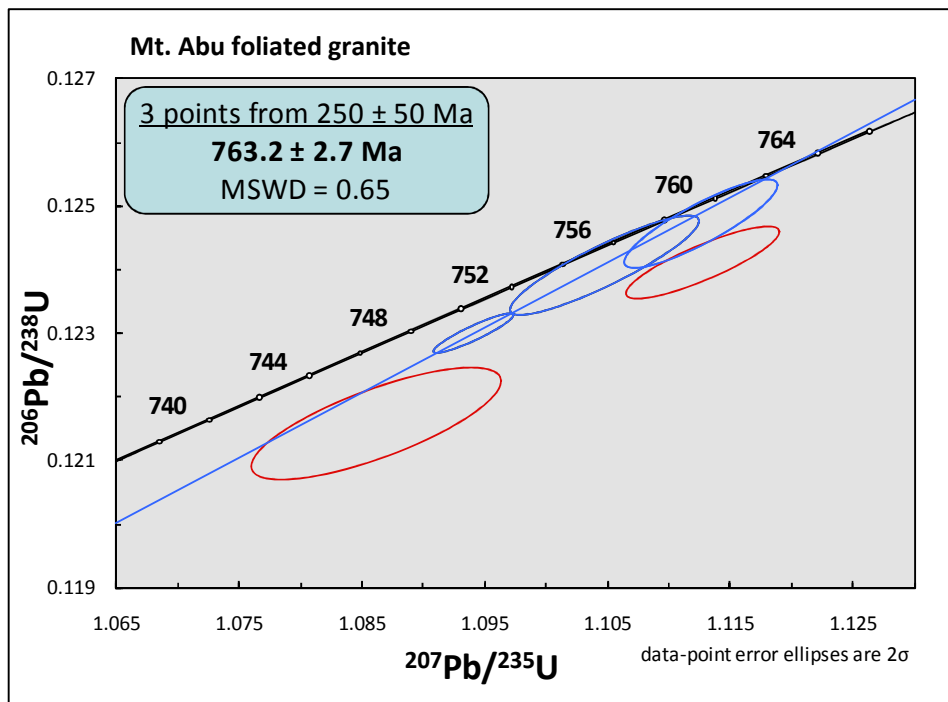


Figure 6.15. The U-Pb concordia age for the Mt. Abu foliated granite. The three ellipses outlined in blue were used to calculate the age of crystallization while the two ellipses outlined in red are more discordant.

6.2.2 Mt. Abu undeformed orange-pink granite (AA6-9)

This is the type-granite for the Mt. Abu pluton. It is phaneritic and undeformed massive, with randomly distributed feldspar, quartz and mafic minerals. The location of the sample is adjacent to other variably deformed phases of the pluton and the contacts sometimes show shearing and subsequent deformation and elongation of minerals in the rock close to the contact. However, contacts between granitoid-types are diverse and vary from diffuse to gradational and sheared.

Zircon morphology is similar to other Mt. Abu samples dated. Most zircons contain clear (maybe fluid) inclusions as well as more common mafic biotite or hornblende inclusions, but after being well-abraded, most of these defects were destroyed (Fig. 6.16). Five analyses were carried out on SP, tips, fragments and two LP subsets. To constrain the age more accurately, a second analysis was done. LP crystals were chosen, as they were shown in the previous round of dating to be highly concordant. Various permutations were carried out in the Isoplot plug-in for Excel (Ludwig, 2001) and the final age of formation was calculated as a four-point isochron anchored at 0 Ma. It yielded an age of 766.0 ± 4.3 Ma (Fig. 6.17), which is within error of the foliated Mt. Abu granite (AA6-14B).

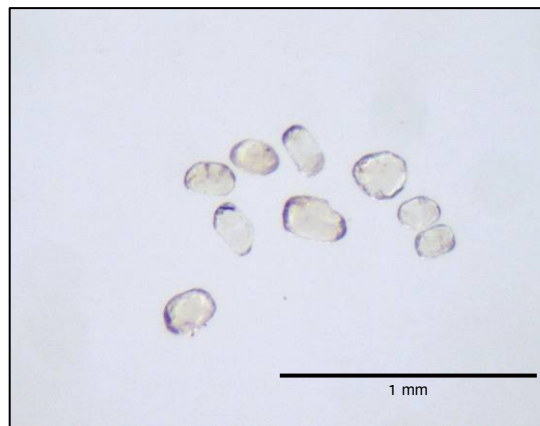


Figure 6.16. Air abraded prismatic crystals from the undeformed Mt. Abu granite; there are some variations in hue (a yellow tint). Most are clear and free of inclusions and fractures.

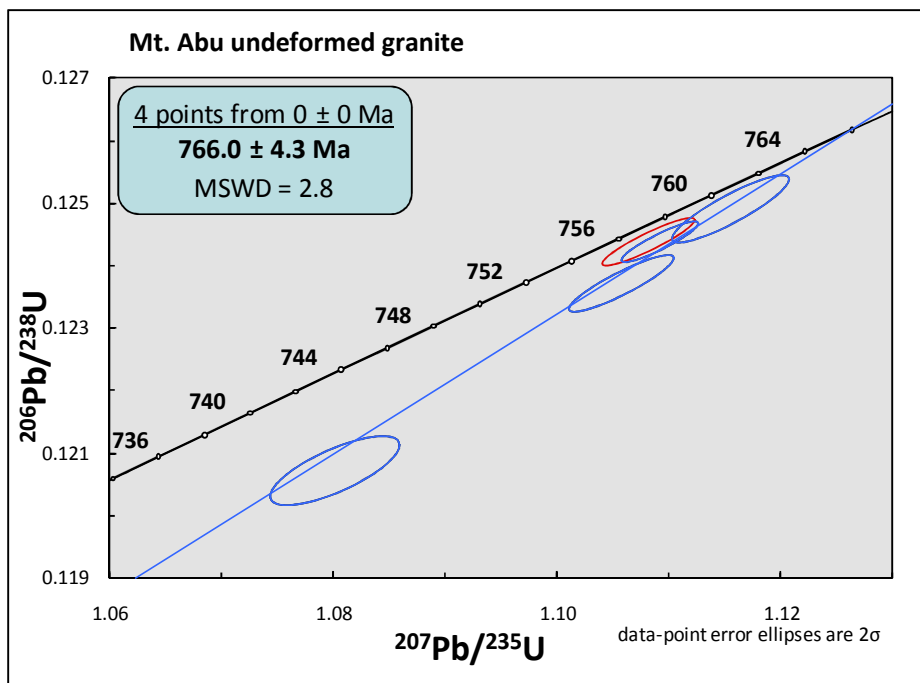


Figure 6.17. The U-Pb concordia age of the undeformed Mt. Abu granite. The four ellipses outlined in blue were used to calculate the crystallization age. The ellipse outlined in red increased the error on the crystallization age appreciably when combined with the others and was therefore not included in the age calculation.

Figure 6.18 (A) is a CL-image of a simple grain with a few bands of zoning, indicating that it is probably a magmatic zircon which is quite pristine. However, Figures 6.18 (B-D) do show fracturing with more luminescent material concentrated along the fracture, lobate growth, disturbed magmatic zoning along the outer edges and local recrystallization due to remobilization. These are indications of disturbance due to a later metamorphic event (Corfu et al., 2003).

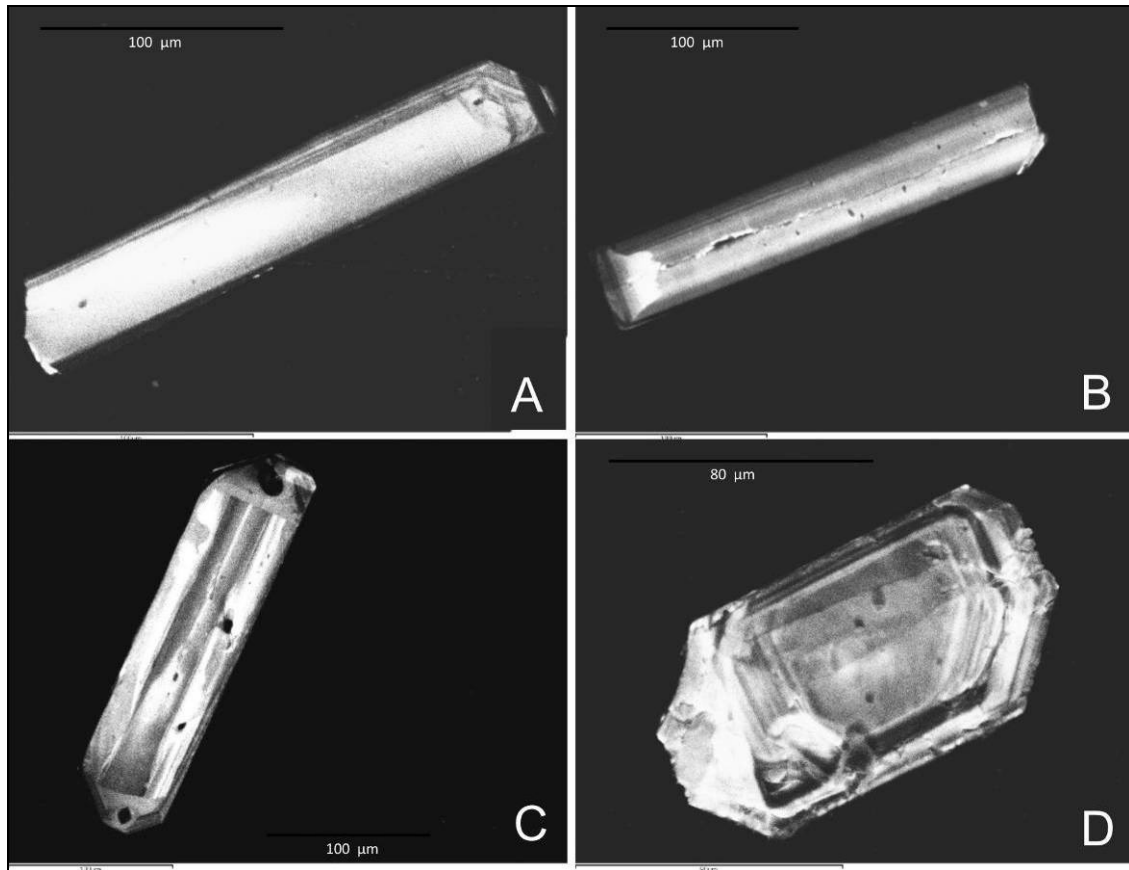


Figure 6.18. Zircons imaged using CL from the undeformed orange-pink Mt. Abu granite. A- long prismatic zircon with featureless interior and thin bands of zoning on edges. B- long prismatic zircon with fracture running lengthwise through crystal. The fracture seems to be annealed, with remobilisation along it (lighter edges). C- long prismatic zircon with recrystallization along margins, shown by lighter-coloured material in lobate structures as well as disturbed magmatic zoning. This grain also has inclusions at prism-edges. D- short prismatic crystal with visible disturbance of the magmatic zoning and growth due to local recrystallization.

6.2.3 Mt. Abu augen gneiss (AA6-35)

This is the Mt. Abu sample with the greatest amount of deformation. It is an augen gneiss with well-defined composite feldspar and quartz augens separated by micas and quartz.

Zircons separated from this sample are similar to both previous Mt. Abu samples, with well-defined crystal faces. Most crystals also contain inclusions and some are fractured, which made sampling of crystals for analysis challenging. As can be seen, even when abraded, most still contained a few clear inclusions.

Three groups (tips, fragments and LP crystals) were the first analyzed. Of these, the group analysis consisting of zircon tips (Fig. 6.20) was discarded because the error ellipse was too far off Concordia, probably due to Pb-loss or a component of inheritance, although the zircons were relatively clear with no visible inherited cores. Two more groups consisting of fragments and LP crystals were subsequently analyzed. An age of 767.7 ± 2.3 Ma was obtained with an isochron anchored at 250 ± 50 Ma (Fig. 6.19).

Figure 6.21 (A) shows a zircon fragment with fractures clearly radiating outward from an inner core. A CL image of the same grain (Fig. 6.21 B) shows a well-defined irregularly-shaped core with a more highly-luminescent outer shell. Magmatic zoning surrounds this area. Figures 6.21 (C-D) illustrate a zircon with a well-defined morphology; however, the interior of the zircon has been recrystallized in some areas (lobate growth into centre and wavy banding) and has many fractures. This is indicative of a zircon that has undergone a great deal of deformation during a later metamorphic event (Corfu et al., 2003).

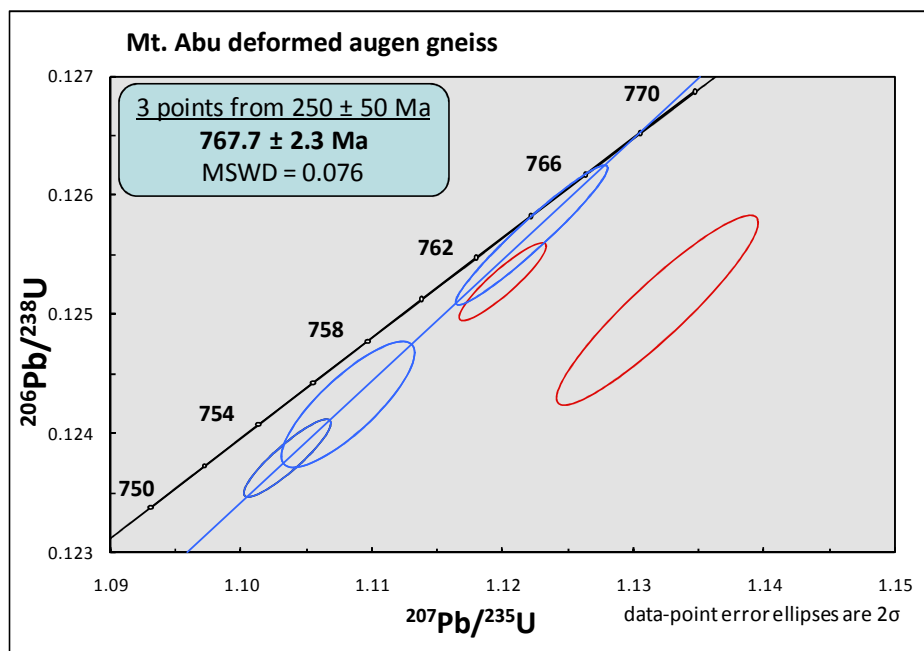


Figure 6.19. U-Pb concordia age for the deformed Mt. Abu augen gneiss. The two ellipses outlined in red were not used in the age calculation due to their greater degree of discordance.

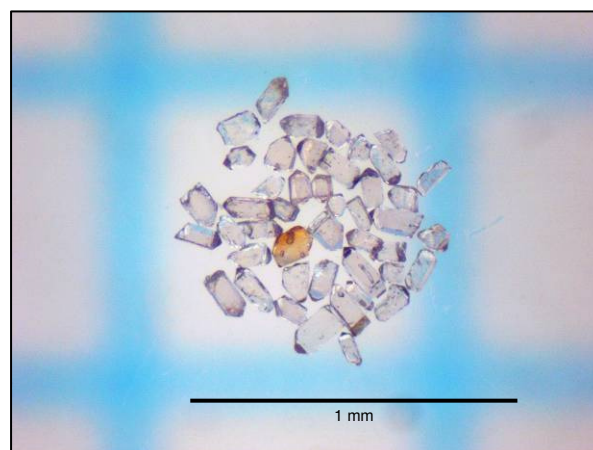


Figure 6.20. Zircon tip fragments from the deformed Mt. Abu augen gneiss. Many have mineral inclusions (hornblende or biotite) while others have clear inclusions.

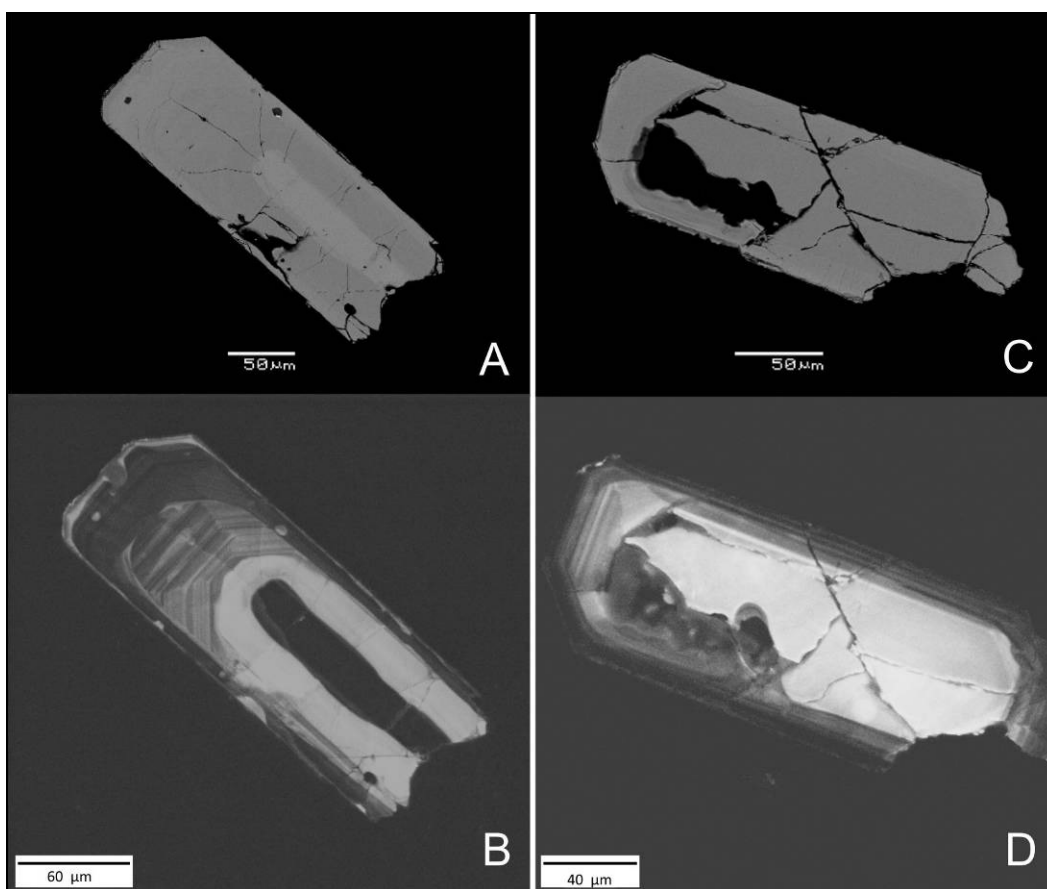


Figure 6.21. CL- and BSE- images illustrating the disturbed nature of zircons from the deformed Mt. Abu sample. A and B: zircon fragment showing faint fractures radiating out from a central core. This is made visible on the CL-image, which defines the dark, irregular inner core surrounded by a band of highly-luminescent material. This relict core has been overgrown and magmatic zoning is well-defined. C and D: zircon which is extremely fractured with a featureless interior (CL-image) which has been partially recrystallized (darker material in lobate forms).

6.3 Kishengarh nepheline syenite gneiss (AA6-52A)

This sample is part of the Kishengarh Nepheline Syenite Complex, approximately 100 km SW of Jaipur (and 300 km NE of Mt. Abu), in Rajasthan. This specimen is deformed with a visible fabric caused by mafic minerals that form a foliation throughout the sample, which consists of snowy-white nepheline as well as microcline (\pm plagioclase) feldspar.

Zircons from this sample were hard to distinguish, even after magnetic and heavy mineral separation. Most zircons were fragmented, not well faceted and turbid (Fig. 6.22 A). Many were murky and had many mafic inclusions, making it difficult to distinguish between large brown-hued zircons and titanite, although titanite was generally softer. Both larger (murky) and smaller (fewer inclusions and generally clearer) zircons were abraded (Fig. 6.22 B). Twenty-eight abraded zircons were recovered, of which fifteen were chosen for the first analysis. One large relatively clear zircon was separated for individual analysis while the

rest (smaller, without inclusions) were analyzed together. More zircons (two groups consisting of two and six grains each, respectively) were analyzed in the second round of analysis in order to get a good spread of ellipses for the concordia diagram.

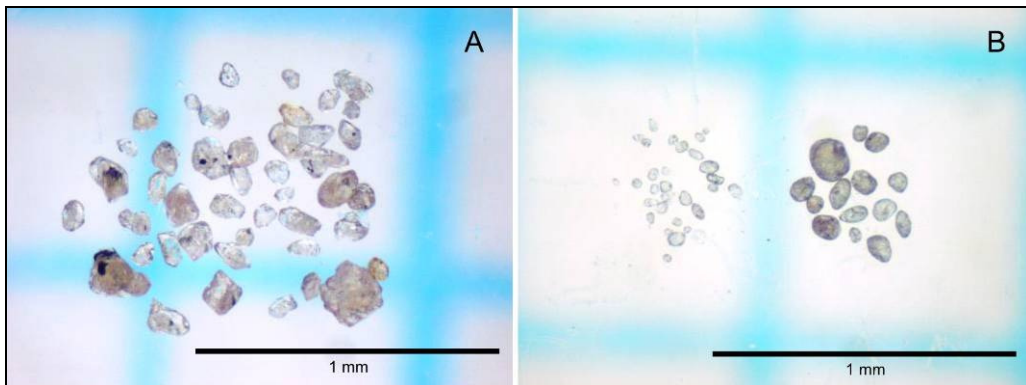


Figure 6.22. Anhedronal zircon fragments from the Kishengarh nepheline syenite. A- Unabraded zircon, most (especially larger crystals) with no distinct morphology, inclusion-riddled and murky. B- Abraded zircons chosen for analysis, with zircons to the left of the image being smaller and clearer with fewer inclusions, while those to the right of the image are larger and murkier.

Titanite (clear to a light rust-brown) was more abundant in this sample as it was found in both (magnetic and non-magnetic) fractions (Fig. 6.23 C). The majority were, however, riddled with biotite- and chlorite-inclusions (Fig. 6.23 A). Preference was given to darker-hued titanite (with the darker colour indicating enrichment on U), as these seemed to be the earliest, primary magmatic growth of titanite. Some of the titanites have darker cores and a lighter, (presumably) new growth of surrounding titanite (Fig. 6.23 A-B). Approximately a hundred were recovered from the abrader and thirty-two with the least inclusions were chosen and divided into two sets for analysis. These analyses, however, were problematic, as the measurements had large errors. During measurement, the loaded filaments behaved very erratically, resulting in an incomplete dataset for one analysis. Both analyses then had to be discarded, as the errors were so large as to make the ages meaningless.

Two subsequent titanite analyses (Fig. 6.23 D: consisting of two and six grains, respectively) were, however, successful and yielded near-concordant ages.

The results were calculated using the Isoplot plug-in for Excel (Ludwig, 2001), and the four combined analyses of the zircons give an age of formation of 989 ± 8 Ma (MSWD = 0.05) when anchored at 0 Ma (Fig. 6.24 A). When the two zircons and two titanites from the second set of analyses are combined and plotted together, the age of the zircons (lower intercept) is calculated to be a younger and more inaccurate age of 933 ± 21 Ma (Fig. 6.24 B). The upper intercept yields an age of 1365 ± 99 Ma (MSWD = 1.2). The error is large, due to the fact that although both analyses are close to concordia, their individual $^{207}\text{Pb}/^{206}\text{Pb}$ ages differ widely at 1357.2 ± 49 Ma and 1286.6 ± 53 Ma.

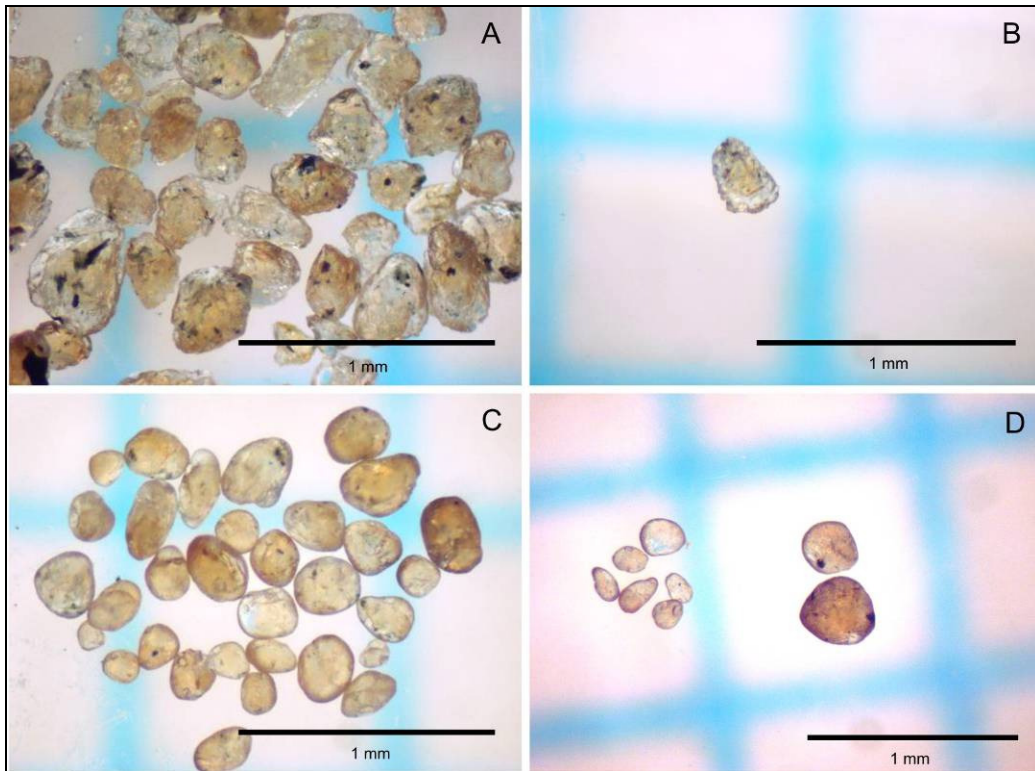


Figure 6.23. Various images of titanite separated from the Kishengarh nepheline syenite. A-inclusion-riddled titanite, many with distinct pale yellow cores surrounded by clear rims. B- A titanite with distinct core. C- Abraded titanite, many different hues/tones of colour. D- two groups of titanite, with LHS group much clearer and lighter in colour than the two grains to the right.

This combined age is taken as a minimum age of formation of the titanites. In this sample, the titanites are older than the zircons dated. This could be due to titanite inheritance (due to relict xenocrystic titanite cores which have been entrained) because as mentioned previously, some cores of a darker colour were visible.

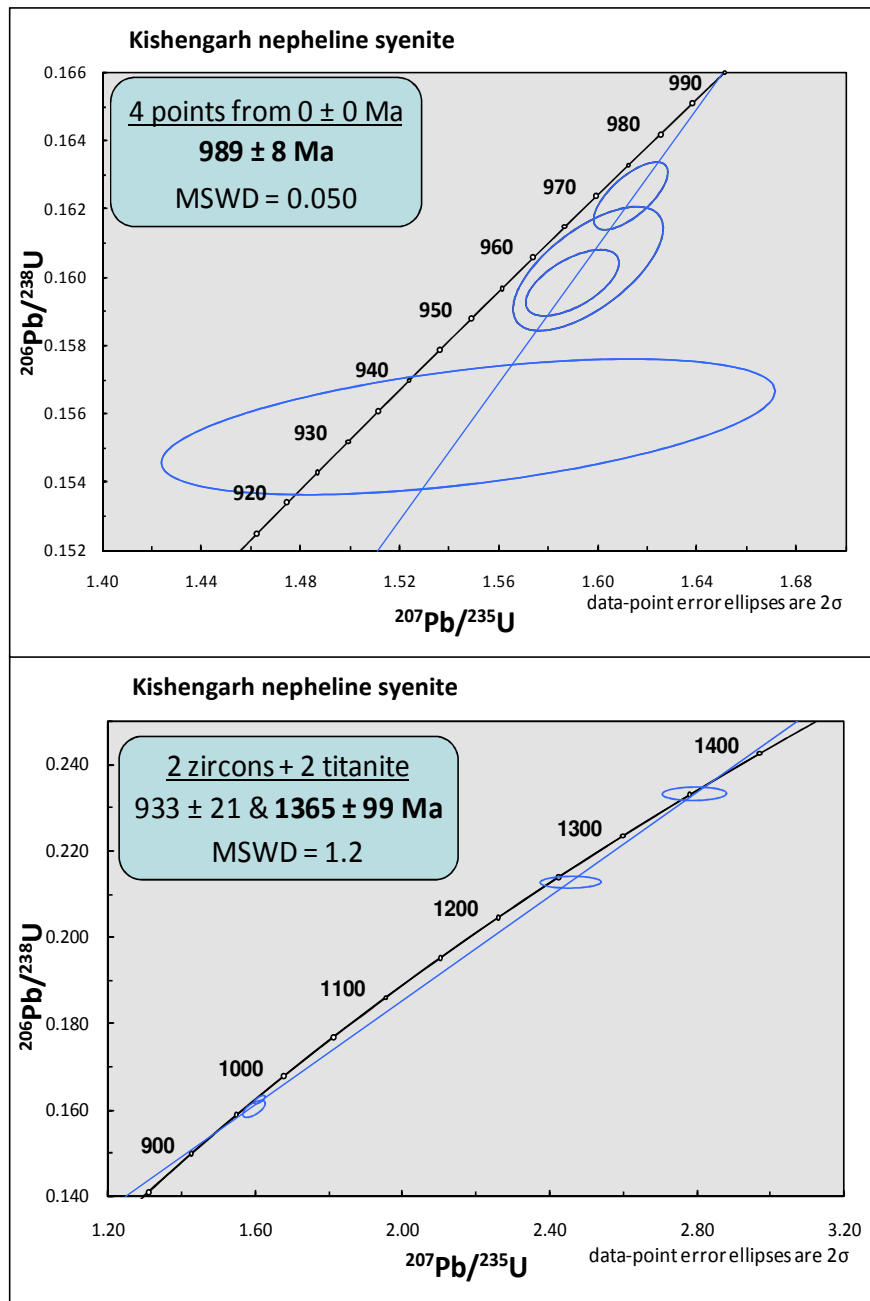


Figure 6.24. Concordia diagram age results for the Kishengarh nepheline syenite sample. A- U-Pb zircon concordia age for sample AA6-52A, utilising all four analyses. B- two near concordant zircon analyses (near the 1000 Ma mark on concordia) combined with the two titanite analyses (spread out above 1200 Ma on concordia) to give a minimum age for the inherited component within these zircons.

The other alternative is to assume that the titanites dated represent the minimum age of magmatic formation, with the zircons (younger, near-concordant age) being metamorphic or highly-reset due to a major (post-crystallization) regional metamorphic event. Conventionally, the upper intercept age of concordant titanite is interpreted to represent the age since first mineral growth or the resetting event that re-equilibrated the U-Pb isotopic system in the minerals (Tucker et al., 1987).

Generally, BSE and CL images (Fig. 6.25 A-C) of the Kishengarh zircons show them to be very anhedral and irregular, with few well-defined planes or pyramids. Zircons are typically fractured, with remobilization of Zr and other elements (such as U, Pb, REE, Hf) surrounding many fractures, induced by metamorphism (Corfu et al., 2003).

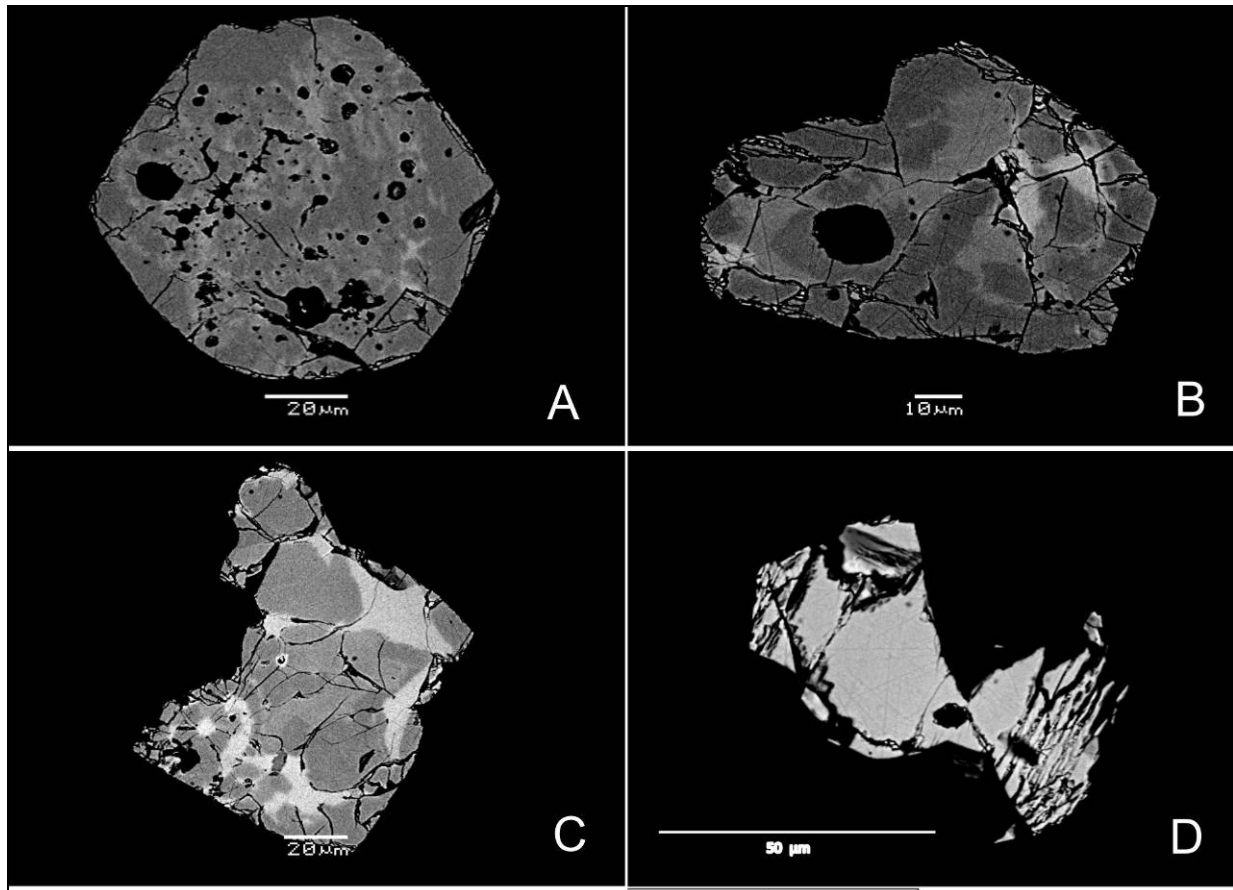


Figure 6.25. CL- and BSE- images of zircons from the Kishengarh sample. A- dissolution and fracturing throughout zircon. B- Very fractured zircon with disturbed domains (light and dark contrasts) as well as remobilization of elements around fractures. C- Concentration of highly-luminescent material around arcuate fractures within the zircon. D- This CL image shows what could be micro-veining on the edges of a zircon fragment and therefore high degrees of strain experienced during metamorphism.

Figure 6.25 (A) shows areas of fracturing and dissolution of the crystal. Figures 6.26 (A, B) show that original oscillatory zoning has been disturbed during metamorphism. Figure 6.25 (D) shows progressively greater amounts of shearing from the centre of the crystal to the sides, which are riddled with microveins that have annealed.

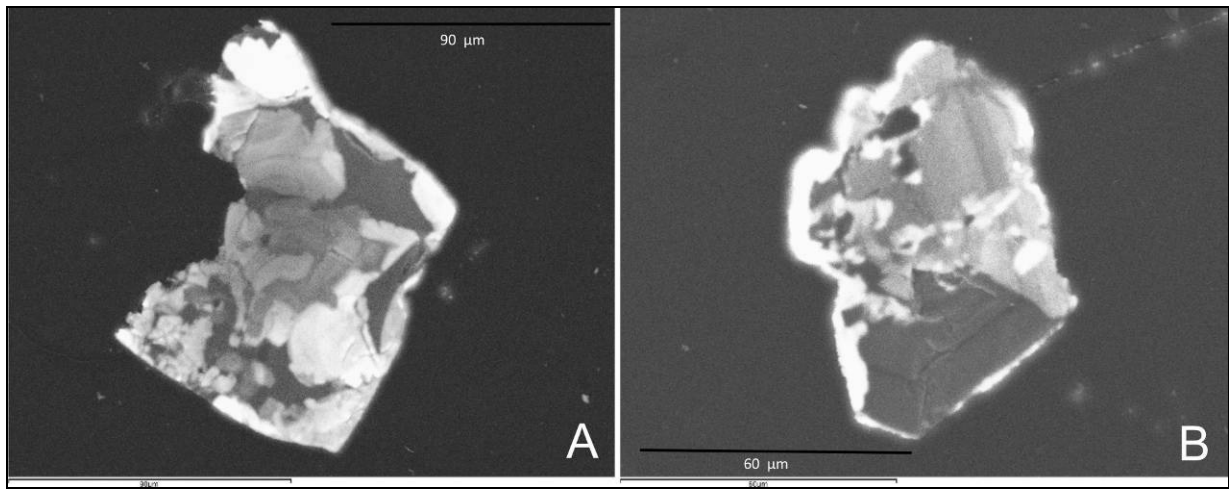


Figure 6.26. Kishengarh zircons that show interrupted and disturbed magmatic zonation. A- highly deformed, patchy and irregular convoluted zoning. B- disturbed and uneven oscillatory zoning as well as irregular zones of homogenous zircon, probably recrystallized.

6.4 Discussion

6.4.1 Erinpura, Ranakpur and Revdar Rd. granitoids

Zircons from all above-mentioned samples show evidence (CL- and BSE- images) of secondary disturbance varying from disturbed primary magmatic zoning to domains of recrystallization as well as microveins and fracturing. The analytical data also indicate Pb-loss and inheritance in many analyses. This is reflected in samples by analyses that are offset and below the concordia line due to subsequent Pb-loss. However, other samples also showed evidence of inheritance of older zircon cores with much older ages for the upper intercept and error ellipses that are far removed from the concordia line.

Two of the older group of samples (Ranakpur and Revdar Rd.) fall within error of each other (841 Ma and 848 Ma, respectively; Figure 6.27), although the Revdar Rd. sample has a large error on the age (21 Ma). It may thus not be related to the Ranakpur sample, as their geochemical signatures are very different. The Revdar Rd. mylonitic gneiss has similar geochemistry to that of the type-locality Erinpura augen gneiss, and may have formed in the latter stages of the same orogenic event.

The Erinpura augen gneiss does not fall within error of any other granitoid dated from this study. However, the two other older samples (the Ranakpur quartz monzonite and the Revdar Rd. mylonite), with ages of 848.1 ± 7.1 Ma and 841 ± 21 Ma, respectively, do fall within error of each other. This is due to the larger error on the age of the Revdar Rd. mylonite, where, due to the relatively poor condition of the zircons, a tighter and more accurate age could not be calculated. These two samples are ~60 km apart, one at the southern foot of the Mt. Abu pluton, and the other within the flatter area to the north and east of Mt. Abu.

The Ranakpur massive granitoid has never been correlated with any granitoids to the southwest of Mt. Abu in any of the previous literature. They have previously been grouped under the umbrella term 'Erinpura granite', as most authors refer to the regionally extensive Rb-Sr age dating done by Choudhary et al. (1984), which implies a single formative event at $\sim 800 \pm 50$ Ma for all granitoids south of Ajmer. This is not the case, as newer geochronological data show that most granitoids within this region range in age from ~ 1.1 - 0.75 Ga. The Ranakpur granitoids have subsequently been classified as part of the Ambaji-Sendra granite gneiss terrane of ~ 1.1 - 0.9 Ga time span (Tobisch et al., 1994; Deb et al., 2001).

The results of this study show that these two granitoids are related geochronologically, although they differ spatially, geochemically and compositionally as well as in their degree of deformation. The Revdar Rd. mylonite has also not been classified in any of the geological maps of the area, and this study shows that geochronologically, it does not belong to the Mt. Abu pluton granitoids. The similarity in ages between the Ranakpur quartz monzonite and the Revdar Rd. mylonite gneiss may indicate that a regional felsic magmatic event occurred at ~ 841 Ma. Other samples from Ranakpur (a diorite and metagabbro), have been dated by Volpe & Macdougall (1990) at 835 ± 43 Ma and 838 ± 36 Ma, respectively. A sample of the Siwaya granite-gneiss (~ 15 km south of Mt. Abu) was dated by Deb et al. (2001) at $836 \pm 7/-5$ Ma, while the Sai granite (southeast of the Ranakpur sample from this study) was dated by Choudhary et al. (1984) at ~ 835 Ma as well. The similarity in these ages may indicate a separate felsic magmatic event to that of the (older; this study) Erinpura granitoid intrusion as well as the younger MIS event. Alternately, this age of ~ 841 Ma has been taken as the maximum age of the end of the Delhi orogeny by Deb et al. (2001).

The Erinpura gneiss dated in this study is from the type-locality of Jawai dam. The term 'Erinpura granite' has been used to define all granitoids that intrude south of Ajmer, in the SDFB by Heron (1953) and Choudhary et al. (1984). However, the type-locality gneiss has never been dated to ascertain its age. Various authors have dated what is termed the Erinpura granite at between ~ 873 Ma and ~ 740 Ma (Crawford, 1970; Choudhary et al., 1984; Volpe & Macdougall, 1990; Deb et al., 2001 & Van Lente et al., 2009).

The Erinpura gneiss sample dated in this study is very similar in age to the tonalite from the Punagarh area of Van Lente et al. 2009; Figure 6.29). All other Erinpura granite ages have been either Rb-Sr or Sm-Nd whole rock studies and most ages are not well-constrained. The age of 880.5 ± 2.1 Ma confirms that the Erinpura granite is older than most other granitoids within the SDFB, as well as being more than 100 m.y. older than the Mt. Abu granitoid pluton. A $^{235}\text{U}/^{207}\text{Pb}$ age of monazite separated from the Erinpura sample of 820.6 ± 4.2 Ma may reflect very slow cooling of the Erinpura granitoid, or a separate, younger igneous/metamorphic event. The monazite here has experienced U- or Pb-loss, because it plots slightly above concordia. A similar age of 826 ± 5 Ma for a monazite was obtained from the Siwaya granite-gneiss

and may also reflect slow cooling of the Siwaya granitoid (age of crystallization: $836 \pm 7/-5$ Ma, Deb et al., 2001) or a separate thermal event, although the difference in ages of zircon (crystallization) and monazite in this case is significantly lower than for the Erinpura granitoid dated here. This is also the case for the age of titanite (814.2 ± 2.4 Ma) from the Ranakpur quartz monzonite, when compared to the age of crystallization of 848.1 ± 7.1 Ma. Both the monazite from Erinpura and the titanite from Ranakpur have ages that are within error of each other (Fig. 6.27), implying a similar span of time for cooling, or a common, younger metamorphic event.

Erinpura augen gneiss

This sample's zircons are varied in age, although morphology is uniform. This can be explained by cryptic xenocrystic cores within some zircons that do not show up under a binocular microscope. These cores cause the analyses to plot far to the right of the concordia curve. Subsequent analyses consisted of LP crystals and fragments. The result, when a tie-line was drawn between 2 concordant analyses, was a younger intercept age, taken as that of crystallisation of the magma, while the upper, older intercept is equivalent to the lower age limit of the rock/magma from which the cores originate. This older age is within the broad limit of the formation of the Aravalli SG.

The age of crystallization is more than 100 m.y. than that of the Mt. Abu samples, so the younger pluton being related to the Erinpura granite is not likely.

Revdar Rd. mylonite gneiss

The age of this sample is evidence of older components close to or juxtaposed with the Mt. Abu pluton. Error ellipses for analyses are small, but fall a distance apart and off concordia, which is possibly the result of Pb-loss due to the metamorphic event that caused the intense deformation of this sample (a migmatite).

This rock may be related to the Erinpura magmatism; however, even when the maximum errors are taken into account, the age does not approach that of the Erinpura sample.

Ranakpur quartz syenite

The age (848.1 ± 7.1 Ma) of this Ranakpur sample is much younger than that of the diorites dated at ~ 1 Ga by Volpe & MacDougall (1990). This sample is classed as part of the Erinpura granite and may possibly be a late-stage product of this magmatism, but this is unlikely as there is a ~ 30 m.y. difference between ages. It is closer in age to the sample from Revdar Rd (AA6-38), within error of this rock.

The titanite age of 814.2 ± 2.4 Ma is younger than the age of crystallization, but this can be explained by later growth of titanite, possibly during cooling after intrusion, or during the peak metamorphism of this sample. Alternately, it may be a separate, later metamorphic event during which the titanite formed.

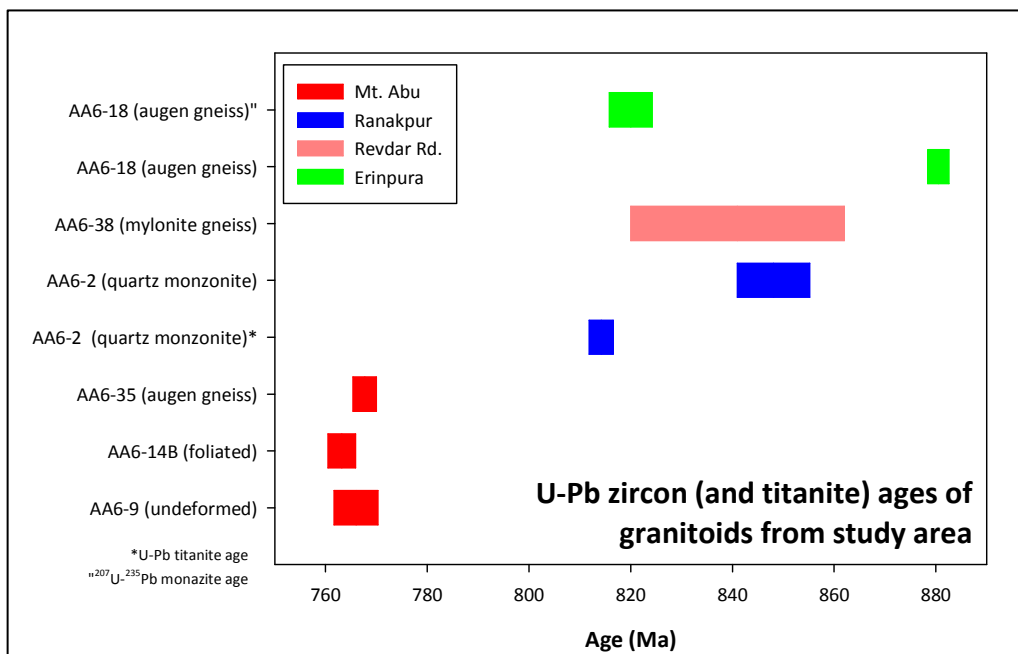


Figure 6.27. A visual summary of all samples dated in this study (errors on the age are included), excluding the Kishengarh nepheline syenite sample.

6.4.2 Younger Group (Mt. Abu granitoids)

The Mt. Abu granitoid pluton has traditionally been grouped with the Erinpura granite since Heron (1953) and is seen to represent the late- to post-magmatic phase of the Delhi orogeny (Choudhary et al., 1984; Gupta et al., 1989). However, De Wall & Pandit (2007), through AMS studies, have concluded that it is a syntectonic pluton, possibly part of the Sirohi orogeny. Previous geochronological data span an age range of ~850-720 Ma for the Mt. Abu pluton. Sivaraman & Raval (1995) dated a Mt. Abu granite at ~770 Ma, but no field or analytical data were given.

Zircons separated from the three Mt. Abu samples dated are all similar in morphology (ranging from long prismatic with clear and mafic mineral inclusion to short, stubby and equant grains) and are assumed to be of magmatic origin owing to their well preserved, oscillatory magmatic zoning and prismatic shape.

All samples from this study, whether deformed, foliated or massive in texture, are similar in age to each other. This confirms that the Mt. Abu intrusive is a simple pluton that has been variably deformed. Mt. Abu samples from this study have a maximum age range of 760.5-770 Ma (Fig. 6.28). They are younger than the

Erinpura gneiss dated in this study by more than 100 m.y., making it unlikely that the Mt. Abu pluton is related to the Erinpura granite. This age range places the Mt. Abu pluton within the time limits of the MIS. A precise U-Pb zircon age of 771 ± 5 Ma by Gregory et al. (2008) obtained on a rhyolitic tuff is thought to constrain the age of the first phase of the MIS magmatism. Unpublished U-Pb zircon ages (Tucker unpubl.; mentioned in Torsvik et al., 2001b) of 771 ± 2 and 751 ± 3 Ma for rhyolites from the MIS also confirm that the Mt. Abu pluton is related to this magmatism. U-Pb zircon ages (TIMS method, Van Lente et al., 2009) of 761 ± 16 and 767 ± 3 Ma, respectively, for interlayered rhyolite and dacite within the Punagarh Group (~30 km north of Mt. Abu) are also within error of the Mt. Abu granitoids from this study. As these dates represent the age of primary magmatic activity in the Sindreth and Punagarh Groups, it may be concluded that the Mt. Abu pluton is related to this magmatism as well. The Seychelles granitoids of age ~750 Ma have also been proven to have been spatially contiguous with the MIS (<200 km separation) through robust palaeomagnetic data (Torsvik et al., 2001a, 2001b; Ashwal et al., 2002). The implication is that the formation of these four felsic (and mafic-ultramafic) suites is related to the same geotectonic event, which Ashwal et al. (2002) postulate as subduction of an Andean-type margin on the western outboard of Rodinia.

The observed variation in textures between Mt. Abu granitoids may be the result of multiple injections from different feeder dykes. The differing conditions in H₂O-fugacity and time spent in the magma chamber would contribute towards the different textures (from massive to porphyritic) observed. New pulses of magma and magma-mixing may also be a contributing factor.

Certain zircon analyses in the Mt. Abu samples that drop below concordia are an indicator of Pb-loss caused by a younger metamorphic event having affected the granitoids of the Mt. Abu pluton. This metamorphism may have caused damage to the zircons through fractures and defects which resulted in remobilization of U- and Pb-rich material.

Rathore et al. (1999) reported a $^{40}\text{Ar}/^{39}\text{Ar}$ plateau age of 548 ± 7 Ma and a pseudo-plateau age (on a saddle-shaped spectrum) of 515 Ma for granites from the Jalore region to the west of Mt. Abu. The event that affected the Jalore granites may also have affected the Mt. Abu pluton.

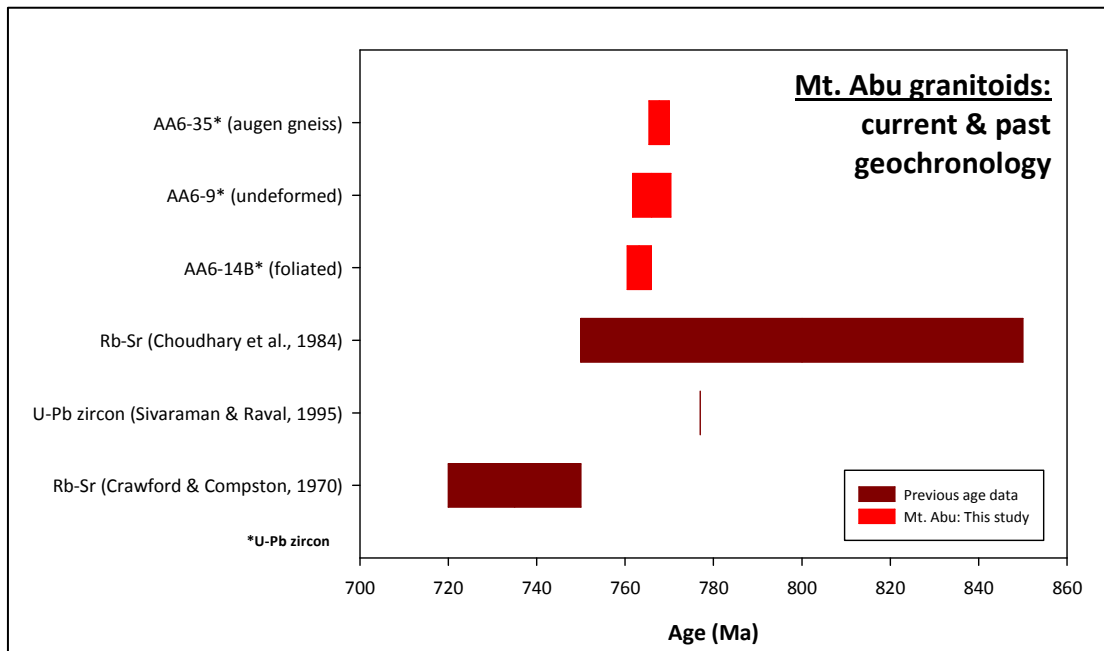


Figure 6.28. Combined previous work and age data from the current study for the Mt. Abu granitoid pluton. Uncertainties within previous work give the Mt. Abu pluton an age range in excess of 130 m.y. The U-Pb zircon age of Sivaraman & Raval (1995) of 777 Ma is without error uncertainties, as these were not published, hence the uncertainty in the age cannot be shown.

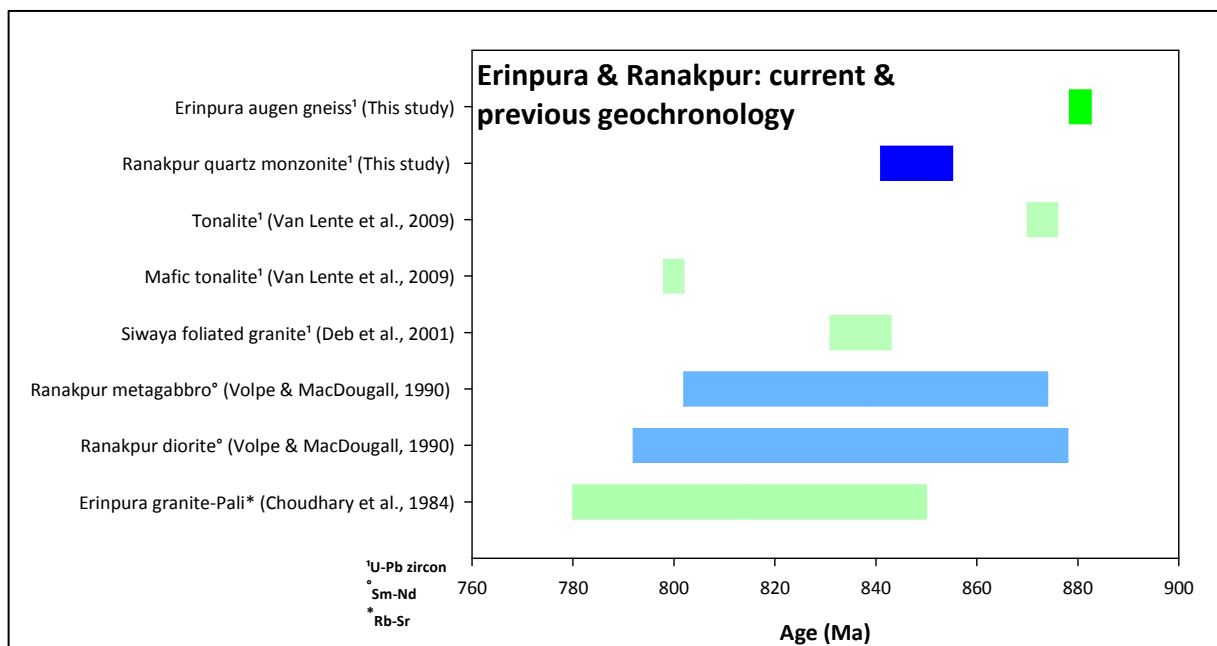


Figure 6.29. Combined previous work and age data from the current study for the Erinpura augen gneiss and the Ranakpur quartz syenite. The Erinpura and Ranakpur U-Pb zircon ages from this study are the ages of crystallization or formation of these samples.

6.4.3 Kishengarh nepheline syenite gneiss

The Kishengarh nepheline syenite zircons are similar in age to other ~1 Ga granitoids and rhyolites from this region (Fig. 6.30). Deb et al. (2001) obtained U-Pb zircon ages of ~986 Ma on rhyolites from the Sendra-Ambaji arc terrane, while Pandit et al. (2003) dated a granitic gneiss (U-Pb zircon) from the Sendra granite

suite at ~968 Ma. Biotite from an inclusion was also dated by Rb-Sr methods at 970 Ma (Crawford, 1970). A diorite from Ranakpur gave a whole rock Sm-Nd isochron age of 1.1 Ga as well (Volpe & Macdougall, 1990). This felsic magmatism may be related to-/or a reflection of- the formation of the supercontinent Rodinia (Roy & Kataria, 1999), which was postulated to have existed from ~1.3-1.0 Ga (the so-called Grenvillian-type orogenies) (Hoffmann, 1991; Moores, 1991; Trompette, 2000; Torsvik & Meert, 2003; Torsvik, 2003).

The age of the titanite cores (1365 ± 99 Ma) places them within the age range of the Phulad Ophiolite Suite (1.7 -1.3 Ga, Volpe and MacDougall, 1990), which may imply formation related to the same event. These cores may be assumed to be inherited, as the age of the zircons is younger. However, it is likely that these titanite grains represent the actual age of crystallization of the nepheline syenite and are primary in nature, while the zircons are highly reset and metamict. Thus, the cores of titanite give the age of formation, while their lighter coloured rims formed during the same event that reset the zircon grains. Some evidence for the primary nature of the age of the titanite grains comes from other studies undertaken on differentially deformed specimens of the nepheline syenite. Crawford (1970) dated the Kishengarh nepheline syenite at 1490 ± 15 Ma, although this was done by Rb-Sr age dating. As rocks usually lose Rb during metamorphism and fluid movement, this older age can be assumed to approach the crystallization age. A biotite inclusion was also dated, which was found to be younger in age at 970 Ma. This younger age was assumed to represent the age of metamorphism.

The zircons from the Kishengarh nepheline syenite in this study have been fractured, with remobilization of material clear within CL-images, which show concentrations of highly luminescent material surrounding fractures. They are not pristine in nature and thus, ages obtained may be suspect due to Pb-loss. A zircon imaged has parallel fracturing and what may be annealing of the fractures on edges of the grain. These features may indicate shearing and a great degree of deformation (Corfu et al., 2003). Zircons are not prismatic and seem to show hallmarks of metamorphic recrystallization or resetting, implying that they are not primary magmatic, but have been heavily modified during the ~1 Ga metamorphic event. Titanite can sometimes be preserved (Corfu. F, personal comm.), and since both analyses show consistently older ages that are not within error of the zircons, it must be assumed that the titanite is older.

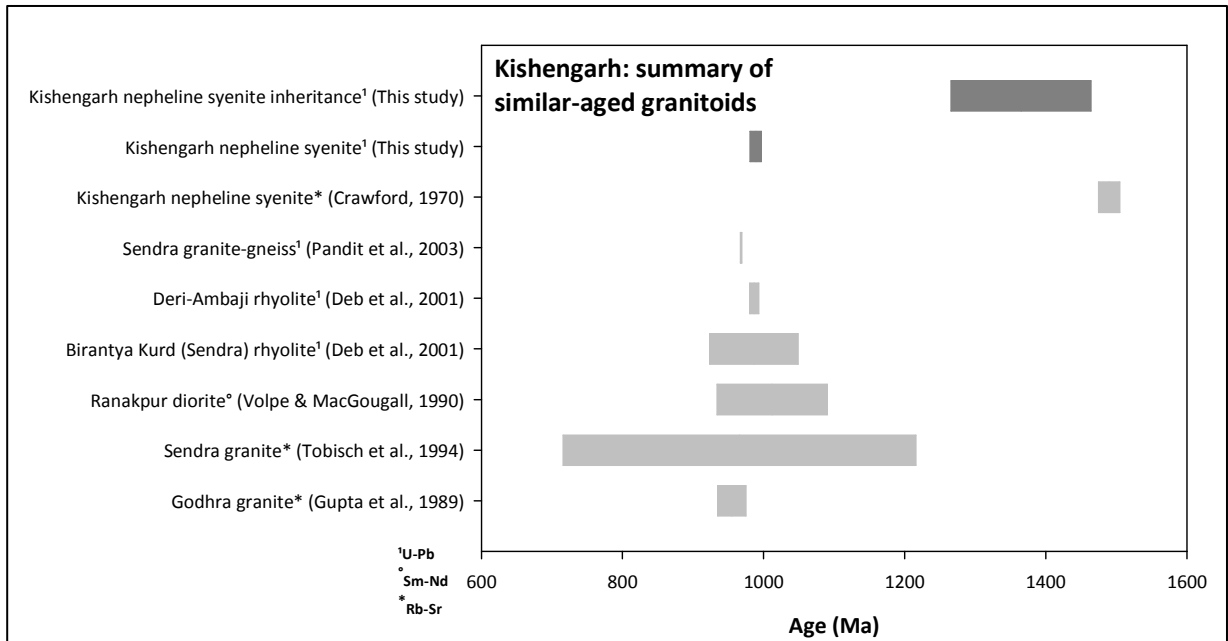


Figure 6.30. A visual summary box diagram of all samples dated within the U-Pb zircon age range of the Kishengarh nepheline syenite of this study. The only other age dating done on this sample was by Crawford (1970). This Rb-Sr age is greater than the age of inheritance of the zircons in this study.

The zircons were affected by the widespread ~1 Ga mostly felsic magmatism (which may be a reflection of the formation of Rodinia) while the titanites (when combined with the two zircon to describe a line of discordia) have a lower limit age of 1365 ± 99 Ma (taken as the age of formation), within error of the Rb-Sr age obtained by Crawford (1970) of 1490 ± 15 Ma.

6.4.4 Primary, metamorphic and inherited ages within the Erinpura and Ranakpur granitoids and Kishengarh nepheline syenite gneiss

Ages other than that of primary magmatic activity have been obtained in this study for the Erinpura and Ranakpur granitoids and Kishengarh nepheline syenite gneiss. The ages on monazite and titanite are younger than the zircon ages, which may represent slow cooling rates within the intrusions or a separate metamorphic event, as monazite is commonly found as an accessory mineral in metamorphic rock types (Foster et al., 2002). The $^{235}\text{U}/^{207}\text{Pb}$ age of 820.6 ± 4.2 Ma obtained for a monazite from the Erinpura gneiss is not far off the age of 814.2 ± 2.4 Ma for titanite from the Ranakpur quartz syenite. Both may be related to a separate, younger event, as the differences in age between zircon and the monazite and titanite ranges from ~33 m.y. for the Ranakpur sample, to ~57 m.y. for the Erinpura gneiss.

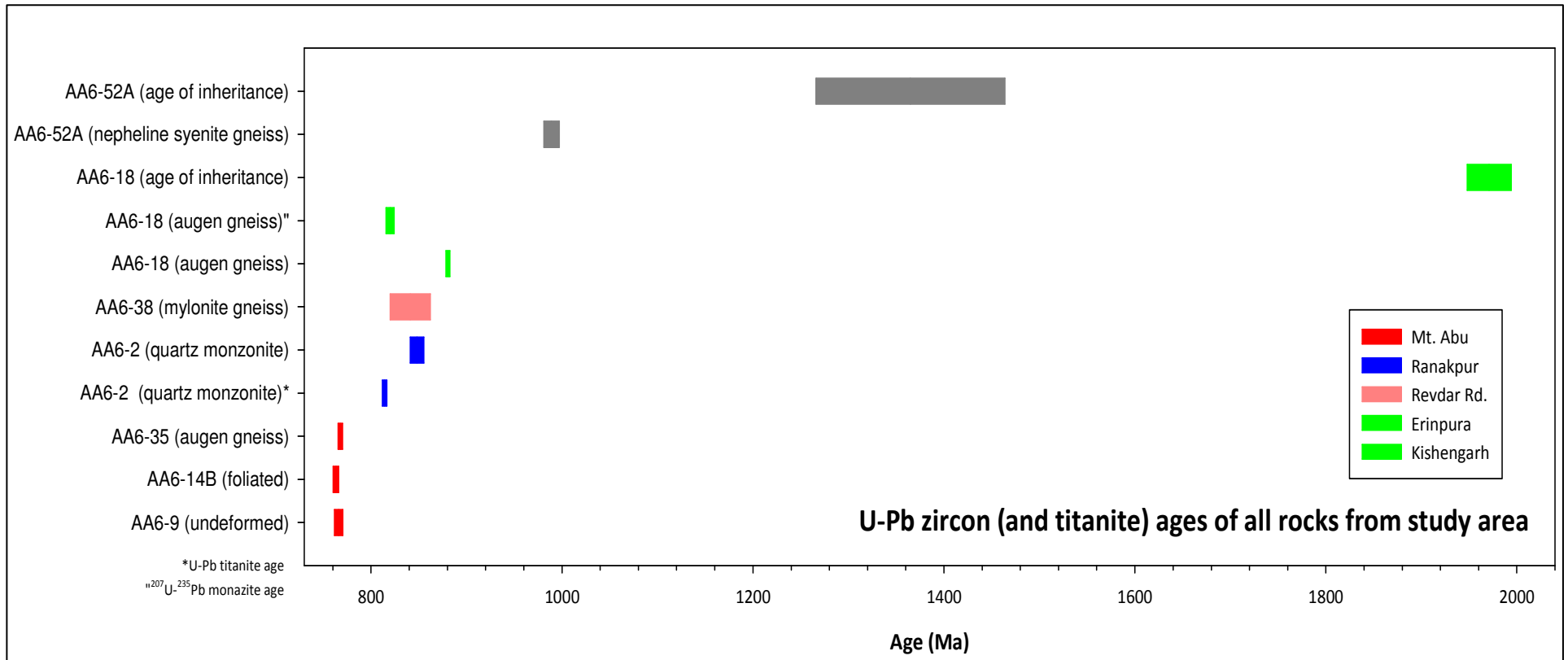


Figure 6.31. A visual summary box diagram of all samples dated in this study, including the ages of inheritance of both the Erinpura augen gneiss and Kishengarh nepheline syenite. All plots include the error on the ages.

However, both granitoids have been variably deformed, which may explain the extended age range between crystallization and other ages, as the length of time of the deformation is not well constrained, although that within the Erinpura granitoids is thought to be syntectonic in nature. Deformation may have extended the period of cooling for the intrusives.

Some analyses in the Erinpura and Kishengarh samples plot to the far right of their concordia diagrams. This is due to older inherited cores, which are cryptic and not easily discernable under the binocular microscope used to select zircons.

Two analyses plot far to the right of concordia for the Erinpura samples. These have been affected by inheritance and form a line of discordia with the other analyses. The upper intercept so-defined of 1971 ± 23 Ma is the minimum age of the inherited cores. These xenocrystic cores may have originated within the felsic plutons that intrude the Palaeoproterozoic Aravalli SG, which has poor age constraints of ~ 2.5 - 1.7 Ga due to unreliable dating methods. The Derwal Granite, emplaced into the Aravalli rocks during the first phase of deformation, was dated by Choudhary et al. (1984) at 1900 ± 80 Ma, using Rb-Sr errorchron data and is thus easily prone to resetting.

The titanites analyzed for the Kishengarh nepheline syenite are older than the zircons dated. When both zircon and titanite analyses are combined to describe a line of discordia, the upper intercept gives an age of 1365 ± 99 Ma, which is not well-constrained, but gives an idea of the age of the inherited cores of titanite. This age places their time of formation within the Meso-Neoproterozoic Delhi SG (~ 1.6 - 1.0 Ga). Plutons with ages that fall within the error of the Kishengarh nepheline syenite are scarce. The Ajitgarh granitoid pluton from the NDFB has been dated by Rb-Sr methods (Choudhary et al., 1984; Crawford, 1970) at ~ 1450 Ma, while monazite from a quartz mica schist in the Ajitgarh area yielded a peak age between ~ 1.5 - 1.3 Ga, although the significance of this age is not understood.

Granitoids from this, the Sirohi region of Rajasthan, within <70 km from each other, have shown themselves to be diverse in lithology, texture and age, with Mt. Abu granitoids being the youngest (Figure 6.31), and the Erinpura augen gneiss being the oldest in this area. This spread in ages implies a complex history involving multiple intrusive/tectonic and metamorphic events. The Mt. Abu granitoids form a separate younger group distinct from the Erinpura, Ranakpur and Revdar Rd. granitoids, which are all older than ~ 840 Ma. The Ranakpur and Revdar Rd. samples are dissimilar in texture and degree of deformation and are spatially unrelated, but are within error of each other in age. The Erinpura granite, juxtaposed with the Mt. Abu granite pluton, is more than 100 m.y. older than the Mt. Abu granitoids, which also implies that they are not related to a single tectonic event.

7. $^{40}\text{Ar}/^{39}\text{Ar}$ AR GEOCHRONOLOGY

It has been shown in Chapter 6 that U-Pb ages on titanite and monazite for the Ranakpur and Erinpura samples, respectively, are younger than their ages of crystallization. $^{40}\text{Ar}/^{39}\text{Ar}$ age dating is utilized here to try to constrain the ages of the later resetting event (s) that the younger U-Pb ages of the monazite and titanite hint at. $^{40}\text{Ar}/^{39}\text{Ar}$ age dating was performed on only four samples from this study, as the other samples' mafic mineral separates were found to be unsuitable for use in $^{40}\text{Ar}/^{39}\text{Ar}$ age dating. Samples dated include the type-locality massive granite from Mt. Abu, the type-locality gneiss from Erinpura, the Ranakpur quartz syenite and the Kishengarh nepheline syenite-gneiss.

Hornblende and biotite are preferred over K-feldspar in $^{40}\text{Ar}/^{39}\text{Ar}$ age dating, as they have greater retentive properties for Ar. Retentivity of Ar is greatest in hornblende, as the blocking temperature of hornblende is $\sim 550^\circ\text{C}$, while biotite has a blocking temperature of 350°C (Faure & Mensing, 2005). The blocking temperature is the temperature below which a mineral is closed to diffusion of an element, in this case, argon. The system must be closed with respect to Ar, meaning that Ar in the sample was completely outgassed at the time of formation or metamorphism. Thus, all ^{40}Ar contained in the mineral is radiogenic, allowing for measurement of the age of formation or metamorphism. All samples below show disturbances within their U-Pb Concordia (Chapter 7). The $^{40}\text{Ar}/^{39}\text{Ar}$ age dating has been utilized here to try to elucidate the ages of these metamorphic disturbances, as they form part of the history of these felsic samples.

7.1 Mt. Abu orange-pink granite: AA6-9

This phaneritic orange-pink granite is undeformed in hand specimen. Mt. Abu samples with greater deformation were not used, as the biotite and hornblende separated was riddled with inclusions and was therefore unusable. In thin section, however, this sample showed evidence of strain deformation in the form of slickenside surfaces (~ 1.5 mm in width) that are formed from extremely fine-grained recrystallized material (quartz and biotite), undulatory extinction of quartz and subgrain formation. The latter two may have formed within the high temperature submagmatic regime, while the slickenside surfaces may be post-magmatic/intrusive in nature. The sample has also undergone alteration in the form of highly sericitized K-feldspar and plagioclase.

The age of crystallization this rock, according to U-Pb zircon age dating (this study), is 766.0 ± 4.3 Ma. There is some evidence of Pb-loss, possibly caused by a later event, as some error ellipses plot further down and away from the line of concordia. Foliations within the Mt. Abu pluton that this sample is part of have been

attributed to syntectonic- as well as submagmatic- deformation (microstructures in thin-section) (De Wall et al., 2006; De Wall & Pandit, 2007). Thus, it is expected that the ^{40}Ar - ^{39}Ar age would not be much younger than that of crystallization, since, barring slow cooling rates within the pluton (which would cause large differences between U-Pb zircon and Ar-Ar ages: Dalrymple et al., 1999; Faure & Mensing, 2005), there is little evidence of deformation post-intrusion in this granitoid.

Biotite in this sample is found in fine-grained aggregates with many inclusions and is thus unsuitable for analysis, but hornblende is euhedral and distinctly blocky when separated (Fig. 7.1 A), with fewer inclusions and generally less alteration. Enough hornblende of good quality was thus separated out and used to calculate a $^{40}\text{Ar}/^{39}\text{Ar}$ age of 508.7 ± 4.4 Ma, which includes the J-value (Fig. 7.2).

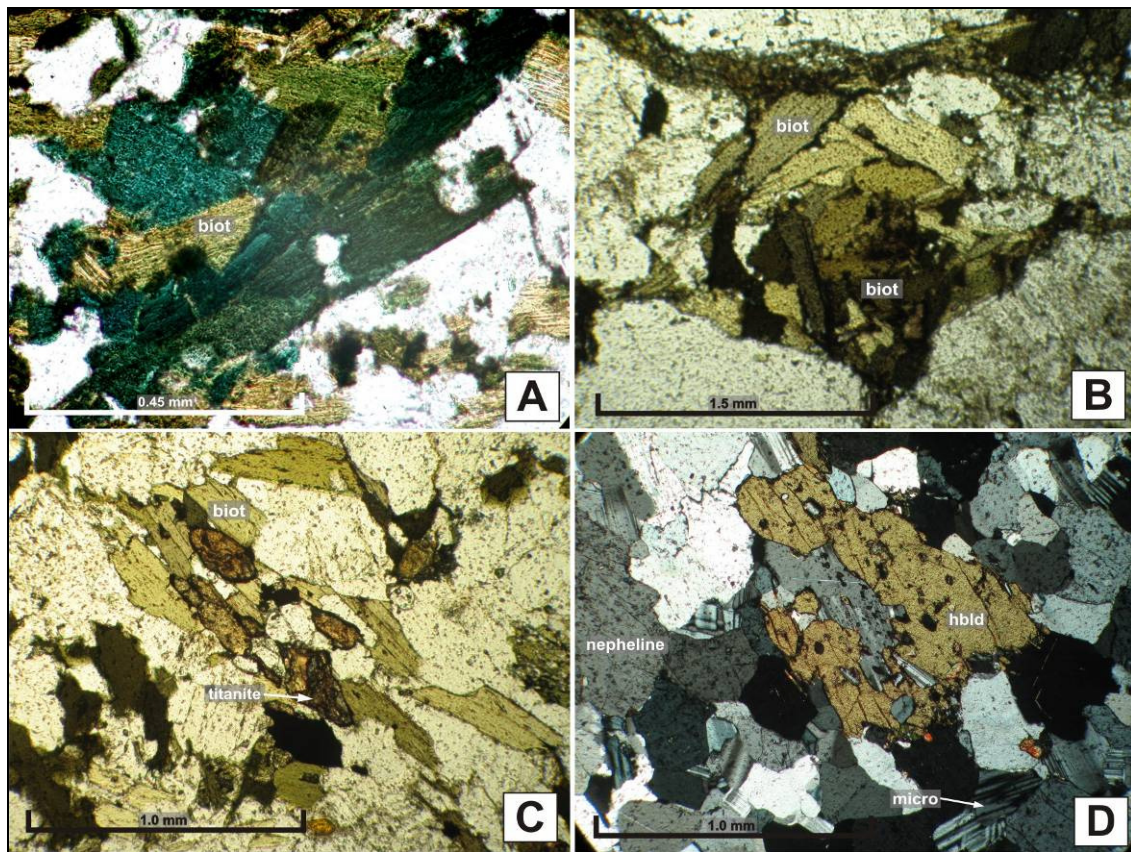


Figure 7.1. Thin section images of mafic minerals within samples dated. A- a mafic cluster from the orange-pink Mt. Abu granite. Fine-grained green-blue hornblende and green-brown biotite are intergrown. Both mafic minerals have inclusions, but hornblende is larger, less altered and more well-formed than the biotite, making it easier to separate and provide a reliable age (AA6-14B, FOV=0.9 mm). B- a medium-grained biotite cluster from the Erinpura gneiss (AA6-18), with crystals that are subhedral to euhedral and are usually partially interstitial to the larger feldspars and quartz. The larger grains have few inclusions, are affected less so by alteration and are therefore useful in Ar-Ar dating (AA6-18, FOV=3mm). C- disseminated biotite intergrown with subhedral titanite within the Ranakpur quartz syenite. The biotite is relatively inclusion-free, making it suitable for Ar-Ar age dating (AA6-2, FOV=2mm). D- large, well-formed hornblende from the Kishengarh nepheline syenite. However, it is inclusion-rich, as can be seen from the image. This makes it difficult to choose grains for Ar-Ar analysis, as inclusions skew the data and contribute to erratic values within the spectrum (AA6-52A, FOV=2mm).

This sample shows an undisturbed relatively flat step-heating spectrum (Fig. 7.2), with the expected drops in all Ar-species/isotopes at the beginning and end of the step heating process. The flat age spectrum is indicative of both ^{40}Ar and ^{39}Ar (formed from decay of ^{39}K , which is a proxy for ^{40}K ; McDougall & Harrison,

1999; Koppers, 2002; Faure & Mensing, 2005) being contained in the same sites within the grains. This would mean that the ^{40}Ar is radiogenic in origin and therefore originally from the decay of ^{40}K in those sites (McDougall & Harrison, 1999). Thus, the system can be considered closed and is reliable (McDougall & Harrison, 1988, 1999).

The drop in Ar at the beginning and end of step-heating is due to Ar-loss from the less-retentive sites at the edges of the crystals, where Ar is not held so strongly in the lattice (McDougall & Harrison, 1988, 1999; Dickin, 2005). The age-spectrum has a good, flat plateau from steps 4 to 7. Steps 5 to 7 were used in the age calculation, because including step 4 increased the MSWD (including the J-value, the error on the calculated age) considerably while the age was not appreciably changed.

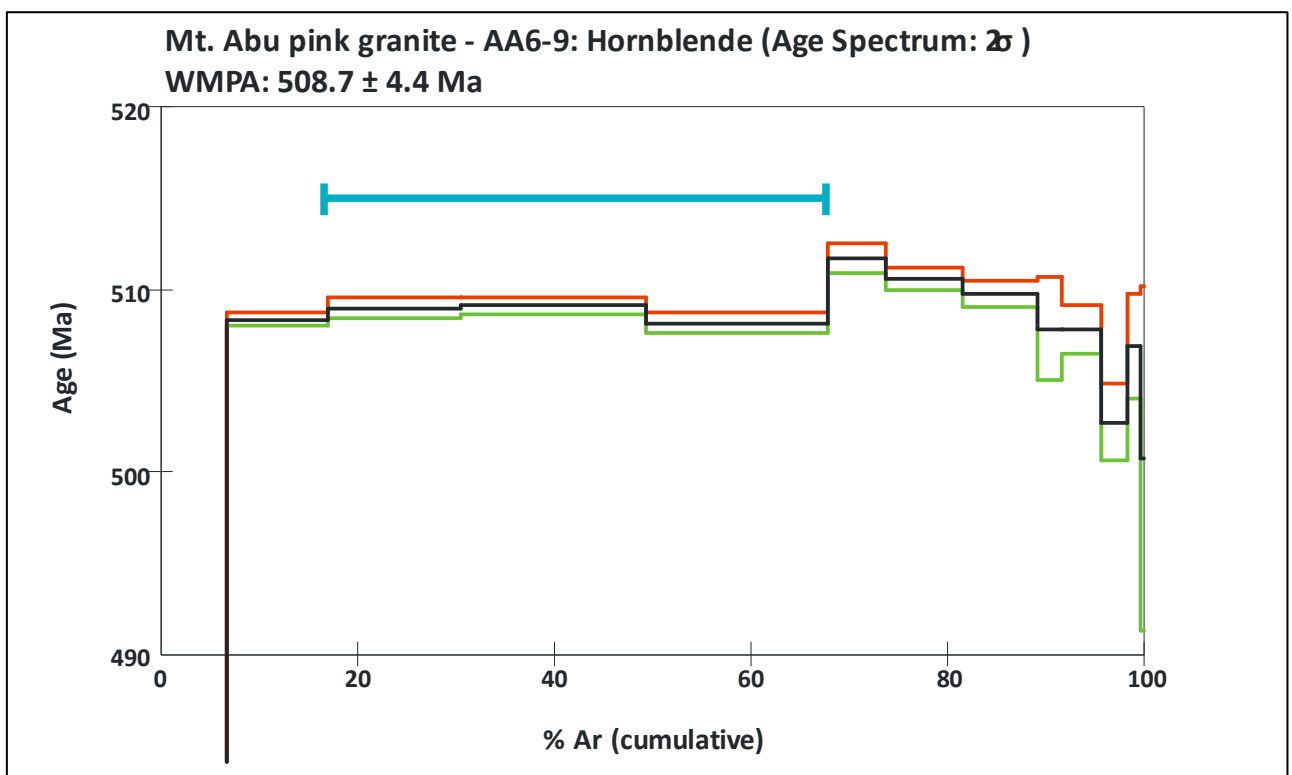


Figure 7.2. The $^{40}\text{Ar}/^{39}\text{Ar}$ step-heating spectrum for the orange-pink Mt. Abu granite (AA6-9). The spectrum has a relatively flat plateau indicating little disturbance and Ar-loss from within the crystal structure of the hornblende. The horizontal blue bar indicates the steps used to calculate the age.

7.2 Erinpura augen gneiss: AA6-18

This sample is a deformed augen gneiss in hand specimen, with augens composed of composite feldspar and quartz grains separated by mafic bands. In thin section, the biotite is found in fine-to medium grained clusters at grain boundaries of larger felsic minerals (Fig. 7.1 B). Biotite, when separated out, occurs as distinct flakes which are good for analysis.

The age of crystallization of this rock is 880 ± 2.1 Ma (U-Pb zircon age dating, this study); much older than the previous Mt. Abu sample, and has clearly experienced a higher degree of deformation. The biotite used to date the age of this deformation yields an age of 515.7 ± 4.5 Ma. The biotite in this sample, though a good size, was not as large or well-formed (alteration of the biotite through chloritization and sericitization was noted) as the hornblende in the Mt. Abu sample and this is reflected in the step-heating spectrum (Fig. 7.3) which is disturbed, although Ar-concentration does increase with temperature up to a pseudo-plateau.

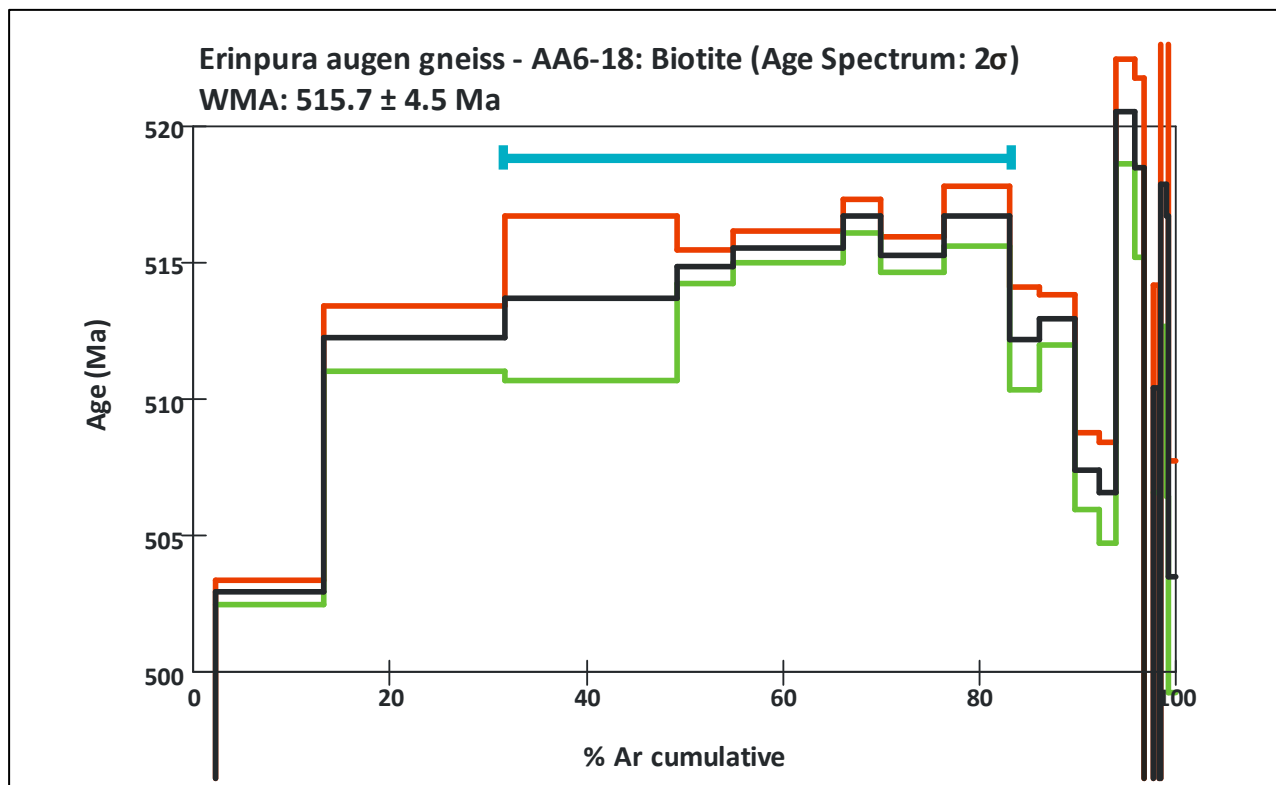


Figure 7.3. The age-heating spectrum for the Erinpura augen gneiss (AA6-18) is erratic, with many dips and increases within the middle part of the spectrum, where the majority of the Ar gas is released. The horizontal blue bar indicates the steps used to calculate the age. This sample has undergone post-magmatic alteration and metamorphic processes that have deformed the lattice-structure in the biotite and cause Ar-loss/gain.

There are several dips within the middle part of the spectrum and large differences in Ar between consecutive steps. These are indications that some Ar has been lost from the more retentive cores of crystals and that decoupling of the Ar and K has occurred, which may also be due to previous Ar-loss (Dalrymple & Lanphere, 1974; McDougall & Harrison, 1999). There is no true plateau age, and only a MWA could be calculated. A monazite $^{235}\text{U}/^{207}\text{Pb}$ age of 820.6 ± 4.2 Ma from this sample may reflect a previous Ar-loss event. This could indicate that the Erinpura augen gneiss has undergone multiple episodes of Ar-loss.

7.3 Ranakpur quartz syenite: AA6-2

This sample is a phaneritic grey granitoid dominated by plagioclase, with well formed mafic biotite and hornblende clusters that are evenly disseminated throughout the rock (Fig. 7.1 C). Parts of the pluton close to the cryptic contact between the surrounding calc-silicate and the granitoid are deformed, with boudinaged granitoid veins and pygmatic folding of the calc-silicate. The sample used for both U-Pb zircon and Ar-Ar geochronology is, however, relatively undeformed in hand specimen. In thin section, recrystallization textures such as interfingering of grain boundaries, many sub-grains on boundaries as well as ophitic textures and undulatory extinction in quartz are abundant.

This sample has an erratic spectrum where Ar-concentration increases with temperature throughout the bulk of the spectrum, with no true plateau being reached (Fig. 7.4).

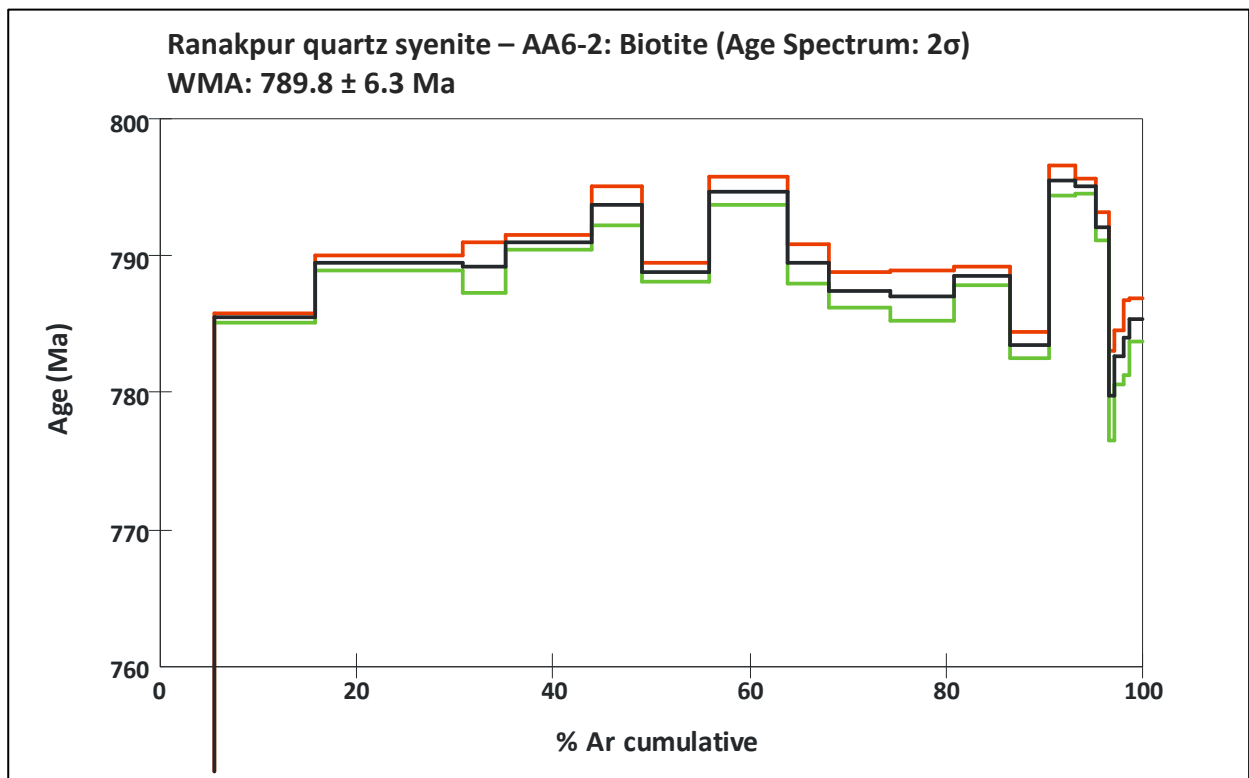


Figure 7.4. The step-heating spectrum for the Ranakpur quartz syenite (AA6-2). It is disturbed and erratic, with large differences between successive steps and no true plateau.

The uneven distribution indicates disturbance due to Ar-loss during a post-crystallization metamorphic event (Dalrymple & Lanphere, 1971, 1974; Dalrymple et al., 1999; Faure & Mensing, 2005).

The U-Pb zircon age of this sample is 848.1 ± 7.1 Ma. Comparatively, the $^{40}\text{Ar}/^{39}\text{Ar}$ weighted mean age on biotite from this sample is 789.8 ± 6.3 Ma, which is approximately 60 m.y. younger than the U-Pb age calculated. This sample is clearly disturbed, as is evident from the irregularity between consecutive steps of

the spectrum. However, the range of ages (from 787 ± 1 Ma to 795 ± 0.5 Ma; 70.6% of cumulative ^{39}Ar) used to calculate the average is meaningful, as the spectrum is fairly tight over this range. An age of 814.2 ± 2.4 Ma was obtained on titanite from this sample. This younger age may reflect cooling or a separate thermal event, for which the Ar-Ar age calculated here may be a minimum.

7.4 Kishengarh nepheline syenite: AA6-52

This is a nepheline syenite gneiss, with foliations formed by hornblende, although hornblende crystals are not aligned parallel to the direction of foliation. The hornblende is relatively well-formed (<1.1 mm diameter) and found in discrete clusters with associated titanite, surrounded by nepheline and plagioclase (Fig. 7.1 D).

The U-Pb zircon age of this sample is 989 ± 8 Ma. This sample is foliated, either during intrusion of the pluton or during a later deformation event. An $^{40}\text{Ar}/^{39}\text{Ar}$ of 944.2 ± 7.4 Ma can be calculated from the isochron (Fig. 7.5). However, the Y-axis (the $^{40}\text{Ar}/^{36}\text{Ar}$ ratio) intercept on the inverse isochron for steps 3-6 (61.9% of cumulative ^{39}Ar) gives an age of 6.07 ± 0.19 Ga, which is a clear indication of excess argon (Fig. 7.6 A, B). Thus, the age of 944.2 ± 7.4 is necessarily a maximum age.

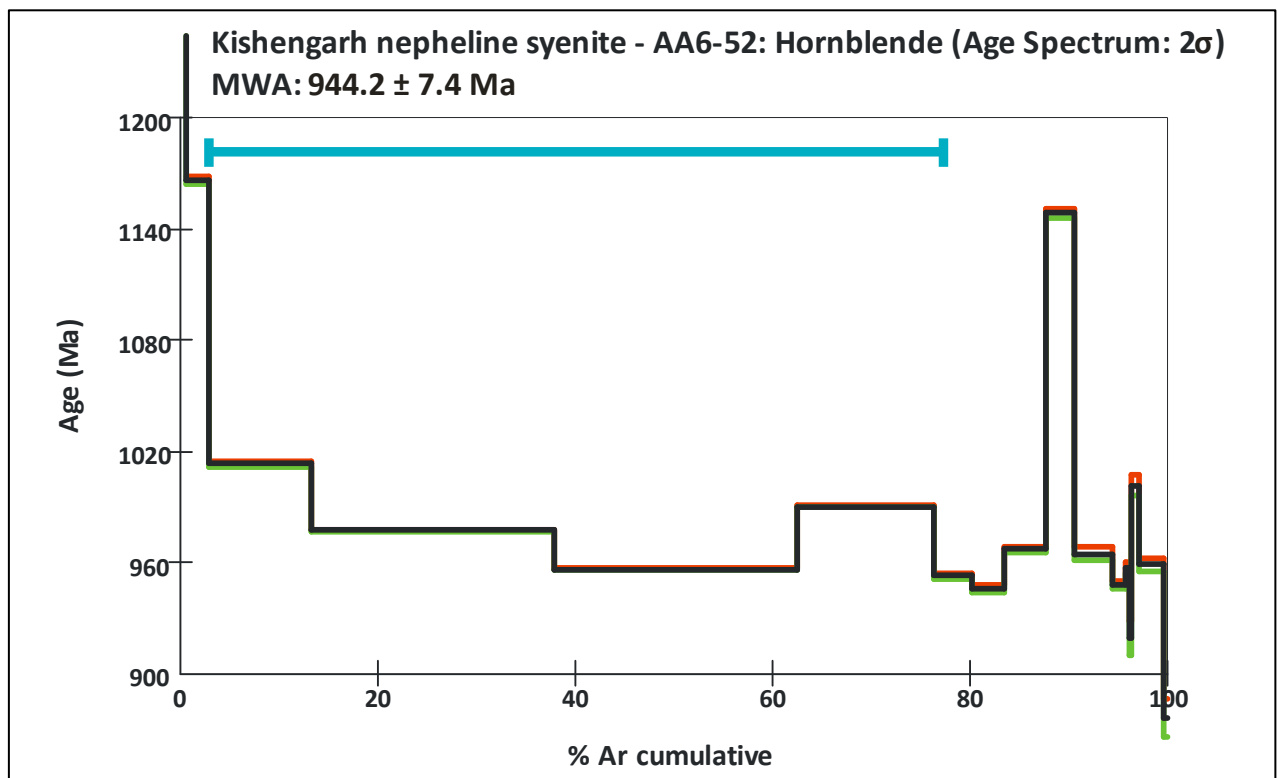


Figure 7.5. The clearly disturbed spectrum of the Kishengarh nepheline syenite gneiss, with anomalously high ages at the beginning and end of heating and no true plateau in the middle of the spectrum. The horizontal blue bar indicates the steps used to calculate the age. The spectrum is saddle-shaped, a clear indicator of excess argon.

The saddle-shaped step-heating spectrum is also another indicator of excess argon (Lanphere & Dalrymple, 1976; McDougall & Harrison, 1999; Faure & Mensing, 2005), with ages for the first few steps that are greater than that of the earth, although the middle of the spectrum might be an age close to that of the true age of the geological event (crystallization or metamorphic age). The coincident K/Ca ratio in Figure 7.7 (it rises and falls in tandem with the step-heating spectrum) is possibly an indicator of excess mobilised K that has also been adsorbed into the crystal lattice at the edge of the grains (McDougall & Harrison, 1999).

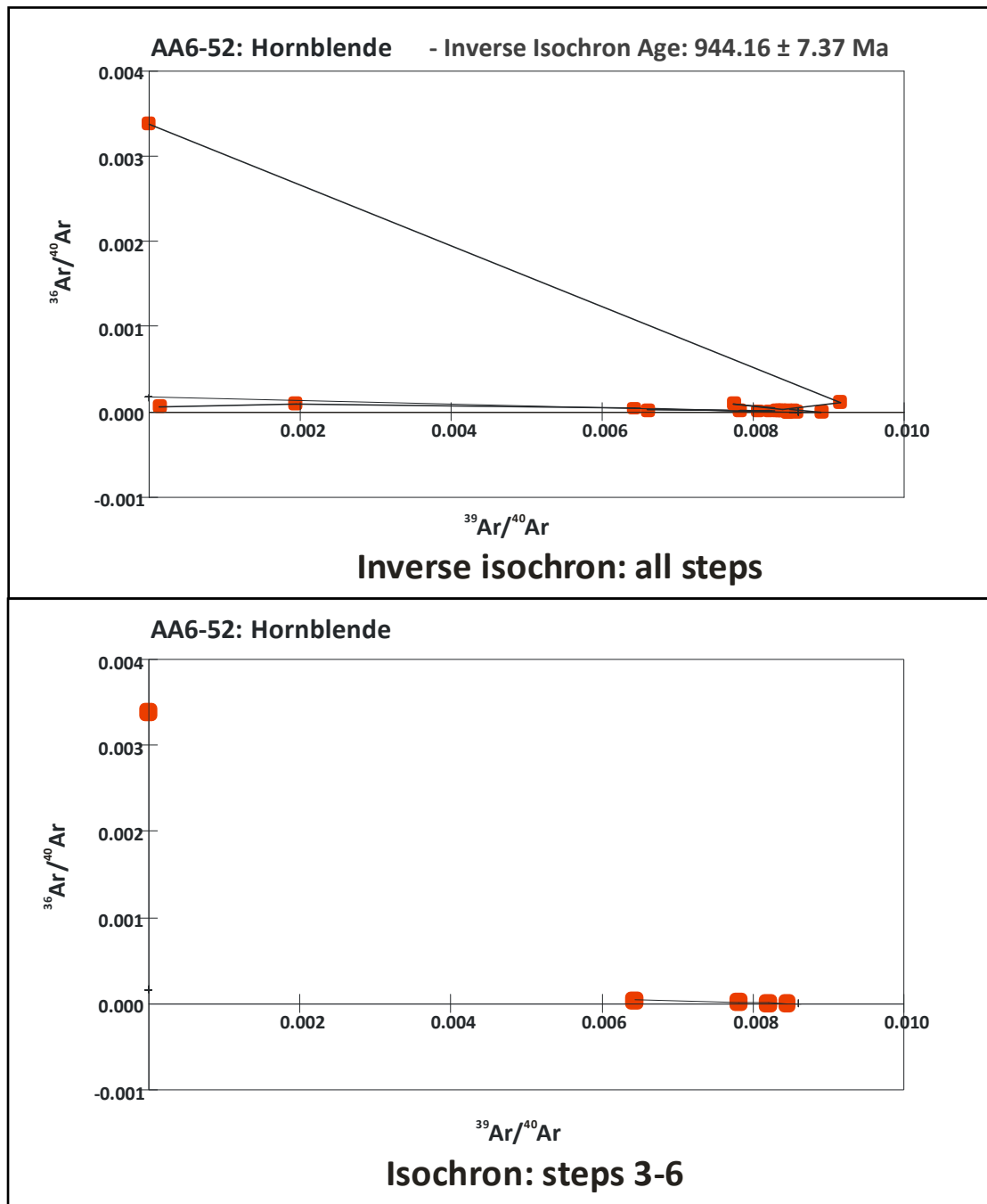


Figure 7.6. A- As can be seen the inverse isochron is generally level and yields a good age (stated in text). B- The inverse isochron for the Kishengarh nepheline syenite, showing steps 3-6, with a large jump in value to the Y-axis intercept. The Y-intercept on steps 3-6 is anomalously high, yielding a Y-intercept age anomalously high (older than that of the earth).

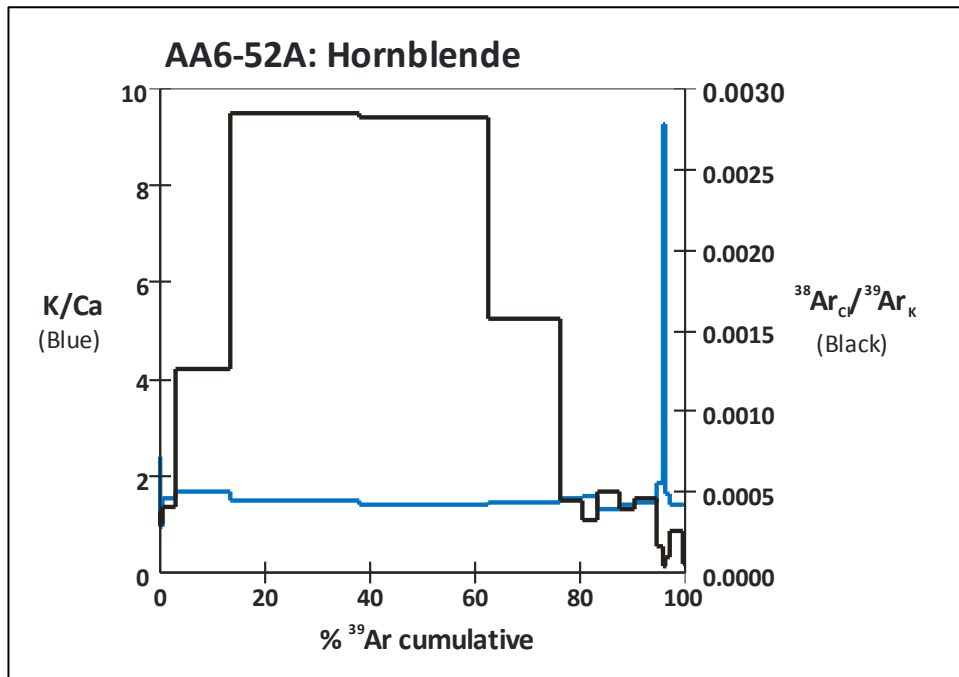


Figure 7.7. The Kishengarh nepheline syenite sample has a very low K/Ca ratio for most of the diffusion process because Ca is a major constituent of hornblende. However, since the ratio is >1, this is not a problem for corrections due to interference from Ca-isotopes.

7.5 Interpretation

Mt. Abu pink granite: AA6-9

The Ar-Ar age of this rock indicates that it has experienced a major resetting (possibly regional) during a metamorphic event. It has the youngest Ar-Ar age of all samples dated (Figure 7.8). The age of this resetting is within that of Pan-African tectonic activity (~800-500 Ma; Bonin et al., 1998) which is recognized in many former east Gondwana continents, and involved supercontinental breakup (Rodinia) and formation (Gondwana) (Rajesh et al., 1996; Liégeois et al., 1998; Paquette & Nédélec, 1998). Pan-African granulite facies metamorphism in the Eastern Ghats, Southern Granulite Belt (south India) and northwest Aravalli Mountains has also been recognized (Roy, 2001). These are the first Pan-African ages recorded for the Aravalli-Delhi mobile belt (Sirohi region) of northwest India. These ages suggest that this part of India may also have been part of late Pan-African activity, during the amalgamation of Gondwana.

Due to metamorphism and the higher temperatures experienced (as well as the attending fluid movement and diffusion) the “Ar-clock” has been reset in the hornblende, and the $^{40}\text{Ar}^*$ present has only been produced since the timing of the metamorphism. The undisturbed step-heating spectrum (well-developed plateau) likely indicates that this sample has not undergone further (later than the Pan-African event) major metamorphism and Ar-loss. The flat age spectrum also implies that both ^{40}Ar and ^{39}Ar are contained

in the same sites within the grains, and that the ^{40}Ar is radiogenic in origin (and therefore originally from the decay of ^{40}K in those sites). The system is therefore, likely to be closed, and thus reliable.

Erinpura augen gneiss: AA6-18

The biotite used to date the deformation in this sample yields an age of 515.7 ± 4.5 Ma, within error of the age from the Mt. Abu sample (Figure 7.8). It may be concluded that both samples (Mt. Abu and Erinpura) experienced the same metamorphic event of duration ~ 508 -515 Ma (coinciding with Pan-African activity in southern India as well) which was probably regional in scale. The primary biotite grains have been reset with respect to their $^{40}\text{Ar}^*$ abundances due to the intensity of the metamorphism and resulting fluid movement experienced. The Erinpura granite likely experienced multiple metamorphic events (unlike the Mt. Abu samples), contributing to the somewhat erratic nature of the spectrum. Both Erinpura and Mt. Abu samples have experienced temperatures in excess of that of closure to argon for both biotite and hornblende (allowing almost complete resetting of the "Ar-clock" for both AA6-18 and AA6-9). This is borne out by the much younger $^{40}\text{Ar}/^{39}\text{Ar}$ ages compared to the U-Pb crystallization ages.

Regional metamorphism in this area varies from low grade greenschist to upper-amphibolite facies, with both the older Aravalli SG and the younger Delhi SG having undergone complex deformation and metamorphism, with polyphase folding and shearing events (Roy & Kataria, 1999, Pandit et al., 2003). In the Delhi SG, staurolite-kyanite grade metamorphism is present in the east, while sillimanite-muscovite grade metamorphism dominates in the west of the belt (Sharma, 1999). Contact metamorphism up to pyroxene-hornfels facies occurs associated with the Erinpura granite magmatism (Gupta et al., 1989; Sharma, 1999).

Ranakpur quartz syenite: AA6-2

This sample has an erratic spectrum, where Ar concentration increases with temperature throughout the bulk of the spectrum, with no true plateau being reached. This sample has definitely been disturbed, with Ar-loss due to one or multiple post-crystallization metamorphic events. Although this sample is undeformed and massive, the pluton it is part of has boudinaged structures between the metasediments and the granitoid, crosscutting granite veins and pygmatic folds, indicating a definitive episode of deformation.

The U-Pb zircon age of this sample is 848.1 ± 7.1 Ma, which is the age estimated for the syntectonic Erinpura granite from earlier-and less precise and accurate- Rb-Sr age dating (a more accurate age of 880 ± 2.1 Ma was calculated for the Erinpura granite from this study). Two titanites were also dated (both had

excess ^{206}Pb and were corrected with K-feldspar Pb), at 814.2 ± 2.4 Ma. Comparatively, the $^{40}\text{Ar}/^{39}\text{Ar}$ weighted mean age on biotite from this sample is 789.8 ± 6.3 Ma, which is approximately 60 Ma younger than the U-Pb age, and ~ 24 Ma younger than the age on the titanites. The implications of these ages are that either cooling of the pluton occurred over a large time span of ~ 50 m.y., or that a younger metamorphic or tectonic event occurred around the age of the titanite dated, and continued cooling until Ar closure temperatures were reached, giving us the Ar-Ar age. Since the Ar-Ar age is much older than that of either the Mt. Abu or Erinpura samples (Figure 7.8), it can be concluded that this pluton did not experience the same younger event that the other two have

Kishengarh nepheline syenite: AA6-52

The U-Pb zircon age of this sample is 989 ± 8 Ma, which is likely the age of a major metamorphic event, as U-Pb dates on titanite from the same sample are in the region of ~ 1365 Ma, and are thought to be the primary age of crystallization of the nepheline syenite. The U-Pb zircon age may be the age of the event that deformed the nepheline syenite into gneiss. The zircons may thus also be either highly reset, metamict or metamorphic in nature. The resetting of the zircon would imply a high temperature during metamorphism ($\sim >900^\circ\text{C}$).

This sample is foliated, either during intrusion of the pluton or during a later deformation event. An $^{40}\text{Ar}/^{39}\text{Ar}$ age of 944.2 ± 7.4 Ma was calculated from the Ar-Ar isochron. The co-incident K/Ca ratio (it rises and falls with the step-heating spectrum) is possibly an indicator of excess mobilised K that has also been adsorbed into the crystal lattice at the edge of the grains. The difference in ages between the U-Pb zircon and the Ar-Ar on hornblende is ~ 45 Ma. This may suggest a later deformation event, or slow cooling of the pluton after metamorphism and deformation (at ~ 990 Ma).

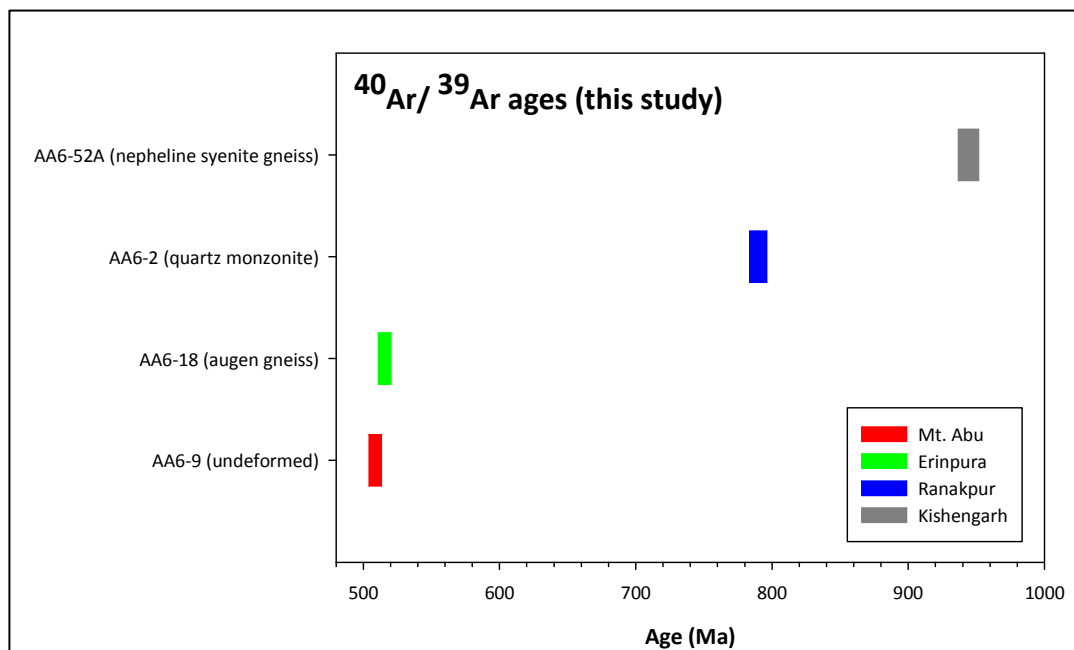


Figure 7.8. A visual box plot of all $^{40}\text{Ar}/^{39}\text{Ar}$ dates obtained in this study. The youngest sample, AA6-9, is the Mt. Abu massive granite, which is undeformed in hand specimen. However, the $^{40}\text{Ar}/^{39}\text{Ar}$ age is ~ 260 m.y. younger than that of the age of crystallization. This is evidence of a younger resetting by a tectono-metamorphic event. The $^{40}\text{Ar}/^{39}\text{Ar}$ age of the Erinpura augen gneiss (AA6-18) is within error of the Mt. Abu granite. This could imply that the event that reset the Mt. Abu granitoid was also experienced by the Erinpura augen gneiss. This event was not the cause for the deformation seen within the Erinpura augen gneiss, as a similar degree of deformation would have to be present within the Mt. Abu pluton as well. The Mt. Abu pluton, however, is variably deformed, with much of the pluton composed of undeformed massive to porphyritic varieties., which, through the Ar-Ar age dating, have been shown to have been affected by the ~ 510 Ma event, but not deformed by them. It has been concluded by De Wall & Pandit (2007) that the deformation within the Mt. Abu pluton is due to syntectonic intrusion. Thus, the ~ 510 Ma event is possibly a thermal/metamorphic expression of the Pan-African event experienced in other parts of India. The quartz syenite from Ranakpur yields a $^{40}\text{Ar}/^{39}\text{Ar}$ age of 789.8 ± 6.3 Ma, approximately 50 m.y. younger than the U-Pb zircon age calculated in this study. This could be the result of prolonged cooling of the intrusion or a younger resetting event. It has not been affected by the resetting event experienced by both the Mt. Abu and Erinpura granitoids, as evinced by the older Ar-Ar age. The Kishengarh nepheline syenite has the oldest $^{40}\text{Ar}/^{39}\text{Ar}$ age calculated (944.2 ± 7.4 Ma), which is ~ 44 m.y. younger than the U-Pb zircon age obtained. This younger Ar-Ar age may be the result of prolonged cooling, or may also be related to a separate deformatory event that transformed the nepheline syenite into gneiss.

8. SUMMARY COMPARISON OF MT. ABU TO SIMILAR GRANITOIDS FROM SEYCHELLES AND MALANI IGNEOUS SUITE (MIS)

Neoproterozoic granitoids and felsic dykes (the latter present in the MIS) from the Seychelles and the MIS have been robustly dated using U-Pb zircon geochronology (in Ashwal et al. (2002) and Carter (2005)). These felsic samples, together with other MIS felsic geochemical results (Maheshwari et al., 2001; 2002) have been used as a comparison to Mt. Abu and Erinpura felsic samples from the present study. The intermediate (more mafic) samples from the Seychelles were not included in this comparison. Sample locations for all can be obtained from the relevant publications mentioned above.

8.1 Summary comparison of Mt. Abu granitoids (and felsic dykes) to similar granitoids from Seychelles and MIS

Seychelles granitoids (Ashwal et al., 2002)

Seychelles granitoids can be divided on the basis of field observations into a grey-granite (Mahé type), grey-gneissose granite and a pink/red-granite (Praslin type) (Ashwal et al., 2002). Textures also vary between massive (medium-grained) to porphyritic, with aplitic dykes and mafic enclaves also present. These features are also present in Mt. Abu samples. The gneissose slightly foliated varieties are thought to be due to magmatic banding which may occur near contacts of the intrusion (Ashwal et al., 2002). Most Mahé and Praslin granitoids are subsolvus (plagioclase dominant), with biotite as the dominant mafic mineral (\pm hornblende). Seychelles granitoids, unlike those of Mt. Abu, have well-preserved magmatic textures (subhedral K-feldspar and plagioclase with interstitial quartz), with only some recrystallized grain boundaries, while accessory minerals are similar to those found in Mt. Abu samples.

These granitoids are also intruded by subvertical dolerite dykes, which are partially to almost-completely altered to amphibolite, epidote, chlorite and muscovite (preservation of magmatic clinopyroxene and plagioclase in most samples). These have a similar mineral assemblage to Mt. Abu dolerites, although Mt. Abu samples preserve no magmatic clinopyroxene and usually have an amphibolitic schistose texture.

Malani Igneous Suite (MIS) peralkaline Barmer granitoids (Maheshwari et al., 2001)

These highly silicic granitoids vary in outcrop from phaneritic massive to porphyritic to aplitic. They are crosscut by associated felsic and mafic dykes. These are hypersolvus granitoids, with perthitic orthoclase being the dominant feldspar (although some samples have minor microcline and plagioclase). Clinopyroxene (altered in rims to riebeckite) \pm amphibole is the major mafic minerals with associated accessories such as zircon, titanite, rutile and magnetite.

Geochemically, they are peralkaline, with high SiO₂ contents. They are similar to other A-type granites with high concentrations of the alkalis, Zr, Nb, Ce, Y and Zn, as well as Rb and U and low concentrations of Al₂O₃, CaO and Sr. They are also depleted in Fe, MgO and TiO₂.

MIS peraluminous Jalore granitoids (Maheshwari et al., 2002)

In the field, three varieties are observed, which are, from oldest to youngest, biotite (and 2-mica types) granite, hornblende granite and biotite ± hornblende granite. These have been intruded by late-stage rhyolitic porphyry dykes and dolerite dykes. The two older varieties also contain mafic enclaves. In thin section, textures can be massive fine- to coarse-grained and porphyritic. The main feldspar is plagioclase in the biotite granite, and k-feldspar in the others, while quartz, biotite and hornblende are the major constituents. Accessory minerals are zircon, muscovite, apatite, sericite, titanite, rutile and Fe-oxides. Hornblende granites are deformed and stretched, with recrystallized groundmass in a preferred orientation around porphyroclasts. Retrograde alteration to epidote and sericite also occurs.

Geochemically they have a restricted range of compositions, although comparative variations occur in major and trace elements. Biotite granites are enriched in SiO₂, MgO, FeO and CaO, while hornblende granites are enriched in the alkalis, Zr, Nb, La and Ba with depletion in Rb, Sr and Al₂O₃. The youngest biotite (± hornblende) granite is enriched in SiO₂, Al₂O₃ and Rb, and depleted in Zr and Nb, comparatively.

8.2 Geochemical comparison of Mt. Abu and Erinpura granitoids (and felsic dykes) with those from the Seychelles and MIS

Modal proportions of Seychelles granitoids in the classification scheme of Fig 8.1 show a clustering of samples in the monzogranite field, with three samples within the alkali-feldspar field. There is a clear separation of Seychelles granitoids from the Mt. Abu and Erinpura felsic suites. This may be due to the fresh, undeformed and unaltered nature of the Seychelles samples when compared to those from India in this study.

Classification in the normative Q'-ANOR diagram of Streckeisen and Le Maitre (1979) is less distinct, as Seychelles granitoids span the range from alkali-feldspar granites to syeno- and monzo-granites, as well as one quartz diorite outlier (Fig. 8.2). MIS rhyolites are classified similarly to Mt. Abu granitoids and felsic dykes. In this diagram, Erinpura samples are classified as containing a greater proportion of plagioclase, and plot as monzogranites.

Mt. Abu samples spread across the metaluminous (predominant) to peralkaline sectors of the ASI diagram, while Seychelles granitoids are almost exclusively metaluminous in nature. The MIS felsics from Barmer plot

exclusively within the peralkaline sector. This is in contrast to the MIS-Jalore “peraluminous” felsics, which are in fact metaluminous to peraluminous in nature (Fig. 8.3). Erinpura granitoids plot on the boundary between the metaluminous and peraluminous sectors as well as farther into the peraluminous field. MIS samples from Carter (2005) are arrayed across all three sectors, with peralkaline samples in the minority.

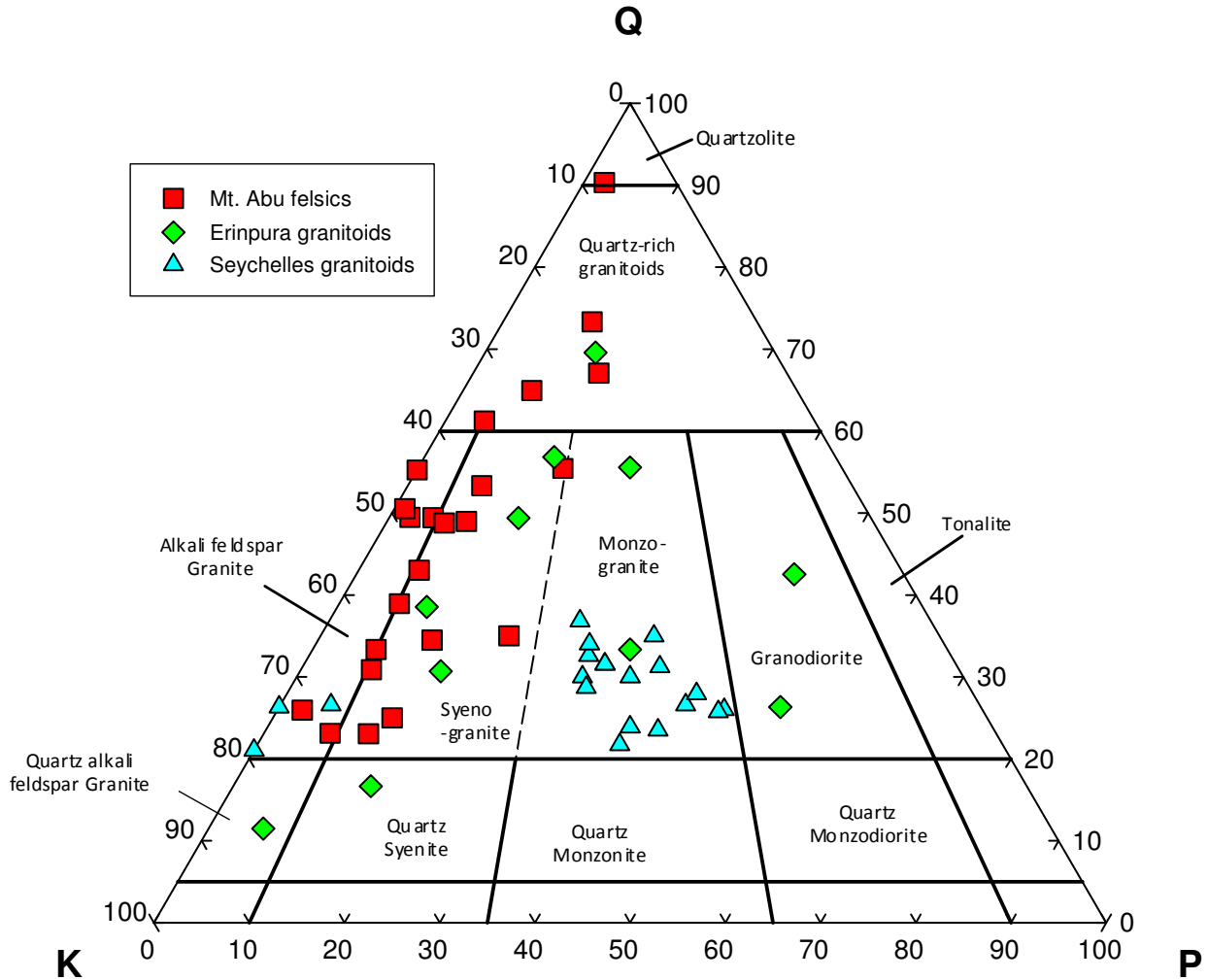


Figure 8.1. Ternary diagram for major mineral rock-classification, according to modal mineralogy proportions of K-feldspar, plagioclase and quartz (after Streckeisen, 1976).

Mt. Abu and Seychelles samples generally exhibit similar gradients and are the most consistent in exhibiting the expected granitic trend of a decrease in all major elements shown with increasing silica (Fig. 8.4); however, Mt. Abu samples exhibit a weaker correlation for CaO and P₂O₅ compared to Seychelles granitoids. Erinpura and MIS (Carter, 2005) felsic rocks are in general more scattered and therefore not well-correlated in some of the diagrams.

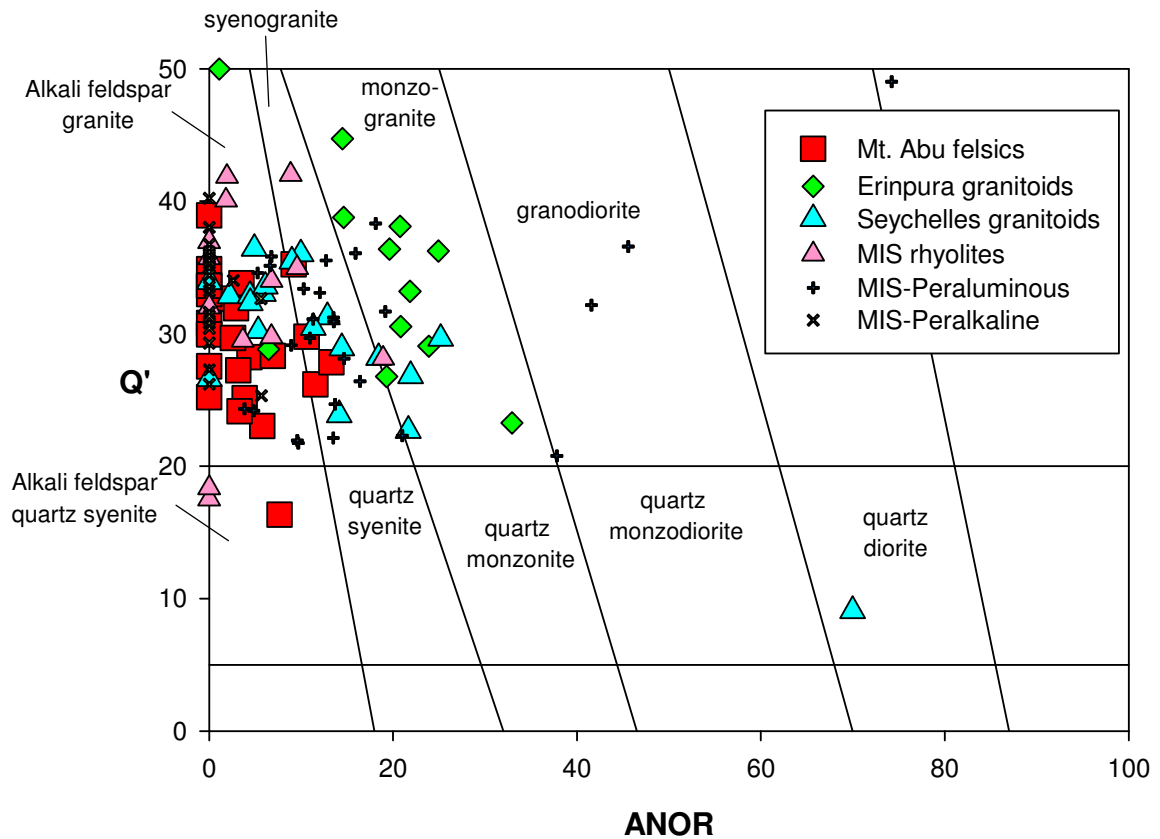


Figure 8.2. Normative classification of the Mt. Abu, Erinpura, Seychelles and Malani Igneous Suite samples, according to Streckeisen and Le Maitre (1979).

The relationships between major elements and silica in the peralkaline and peraluminous samples of Maheshwari et al. (2001; 2002) are generally poorer, although the Jalore samples generally follow the Mt. Abu and Seychelles trend. The peralkaline samples however, show no correlations and are highly enriched in silica. LOI is greater in Mt. Abu samples (average LOI= 0.94) than in those of Seychelles granitoids (average LOI= 0.37), which may indicate a greater degree of alteration (due to deformation) within the Mt. Abu granitoids.

All samples show scatter in the relationships between K_2O and Na_2O , although Mt. Abu samples cluster levelly, showing negligible change with increasing silica content (Fig. 8.5). Seychelles and Erinpura granitoids show a trend of decreasing MgO with increasing silica.

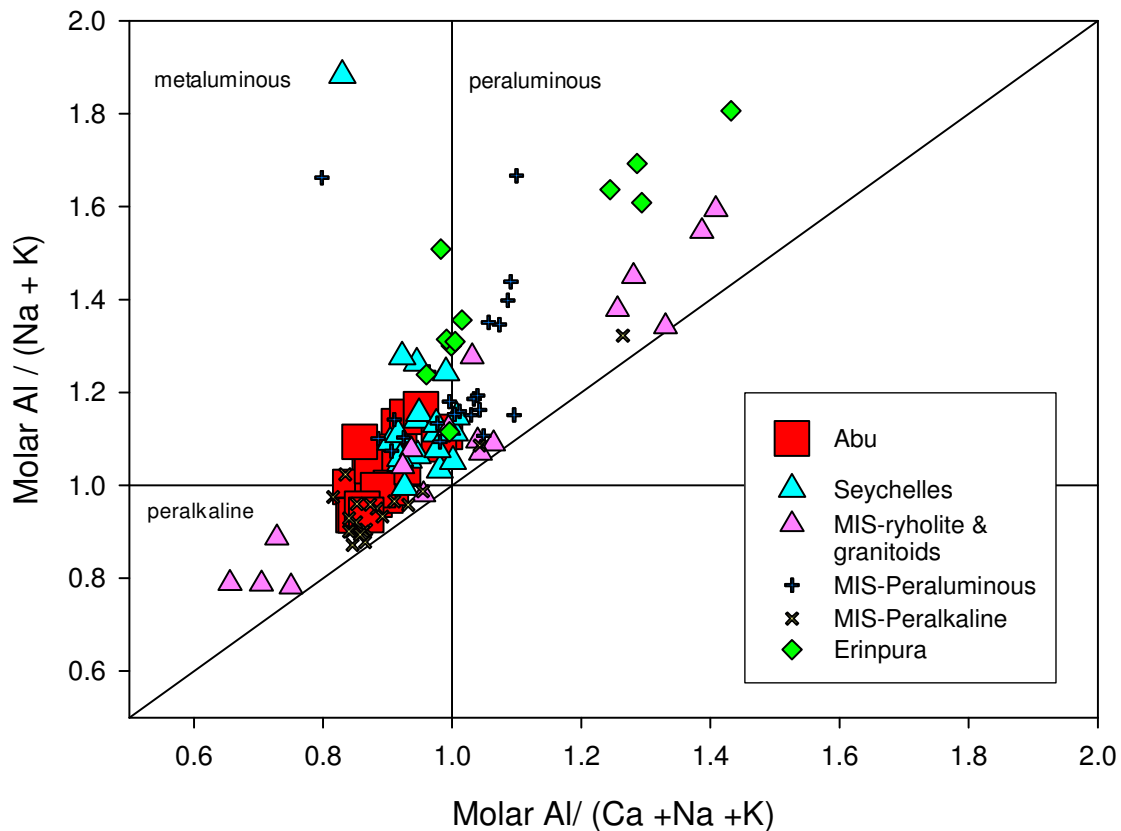


Figure 8.3. Aluminium saturation index (ASI) plot for granitoids from Mt. Abu, Erinpura, MIS and Seychelles. Mt. Abu and Seychelles samples are predominantly metaluminous, with a few peralkaline samples, while MIS samples span all fields (after Maniar & Piccoli, 1989).

Most felsic suites here do not show any strong correlations between silica and trace element abundances (Fig. 8.6). Mt. Abu samples show trends of increasing abundance in LILE (Th, U and Rb), and a slight decrease in Ba and Sr with an increase in silica. The latter relationship is also observed in the Erinpura and Seychelles samples. The peralkaline MIS-Barmer samples (and to a certain extent, the MIS-Jalore samples) are highly enriched in Zr over Mt. Abu, Seychelles, Erinpura and MIS felsics of Carter (2005).

Mt. Abu and MIS samples are positively- and negatively- correlated for Ba and Rb, with respect to Sr (Fig. 8.7). The good correlation between Ba and Sr may be attributed to plagioclase and K-feldspar removal, while the negative correlation of Rb with respect to Sr is due to the preferential enrichment of Rb in the magma/melt due to its larger ionic radius. Erinpura and Seychelles granitoids do decrease in Rb with increasing Sr, but the correlation is weaker. MIS peraluminous and peralkaline samples tend to scatter (or cluster, in the latter) with no relationships between the elements. The generally positive correlation between CaO and Sr in all sample suites (excluding the MIS-Barmer peralkaline samples) may have been caused by the early removal of plagioclase from the source of these felsic samples or may reflect source variations.

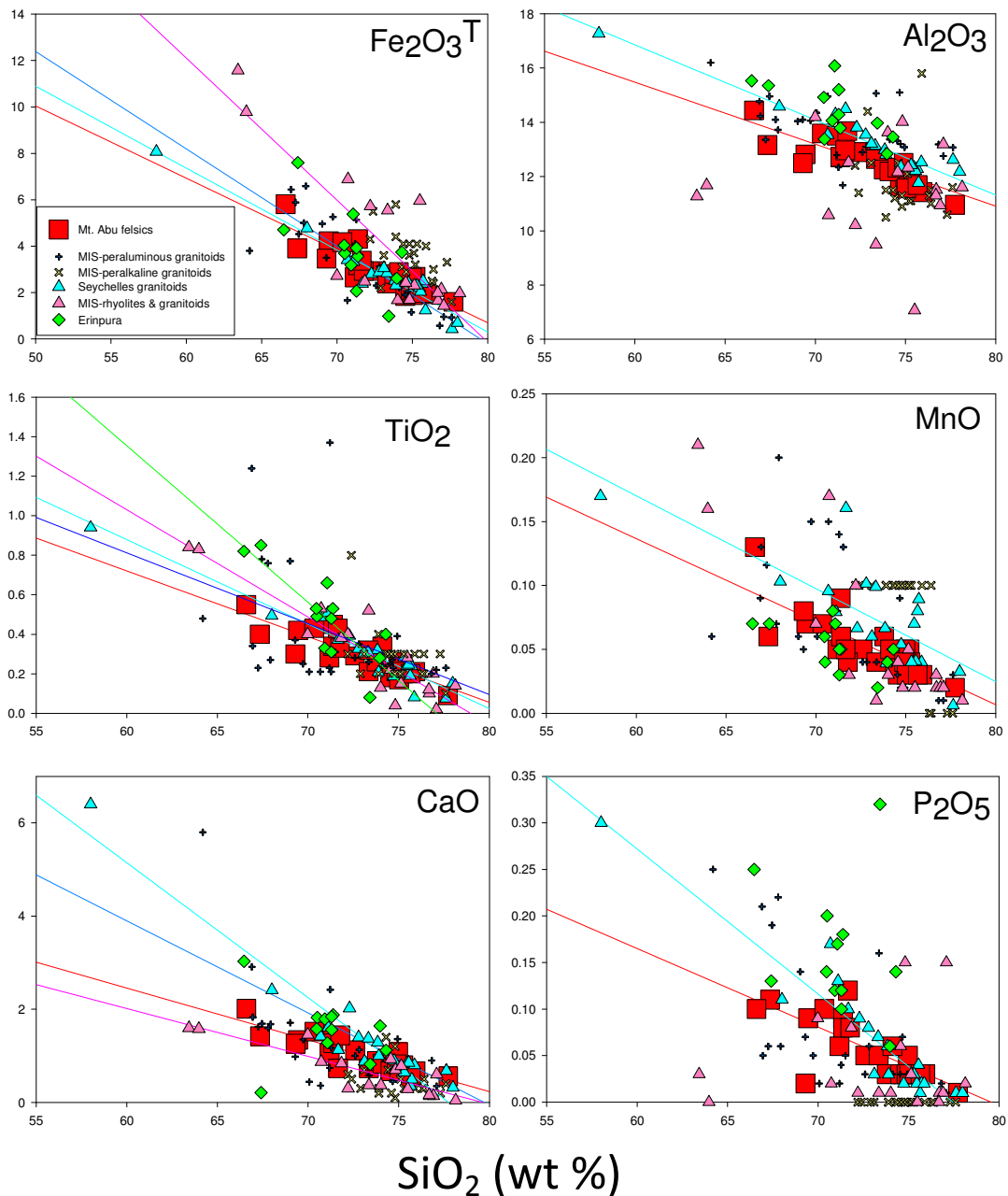


Figure 8.4. Harker diagrams of major elements (in wt %) versus silica (wt %) for Mt. Abu, Erinpura, MIS peraluminous, MIS peralkaline and Seychelles granitoids. Data for Seychelles granitoids are from Ashwal et al., 2002 and data for MIS samples are from Maheshwari et al., 2001, 2002).

The La vs. La/Yb graph demonstrated the similar nature of the Mt. Abu, Seychelles and MIS samples in terms of incompatible elements, as they have similar shallow gradients indicating enrichment of both light rare earth elements (LREE) and heavy rare earth elements (HREE). This may be due to the more evolved composition compared to the that of the Erinpura samples, which have a steep positive gradient, indicative of the greater difference in values between the LREEs and HREEs. The MIS samples (not shown here) of Maheshwari et al (2001; 2002) have the shallowest slopes of all samples due to the great enrichment in both LREEs and HREEs.

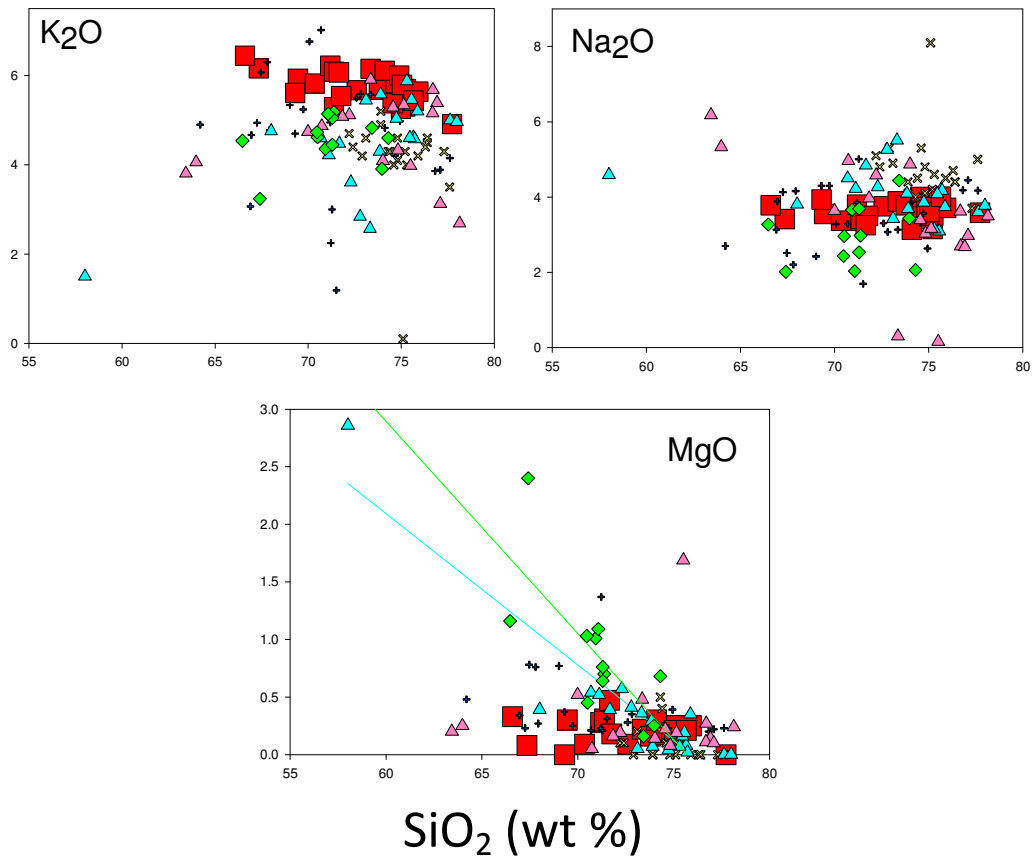


Figure 8.5. Harker diagrams of major elements (in wt %) versus silica (wt %) for Mt. Abu, Erinpura, MIS peraluminous, MIS peralkaline and Seychelles granitoids.

In terms of rare earth element (REE) chondrite-normalized plots (Fig. 8.8), the overall shape and slope of the Praslin Group granitoids are most similar to Mt. Abu, with a similar average $(La/Lu)_N$ gradient of 6.28, slightly greater than the Mt. Abu average (5.84), as well as similar LREE and HREE slopes. Similarities also exist between overall abundances of REEs and size of the Eu-anomaly (and the Eu-anomaly also increases with silica content). The Praslin Group granitoids are more tightly grouped than Mahé samples. Mahé granitoids have lower average abundances and smaller Eu-anomalies, but similar slopes to both Praslin and Mt. Abu samples. Both groups have steeper LREE- and flatter HREE-slopes, with weak negative Ce-anomalies as well. MIS peraluminous (Jalore) granitoids are very similar in shape, as well as average REE abundances and LREE and HREE slopes, as Mt. Abu samples (although the overall $(La/Lu)_N$ of 11.52 is greater than that of Mt. Abu samples). MIS peralkaline samples are highly enriched in all REEs over other samples, with a shallower overall $(La/Lu)_N$.

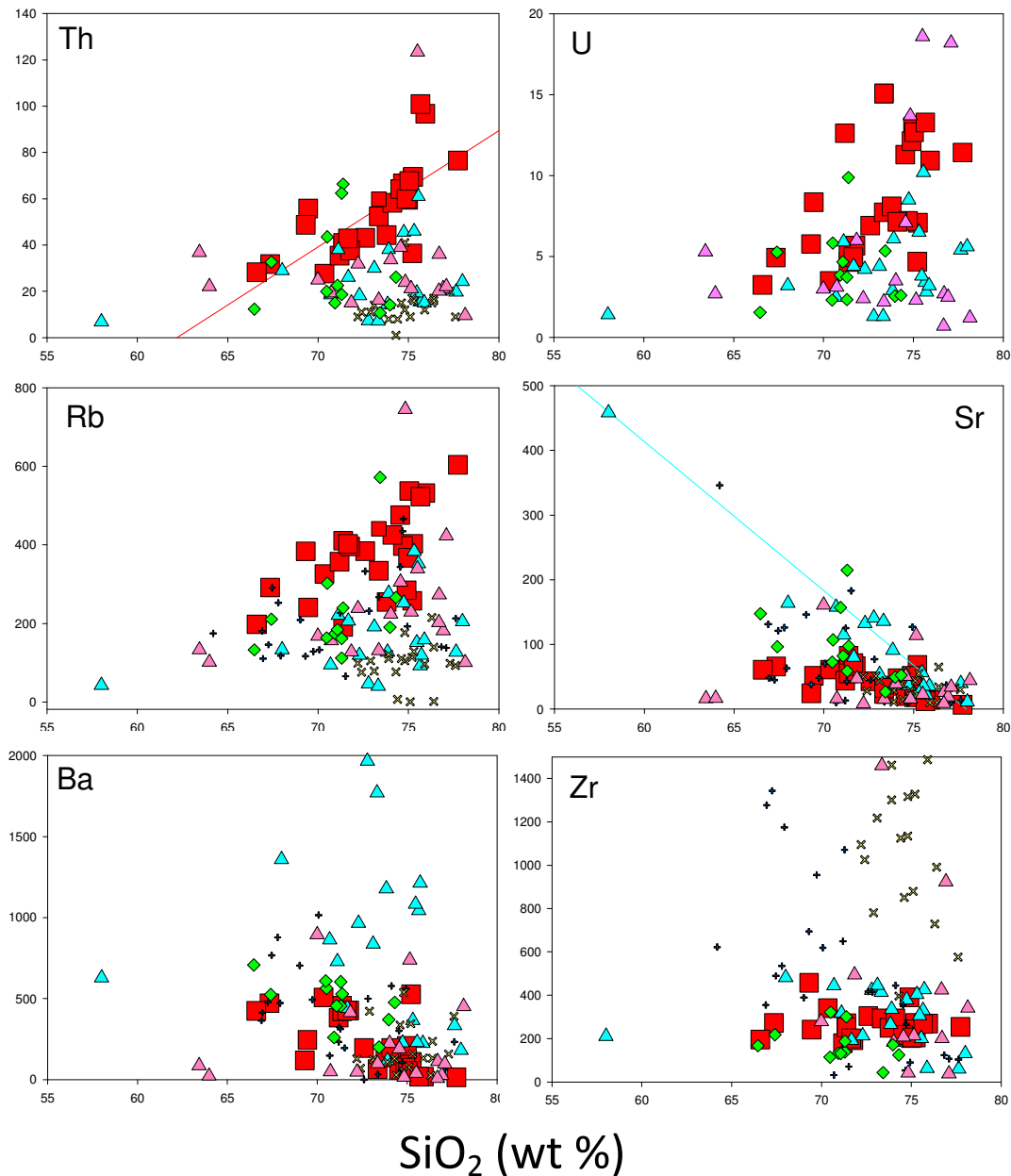


Figure 8.6. Harker diagrams of incompatible trace elements (in ppm) versus silica for Mt. Abu, Erinpura, MIS peraluminous, MIS peralkaline and Seychelles granitoids. All are LILE, save for Zr, which is a HFSE.

The MIS samples from Carter (2005) vary considerably. A comparison of the $(La/Lu)_N$ slope in the four granitoids from this MIS study to samples from Mt. Abu shows that they are similar, although the Eu-anomaly is smaller in magnitude. These granitoids are also similar to the MIS-Jalore samples from the Maheshwari et al. (2002) study. The shape of the REE plot is also similar, with the LREEs gradient being greater than that of the HREEs. The rhyolites from this MIS have shallower LREE, HREE and $(La/Lu)_N$ gradients as compared to the granitoids of the study or the Mt. Abu samples.

The spider diagrams for Praslin Group granitoids (Fig.8.9) are similar in abundance as well as shape to Mt. Abu samples. Mahé Group granitoids have lower abundances, but the overall shape is similar, with well-developed Sr, P and Ti anomalies. The negative Nb-anomaly is more greatly developed than either Mt. Abu

or Praslin Group samples, while the Ba-anomaly is weakly-developed or positive in some samples, indicating lesser removal of K-feldspar from these samples. K-values are also not depleted relative to Th-values, as in Praslin Group and Mt. Abu samples.

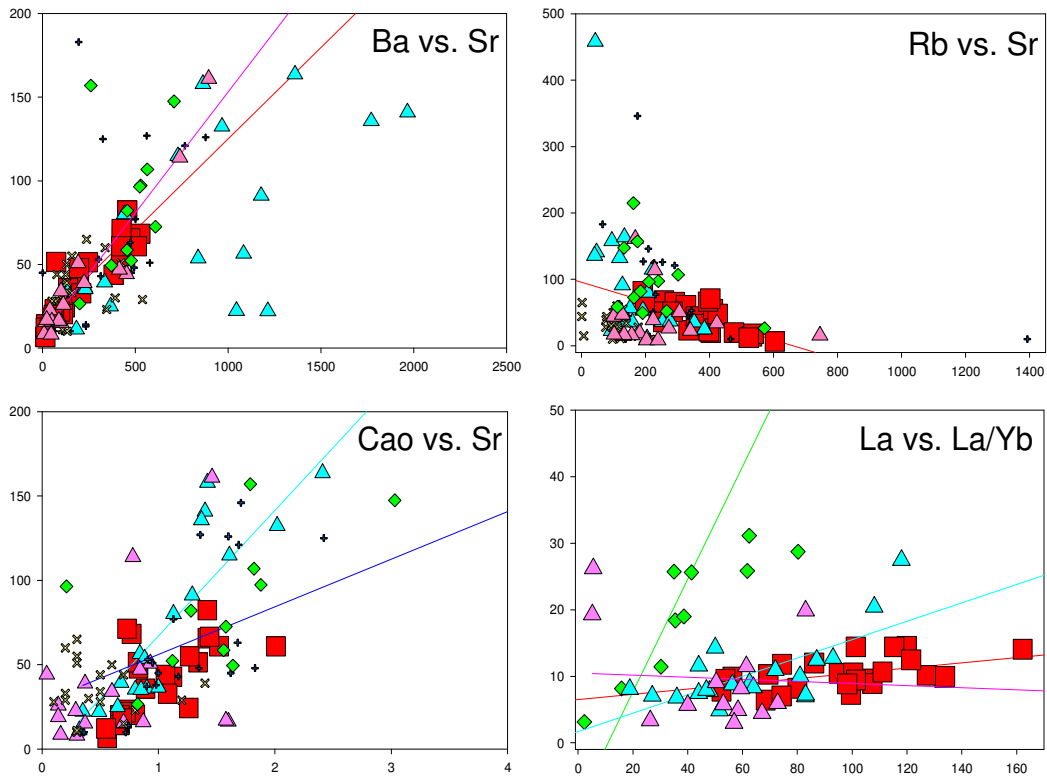


Figure 8.7. Inter-element diagrams (in ppm) for Mt. Abu, Erinpura, MIS peraluminous, MIS peralkaline and Seychelles granitoids.

MIS samples differ in that they have high abundances of the more incompatible elements (to the right of the graph) with the result that the slope from highly incompatible to moderately incompatible elements (from La to Y) is very shallow and the Sr, P and Ti anomalies are extremely well-developed. The LIL and radioactive elements to the left of the graph are present in lower abundances relative to those of Mt. Abu, Praslin Group or other MIS (Carter, 2005) samples. They also have moderate to strong Ba and Nb anomalies. Some MIS-Barmer peralkaline samples have negative Rb-anomalies as well.

The positive ϵNd_{750} MIS samples from Carter (2005) have a spider diagram shape similar to the MIS peralkaline samples from Maheshwari et al. (2001), while the negative ϵNd_{750} samples, which include the Jalore granitoids, are similar in shape and element-abundance to the Mahé Group granitoids from the Seychelles.

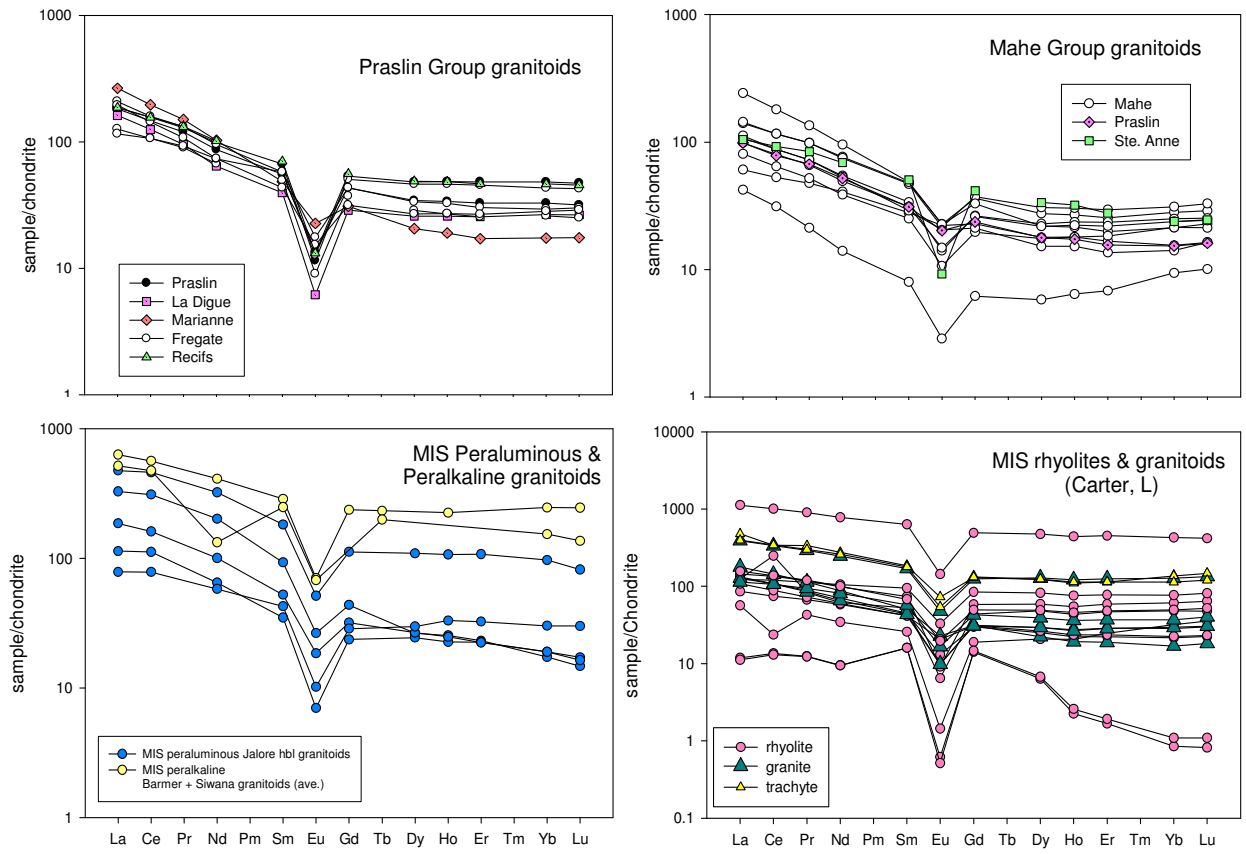


Figure 8.8. REE diagrams for Seychelles, Malani Igneous Suite peraluminous and Malani Igneous Suite peralkaline granitoids.

Mt. Abu and Seychelles dolerites - The spider diagram comparing Mt. Abu and Seychelles dolerite dykes is designed to show the similarity in immobile trace element patterns between the two sample suites. The more mobile (in aqueous solutions) LILE such as Rb, Ba and K are elevated in Mt. Abu dolerites, which can be explained by their higher degree of alteration and metamorphism (Mt. Abu samples are metamorphosed to upper-greenschist lower-amphibolite mineral assemblages and also have a schistose fabric). Both suites have moderate to strong Ba and Nb anomalies. Mt. Abu and Seychelles dolerites show similarities in their HFS and immobile elements (save for Nb, where Mt. Abu dolerites have a higher value than Seychelles).

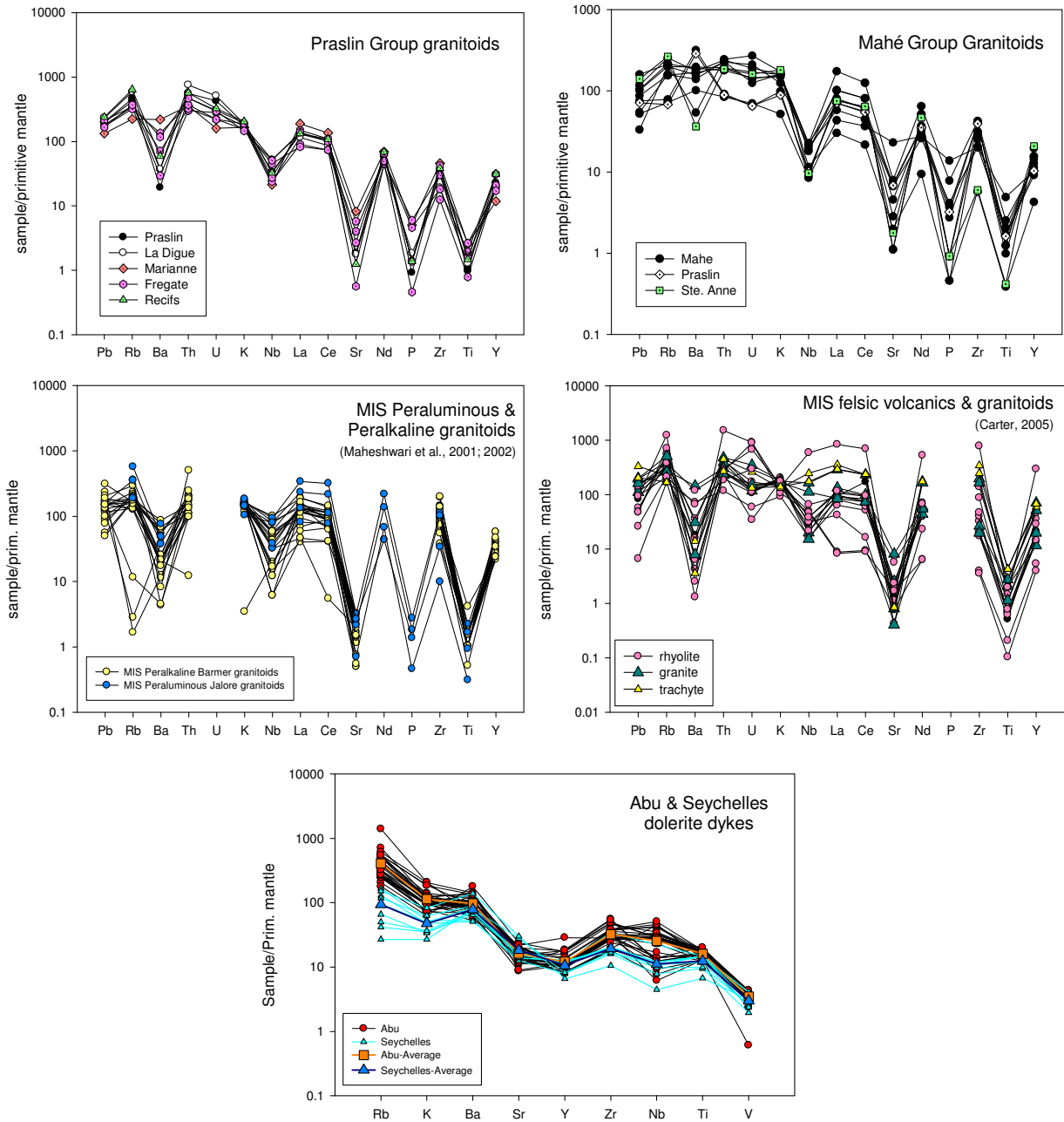


Figure 8.9. Spider diagrams for Seychelles, MIS peraluminous and MIS peralkaline granitoids and Seychelles and Mt. Abu dolerite dykes.

9. DISCUSSION

Mt. Abu Granitoids

In previous geological maps, the Mt. Abu pluton has either been split into a deformed older (Erinpura granite age) component and a younger undeformed massive (pink Jalore granite of the Malani Igneous Suite (MIS)) component, or it has been mapped (Geological Survey of India, 1998) as belonging to the Erinpura granite suite, which is estimated to be between ~800-870 Ma, although most ages cluster around ~840 Ma. This ambiguity in the age is due to a lack of geochronologically reliable and precise data, as well as sound geochemical and petrographical characterization.

The Mt. Abu pluton is simple in nature and was intruded at mid-crustal to shallow levels, implied by the lack of garnet in the source (relatively flat slope of HREEs) as well as rhyolite dykes that intrude the granitoids. The Mt. Abu granitoids are classified as syenogranite to alkali feldspar granite, which are highly evolved and form at shallow depth in the crust. The granophyric texture in the groundmass of many granitoids also supports a shallow level of intrusion, as micrographic intergrowth is formed by rapid co-crystallizing of quartz and K-feldspar due to the loss of vapour pressure during volatile release/loss (Mason, 1985; Vernon, 2004; Villaseca et al., 2009) as the magma nears the surface.

The relatively uniform and restricted composition of this pluton, together with the enrichment (relative to other granitoids in this study) of incompatible elements, may be due to derivation from- and partial melting of a single batch of magma, with mixing and assimilation of various components early on in the magma's evolution (Chappell, 2010). Rare mafic enclaves with diffuse contacts also support mixing/assimilation within these granitoids. The source (s) of the magma would have to be confirmed by Sm-Nd and other isotopic data. The lack of evolution from more mafic granodioritic compositions to the more felsic monzogranites and alkali feldspar granites as well as the lack of a decrease in compatible elements with increasing SiO₂ signifies that fractional crystallization was not the major process controlling evolution of the Mt. Abu granitoids (Villaseca et al., 1998; Cobbing, 2000; Martin & Moyen, 2002; Villaros et al., 2009). A lack of correlation between the mafic (Mg+Fe) molar ratio and refractory elements in the Mt. Abu samples is taken as evidence of there being few refractory minerals (such as zircon, Fe-oxides and garnet) entrained from the source, as is the case in the S-type granites of Villaros et al. (2009).

The varying textures within the pluton may be explained by injection from the magma chamber through a system of feeder dykes and pipes. The diffuse to sharp contacts within the Mt. Abu pluton make the mechanism of intrusion by feeder dykes and pipes plausible (Cobbing, 2000). This mechanism may allow for slight variations in the magma (fO_2 , volatile content, rates of cooling and time taken for ascent). An increase in oxygen fugacity causes bonds between the silica and oxygen to break, resulting in slow nucleation rates

and porphyritic growth (Vernon, 2004). The S-C foliations (trending NW-SE) in the shear zone that grade to mylonitic gneiss indicate that the Mt. Abu pluton underwent a period of compressive stress. Possibilities for formation of the foliated and augen gneiss textures are either, i) during intrusion or ii), subsequent deformation post-intrusion. The deformatory fabric possibly formed during initial intrusion, with reactivation during a later event. This later event may be Pan-African in age, as these granitoids record a Pan-African argon resetting age. The greatest degree of deformation (augen gneiss and a shear zone) is found at the western edge of the pluton, which would suggest a compressive environment and possibly space constraints during intrusion.

Mt. Abu felsic samples are alkali-calcic to alkali within the silica vs. MALI diagram of Frost et al. (2001), and plot as alkaline syenogranites and alkali feldspar granites. These felsic rocks are characteristic of extensional environments, such as rifts or plume-settings (Whalen et al., 1987; Eby, 1990). These A-type granitoids are thought to be the most highly differentiated products of fractional crystallization of mafic mantle-derived magma and as such, usually also have a mafic association. They are also enriched in incompatible elements such as the REEs, HFSEs and alkalis (Bonin, 2007). A-types are usually metaluminous to mildly peraluminous or peralkaline (Eby, 1990; Bonin, 2007), with more evolved phases having alkali rich amphiboles and pyroxenes in the former, or muscovite in the latter.

Mt. Abu granitoids are dominantly metaluminous in character, with only the late-stage rhyolite dykes and foliated granitoids being peralkaline, although all samples are classified as highly evolved syenogranite and alkali feldspar granite. These weakly peralkaline samples are similar petrographically and geochemically to the metaluminous samples and do not display any significant increase in the concentrations of incompatible elements, unlike the highly-enriched late-stage alkali-feldspar granite products of fractional crystallization within A-type granitoids. The rare earth element (REE) diagrams for Mt. Abu have appreciable $[La/Lu]_N$ slopes with light REE enrichment, indicative of upper-crustal derivation (Chappell & White, 2001; Bagas et al., 2010). No samples from Mt. Abu, even the most silica- and K-rich, display the “gull-wing” shape of overall light REE depletion and heavy REE enrichment in REE profiles that is typical of rift- or extensional-related environments (Bonin, 1998). These samples do not display the typical sodic amphiboles and pyroxenes (riebeckite, arfvedsonite and aegirine) either, while fluorite, another late-stage fractionate, is also rare.

The deformed nature of the Mt. Abu granitoids is also unlike rift-related granitoids, with De Wall et al. (2006) concluding that the Mt. Abu pluton was intruded within a compressive strain field. The lack of peraluminous or corundum normative samples implies that these are not enriched A-type granitoids, which have a large degree of crustal (metasedimentary) interaction and contamination (Rämö & Haapala, 1995; Dall’Agnol et al., 2005). These are most similar to Praslin Group granitoids from the Seychelles, as described

in Ashwal et al. (2002), which are not alkaline in character, but I-type metaluminous. The high alkali-content in Mt. Abu samples may be explained by derivation from a high-K source, which may be of crustal (including meta-igneous andesite) origin, (Roberts & Clemens, 1993; Liégeois et al., 1998). The high Zr-values of Mt. Abu granitoids can also be linked to the high alkali-content, because as the alkali concentration increases, so do Zr-saturation levels (Watson & Harrison, 1983). Alkaline and peralkaline magmas are very high temperature (~800-900°C; Dall'Agnol et al., 2005) with no inherited zircons present as they have been dissolved. Zr is anomalously enriched in these granitoids, as Zr-saturation levels increase with an increase in temperature (Watson & Harrison, 1983). The presence of xenocrystic cores in the Mt. Abu zircons (samples AA6-35, the augen gneiss; see Fig. 6.21) implies that the magma may not have been of a high enough temperature to dissolve all zircon inherited from the source (Villaros et al., 2009), unlike alkaline rift-related magmas (Hoskin & Schaltegger, 2003; Miller et al., 2003).

Although the Mt. Abu granitoids plot as K-rich syenogranite and alkali feldspar granite, their metaluminous nature, immobile REE diagram shapes, REE ratios, lack of alkali rich mafic minerals and syndeformational nature suggest that these granitoids should not be typified as A-type alkaline rift-related granites. The high K, LREE and HFSE values may be derived from an enriched source rock. Mt. Abu granitoids also have moderate Nb-anomalies in the spider diagram, which are due to the large crustal component and also suggest that the source was upper crustal in nature, and hence rich in the elements mentioned above. However, the source was not metasedimentary or supracrustally derived, as these would impart signatures to the Mt. Abu granitoids such as peraluminosity and/or being corundum normative. The source magma may have had an ancient crustal component or contamination in the form of the Archaean Banded Gneiss Complex (BGC; ~3.5 -2.5 Ga), which forms the basement to this region. Fractional crystallization of a mantle-derived mafic magma is an unlikely origin for these samples as well, due to the lack of exposure of large volumes of mafic intrusives or an array from more mafic to more felsic granitoids. The Nb-anomalies may also reflect an arc component in the source (Roberts & Clemens, 1993; White, 2007). These felsic rocks may be a distal expression of a subduction zone, as magmatism within a magmatic arc may change from more tholeiitic, to calc-alkaline I-type and then become progressively more evolved as distance from the arc increases. The Seychelles granitoids are compositionally less evolved (especially if one takes into account the mafic intermediate group) than the Mt. Abu granitoids, plotting as an array from quartz diorite (intermediate rocks) → monzogranite → syenogranite → alkali feldspar granite. The Mahé Group granitoids and the intermediate group granitoids here are more primitive geochemically as well. Thus, the Seychelles granitoids may represent a source that is intermediate between an arc and crustal setting, while the Mt. Abu samples would represent a distal facies, intermediate between subduction-related I-type and within-plate, anorogenic A-type magmatism, possibly within a back-arc setting.

The Mt. Abu granitoids are Neoproterozoic in age, and have been dated in this study at ~765 Ma. Samples of massive orange-pink granite, mafic-foliated granite and augen gneiss from the pluton were dated using U-Pb zircon ID-TIMS methods at 766.0 ± 4.3 Ma, 763.2 ± 2.7 Ma and 767.7 ± 2.3 Ma, respectively. This overlap in ages is taken as evidence that despite the textural variations, all granitoids within the pluton are similar in age and formed coevally, which also implies a common source magma. This age is taken as that of separation and crystallization of the Mt. Abu magma. The U-Pb zircon age is believed to be magmatic because the zircons are transparent, colourless, have euhedral morphology with well-defined faces as well as primary magmatic zoning seen in CL-images, similar to those seen in Corfu et al. (2003). The Mt. Abu pluton is younger than the Erinpura gneiss dated in this study by more than 100 m.y., making it unlikely that the Mt. Abu pluton is related to the Erinpura granite.

The error ellipses on the U-Pb concordia do not show signs of inheritance, but several show some signs of Pb-loss. This Pb-loss is interpreted as disturbance caused by the younger Pan-African tectonic event dated by Ar-Ar methods in this study. This event also caused dissolution and recrystallization of some of the zircons in the augen gneiss samples (see Fig. 6.21 B-C).

The Mt. Abu granitoid pluton has been related to the Erinpura granitoid suite in the Geological Survey of India (1998) maps. This suite was thought to be intruded during the last stages of the Delhi orogeny (Bhushan, 1995), with the Mt. Abu pluton being the post-orogenic expression of this event (800 ± 50 Ma; Choudhary et al., 1984). Alternately, it has been linked to the younger MIS by Choudhary et al. (1984) and Gupta et al. (1989) on the basis of Crawford's (1970) Rb-Sr age of 735 ± 15 Ma.

The magmatic age of formation (~765 Ma: U-Pb zircon) results places the Mt. Abu pluton within the time limits of the MIS. A precise U-Pb zircon age of 771 ± 5 Ma by Gregory et al. (2008) obtained on a rhyolitic tuff is thought to constrain the age of the first phase of the MIS magmatism. Unpublished U-Pb zircon ages (Tucker unpubl.; mentioned in Torsvik et al., 2001b) of 771 ± 2 and 751 ± 3 Ma for rhyolites from the MIS also confirm that the Mt. Abu pluton is related to this magmatism. U-Pb zircon ages (TIMS method, Van Lente et al., 2009) of 761 ± 16 and 767 ± 3 Ma, respectively, for interlayered rhyolite and dacite within the Punagarh Group are also within error of the Mt. Abu granitoids from this study. This intermediate to felsic volcanic activity is ~30 km north of Mt. Abu, implying a spatial connection between the two terranes. As these dates represent the age of primary magmatic activity in the Sindreth and Punagarh Groups, it may be concluded that the Mt. Abu pluton is related to this magmatism as well.

This set of Mt. Abu ages is within error of the age of Seychelles and MIS granitoids as well as the Sindreth-Punagarh mafic-ultramafic volcanics (proposed as a remnant of ophiolitic mélange). The latter two suites are within ~70 km of the Mt. Abu pluton, implying a spatial as well as temporal connection. The Mt. Abu

granitoids are also similar in outcrop and geochemistry (REE- and spider-diagrams) to the Praslin Group granitoids of the Seychelles. The Seychelles granitoids have also been proven to have been spatially contiguous with the MIS (<200 km separation) through robust palaeomagnetic data. Both the Seychelles and MIS have also been shown to have arc-type ϵ_{Nd} signatures (unpublished data, Tucker, R. & Carter, L., 2001, in Ashwal et al., 2002). The implication is that the formation of these four igneous suites is related to the same geotectonic event, which is postulated by Ashwal et al. (2002) as an Andean-type arc off the western outboard of the Proterozoic supercontinent Rodinia (Fig. 9.1). This provides further evidence that Rodinia as such, was not a static, amalgamated continent, but continued to grow and evolve, at least until ~750 Ma.

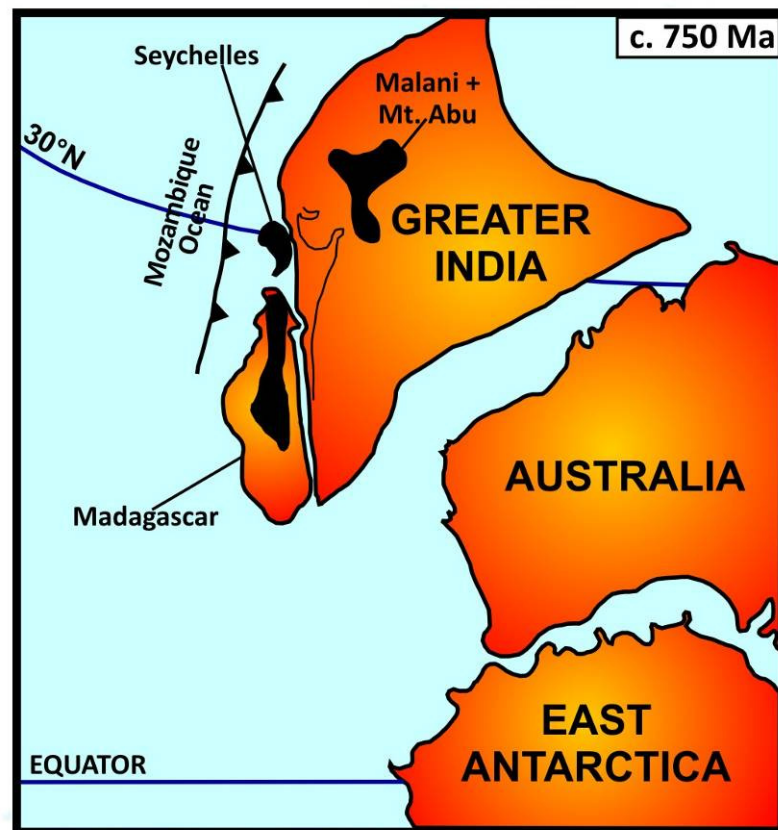


Figure 9.1. Proposed reconstruction (including Mt. Abu pluton) of part of the Rodinian supercontinent at ~750 Ma, with postulated subduction (eastward) along the western margin of India and Madagascar (after Ashwal et al., 2002).

Other igneous intrusions that are within the spatial environs of Mt. Abu include the gabbro-norite-mafic granulite intrusions to the south of Mt. Abu, which were dated by A. B. Roy & A. Kröner (mentioned in Roy, 2001) using single zircon geochronology at ~750 Ma, although the data are unpublished.

The Antsirabe Nord Suite of calc-alkaline plutons situated in northern Madagascar have also been dated at ~750 Ma and have geochemical characteristics associated with arc-related magmatism. The dominance of felsic over intermediate rocks suggests that these were formed at a continental margin, in an 'Andean' type setting. This subduction zone developed outboard of cratonic Madagascar (Thomas et al., 2009).

Similar palaeomagnetic data, ages and isotopic constraints between the Bemarivo Belt of northern Madagascar, Seychelles and the Rajasthan Belt of NW India have led some authors to propose a genetic link between the three terranes (Thomas et al., 2009). The Mt. Abu pluton can be considered as part of the Rajasthan Belt mentioned here, as has been shown by the similarities in age and spatial position to the MIS, as well as the Seychelles granitoids.

The partially altered (sericitization, recrystallization textures, bubbles within the quartz and fractures within feldspars and quartz) nature of all Mt. Abu thin sections also indicates that the pluton has undergone a major episode of metamorphism and alteration. The augen gneiss samples from this pluton indicate deformation experienced, either syn- or post-intrusional. Deformation in thin section manifests as high-strain solid-state deformation microstructures. The high strain microstructures (S-C foliations, gneissose texture) dominate in the highly deformed augen gneiss samples, while the submagmatic microstructures are prevalent within all variations. These augen gneisses are samples from the western edge of the pluton, which may suggest high strain areas around the pluton boundaries and space constraints during intrusion. The pluton may have also experienced reactivation during a later event. This later event likely occurred together with- or just prior to- the metamorphism that affected the Mt. Abu pluton. This was a regional metamorphic event, as the surrounding metasediments and the Erinpura granite of Jawaidam also show similar grades of metamorphism.

This thermal metamorphic event can be timed, as Ar-Ar ages on hornblende and biotite allow dating of the last event that reset the argon within these minerals. The age of the resetting event in the Mt. Abu granite is 508.7 ± 4.4 Ma, which constrains the timing of the deformation and metamorphism within the pluton. Hornblende is reset above ~ 550 °C (Faure & Mensing, 2005), giving us a minimum temperature of metamorphism as well. The timing of the metamorphism is Pan-African (800-500 Ma; Bonin et al., 1998; Paquette & Nédélec, 1998). Kennedy (1964) termed the Pan-African as a thermo-tectonic event resetting isotopic dates at ca. 500 Ma, which corresponds with the Ar-Ar results from Mt. Abu. Other imprints of the Pan-African reported are the granulite facies metamorphism in the Eastern Ghats, Southern Granulite Belt (south India) and in the northwest Aravalli Mountains (Roy, 2001). This age, together with that from the Erinpura augen gneiss, are the first Pan-African ages recorded for the southern Aravalli-Delhi mobile belt (Sirohi region) of northwest India, and suggest involvement within the Pan-African amalgamation of Gondwana.

Subvertical dolerite dykes that crosscut the granitoids (usually sharp contacts) have been totally altered (hornblende-actinolite-epidote assemblages), with the metamorphic grade ranging from the upper-greenschist to lower amphibolite facies ($< \sim 650$ °C). This metamorphism may have coincided with the

intrusion of the granitoid. Alternately, it may have occurred during the later Pan-African regional resetting of Ar in the hornblende and biotite of the Mt. Abu and Erinpura granitoids. The coincidence of the resetting temperature for Ar in hornblende (~550°C; Faure & Mensing, 2005) with the estimated temperature range of the metamorphism in the dolerite dykes (lower amphibolite grade) may indicate that this late Pan-African age was the likely cause of the metamorphism as well as the deformation seen within the Mt. Abu pluton. Ar-Ar ages on the dolerite dykes need to be done in order to confirm that this is true.

Erinpura Granitoids

These granites are composed of various intrusives from Sendra in the north to Sai in the south (~445 km extent), the majority of which have been poorly dated by Rb-Sr errorchron methods (Choudhary et al., 1984) to 850 ± 50 Ma. However, other more recent and accurate dating (U-Pb zircon; Sm-Nd isochron) of felsic plutonics classified as Erinpura granite has led to ages in the range of ~800-873 Ma (Volpe & MacDougall, 1990; Deb et al., 2001; Van Lente et al., 2009). As a number of ages are clustered around the ~840 Ma mark, this is thought to represent the maximum age of the end of the Delhi orogeny (Deb et al., 2001). The type-locality granitoid (an augen gneiss) at Jawai dam, the basis upon which all other Erinpura granitoids are classified, has been accurately dated in this study.

The Erinpura granite suite is thought to have intruded syntectonically (deformation fabric) during the closing stages of the Delhi orogeny and is thus classified as a syn- to late-tectonic granitoid (Bhushan, 1995). The Mt. Abu pluton, because of its close spatial relation to the Erinpura granite suite, has been classed in the literature as the late- to post-orogenic part of the Erinpura granite suite. However, U-Pb zircon age-dating performed on the Mt. Abu pluton has shown it to be geochronologically similar to the younger MIS and is hence not related to the Erinpura granite suite.

The U-Pb zircon age from this study on the type-locality Erinpura augen gneiss is 880.5 ± 2.1 Ma, ca. 100 m.y. older than the oldest Mt. Abu sample dated in this study. This age is taken as that of crystallization of the Erinpura granitoid, as the analyses with small error ellipses plot close to concordia. Zircons from this sample have sub-rounded edges and a purple tint. They are not as pristine or prismatic as those from the Mt. Abu granitoids. CL-and BSE-imaging show areas of inhomogeneity within zircon interiors, disturbed magmatic layering and Zr-dissolution within Erinpura zircons. These are caused by the deformation to an augen gneiss texture, which is commonly seen in outcrop (Corfu et al., 2003).

The disparity in the ages of the two granitoids negates the conventional view that these two intrusives are related and that the Mt. Abu pluton is a part of the Erinpura plutonism. The reliable U-Pb zircon ages indicate that the Mt. Abu and Erinpura granitoids should not be placed together stratigraphically and that

although they are adjacent spatially, they belong to different events of formation. The Erinpura granitoids belong to a continental collisional-type event, within the Delhi orogeny.

Erinpura granitoids have a distinctive megaporphyritic texture, which, according to Vernon (2004), is caused by slow undercooling and nucleation rates within the magma chamber. In the field Erinpura samples vary from megaporphyritic to augen gneiss, while mylonitic gneiss is present in the Sirohi shear zone. Contacts with the metasediments are tectonized, which, together with the prevalence of deformed gneissic granitoids, indicates intrusion during a compressional phase (Schulmann et al., 1996).

Thin section alteration of K-feldspar and plagioclase to sericite is prevalent, while plagioclase and rare hornblende are altered to tremolite/actinolite, epidote and chlorite. The hornblende (Fig.4. 8 B) has a relict core (subhedral) surrounded by growth rims/layers which are now totally altered. This brownish totally altered hornblende is interpreted to represent relict igneous hornblende (Dennis et al., 2004). The alteration to more hydrous minerals is due to hydrothermal fluid movement during metamorphism (Vernon & Clarke, 2008). The presence of sillimanite indicates that the metamorphism reached temperatures and pressures in excess of $\sim 550^{\circ}\text{C}$ and $\sim 3\text{-}4$ kbars (Vernon & Clarke, 2008).

The dominance of high strain deformation microstructures (deformation cleavage in mica and separation and anastomosing of less competent material around more competent porphyroclasts) in thin section and abundance of granitic-gneiss, augen gneiss and mylonitic gneiss in outcrop implies that the strain and deformation experienced by the Erinpura granitoids was more widespread than that within the Mt. Abu pluton (localized occurrences). The higher proportion of plagioclase in the mode compared to the Mt. Abu samples is reflected by the higher Sr-values, and indicates that the source of the Erinpura granitoids was more primitive or less differentiated than that of the Mt. Abu samples (Martin & Moyen, 2002).

The differences between the two suites are also apparent in the mafic mineral assemblage, as, although biotite dominates in both suites, muscovite is the subsidiary mafic mineral found in Erinpura granitoids and hornblende is almost totally absent. Sillimanite is also present in one Erinpura sample. The presence of these Al-rich minerals indicates that the source of the Erinpura magma must have been Al-enriched. The metaluminous to strongly peraluminous nature of the Erinpura granitoids confirms that the magma was enriched in Al, as does the presence of corundum in the norm and muscovite and sillimanite in the mode (Chappell & White, 2001). The Erinpura magma, during its ascent, may have incorporated metasediments (of supracrustal origin) such as weathered argillaceous shales, which are Al-rich (Chappell & White, 2001; Vernon & Clarke, 2008) during crustal anatexis. The above factors are evidence that the Erinpura two-mica granitoids are S-type in nature.

The greater proportion of mafic minerals present in the Erinpura granitoids compared to Mt. Abu samples may be due to various factors such as source composition, differing degrees of partial melting or a greater degree of entrainment within the Erinpura granitoids. Entrainment of source materials would include refractory zircon, mafic minerals and Fe-Ti oxides (Villaros et al., 2009; Chappell, 2010). Entrainment is a valid possibility, as the U-Pb concordia do show an inherited component within zircons from the Erinpura granitoid dated (Chappell et al., 1998; Chappell, 2010). Erinpura samples also display stronger relationships between the maficity index and major elements such as Al, Ti, Mn (positive trends) and Na (negative trend). Transition elements V, Co, Ni and Zn are all positively correlated with regards to the mafic (Mg+Fe) molar ratio. These relationships reflect the higher mafic component in the Erinpura granitoids, which is possibly due to a greater proportion of restite (Fe-Ti oxides, mafic minerals) entrained (as these transition elements are compatible to only moderately incompatible), similar to the S-type granites of Villaros et al. (2009).

Partial melting and entrainment may have been the dominant processes acting upon the Erinpura magma, and the scatter in inter-element diagrams is possibly due to heterogenous source rocks (Chappell, 2010).

The slope of the Erinpura granitoids in the La vs. La/Yb diagram, when compared to those of Mt Abu granitoids is steeper. This steeper slope is caused by greater partitioning of the relatively more incompatible LREES over the more compatible HREEs, due to a smaller degree of partial melting (White, 2007). However, smaller degrees of partial melting should lead to greater concentrations of these REEs as well. This is not the case, as the Mt. Abu granitoids are slightly more enriched than the Erinpura granitoids. The Mt. Abu samples have greater concentrations of all incompatible elements, but this may be explained by derivation from a source that is more enriched in incompatible trace elements. This enrichment can be seen in the K_2O-SiO_2 diagram of Le Maitre et al. (1989), where Mt. Abu granitoids plot within the high-K to shoshonitic sector, while Erinpura granitoids are less enriched in terms of potassium. Since Mt. Abu granitoids are more K-rich than Erinpura samples, this would mean that they are also more enriched in incompatible elements (seen in the REE- and spider-diagrams), explaining their greater degree of enrichment compared to the Erinpura granitoids. This implies that the source of the Erinpura granitoids differs from that of Mt. Abu.

The HREE slope of Erinpura granitoids is slightly concave upwards, which would indicate retention of hornblende in the source (the brown altered hornblende crystal in Fig. 4. 8 B may be representative of this) (Rollinson, 1993). This concavity in the HREE slope is not present in Mt. Abu samples. The Eu-anomaly is not as well-developed as in the Mt. Abu granitoids, indicating that less plagioclase has been left behind in the source, or that the Erinpura granitoids have experienced a lesser degree of differentiation. The spider diagram is similar to that of the Mt Abu granitoids in most respects, with anomalies that are less well-developed, except in the case of Nb, for which the Erinpura granitoids have more intensely developed

anomalies. This could indicate a greater crustal/arc component involved in the generation of the Erinpura magma (Roberts & Clemens, 1993).

Monazite separated from the Erinpura augen gneiss was also dated, giving a reliable $^{238}\text{U}/^{207}\text{Pb}$ age of 820.6 ± 4.2 Ma. Monazite ages usually represent the peak cooling age after intrusion or metamorphism (Foster et al., 2002). As there is a 40 m.y difference in the ages on zircon and monazite, the monazite age is unlikely to represent cooling after intrusion and instead may be a record of a younger regional metamorphic event. Other geochronological evidence for such an event are from ages on titanite (this study; 814.2 ± 2.4 Ma) from Ranakpur, which also record an age close to that of the Erinpura monazite, as well as on monazite from the Siwaya pluton (826 ± 5 Ma; Deb et al., 2001), 75 km south of the Erinpura granite.

The evidence of older xenocrystic components within the Erinpura zircons (inherited age component) is an indication that this magma entrained older components from its source and was not able to dissolve all the older zircon. Thus, the temperature of the magma did not exceed that of zircon dissolution, or the magma reached zircon saturation early on (Hoskin & Schaltegger, 2003; Miller et al., 2003). The presence of inherited zircon has been interpreted by Chappell et al. (1998) as due to relatively lower temperature crustal melting in the source.

The inherited component of the Erinpura granitoids was dated at 1971 ± 23 Ma, which is taken as the minimum age of the inherited cores and the rocks that they originated from. This age is within the time frame of the felsic plutonic intrusions (Derwal Granite, $\sim 1900 \pm 80$ Ma; Choudhary et al., 1984) of the Paleoproterozoic Aravalli Supergroup, which has poor age constraints of 2.5-1.7 Ga due to a paucity of age data.

Ar-Ar age dating was also done on biotite separated from the Erinpura augen gneiss sample. The age spectrum is clearly disturbed, but gives a mean weighted age of 515.7 ± 4.5 Ma that falls within error of the more accurate and reliable Ar-Ar age on hornblende from the Mt. Abu sample (508.7 ± 4.4 Ma). That the ages are similar to each other implies that the event causing the resetting of the argon affected both granitoid suites. The timing of the resetting event falls within the age boundaries of the Pan African orogenic event (Bonin et al., 1998; Paquette & Nédélec, 1998). This event was the cause of the latest regional lower-amphibolite grade metamorphism that affected these granitoids as well as the variable deformation within the Mt. Abu pluton (and may also have contributed to deformation within the Erinpura pluton as well).

These Pan-African Ar-Ar ages are the first such reported for the Sirohi region and may reflect an important orogenic event that has previously not been dated in this region.

Ranakpur Granitoids

The Ranakpur granitoid pluton intrudes metasediments of the Delhi SG, with granitoid veins that are boudinaged as well as folded within the calc-silicate. These are caused by deformation either during- or post-intrusion. This deformation was accompanied by metamorphism and hydrothermal fluid movement, as samples further away from the intrusive contact are very friable and yellow Fe-staining around grain boundaries can be seen in hand specimen and thin section.

The Ranakpur samples form a tight cluster on most geochemical plots. The anomalously high Sr- and Ba- and low Rb- and U-concentrations are, together with the low SiO₂-content and high (Na₂O+CaO) values, indications that the Ranakpur granitoids evolved from a more primitive parental magma, with less differentiation occurring (Martin & Moyen, 2002).

More evidence that these Ranakpur granitoids are derived from a different source are the REE profiles, which have the highest LREE enrichment and [La/Lu]_N gradients of all granitoids from this study. This large gradient is due to a mineral in the source that has a high K_D for the HREEs. The most likely mineral is garnet, which would imply pressures of greater than ~7 kbars (Martin & Moyen, 2002; Vernon & Clarke, 2008) for the generation of this pluton. The Eu-anomaly is also small or absent, implying that plagioclase was not present or stable within the source. Sr-content is controlled by the presence or absence of plagioclase in the source and will increase in the melt if there is no plagioclase in the source to buffer the concentration (Martin & Moyen, 2002). The high Sr-values, small to absent Eu-anomaly and high (Na₂O+CaO) indicate that plagioclase was not present and may not have been stable within the parental magma. The Ranakpur magma was deep-seated, as well as being relatively primitive and less differentiated (highest Mg#, (Na₂O+CaO) and Sr-values) (Martin & Moyen, 2002). The highly-developed Nb-anomaly is an indicator that this magma has a large arc component, as the SiO₂-content (and hence crustal component) is not very high.

A U-Pb zircon age of 848.1 ± 7.1 Ma was obtained from a Ranakpur granitoid and indicates that this granitoid is unlikely to be related to the type-locality Erinpura augen gneiss sample dated in this study. The different geochemistry also provides evidence of this.

The similarity in ages between the Ranakpur quartz syenite and the Revdar Rd. mylonite gneiss may indicate that a regional felsic magmatic event occurred at ~841 Ma, which could possibly be a later expression of the Delhi orogeny. Other samples from Ranakpur (a diorite and metagabbro), have been dated by Volpe & MacDougall (1990) at 835 ± 43 Ma and 838 ± 36 Ma, respectively. A sample of the Siwaya granite-gneiss (~15 km south of Mt. Abu) was dated by Deb et al. (2001) at 836 +7/-5 Ma, while the Sai granite (southeast of the Ranakpur sample from this study) was dated by Choudhary et al. (1984) at ~835 Ma as well. The similarity in these ages may indicate a separate felsic magmatic event to that of the (older,

~880 Ma; U-Pb zircon this study) Erinpura granitoid intrusion as well as the younger MIS event. Alternately, this age of ~841 Ma is taken as the maximum age of the end of the Delhi orogeny by Deb et al. (2001).

The U-Pb titanite age obtained from the Ranakpur sample of 814.2 ± 2.4 Ma is significantly younger than the U-Pb zircon age of formation, and as previously stated, may be an indicator of a separate metamorphic and/or intrusional event that affected both the Ranakpur and Erinpura granitoids. The surrounding amphibolite contains clinopyroxene and phlogopite, which indicates that temperatures reached the amphibolite-facies in this metamorphic event (Blatt & Tracey, 1995).

Ar-Ar age dating was also performed on this sample, and although the spectrum was erratic and disturbed, a mean weighted age of 789.8 ± 6.3 Ma was obtained. This age may reflect cooling after the metamorphic event dated by the titanites in this sample.

Revdar Rd. Granitoids

Revdar Rd. granitoids range from massive orange-pink granite, to foliated granitoids (mafic clusters defining foliation) and megaporphyritic augen gneiss in outcrop. Most have similarities in texture to either Mt. Abu or Erinpura granitoids and were divided on the basis of field appearance into Mt. Abu-type or Erinpura-type or those that resemble neither.

The petrography largely supported this division, as those classed as Erinpura-type has biotite and muscovite as the major mafic minerals, while Mt. Abu-type granitoids has hornblende in addition to biotite, which occurred commonly as clusters. Granophyric texture in the groundmass of Mt. Abu-type granitoids would imply a relatively shallow level of intrusion, and is similar to Mt. Abu granitoids (Mason, 1985; Vernon, 2004).

The Revdar Rd. granitoids span the range from granodioritic to ultrapotassic on Streckeisen's (1976) diagram, although the majority are monzogranitic in composition. Some granitoids plot outside the granitic fields of the diagram, most likely due to pervasive alteration, weathering and deformation of these samples, as these samples were not as fresh as those from the main Mt. Abu pluton.

Revdar Rd. granitoids plot either on the Mt. Abu or Erinpura trend-lines in the La vs. La/Yb diagram, which supports the field evidence of their being two or more granitoid subsets. This distinction is further supported by the trace element data, where there is a clear division between Mt. Abu-type and Erinpura-type granitoid. Samples falling on the Mt. Abu trend line of the La vs. La/Yb diagram have REE patterns that

are similar to those of the Mt. Abu pluton granitoids, while the same is true of the Erinpura-type granitoids, which have a slope and enrichment similar to the Erinpura granitoids.

A U-Pb zircon age for a mylonitic gneiss of 841 ± 21 Ma gives the age of the older components sampled here. This mylonitic gneiss belongs to the Erinpura-type subset, but the age is younger than that of the Erinpura type-locality augen gneiss. Later intrusion within the same event (Delhi orogeny) as the Erinpura granitoid cannot be ruled out, as the age constraints are quite large. The Revdar Rd. mylonite has also not been classified in any of the geological maps of the area, and this study shows that geochronologically, it does not belong to the Mt. Abu pluton granitoids. This implies an older granitoid component is present immediately south of the Mt. Abu pluton, within the Sirohi Group metasediments.

Sumerpur Granitoids

These samples have been classified as late stage fractionates of the Erinpura granite (Geological Survey of India (1998) map), although they are undeformed and massive with faint uneven magmatic flow-banding in outcrop, unlike the megaporphyritic Erinpura augen gneiss. Mafic enclaves with diffuse contacts also occur, as well as rare perfectly tabular to rounded mega-phenocrysts (up to 5 cm width) of white feldspar.

These samples, although undeformed, have a cloudy texture due to sericitization of the feldspars. Some submagmatic solid-state deformation microstructures are present in thin section, such as recrystallized quartz and subgrain formation. There is no evidence of strain deformation in outcrop or thin section to indicate that this granitoid has been intruded syntectonically, as is the case in the Erinpura granite. Feldspar phenocrysts also show faint primary zoning, indicating their magmatic nature. The alteration of the biotite to chlorite is due to retrograde alteration, possibly during cooling of the pluton, while muscovite is present as well.

In REE diagrams, they follow the enrichment trend of the Erinpura samples, although the overall slope of the graph is intermediate between Erinpura and Mt. Abu values. The spider diagram enrichments and depletions are similar to those of the Erinpura samples in terms of abundance, so that these can be most closely correlated to the Erinpura granitoids in terms of geochemistry, but not, however, in outcrop or thin section. Further geochronological work needs to be done to confirm the grouping/classification of this granitoid.

Swarupganj Rd. Granitoid

This isolated outcrop of granodiorite has snowy white feldspar (predominantly plagioclase) and mafic biotite that gives the sample a weak foliation, possibly magmatic in nature. This granitoid intrudes amphibolite of the Delhi SG.

This sample has the highest SiO₂-values and is a plagioclase-dominant granodiorite with weak biotite foliation. This sample also shows no signs of deformation in thin section and is unlike either the Mt. Abu or Erinpura samples modally. The Swarupganj Rd. granodiorite has a high SiO₂-content, but the lowest degree of incompatible- and rare earth element enrichment of all granitoids in this study, with almost equal light- and heavy- REE enrichment and a weak Eu-anomaly. This implies high degrees of partial melting for this granitoid magma and a source that may be depleted in incompatible elements, as it plots within the low-K calc-alkaline field of Le Maitre (1989). The petrography and geochemistry indicate that it is not similar to the Erinpura or Mt. Abu granitoids and is unlikely to be related to them.

Kishengarh Nepheline Syenite-Gneiss

This pluton is variably deformed and the sample dated is foliated. This sample does preserve its magmatic texture, although microcline has deformation twinning. The age of the zircons (989 ± 8 Ma) reflects the age of a major tectonothermal event at ~ 1 Ga. The older titanite age (1365 ± 99 Ma) is assumed to be the age of formation. Evidence for the primary nature of the age of the titanite grains comes from other studies undertaken on differentially deformed specimens of the nepheline syenite. Crawford (1970) dated the Kishengarh nepheline syenite at 1490 ± 15 Ma and although this was done by Rb-Sr dating, the age is much older than that of the zircons dated here, and much closer to that of the titanites. A biotite inclusion was also dated, which was found to be younger in age at 970 Ma. This younger age was assumed to represent the age of metamorphism. This age comes close to the age of the zircons, making it likely that the zircons have been reset during a high-grade metamorphic event. The resetting event may be related to-/or a reflection of- the formation of the supercontinent Rodinia (Roy & Kataria, 1999), which was postulated to have existed from ~ 1.3 -1.0 Ga (the so-called Grenvillian-type orogenies) (Hoffmann, 1991; Moores, 1991; Trompette, 2000; Torsvik & Meert, 2003; Torsvik, 2003). The alkaline nature of the intrusive is related to the environment of formation, which is likely extensional, such as a rift- or plume-type setting.

10. CONCLUSIONS

1. The Mt. Abu felsic pluton shares some similarities with the Erinpura granite suite, in terms of basic mineralogy and chemical composition. However, U-Pb zircon geochronology clearly indicates that the Mt. Abu felsic pluton is not related to- or contiguous with- the Erinpura granite suite. All phases within the Mt. Abu pluton were intruded coevally and should not be separated on the basis of either age or textural variations. Revdar Rd. granitoids that are similar in outcrop appearance and petrography to Mt. Abu granitoids also conform to Mt. Abu granitoids geochemically and are classified as part of the Mt. Abu felsic pluton.

The simple Mt. Abu pluton is considered an intermediate between an enriched I-type intrusion and an A-type intrusion due to its predominantly metaluminous, high-K nature, the presence of hornblende in the mode, immobile element geochemical signatures and enrichment in alkalis and incompatible elements. It intruded at a relatively shallow level of the crust, implying that the source magma was also not deep-seated. The fairly restricted composition of Mt. Abu granitoids suggests that partial melting and a degree of assimilation/mixing may have been the major factors affecting the evolution of this granitoid pluton; fractional crystallization was not the major control on evolution of these granitoids.

The source of the Mt. Abu magma is alkali-enriched, which may be explained by partial melting of a crustal source such as the high-K meta-igneous (andesite) one suggested by Roberts & Clemens (1993) or the Banded Gneiss Complex basement, which has been shown to be a likely mixing component for the Seychelles granitoids. There is no excess Al in the Mt. Abu magma, nor are any phases peraluminous, which implies very little supracrustal sedimentary contamination, unlike most A-type magmas. It cannot be considered strictly alkaline or rift-related due to the predominantly metaluminous nature, lack of sodic-rich amphiboles as well as lack of extreme LREE-depletion and HREE-enrichment, even in high silica samples.

Mt. Abu samples from this study have a maximum age range of 760.5-770 Ma, placing the Mt. Abu pluton within the time limits of the Malani Igneous Suite (MIS) as well as ~750 Ma granitoids from the Seychelles. Ages of the Sindreth-Punagarh Groups are also similar. These mafic-ultramafic volcanics are thought to be remnants of an ophiolitic mélange within a back-arc basin setting at ~750-770 Ma. The three Indian terranes are spatially and temporally contiguous. The same contiguity in space and time has been demonstrated by robust paleomagnetic data for the Seychelles and MIS. These similarities imply formation within a common geological event, the proposed Andean-type arc (Ashwal et al., 2002) on the western outboard of Rodinia. The petrographic and geochemical classification of the Mt. Abu pluton as well as the deformed nature suggests intrusion distal to the purported arc, on the continental side, similar to Seychelles granitoids. This, together with the back-arc basin signature of the Punagarh and Sindreth Groups

provide evidence for the magmatic arc interpretation and not the traditionally held view of these rocks having formed within a rift setting or due to plume activity during terrane (and supercontinent) dispersal. This would also imply that peninsular India did not become a coherent entity until after this Neoproterozoic magmatism; Rodinia was not a static supercontinent that was completely amalgamated by 750 Ma, as subduction was occurring here simultaneous with rifting elsewhere.

2. The Mt. Abu pluton differs from both the MIS and Seychelles granitoids in the greater level of deformation, with much of the pluton being foliated or deformed to augen gneiss textures. The timing of some of the deformation, particularly the augen gneiss and shear zone deformation, is thought to have occurred during intrusion. Reactivation of deformatory trends is also thought to have occurred concurrently or just before a major thermal event at ~509-515 Ma (Ar-Ar ages on Mt. Abu and Erinpura granitoids). This event was regional as it caused resetting of Ar-Ar isotopic clocks in the Mt. Abu granitoids as well as the Erinpura augen gneiss intrusive 40 km north of the Mt. Abu pluton. The temperature of resetting of argon in hornblende coincides with temperatures experienced during upper-greenschist to lower-amphibolite facies metamorphism. Evidence for this metamorphism occurs in the altered dolerite dykes (now amphibolite schist) that intrude the Mt. Abu pluton, which are thought coeval with granitoid intrusion. In addition, sillimanite within an Erinpura granitoid indicates that the metamorphism reached temperatures in excess of ~550°C and ~3-4 kbars.

Ar-Ar age dating on the dolerite dykes needs to be done in order to confirm that the alteration in them occurred at the same time as the resetting in the Mt. Abu pluton granitoids.

These late Pan-African ages are the first such ages reported for the Sirohi region and southern part of the Aravalli mountain range. They offer evidence for the extension of Pan-African amalgamation tectonics (evidence from southern India) into NW India.

3. The age of separation of the Erinpura augen gneiss magma is close to 900 Ma, thus placing the Erinpura granitoids within the age limits of the Delhi orogeny (~900-800 Ma; Bhushan, 1995). Most deformation observed here would have been caused by compression during intrusion. The Erinpura granitoids are S-type granitoids due to their predominantly peraluminous nature, highly restricted SiO₂-content, normative corundum and the presence of Al-rich muscovite and sillimanite in the mode. Weathered argillaceous metasedimentary material was incorporated into this magma, while the presence of inherited cores suggests relatively lower temperatures of formation for these granitoids as compared to I- or A-type granitoids.

The age of inheritance (1971 ± 23 Ma) in the Erinpura augen gneiss is taken as the age of the source component, which coincides with Aravalli SG formation. The monazite age (~ 820 Ma) is taken as the age of a younger resetting thermal event, while the Ar-Ar age is thought to represent a regional Pan-African tectonothermal imprint.

Although the Sumerpur granitoids differ from the Erinpura granitoids in terms of macroscopic and microscopic texture (undeformed, rarely megaporphyritic), they conform geochemically to the Erinpura granitoid characteristics and therefore may be related to the Erinpura granitoid suite. Geochronology would have to be done in order to constrain and compare the age of this pluton.

The Revdar Rd. granitoids that are similar in macroscopic appearance to Erinpura granitoids also conform geochemically, and may thus belong to the Erinpura granite suite. A Revdar Rd. mylonite gneiss with the Erinpura granitoids' geochemical signature was dated at ~ 841 Ma, which does not conform to the age of the type-locality Erinpura augen gneiss dated here, but later intrusion within the same event cannot be ruled out because of the uncertainty in the age (~ 21 Ma). This Revdar Rd. mylonite gneiss may also be expressive of a reactivation or younger event that occurred around ~ 840 Ma, an age common to other granitoid plutons dated within the region. The presence of garnet in one Revdar Rd. (Erinpura-type) sample implies generation of these granitoids at depth and/or entrainment from the source, similar to the S-type Erinpura granitoids.

4. The Ranakpur granitoids differ significantly from both the Erinpura and Mt. Abu intrusives due to their low SiO_2 -content and steep REE profiles (garnet present in the source magma); they are thought to have been generated under higher pressures from a more primitive source. The deeper pressure of generation is confirmed by the absence of a negative Eu-anomaly signalling that plagioclase may not be as abundant in the source rocks at the depths that this magma was generated at.

The Ranakpur quartz syenite dated (U-Pb zircon) is younger by ~ 30 m.y. than the Erinpura augen gneiss. It is within the same time range as numerous other granitoids from this region as well as the Revdar Rd. granitoid dated in this study. The prevalence of 830-840 Ma ages may indicate that a major tectonic event occurred at this time. The Ranakpur quartz syenite may have been generated near a subduction or collision zone, where crust is thickened and magmas can be generated at depth. The deeply-developed Nb-anomaly in the spider diagram also implies a larger subduction component to the magma.

This granitoid does not record the younger Pan-African event of the Mt. Abu and Erinpura granitoids, but the ages of titanite (~ 814 Ma) are similar to the monazite age (~ 820 Ma) reported from the Erinpura granitoid. These could represent very slow cooling from the ~ 848 Ma age of formation, or more likely a

separate and younger event. The ~789 Ma Ar-Ar age may represent slow cooling rates after the tectonic event of 814-820 Ma. The calc-silicates surrounding the Ranakpur granitoid are metamorphosed to the amphibolite grade facies, and may likely reflect the 814-820 Ma metamorphic event.

7. The Swarupganj Rd. monzogranite is interpreted to have formed by high degrees of partial melting from a depleted crustal source and is dissimilar to other granitoids from this study. More sampling, geochemical and geochronological work needs to be done in order to characterize this intrusion.

8. The Kishengarh nepheline syenite gneiss is the oldest sample dated within this study. The deformation was due to arc- or continental- collision during a Grenvillian-type orogeny related to the amalgamation of the Rodinia supercontinent (and peninsular India), dated by the highly reset zircons at ~990 Ma. This is considered a DARC (deformed alkaline rock and carbonatite) and represents a suture zone (Leelanandam et al., 2006). The primary age of formation of this DARC is older than 1365 ± 99 Ma, which is the age of xenocrystic titanites from the sample.

9. The granitoid rocks from this study area (Sirohi region) range widely in outcrop appearance, petrography and geochemistry. Granitoids from the Sirohi region dated in this study show a range of meaningful ages that represent geological events occurring at ~880 Ma, ~844 Ma, ~817 Ma, ~789 Ma, ~765 Ma and ~511 Ma. Granitoid magmatism (age of formation) in this region is predominantly Neoproterozoic, and the number of events associated with each granitoid intrusion as well as diverse tectonic settings implies a complexity in the South Delhi Fold Belt that is not matched by the conventional and simplified view of a progression from collision and orogeny through late orogenic events to anorogenic, within-plate (rift-related) alkaline magmatism. . Instead, it is envisaged that convergence and subduction during the formation of Rodinia occurred at ~1 Ga (Kishengarh nepheline syenite deformation), with a transition to continental-continental collision at ~880-840 Ma (Erinpura and Ranakpur granitoids). This was then followed by far-field Mt. Abu and MIS magmatism, related to a renewed period of subduction at ~770 Ma. The last deformatory event to affect this region was that associated with the formation of Gondwana in the late Pan-African (~510 Ma).

11. REFERENCES

- Allègre, C. J. (2008). *Isotope Geology*. Cambridge University Press, Cambridge, 512pp.
- Anders, E. & Grevesse, N. (1989). Abundances of the elements: Meteoritic and solar. *Geochim. Et Cosmochim. Acta*, **53**, 17-214.
- Ahmad, T., & Tarney, J. (1994). Geochemistry and petrogenesis of late Archaean Aravalli volcanics, basement enclaves and granitoids, Rajasthan. *Precambrian Res.*, **65**, 1-23.
- Ashwal, L. D., Demaiffe, D., Torsvik, T. H. (2002). Petrogenesis of Neoproterozoic granitoids and related rocks from the Seychelles: the case for an Andean-type arc origin. *J. Petr.* **43**, 45-83.
- Atherton, M. P. & Sanderson, L. M. (1985). The chemical variation and evolution of the super-units of the segmented Coastal Batholith. In: Pitcher, W. S., Atherton, M. P., Cobbing, E. J. & Beckinsale, R. D. (eds). *Magmatism at a Plate Edge: The Peruvian Andes*. Blackie Halstead, New York, 328pp.
- Bagas, L., Bierlein, F. P., Anderson, J. A. C. & Maas, R. (2010). Collision-related granitic magmatism in the Granites-Tanami Orogen Western Australia. *Precamb. Res.*, **177**, 212–226
- Balasubrahmanyam, M. N. (2006). *Geology and tectonics of India: an overview*, Intl. Assoc. Gond. Res. Mem. 9, Kochi University, Akebono-cho 2-5-1, Kochi, Japan, 204pp.
- Best, M. (2003). *Igneous and Metamorphic Petrology (2nd edn)*. Blackwell science Ltd., Oxford, U. K., 729pp.
- Bhushan, S. K. (1995). Late Proterozoic continental growth: implications from geochemistry of acid magmatic events of West Indian craton, Rajasthan. *Geol. Soc. Ind. Mem.* **34**, 339-355.
- Bhushan, S. K. (1999). *Neoproterozoic magmatism in Rajasthan. Proc. Seminar on Geology of Rajasthan: Status and Perspective*. P. Kataria (Ed.) MLS University, Udaipur, 101-110.
- Bhushan, S.K. (2000). Malani rhyolites-a review. *Gondwana Res.*, **3**, 65–77.
- Biju-Sekhar, S., Yoshida, M., Santosh, M., Pandit, MK. (2001). Magmatism in north-Delhi fold belt, NW India: Evidence for pre-Rodinia tectonics. *Gondwana Res.*, **4**, 149-150.

Biju-Sekhar, S., Yokoyama, K., Pandit, M. K., Okudaira, T., Santosh, M. (2003). Late Paleoproterozoic magmatism in Delhi Fold Belt, NW Indian and its significance: evidence from EPMA chemical ages of zircons. *J. Asian Earth Sci.*, **22**, 189–207.

Blatt, H. & Tracey, R. J. (1995). *Petrology: Igneous, sedimentary and Metamorphic (2nd edn)*. W. H. Freeman & Company, New York, 529pp.

Bonin, B. (2007). A-type granites and related rocks: Evolution of a concept, problems and prospects. *Lithos*, **97**, 1-29.

Bonin, B., Azzouni-Sekkal, A., Bussy, F. & Ferrag, S. (1998). Alkali-calcic and alkaline post-orogenic (PO) granite magmatism: petrologic constraints and geodynamic settings. *Lithos*, **45**, 45-70.

Bowring, S. A. & Schmitz, M. D. (2003). High-precision U-Pb zircon geochronology and the stratigraphic record, *In*: Hancher, J.M. & Hoskin, P. W. O. (Eds.), *Zircon, Reviews in Mineralogy and Geochemistry*, **53**, 305-326.

Carter, L. (2005). *Granitic and rhyolitic magmatism: constraints on continental reconstruction from geochemistry, geochronology and palaeomagnetism*. Masters thesis (unpubl). Rand Afrikaans University, Johannesburg, 54pp.

Chappell, B. W. (2010). Causes of variation in granite suites. *The Ishihara Symposium: Granites and Associated Metallogensis*, 27-34.

Chappell, B. W., Bryant, C. J., Wyborn, D., White, A. J. R. & Williams, I. S. (1998). High- and Low-temperature I-type granites. *Resource Geol.*, **48**, 225-235.

Chappell, B. W. & White, A. J. R. (2001). Two contrasting granite types: 25 years later. *Austr. J. Earth Sci.*, **48**, 489-499.

Choudhary, A. K., Gopalan, K. & Sastry, C. A. (1984). Present status of the geochronology of the Precambrian rocks of Rajasthan. *Tectonophysics*, **105**, 131-140.

Christiansen, C. H., Haapala, I. & Hart, G. L. (2007). Are Cenozoic topaz rhyolites the erupted equivalents of Proterozoic rapakivi granites? Examples from the western United States and Finland. *Lithos*, **97**, 219-246.

Crawford, A. R. (1970). The Precambrian geochronology of Rajasthan and Bundelkhand, northern India. *Can. J. Earth Sci.*, **7**, 91-110.

Cobbing, J. (2000). *The Geology and Mapping of Granite Batholiths*. Berlin, Springer, 141pp.

Corfu, F. (2004). U-Pb age, setting, and tectonic significance of the anorthosite-mangerite charnockite granite-suite, Lofoten-Vesterålen, Norway. *J. Petrology*, **45**, 1799-1819.

Corfu, F., Hancher, J. M., Hoskin, P. W. O. & Kinny, P. (2003). Atlas of zircon textures. In: Hancher, J.M. & Hoskin, P. W. O. (Eds.), *Zircon, Reviews in Mineralogy and Geochemistry*, **53**, 469-500.

Crawford, A. R. (1975) Rb-Sr age determination for the Mt. Abu granite and related rocks of Gujarat. *J. Geol. Soc. Ind.*, **16**, 73.

Crawford, A. R. & Compston, W. (1970). The age of the Vindhyan System of Peninsular India. *Quart. J. Geol. Soc. London*, **125**, 351-372.

Dall'Agnol, R., Teixeira, N. P., Rämö, T., Moura, C., Macambira, M., Oliveira, D. (2005). Petrogenesis of the Paleoproterozoic rapakivi A-type granites of the Archean Caraja's metallogenic province, Brazil. *Lithos*, **80**, 101– 129.

Dalrymple, G. B. & Lanphere, M.A. (1971). $^{40}\text{Ar}/^{39}\text{Ar}$ technique of K-Ar dating: a comparison with the conventional technique. *Earth Plan. Sci. Letters*, **12**, 300-308.

Dalrymple, G. B. & Lanphere, M.A. (1974). $^{40}\text{Ar}/^{39}\text{Ar}$ age spectra of some undisturbed terrestrial samples. *Geochim. Cosmo. Acta*, **38**, 715-738.

Dalrymple, G. B., Alexander, E. C., Lanphere, M. A. and Kraker, G. P. (1981). Irradiation of samples for $^{40}\text{Ar}/^{39}\text{Ar}$ dating using the Geological Survey TRIGA reactor. *Geological Survey Professional Paper*, **1176**, 1-55.

Dalrymple, G. B., Grove, M., Lovera, O. M., Harrison, M. T., Hulen, J. B. & Lanphere, M. A. (1999). Age and thermal history of the Geysers plutonic complex (felsites unit), Geysers geothermal field, California: a $^{40}\text{Ar}/^{39}\text{Ar}$ and U-Pb study. *Earth Planet. Sci. Lett.*, **173**, 285-298.

De Wall, H., Pandit, M. & Dietl, C. (2006). Synkinematic intrusion of the Mt. Abu granitoids, NW Indian craton: evidence from combined magnetic fabric and microstructural studies. *Geophysical Research Abstracts*, **8**, 10496.

Deb, M. & Sarkar, S. C. (1990). Proterozoic tectonic evolution and metallogenesis in the Aravalli-Delhi Orogenic Complex, northwestern India. *Precamb. Res.*, **46**, 115-137.

Deb, M., Thorpe, R. I., Krstic, D., Corfu, F. & Davis, D. W. (2001). Zircon U-Pb and galena Pb isotope evidence for an approximate 1.0 Ga terrane constituting the western margin of the Aravalli-Delhi orogenic belt, northwestern India. *Precamb. Res.*, **108**, 195-213.

Dennis, A., Shervais, J., Mauldin, J., Maher, Jr., H. & Wright, J. (2004). Petrology and geochemistry of Neoproterozoic volcanic arc terranes beneath the Atlantic Coastal Plain, Savannah River Site, South Carolina. *GSA Bulletin*, **116**, 572-593.

Dickin, A. (2005). *Radiogenic Isotope Geology (2nd Ed)*. Cambridge University Press, Cambridge, 492pp.

Eby, G. N. (1990). The A-type granitoids: A review of their occurrence and chemical characteristics and speculation on their petrogenesis. *Lithos*, **26**, 115-134.

Faure, G. & Mensing, T. M. (2005). *Isotopes: Principles and Applications (3rd Ed)*. Wiley & Sons, Inc., New Jersey, 897pp.

Foster, G., Gibson, H. D., Parrish, R. R., Horstwood, M. S. A., Fraser, J. & Tindle, A. G. (2002). Textural, chemical and isotopic insights into the nature and behaviour of metamorphic monazite. *Chem. Geology*, **191**, 183-207.

Frost, B. R., Arculus, R. J., Barnes, C. G., Collins, W. J., Ellis, D. J., & Frost, C. D. (2001). A geochemical classification of granitic rocks. *J. Petrology*, **42**, 2033-2048.

Gopalan, K., Trivedi, J. R., Balasubramanyam, M. N., Roy, S. K., & Anjaneya Sastry, C. (1979). Rb-Sr chronology of the Khetri Copper Belt, Rajasthan. *J. Geol. Soc. India*, **20**, 450-6.

Gopalan, K., Macdougall, J. D., Roy, A. B., Murali, A. V. (1990). Sm-Nd evidence for 3.3 Ga old rocks in Rajasthan, northern India. *Precamb. Res.*, **48**, 287-297.

Gregory, L. C., Meert, J. G., Bingen, B., Pandit, M. K. & Torsvik, T. H. (2008). Paleomagnetism and geochronology of the Malani Igneous Suite, Northwest India: Implications for the configuration of Rodinia and the assembly of Gondwana. *Precamb. Res.*, **170**, 13-26.

Gupta, S. N., Arora, Y. K., Mathur, R. K., Iqbaluddin, Prasad, B. & Sharma, S. B. (1989). The Precambrian geology of the Aravalli Region, southern Rajasthan and northeastern Gujarat. *Mem. Geol. Surv. India*, **123**, 262pp.

Hall, A. (1996). *Igneous Petrology (2nd edn)*. Longman Group Ltd., Great Britain, 557pp.

Hanson, G. N. (1978). The application of trace elements to the petrogenesis of igneous rocks of granitic composition. *Earth Plan. Sci. Lett.*, **38**, 26-43.

Heron, A.M. (1953). Geology of Central Rajputana. *Mem. Geol. Soc. India*, **79**, 339.

Hoffmann, P. F. (1991). Did the breakout of Laurentia turn Gondwanaland inside-out? *Science*, **252**, 1409–1412.

Hoskin, P. & Schaltegger, U. (2003). The composition of zircon and igneous and metamorphic petrogenesis. In: Hancher, J.M. & Hoskin, P. W. O. (Eds.), *Zircon: Reviews in Mineralogy and Geochemistry*, **53**, 469-500.

Kaur, P., Chaudhri, N., Biju-Sekhar, S & Yokoyama, K. (2006). Electron probe micro analyser chemical zircon ages of the Khetri granitoids, Rajasthan, India: records of widespread late Palaeoproterozoic extension-related magmatism. *Current Science.*, **90**, 65–73.

Kennedy, W.Q. (1964). The structural differentiation of Africa in the Pan-African (± 500 m.y.) tectonic episode. *Ann. Repp. Res. Inst. Afr. Geol.*, University of Leeds, **8**, 48-49.

Koppers, A. A. P. (2002). ArArCALC – software for $^{40}\text{Ar}/^{39}\text{Ar}$ age calculations. *Computers & Geosciences*, **28**, 605-619.

Krogh, T. E. (1982). Improved accuracy of U-Pb zircon ages by the creation of more concordant systems using an air abrasion technique. *Geochem. Cosmochim. Acta*, **46**, 637-649.

Lanphere, M. A. & Dalrymple, G. B. (1976). Identification of excess ^{40}Ar by the $^{40}\text{Ar}/^{39}\text{Ar}$ age spectrum technique. *Earth Planet. Sci. Lett.*, **32**, 141-148.

Leelanandam, C., Burke, K., Ashwal, L. D. & Webb, S. (2006). Proterozoic mountain building in Peninsular India: an analysis based primarily on alkaline rock distribution. *Geological Magazine*, **143**, 195-212.

Le Maitre, R. W., Bateman, P., Dudek, A., Keller, J., Lameyre, J., Le Bas, M. J., Sabine, P. A., Schmid, R., Sorenson, H., Streckeisen, A., Woolley, A. R. & Zanettin, B. (1989). *A Classification of igneous Rocks and Glossary of Terms: Recommendations of the international union of Geological Sciences Subcommittee on the Systematics of Igneous Rocks*. Blackwell scientific, Oxford, 193pp.

Liew, T. C., Finger, F. & Hock, V. (1989). The Moldanubian granitoids plutons of Austria: Chemical and isotope studies bearing on their environmental setting. *Chem. Geology*, **76**, 41-55.

Liégeois, J.P., Navez, J., Hertogen, J. & Black, R. (1998). Contrasting origin of post-collisional high-K calc-alkaline and shoshonitic versus alkaline and peralkaline granitoids. *Lithos*, **45**, 1-28.

Ludwig, K. R. (2001). Isoplot/Ex rev 2.49. Berkeley Geochronology Centre, Berkeley, CA.

Maheshwari, A., Sial, A. N., Coltorti, M., Chittora, V. K & Cruz, M. J. M. (2001). Geology and petrogenesis of Siwana Peralkaline Granites, west of Barmer, Rajasthan, India. *Gondwana Res.*, **4**, 87-95.

Maheshwari, A., Garhia, S. S., Sial, A. N., Ferreira, V. P., Dwivedi, V. & Chittora, V. K. (2002). Geology and geochemistry of granites around Jaswantpura, Jalore district, southwestern Rajasthan, India. *Gondwana Res.*, **5**, 373-379.

Mahood, G. & Hildreth, W. (1983). Large partition coefficients for trace elements in high-silica rhyolites. *Geochem. Cosmochim. Acta*, **47**, 11-30.

Mamtani, M. A., Karanth, R.V., Merh, S.S. and Greiling, R.O. (2000). Tectonic evolution of the southern part of Aravalli Mountain Belt and its environs-possible causes and time constraints. *Gondwana Res.*, **3**, 175-187.

Maniar, P. D. & Piccoli P. M. (1989). Tectonic discrimination of granitoids. *Geol. Soc. America. Bull.*, **101**, 635-643.

Martin, H. & Moyen, J-F. (2002). Secular changes in tonalite-trondhjemite-granodiorite composition as markers of the progressive cooling of Earth. *Geology*, **30**, 319-322.

Mason, G. H. (1985). The mineralogy and textures of the Coastal Batholith, Peru. In: Pitcher, W. S., Atherton, M. P., Cobbing, E. J. & Beckinsale, R. D. (eds). *Magmatism at a Plate Edge: The Peruvian Andes*. Blackie Halstead, New York, 328pp.

McDougall, I. & Harrison, T. M. (1988). *Geochronology and Thermochronology by the $^{40}\text{Ar}/^{39}\text{Ar}$ Method* (1st edn). Oxford University Press, New York, 212pp.

McDougall, I. & Harrison, T. M. (1999). *Geochronology and Thermochronology by the $^{40}\text{Ar}/^{39}\text{Ar}$ Method* (2nd edn). Oxford University Press, Oxford, 269pp.

Middlemost, E. (1997). *Magmas, Rocks and Planetary Development*. Addison, Wesley, Longman Ltd., England, 299pp.

Miller, C. F., McDowell S.M., & Mapes R.W. (2003). Hot and cold granites? Implications of zircon saturation temperatures and preservation of inheritance. *Geology*, **31**, 529–532.

Moores, E. M. (1991). Southwest U.S.-East Antarctic (SWEAT) connection: A hypothesis. *Geology*, **19**, 425–428.

Naha, K. & Halyburton, R.V. (1974). Early Precambrian stratigraphy of central and south Rajasthan, India. *Precamb. Res.*, **4**, 55-73.

Norrish, K. & Hutton, J. T. (1969). An accurate X-ray spectrographic method for the analysis of geologic samples. *Geochem. Cosmochim. Acta*, **33**, 431-454.

Pandit, M. K., Redfield, T. F., Torsvik, T. H., Ashwal, L. D., Webb, S., Bengen, B. (Unpubl). New palaeomagnetic data from SW Rajasthan (India): implications for Rodinia palaeogeography, indications of True Polar Wander (!), or simply post neo-Proterozoic tilt?

Pandit, M. K. and Khatatneh, M. K. (1998). Geochemical constraints on anorogenic felsic plutonism in North Delhi Fold Belt, western India. *Gondwana Res.*, **2**, 247–255.

Pandit, M. K., Carter, L. M., Ashwal, L. D., Tucker, R. D., Torsvik, T. H., Jamtveit, B., Bhushan, S. K. (2003). Age, petrogenesis and significance of 1 Ga granitoids and related rocks from the Sendra area, Aravalli Craton, NW India. *J. Asian Earth Sci.*, **22**, 363-381.

Pankhurst, R. J., Rapela, C. W. & Fanning, C. M. (2000). Age and origin of coeval TTG, I- and S-type granites in the Famatinian Belt of NW Argentina. In: Barbarin, B., Stephens, W. E., Bonon, B., Bouchez, J-L., Coney, D. B. & Martin, H. (Eds.), Fourth Hutton Symposium on the Origin of Granites and Related Rocks, *Trans. Royal Soc. Edinburgh: Earth Sci.*, **91**, 151-168.

Paquette, J.L. & Nédélec, A. (1998). A new insight into Pan-African tectonics in the East-West Gondwana collision zone by U-Pb zircon dating of granites from central Madagascar. *Earth Planet. Sci. Lett.*, **155**, 45-56.

Rämö, O.T. & Haapala, I. (1995). One hundred years of rapakivi granites. *Mineralogy and Petrology*, **52**, 129–185.

Rathore, S. S., Venkatesh, T. R. & Srivastava, R. K.. (1999). Rb–Sr isotope dating of Neoproterozoic (Malani Group) magmatism from Southwest Rajasthan, India: evidence of younger Pan-African thermal event by ^{40}Ar – ^{39}Ar studies. *Gondwana Res.*, **2**, 271–286.

Rex, D. C. and Guise, P. G. (1995). Evaluation of argon standards with special emphasis on time scale measurements. In: Odin, G.S. (Ed.), *Phanerozoic Time Scale, Bulletin Lias. Information, IUGS Subcommittee on Geochronology*, **13**, 21-23.

Roberts, M. P. & Clemens, J. D. (1993). Origin of high-potassium, calc-alkaline, I-type granitoids. *Geology*, **21**, 825-828.

Rollinson, R. H. (1993). *Using Geochemical Data: Evaluation, Presentation and Interpretation*. Longman Group. Ltd, England, 352pp.

Roy, A. B. (2001) Neoproterozoic crustal evolution of northwestern Indian shield: Implications on break-up and assembly of supercontinents. *Gondwana Res.*, **4**, 289-306.

Roy, A. B. & Dutt, K. (1995). Tectonic evolution of the nepheline syenite and associated rocks of Kishengarh, District Ajmer, Rajasthan. *Mem. Geol. Soc. India.*, **31**, 231-257.

Roy, A. B & Kröner, A. (1996). Single zircon evaporation ages constraining the growth of the Archaean Aravalli craton, northwestern Indian shield. *Geol. Mag.*, **133**, 333-342.

Roy, A. B. & Kataria, P. (1999). Precambrian geology of the Aravalli Mountains and neighbourhood: analytical update of recent studies. *Proc. Seminar on Geology of Rajasthan: Status and Perspective*. MLS University, Udaipur, 1–56pp.

Solanki, A. M. (2005). *A geochemical and petrographic comparison of dolerite dykes from Mt. Abu (Rajasthan) and Seychelles with a view to continental geometry*. Honours thesis (unpubl.). University of the Witwatersrand, Johannesburg, 58pp.

Schulmann, K., Mlcoch B. & Melka R. (1996). High-temperature microstructures and rheology of deformed granite, Erzgebirge, Bohemian Massif. *J. Structural Geol.*, **6**, 710-733.

Sharma, K. K. (2004). The Neoproterozoic Malani magmatism of the northwestern Indian Shield: Implications for crust-building processes. *Earth Planet. Sci.*, **113**, 795-807.

Sharma, K. K. (2007). K-T magmatism and basin tectonism in western Rajasthan, India, results from extensional tectonics and not from Réunion plume activity. *GSA Special Papers*, **430**, 775-784.

Sharma, R. S. (1999). Crustal development in Rajasthan Craton. *Ind. J. Geol.*, **71**, 65-80.

Sinha-Roy, S. (1988). Proterozoic Wilson cycles in Rajasthan. *Mem. Geol. Soc. India.*, **7**, 95-107.

Sivaraman, T.V. & Raval, U. (1995), U-Pb isotope study of zircons from a few granitoids of Delhi-Aravalli belt: *J. Geol. Soc. India*, **46**, 461-475.

Srikarni, C., Limaye, M. A., Janardhan, A. S. (2004). Sapphirine-bearing Granulites from the Abu-Balaram Area, Gujarat State: Implications for India-Madagascar Connection. *Gondwana. Res.*, **7**, 1214-1218.

Stacey, J. S. & Kramers, J. D. 1975. Approximation of terrestrial lead isotope evolution by a two-stage model. *Earth Plan. Sci. Lett.*, **26**, 207–21.

Streckeisen, A. (1976). To each plutonic rock its proper name. *Earth Sci. Reviews*, **12**, 1-33.

Thorpe, R. S., Francis, P.W. & O'Callaghan, L. (1984). Relative roles of source composition, fractional crystallization and crustal contamination in the petrogenesis of Andean volcanic rocks. *Phil. Trans. R. Soc. Lond.*, **A 310**, 675-692.

Thomas, R.J., De Waele, B., Schofield, D.I., Goodenough, K.M., Horstwood, M.S.A., Tucker, R., Bauer, W., Annels, A.E., Howard, K., Walsh, G., Rabarimana, M., Rafahatelo, J.M., Ralison, A.V., Randriamananjara, T. (2009). Geological evolution of the Neoproterozoic Bemarivo Belt, northern Madagascar. *Precamb. Res.*, **172**, 279–300.

Tobisch, O.T., Collerson, K.D., Bhattacharyya, T., Mukhopadhyay, D. (1994). Structural relationships and Sr-Nd isotope systematics of polymetamorphic granitic gneisses and granitic-rocks from central Rajasthan, India - implications for the evolution of the Aravalli Craton. *Precambrian Res.*, **65**, 319-339.

Torsvik, T. H. (2003). The Rodinia jigsaw puzzle. *Science*, **300**, 1379-1381.

Torsvik, T. H., Ashwal, L. D., Tucker, R. D., Eide, E. A. (2001a). Neoproterozoic geochronology and palaeogeography of the Seychelles microcontinent: the India link. *Precamb. Res.*, **110**, 47-59.

Torsvik, T. H., Carter, L. M., Ashwal, L. D., Bhushan, S. K., Pandit, M. K., Jamtveit, B. (2001b). Rodinia refined or obscured: palaeomagnetism of the Malani Igneous Suite (NW India). *Precamb. Res.* **108**, 319-333.

Torsvik, T.H. & Meert, J. G. (2003). The making and unmaking of a supercontinent: Rodinia revisited. *Tectonophysics*, **375**, 261-288.

Trompette, R. (2000). Gondwana evolution; its assembly at around 600 Ma. *Earth Planet Sci.*, **330**, 305-315.

Tucker, R. D., Råheim, A., Krogh, T. A. & Corfu, F. (1987). Uranium-lead zircon and titanite ages from the northern portion of the Western Gneiss Region, south-central Norway. *Earth Plan. Sci. Lett.*, **81**, 203-211.

Tucker, R. D., Ashwal, L. D. & Torsvik, T. H. (2001). U-Pb geochronology of Seychelles granitoids: a Neoproterozoic continental arc fragment. *Earth. Plan. Sci. Lett.*, **187**, 27-38.

Van Lente, B. (2001). *Neoproterozoic rocks of the Punagarh and Sindreth Groups, Rajasthan, northwest India*. Masters thesis (unpubl). Rand Afrikaans University, Johannesburg, 129pp.

Van Lente, B., Ashwal, L. D., Pandit, M. K., Bowring, S. A. & Torsvik, T. H. (2009). Neoproterozoic hydrothermally altered basaltic rocks from Rajasthan, northwest India: Implications for late Precambrian tectonic evolution of the Aravalli Craton. *Precamb. Res.*, **170**, 202-222.

Vernon, R. H. (2004). *A Practical Guide to Rock Microstructure*. Cambridge University Press, Cambridge, 594pp.

Vernon, R. H. & Clarke, G. L. (2008). *Principles of Metamorphic Petrology*. Cambridge University Press, New York, 446pp.

Villaseca, C., Barbero, L. & Rogers, G. (1998). Crustal origin of Hercynian peraluminous granitic batholiths of Central Spain: petrological, geochemical and isotopic (Sr, Nd) constraints. *Lithos*, **41**, 55-79.

Villaseca, C., Pérez-Soba, C., Merino, E., Orejana, D., López-García, J. A. & Billstrom, K. (2008). Contrasting crustal sources for peraluminous granites of the segmented Montes de Toledo Batholith (Iberian Variscan Belt). *J. Geosciences*, **53**, 263-280.

Villaros, A., Stevens, G., Moyem, J-F., Buick, I. S. (2009). The trace element compositions of S-type granites: evidence for disequilibrium melting and accessory phase entrainment in the source. *Contr. Mineral Petr.*, **158**, 543-561.

Vijaya Rao, V., Rajendra Prasad, B., Reddy, P. R. & Tewari, H. C. (2000). Evolution of Proterozoic Aravalli Delhi Fold Belt in northwestern Indian Shield from seismic studies. *Tectonophys.*, **327**, 109-130.

Volpe, A. M. & MacDougall, S. D. (1990). Geochemistry and isotopic characteristics of mafic (Phulad ophiolite) and related rocks in the Delhi Supergroup. Rajasthan India: Implications for rifting in the Proterozoic. *Precamb. Res.*, **48**, 167-191.

Watson, B. & Harrison, M. T. (1983). Zircon saturation revisited. *Earth Plan. Sci. Lett.*, **64**, 295-304.

Whalen, J. B., Currie, K. L. & Chappell, B. W. (1987). A-type granites: Geochemical characteristics, discrimination and petrogenesis. *Contr. Mineral Petr.*, **95**, 407-419.

White, W. (2007). *Geochemistry*. On-line textbook:

<http://www.geo.cornell.edu/geology/classes/geo455/Chapters.HTML>. (last revised 21-11-2007), 413pp.

Wiebe, R. A., Smith, D., Sturm, M., King, E. M. & Seckler, M. S. (1997). Enclaves in the Cadillac Mountain Granite (Coastal Batholith): Samples of hybrid magma from the base of the chamber. *J. Petrology*, **38**, 393-423.

Wiedenbeck M. & Goswami, J. N. (1994). An ion-probe single zircon $^{207}\text{Pb}/^{206}\text{Pb}$ age from the Mewar Gneiss at Jhamarkotra, Rajasthan. *Geochim. Cosmochim. Acta.*, **58**, 2135-2141.

Wiedenbeck, M., Goswami, J.N. and Roy, A.B. (1996). Stabilization of the Aravalli Craton of northwestern India at 2.5 Ga: An ion microprobe zircon study. *Chem. Geology*, **129**, 325.

Winter, J. D. (2001). *An Introduction to Igneous and Metamorphic Petrology*. Prentice-Hall Inc., N. Jersey, U. S. A., 697pp.

Wolhuter, L. E. (1971). Major and trace elements in the Opemisca Lake granite pluto, Quebec, Canada. In: Lister, L. A. (Ed.), Symposium on Granites, Gneisses and Related Rocks, *Geol. Soc. S. Africa Special Publication No. 3.*, Johannesburg, Bardwell & Co., 509pp.

Zhong, H., Zhu, W-G., Chu, Z-Y., He, D-F. & Song, X-Y. (2007). Shrimp U-Pb zircon geochronology, geochemistry, and Nd-Sr isotopic study of contrasting granites in the Emeishan large igneous province, SW China. *Chem. Geol.*, **236**, 112-133.

APPENDIX A

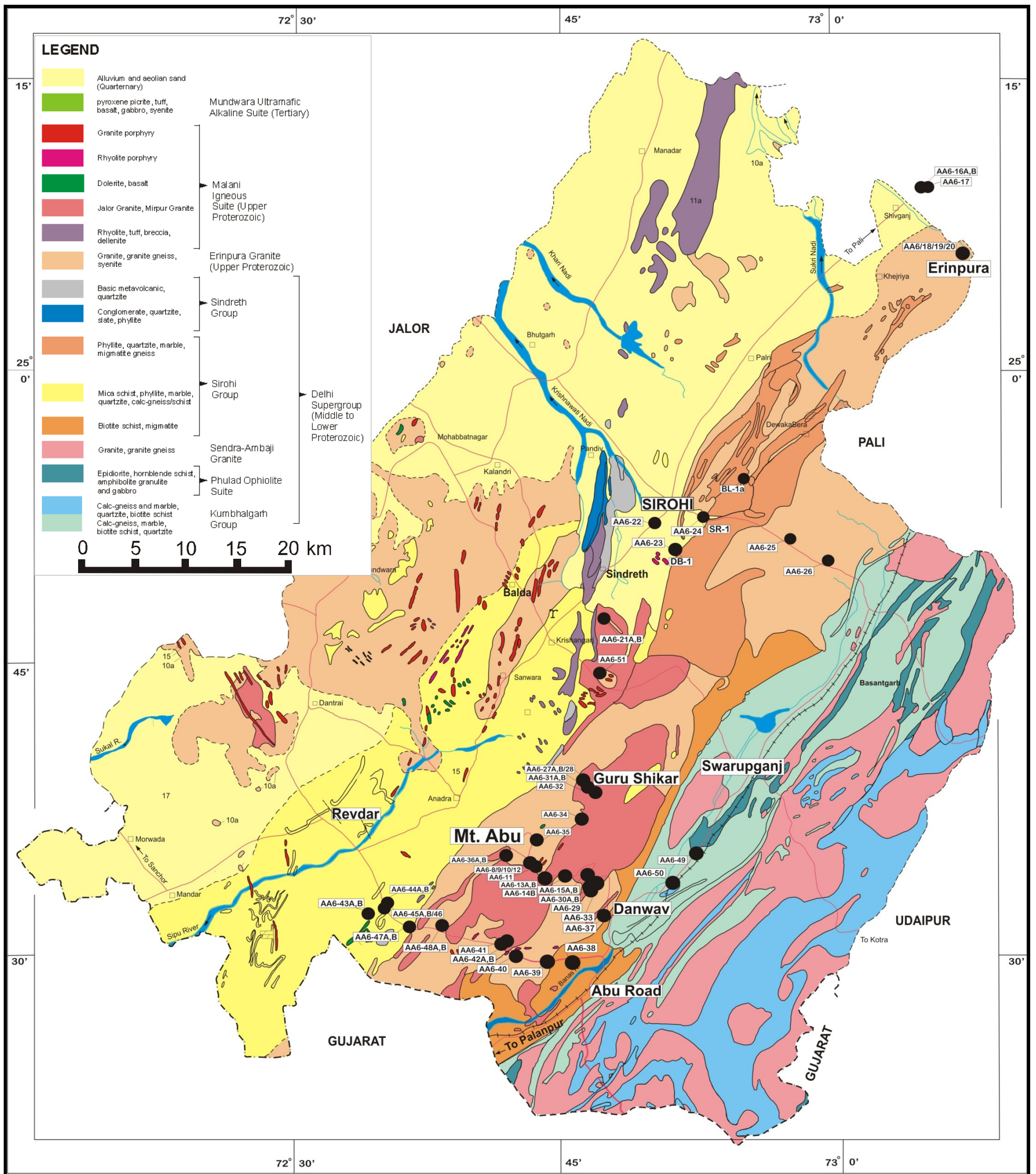


Figure 2.1. Regional geology of the study area and accompanying legend. Sample sites are indicated as yellow dots within the Erinpura and MIS granitoids (after Geological Survey Map of India, 1998).

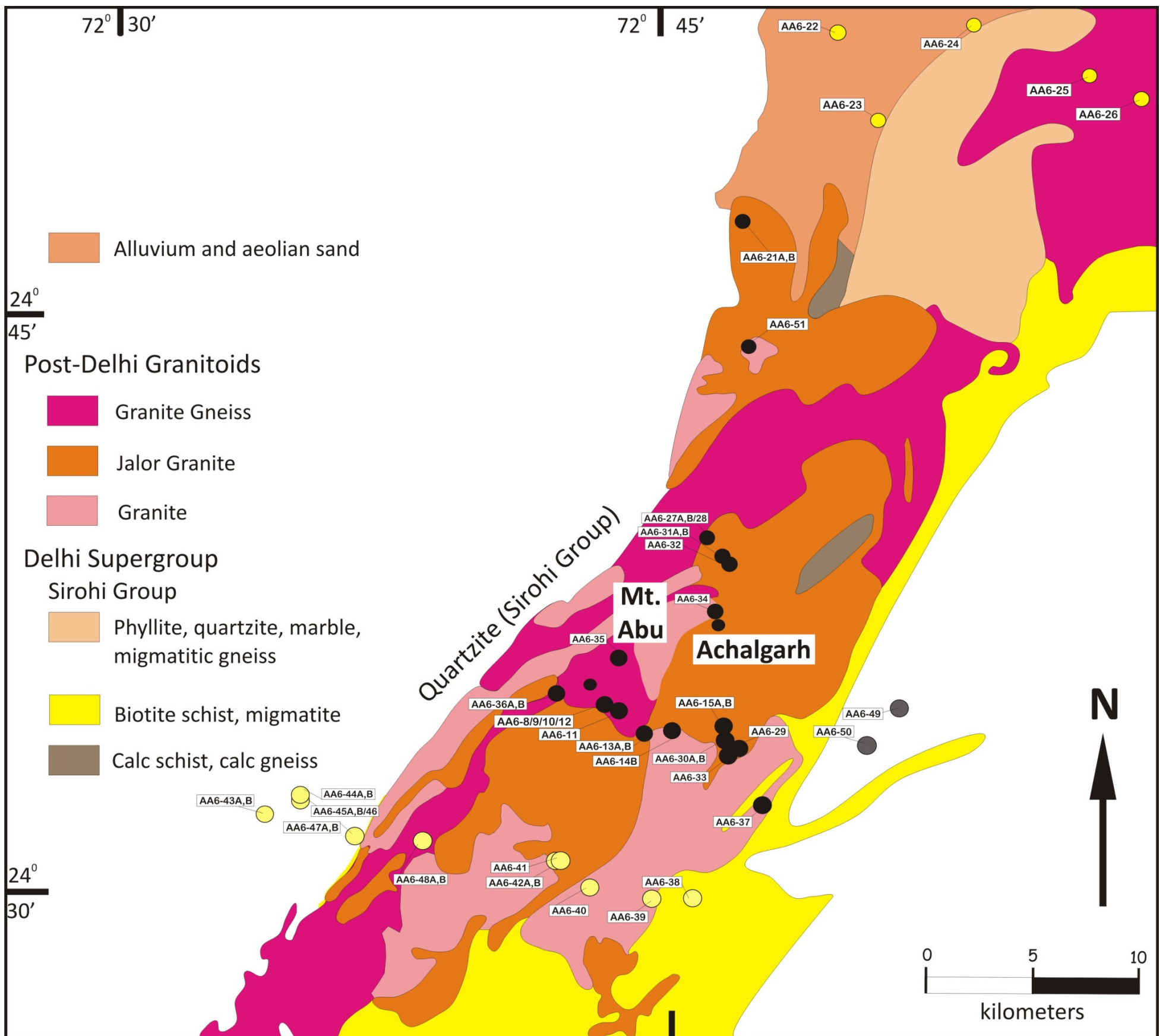


Figure 2.3. Geological map of the Mt. Abu pluton and immediate surrounds. The black circles represent Mt. Abu felsic samples, the pale yellow circles Revdar Rd. samples, the dark grey circles are Swarupganj Rd. samples and the bright yellow circles represent various Erinpura granitoid samples. The type-locality Erinpura granite sample is not shown on this map as it outcrops further north (see Fig. 2.1).

APPENDIX B

MT. ABU GRANITIDS

AA6-8

N 24°34'47.5" E 072°43'33.0"

Phaneritic, with grain size ranging from (1.5mm-15mm).

Composed of K-feldspar (kspar), plagioclase (plag), quartz (qtz) + mafic clusters (2-6mm width) as well as smaller grains of qtz + feldspar (fspar) which are euhedral, unlike the more coarser-grained components.

T/S:

-this section does not look pristine. Grains are fractured, have embayed and altered margins, while qtz has subgrains. The areas between larger fspar grains are infilled by fine-grained recrystallized qtz + fspar (sub-0.1mm in diameter, blocky).

-a lot of graphic or mymerkitic texture.

There is a predominance of perthitic orthoclase over microcline, which are both subhedral, while plagioclase is usually euhedral to subhedral.

-all grains are altered with green to brown biotite within fractures, as well as being sericitized.

-graphic textures sometimes exhibit disparate separate anhedral qtz grains within the fspar going into optical continuity.

-All fspars range from less than 0.1mm to 7mm length.

-The biotite is concentrated into clusters, with associated titanite and opaque minerals. Hornblende is scattered, but found rarely. The biotite is euhedral, being <1mm length.

-titanite (tit) grows at margins of opaque minerals, fine-grained.

Modal:

~50.5 % orthoclase

~20 % qtz

~10 % microcline

~10 % biotite

~6 % plagioclase

~1.5 % opaque minerals

~1 % titanite

<1 % hornblende

AA6-9

N 24°34'48.2" E 072°43'31.5"

Phaneritic: coarse to medium grained kspar (6-10mm, subhedral to euhedral, a lot of fractures), qtz (1-3mm, blocky, euhedral).

Mafics concentrated in clusters of finer-grains (<1mm)

Slickenside surfaces, thin (~1.5mm width) run through sample. Grey, probably mafic minerals like biotite/hornblende form the plane of the slickenside surface.

T/S:

-this is a very altered rock, with a lot of inclusions within the kspar (orthoclase predominant) as well as sericitization.

Medium- to coarse-grained phaneritic texture.

-graphic texture with runic qtz within perthitic kspar.

-microcline also found, which is sericitized and poikilitically enclosing anhedral qtz.

-there is also plagioclase visible, which is similarly sericitized and altered, with microcline-veins of polycrystalline qtz running through it

-there is some anhedral calcite within fspar phenocrysts.

-the mafic clusters consist predominantly of dark brown to sea green/blue hornblende, with some biotite. The largest crystals in the clusters are ~2mm across, most are less. There are associated iron oxides rimmed by titanite as well. Some opaque minerals are euhedral (maybe sulfides?) and not associated with mafics.

-zircons (subhedral) found within the mafic clusters (~0.3mm long).

-texture is magmatic (euhedral to subhedral kspar, plagioclase and microcline with graphic anhedral qtz as well as subhedral qtz grains (1-2mm) but very altered.

-Modal:

~50 % orthoclase

~20 % qtz

~15 % hornblende

~5 % microcline

~5 % biotite

~2 % plagioclase

~1 % titanite

~1 % opaque minerals

Trace zircons

AA6-10

N 24°34'47.6" E 072°43'33.5"

No discernable fabric.

Large fspar phenocrysts seem to have rims of different compositions of fspar.

Porphyritic, phenocrysts of creamy-white fspar (subhedral, 0.5mm-1.5mm) with inclusions of mafic minerals + qtz crystals (~2mm) + smaller, still porphyritic fspar crystals which are tabular, euhedral to subhedral (1mm- 3mm long) + mafic clusters.

Groundmass consists of mafic clusters + mafics disseminated throughout, together with other minerals that are also phenocrysts.

T/S:

-phenocrystic sample, with kspar that is rounded, subhedral (~1mm-1cm in length), sericitized, fractured and full of inclusions kspar, qtz (both anhedral) and mica (euhedral usually). All phenocrysts are microcline, and one grain exhibits a more greatly sericitized core, while others show patches of greater sericitization.

-phenocrysts of qtz are very fractures, ranging from euhedral to subhedral (1mm-5mm), with some phenocrysts being polycrystalline.

- Granophyric intergrowth + fine-grained blocky to tabular plagioclase, qtz grains (<1.25mm).

-The biotite is disseminated throughout slide, but also in clusters, with associated opaques, tit and hornblende (which is subhedral and blue-green. The opaques are euhedral, surrounded by fine-grained titanite.

Modal:

~40 % microcline
~31 % qtz
~17.5 % plagioclase
~8 % biotite
~1.5 % titanite
~1 % hornblende
<1 % opaques

AA6-12

N 24°34'45.7" E 072°43'38.6"

Phenocrystic: fspar (creamy white grey, maybe plagioclase), a mix of euhedral, smaller crystals (~2mm-5mm) to larger, euhedral, slightly rounded off phenocrysts (~7-12mm).

Groundmass consists of (≤1mm to 2mm) crystals of kspar (pink) + qtz, both subhedral as well as clusters of mafics, (~3mm length) which are elongated, forming a fabric.

Slickenside surfaces visible, ~1mm in width.

T/S:

-porphyritic rock, with phenocrysts of plagioclase (which has some deformed twinning) and some qtz and orthoclase. Size varies from 2mm-4mm, with all grains usually subhedral, although plagioclase is euhedral. Grain boundaries are not very well-defined.

Groundmass is recrystallized, blocky qtz, interspersed with subhedral-to-anhedral perthitic orthoclase, plagioclase and microcline. Biotite (<0.5mm across) is disseminated throughout slide, and is anhedral to subhedral. It also forms clusters.

-graphic texture between orthoclase and qtz in groundmass.

Modal:

51 % qtz
20 % orthoclase
14 % plagioclase
7 % microcline
6 % biotite
<1 % titanite
<1 % opaques
Trace calcite

AA6-13A

N 24°34'18.3" E 072°44'05.8"

Phaneritic- (range from 2mm-14mm), with euhedral to subhedral pink kspar + euhedral qtz (up to 6mm)

Grains separated at most boundaries by mafic minerals-biotite + thin streamers/bands of mafic minerals cutting across some felsic grains and forming a fabric (foliation). A post-intrusive fabric, as it cuts across grains.

T/S:

-Slickenside surfaces visible in thin section as they crosscut the fspar phenocrysts. These show up as veins which are filled with euhedral to subhedral biotite (<0.5mm length) and recrystallized blocky qtz (same size as biotite).

-porphyritic, with phenocrysts of microcline, orthoclase and plagioclase, which are usually subhedral with many fractures/cracks filled with finer-grained qtz+biotite+/-calcite (<0.1mm). Spaces between the phenocrysts are filled with blocky qtz which also shows subgrain formation.

-the groundmass is blocky qtz, some smaller crystals of fspar, biotite, opaques and calcite and muscovite (alteration products) (<0.25mm).

Modal:

~45 % orthoclase
~20 % qtz
~10 % plagioclase
~6.5 % biotite
~5 % microcline
~1.5 % opaques
~1 % calcite
~1 % muscovite
Pheno=60 %, groundmass=40%

AA6-13B

N 24°34'18.3" E 072°44'05.8"

Granite, with distinct phenocrysts of fspar which are tabular, euhedral to subhedral (3-11mm) and very fractured. Pink kspar grains are larger, but less well-defined in shape and seem to grow together. Visible qtz rare. The mafics surround the grain boundaries of pink kspar in mm-thin streaks and help to define boundaries of kspars.

T/S:

-Phenocrystic, with groundmass which is very fine-grained (<0.2mm) and consists of blocky qtz, tabular plagioclase and subhedral kspar (microcline+orthoclase).

-phenocrysts of kspar have reacted/altered edges which are also perthitized and inclusions of qtz and other fspars.

Modal:

~56 % qtz
~11 % plagioclase
~11 % orthoclase
~11 % biotite

~5.5 % microcline

~5.5 % zircons

AA6-14B

N 24°34'14.5" E 072°45'33.6"

Similar to AA6-12, but with elongated biotite clusters (~7mm length), with pink subhedral kspar phenocrysts (~0.7mm-2cm length), faintly aligned with the mafic clusters that define the fabric in these rocks. The groundmass is grey, consisting of qtz and fspar.

T/S:

-porphyritic, with qtz, plagioclase, perthite and mafic clusters.

-Phenocrysts of qtz are polycrystalline due to strain deformation and regrowth-they show undulatory extinction and smaller subgrains as well as interfingering at grain boundaries (0.5-3mm diameter, although subgrains contained within are smaller; subhedral).

-there are some plagioclase polycrystalline clusters, the crystals are the same size as the qtz phenocrysts; euhedral, with a "dirty" sericitized texture. There are few phenocrysts.

-the perthite is polycrystalline predominantly, the largest cluster being ~5mm diameter and there is also some mymerkite/graphic texture in one grain.

-the mafic clusters contain biotite (brown and green) and hornblende (sea blue, oblique ext), which are <0.5mm, elongated euhedral grains that are clustered together in random orientations. The associated opaques are Fe-rich, because of the presence of titanite around the edges of some opaques.

-the matrix is very fine-grained qtz and feldspar and biotite scattered randomly. There are elongated mafic clusters within the groundmass, as well as graphic texture.

Modal %:

~25% qtz

~50 % kspar

~12 % biotite

~6% plagioclase

Trace hornblende, opaques, and titanite

AA6-15A

N 24°34'37.4" E 072°46'20.6"

Phaneritic, with grains ranging from 0.2mm to 10mm width.

Mafics are found predominantly in clusters (which have a similar width to other grains). The mafics within clusters appear more-fine-grained (<0.2mm).

Sub-equigranular texture, larger pink and grey fspar grains which are sub- to anhedral, regular qtz grains (euhedral to subhedral), somewhat blocky shaped.

T/S:

-generally medium-to-coarse grained. Magmatic texture of larger grains of orthoclase, microcline and plagioclase, and recrystallized qtz (blocky, euhedral) between fspar grains and infilling fractures in them.

-Blocky qtz varies from 0.1mm-2.4mm, depending on space and position. Fspar grains are usually subhedral, with embayed and ragged margins and holes where qtz has grown.

-hornblende and biotite occur together in clusters. The hornblende is large (1mm-2.5mm), subhedral and has very ragged reacted margins. Biotite is smaller (<0.5mm) and euhedral. Titanite and opaques also associated with mafics.

Modal:

~30.3 % orthoclase

~30 % qtz

~16.3 % microcline

~10.4 % plagioclase

~7 % hornblende

~3 % biotite

~1 % titanite

<1 % calcite

<1 % opaques

AA6-15B

N 24°34'37.4" E 072°46'20.6"

Probably a dyke: porphyritic, with phenocrystic white and pink fspar (tabular), subhedral to euhedral (2mm-12mm length) + qtz which is subhedral, blocky (~2-3mm). They are surrounded by dark grey finer-grained groundmass, looks like silica + fspar (predominantly, as it is difficult to scratch it with a steel knife) and mafics (probably biotite).

Mafics are platy, form a fabric and seem to flow around phenocrysts.

Phenocrysts contain a lot of inclusions of dark material (biotite?) and also they are altered.

AA6-27A

N 24°38'54.9" E 072°46'27.1"

Porphyritic, with phenocrysts of fspar (grey to white; 10 mm-20mm), with medium-grained groundmass (~1mm-3mm) consisting of massive pink kspar and euhedral to subhedral qtz grains as well as elongated mafic spots (~1-2mm long) which form the lineation within the sample.

T/S:

-Porphyritic, with large (~19 mm) phenocrysts of orthoclase, which are very perthitized (small "subgrains" of plagioclase can be seen within the larger grain, in patches). Phenocrysts are very fragmented, which also contain tabular, totally sericitized plagioclase grains, anhedral orthoclase as well as microcline-veins of quartzofeldspathic material. Graphic texture occurs ~1 mm into the phenocryst grain boundary, in a line that mirrors the grain's edge. Euhedral muscovite also occurs on grain boundaries, very fine-grained, <0.1 mm.

-the groundmass composes biotite, forming a faint fabric through the slide. The growth habit of the biotite is in clusters (1-3 mm) as well as single crystals disseminated throughout slide (0.1 mm-2 mm). They are subhedral, and brown-to dark brown/green pleochroic. Euhedral to subhedral (hexagonal) opaques as well as euhedral titanite and apatite are associated with the biotite. The groundmass also consists of smaller perthitic orthoclase (subhedral to euhedral), as well as euhedral to subhedral plagioclase which is almost totally sericitized, both 0.5 mm-1.5 mm in diameter. Quartz in the groundmass is recrystallized, subhedral (0.1 mm-0.7 mm).

Modal:

~20 % phenocrysts (orthoclase)

~80 % groundmass, which consists of:

~55 % quartz

~13 % orthoclase

~7 % plagioclase

~4 % biotite

~1 % opaque minerals

Accessory minerals: titanite, apatite, muscovite (all <1 %)

AA6-27B

N 24°38'54.9" E 072°46'27.1"

Similar to AA6-27A, but mafic blotches are larger, more distinct and elongated (generally > 2mm length).

T/S:

-Sub-granular texture, with most grains of qtz (<1mm, usually) equally well-developed, euhedral to subhedral, while plagioclase grains are tabular and larger (0.5mm-1mm).

-kspars (perthite and microcline) are usually subhedral, with size varying in-between qtz and plagioclase. One large (~5mm length, tabular), perthitic orthoclase phenocrysts has embayed margins.

-clusters of biotite (<1mm length individually; euhedral) as well as disseminated grains found. The clusters include opaques, titanite and zircons

Modal:

~63 % qtz

~17 % orthoclase

~10 % microcline

~7 % plagioclase

~7 % biotite

<1% titanite

<1 % opaques

<1 % zircons

AA6-28

N 24°38'52.5" E 072°46'23.0"

Phaneritic, with very large grains of kspars (5mm-14mm), which are subhedral, fractured, with inclusions of biotite/hornblende. In contrast, qtz grains are more regular-sized (1mm-7mm) and euhedral as well.

Irregular mafic blotches or clusters, which are somewhat elongated, are scattered throughout sample, in between larger feldspar grains.

Smaller, finer-grained crystals of kspars + qtz (both euhedral; <2mm) are also scattered throughout sample.

T/S:

-porphyritic, with a sericitized phenocrysts of perthitic orthoclase, ~2 cm diameter (which contains inclusions of prismatic ~2mm long plagioclase grains).

-other feldspar grains vary from 0.1 mm to ~8 mm. These consist of perthitic orthoclase grains which are subhedral to anhedral as well as sericitized plagioclase grains (~40 % sericitization). Most feldspar grains contain microcline fractures infilled by fine-grained (~0.02mm) quartz, as well as poikilitically enclosing quartz blebs that are optically continuous.

These grains are separated by blocky quartz grains and biotite clusters. The quartz varies from 0.05 mm to 2 mm and shows interfingering on grain boundaries as well as subgrains. The biotite is euhedral to subhedral (0.1-1 mm in length), and is concentrated into clusters. Anhedral opaque minerals and long prismatic zircon grains (0.25/0.5 mm) are associated with the dark-brown to light brown pleochroic biotite. The opaques are surrounded by fine-grained titanite.

Modal:

~53 % orthoclase

~30 % quartz

~9 % biotite

~6 % plagioclase

~1 % microcline

~1 % opaque minerals

Accessories: titanite, zircon

AA6-29

N 24°33'44.4" E 072°46'26.8"

Porphyritic, subhedral to euhedral phenocrysts of grey-pinkish fspars (10mm-25mm long), containing inclusions of biotite.

Slickenside surfaces, which are defined by flat, flaky biotite running through the sample (vary from 1mm-7mm thick) crosscut the planar fabric.

Planar fabric created by elongated mafics (biotite +/- hornblende).

Groundmass consists of medium-to coarse-grained pink fspars + qtz (~1mm-4mm) as well as mafics.

T/S:

-Porphyritic, with large grains of subhedral orthoclase and microcline and euhedral to subhedral plagioclase, which are 1.5 -4 mm diameter, usually in clusters.

-the groundmass consists of finer-grained quartz and biotite and feldspars (0.05 mm-0.8 mm). Biotite is subhedral, with opaque minerals surrounded by titanite as well as prismatic zircons. The quartz is anhedral, with graphic texture and the feldspars are euhedral to subhedral.

Modal:

~38 % orthoclase

~47 % quartz

~8% plagioclase

~3 % microcline

~4 % biotite

~Accessories: opaques, titanite, zircon

AA6-30A

N 24°33'41.0" E 072°46'24.5"

Granite. It is coarse-grained, with large white, subhedral to euhedral fspar grains which vary from 1mm to 2.5mm diameter. Smaller grains of fspar are dispersed. The grains seem sericitized and fractured.

T/S:

-the grain size in this rock varies from 6 mm at its largest to less than 0.1 mm in diameter. The larger grains are generally the feldspars, which are then surrounded by finer-grained blocky, granular quartz, and feldspars as well as biotite clusters.

-the large k-feldspar grains (orthoclase and microcline) are perthitic, subhedral to anhedral (0.8 mm-7.5 mm), with embayed margins and fractures infilled by very fine-grained biotite and quartzofeldspathic material (up to 1 mm).

-clusters of biotite and hornblende are intergrown together with anhedral opaques (surrounded by fine-grained titanite) and zircon. The biotite is euhedral while the hornblende is subhedral (blue green to green pleochroic) with very jagged, reacted margins (0.1 mm-1 mm).

-a large orthoclase grain displays graphic texture.

Modal:

~40 % orthoclase

~20 % microcline

~21 % quartz

~10 % plagioclase

~8 % biotite

~1 % titanite

Accessories:

Hornblende, zircon and opaques

AA6-33

N 24°33'22.0" E 072°46'31."

Quite altered (a lot of red and yellow oxidation).

Somewhat phenocrystic, with large subhedral (~1cm) kspar grains which have fractures that are infilled by mafic minerals (probably biotite). Also Qtz grains that have been stretched out (>7mm).

Biotite also found interstitially.

T/S:

-k-feldspars are common as well as plagioclase. All are subhedral, 0.5-7 mm in size range. The large feldspar grains have veins of recrystallized quartz (0.1-0.2 mm width) as well as anhedral inclusions or growth of blebs of quartz.

-The quartz is recrystallized, forming subgrains between feldspar grains (0.1-1.5 mm).

-biotite is disseminated throughout slide (0.1-0.4 mm), subhedral, as well as in clusters of ~2mm diameter, which also contain euhedral titanite.

Modal:

~60 % quartz

~33 % orthoclase

~4 % plagioclase

~1 % microcline

~3 % biotite

Accessory: titanite

AA6-34

N 24°37'11.9" E 072°45'54.0"

Pink granite which is phaneritic, with coarse pink kspar (up to 23mm diameter) that has many fractures and inclusions of Qtz and mafics. Qtz, subhedral, 3mm-5mm is also present. Interspersed between these minerals are mafic blotches/aggregates/lenses (because they are eye-shaped) of biotite.

T/S:

-a porphyritic rock with phenocrysts of orthoclase, plagioclase and quartz, the latter two forming composite phenocrysts, especially the quartz (may be subgrains growth. Size of phenocrysts ranged from 2 mm-1.4 cm diameter, with feldspars euhedral to subhedral, and quartz anhedral.

-groundmass has a lot of intergrown orthoclase and quartz (graphic texture) as well as smaller grains of feldspar and quartz and biotite (which forms radiating clusters and is disseminated) that are <0.2 mm diameter. Biotite is larger, up to 0.6 mm. it also has associated opaques (and surrounding titanite) as well as zircon and apatite within clusters. Disseminated biotite anhedral and green pleochroic, as opposed to brown pleochroic in the clusters, which may indicate two phases of growth.

Modal:

~52 % orthoclase

~37 % quartz

~6 % plagioclase

~4 % biotite

Accessories: Opaques, titanite, zircon, apatite, calcite

AA6-35

N 24°36'26.5" E 072°43'22.0"

Phaneritic, composed predominantly of creamy white fspar (2mm-20mm), and mafics (biotite and/or hornblende).

Augen gneiss.

Qtz grains (~3mm; subhedral to euhedral) interspersed with fspar.

T/S:

-porphyritic, with phenocrysts of kspar (2-6mm diameter) which are very altered/sericitized as well as being poikilitic to smaller kspar, plagioclase and qtz. The edges of the phenocrysts are sub-ophitic the fine-grained matrix. Calcite and qtz are found in veinlets within the phenocrysts as well.

-mafic clusters contain elongated, brown to light-brown pleochroic biotite, which is clustered in a radiating habit (<0.3mm length). Associated with this is sericite with some visible muscovite flakes (~<0.3mm). There is also titanite and opaque minerals, with the titanite being fine-grained as it surrounds the edges of the opaque minerals.

The groundmass is very altered and sericitic, there is also a lot of graphic texture present, and the qtz and fspar are <0.1mm. There are also a lot of qtz subgrains in the matrix (<0.5mm), which are elongated.

Modal:

~40% perthitic kspar

~34 % qtz

~15 % biotite

~5 % plagioclase

~3 % muscovite

<1 % calcite

~2 % tit

~1 % opaques

AA6-36A

N 24°35'09.1" E 072°41'43.8"

Porphyritic, augen-granite-gneiss, with fspar phenocrysts which are euhedral to subhedral (1-25mm), creamy-white. Subordinate qtz phenocrysts (2mm-5mm) as well is quartzofeldspathic banding.

Bands/foliations of platy minerals, probably biotite/hornblende.

T/S:

-macroscopically the thin section consists of large fspar phenocrysts separated by elongated biotite-rich strain domains.

-one large (~1cm) kspar grain is very altered (~60 % of orthoclase is sericitized) as well as fractured. These are infilled by blocky qtz and/or calcite/muscovite.

-smaller, euhedral, tabular plagioclase (90.5mm-2mm) and subhedral to anhedral orthoclase (1mm-2.5mm) is also found. The orthoclase is full of euhedral muscovite/sericite inclusions.

-recrystallized qtz (strained and/or elongated) is found between the fspar grains, with elongation in the same direction as the "streamers" of biotite.

-the biotite (<1mm length) is found concentrated in elongate clusters together with titanite, opaque minerals and muscovite.

Modal:

~40 % orthoclase

~43 % qtz

~4 % microcline

~10 % biotite

~1 % titanite

~1 % muscovite

~1 % opaque minerals

AA6-36B

N 24°35'09.1" E 072°41'43.8"

A granite which is phaneritic, and dominated by thin (<1mm thick) veins/slickenside surfaces cutting through the sample. Lineated and foliated minerals have grown along these planes, and are probably micas. Disseminated biotite grains also found throughout sample. The mafic domains separate pink-orange kspar and qtz domains. The qtz and kspar are subhedral. Disseminated biotite 'spots' are found within the fspar grains.

T/S:

-porphyritic, with angular to subhedral phenocrysts of perthitic orthoclase and microcline. These are fractured and crosscut by fine-grained muscovite veins/planes. These form a fabric through the slide.

-the groundmass is feldspar grains and quartz (up to 0.3mm diameter) which are subhedral.

-the phenocrysts vary from 1.2-6 mm in length and all orthoclase is subhedral, with grains preferentially lense-shaped and sometimes composite.

Biotite is found together with muscovite in the veins/planes, but is subordinate.

Modal:

~46 % quartz

~45 % orthoclase

~2 % plagioclase

~2 % biotite

~5 % muscovite

Accessory: titanite

AA6-37

Danwav Village

Granite gneiss, with separate mafic and felsic domains. The mafic domains (some are ~4cm across) look like they are biotite rich, platy with grains ~2mm-4mm across. The felsic domains consist of sericitized white fspar which is subhedral (~7mm-25mm length) and qtz, which has subrounded grains (~4mm) and is rare.

T/S:

-the texture is granular-qtz (0.1mm-<1mm; triple-junctions) growing in-between subhedral kspar grains.

-both microcline and orthoclase are heavily perthitized, euhedral to subhedral and vary from 2.5mm-8mm length. They are also full of inclusions.

-plagioclase is minor, tabular and euhedral (~1.25mm length).

The mafic mineral is hornblende (biotite is minor;<1 mm length), which forms large grains that are very fractured along cleavage planes, full of inclusions and that are also associated with euhedral to subhedral titanite and opaque minerals. The hornblende is ~1-5mm length.

Modal:

~40 % qtz

~30 % orthoclase

~15 % hornblende

~7 % microcline

~5 % plagioclase

~1 % biotite

~1 % titanite

~1 % opaque

MT. ABU (SILICEOUS DYKES)

AA6-11

N 24°34'46.3" E 072°43'36.7"

Siliceous rhyolitic porphyritic dyke with phenocrysts of fspar (1mm-6mm length) which are tabular, very fractured and sericitized (cores are greatly altered). Groundmass is fine-grained, siliceous.

T/S:

-silica-rich, fine-grained groundmass (<0.05mm), with phenocrysts of orthoclase and qtz.

-Phenocrystic orthoclase is euhedral, tabular, with some perthite (1mm-3mm length).

-phenocrystic qtz is euhedral to subhedral, blocky, polycrystalline and 0.5mm-1,5mm in length.

-the groundmass is too fine-grained to distinguish between qtz and fspar, but micas (biotite) are disseminated in a definite orientation (elongate in one direction).

-larger concentrations of biotite are themselves elongate and stretched out in same orientation as rest of micas. Opaque minerals are associated with biotite.

Modal:

~59 % groundmass (excl. biotite)

~25 % biotite

~12 % qtz (discernable pheno)

~4 % orthoclase (discernable pheno)

AA6-30B

N 24°33'41.0" E 072°46'24.5"

Siliceous, very fine-grained rhyolitic dyke, with phenocrysts of euhedral to subhedral creamy-white, sometimes sericitized fspar, which is tabular (1mm-7mm length). Subhedral grains of qtz (~1mm-4mm diameter) are also found within the sample. The groundmass is very fine-grained (<1mm, not visible as individual crystals), and is a dark grey. There are subequal amounts of qtz and fspar phenocrysts, with fspar dominating.

T/S:

-porphyritic, with phenocrysts of perthitic orthoclase, microcline and plagioclase (euhedral to subhedral), ~0.5 -4 mm diameter. Other phenocrysts are quartz, which is euhedral blocky, 0.5-3 mm, with undulatory extinction.

-the phenocrysts have new growth of fine-grained quartzofeldspathic material within.

-the groundmass is fine-grained (<0.1 mm) and consists of quartz, plagioclase, k-feldspar and biotite. The biotite is euhedral, plagioclase is subhedral, and orthoclase and quartz are subhedral to anhedral.

Modal:

Phenocrysts: 14 %

~8 % quartz

~3 % orthoclase

~2 % microcline

~1 % plagioclase

Groundmass: 86 %

~10 % biotite

~76 % quartzofeldspathic material

AA6-31A

N 24°38'39.1" E 072°46'37.1"

A porphyritic rock, with phenocrysts of white fspar (which are also fractured), which are euhedral to subhedral and range from ~2mm to 20mm in length. Qtz phenocrysts are subhedral and ~3mm-7mm in diameter. Mafic clusters are also interspersed between the phenocrysts. The groundmass is a light pink colour (therefore kspar-rich).

T/S:

-a porphyritic rock, with phenocrysts of microcline and orthoclase which are euhedral to subhedral (1-7 mm) and sericitized (~40 %). The orthoclase displays a mesoperthitic texture, with almost half the grain exsolved plagioclase. Phenocrysts of quartz which are blocky, euhedral to subhedral, with undulose extinction and subgrain formation. Quartz phenocrysts are also composite. Phenocrysts of plagioclase are subhedral (0.7-1 mm). All phenocrysts are crosscut by blocky fine-grained quartz (0.1 mm width fractures).

-the groundmass consists of disseminated biotite (anhedral to subhedral; 0.01 mm-0.2 mm diameter). Opaque minerals are usually found in rare biotite clusters (1-3 mm diameter). The rest of the groundmass consists of quartz and k-feldspars intergrown in graphic to mymerkitic textures.

Modal:

~47 % quartz

~24 % microcline

~21 % orthoclase

~1 % plagioclase

~7 % biotite
~1 opaques
Accessory: titanite

AA6-31B

N 24°38'39.1" E 072°46'37.1"

Rhyolitic porphyry dyke, with phenocrysts of tabular euhedral white fspar, which is fractured and sericitized (~4mm length).

T/S:

-a porphyritic sample, with phenocrysts of microcline and orthoclase (euhedral to subhedral, blocky to tabular habit, 1-3 mm) as well as subhedral quartz (which can be composite grains or subgrains).

-there is a definite fabric in the groundmass formed by quartzofeldspathic (quartz and plagioclase discernable) material and biotite and hornblende grown with long axes subparallel to each other. The biotite is euhedral (0.05 mm length) and hornblende subhedral, with the same size as biotite.

Modal:

~84 % quartz

~7 % biotite

~5 % microcline

~2 % plagioclase

~2 % orthoclase

Accessories: titanite, opaques

AA6-32

N 24°38'35.7" E 072°46'41.2"

Aplite, with fine-to medium-grained (~1mm-2mm across) grains of pink kspar with disseminated mafics throughout the sample. Qtz is euhedral (~1-2mm diameter) and is dispersed as well.

T/S:

-fine-grained rock, with a sub-granular texture, because there are some larger grains of feldspar.

-the plagioclase is prismatic, euhedral to subhedral, sometimes with kinked/faulted twinning.

-the k-feldspars are subhedral, with 30-40 % sericitization. As well as intergrowth of quartz in a graphic texture.

-the feldspars range from 0.15-2 mm.

-fine-grained muscovite (sub-0.1 mm) in individual crystals are grown around feldspar grain boundaries.

-quartz is blocky to anhedral (0.01 -0.3 mm).

-biotite (generally anhedral, 0.1-0.3 mm), and opaques are scattered throughout slide.

Modal:

~45 % quartz

~32 % orthoclase

~10 % plagioclase

~8 % microcline

~4 % biotite

~1 % muscovite

Accessory: opaques

Mirpur granite

AA6-21A

N 24°47'04.5" E 072°47'11.9"

Pink granite, medium- to coarse-grained with large grains of kspar which are subhedral (~2mm, most >0.7cm reaching a maximum of 2cm). rounded qtz grains (~2-4mm) found in-between larger fspar grains. White to greenish-white fspar grains are also found interspersed with pink kspar. Mafic minerals occur in small (~2mm) clusters/patches throughout the sample, as well as within kspars.

T/S:

-All the orthoclase/K-feldspar is totally sericitized and pale pink in colour. The plagioclase is only partially sericitized and retains its magmatic tabular shape.

This is a coarse-grained rock, with grains between 2 mm to 7 mm diameter, and euhedral to subhedral (the orthoclase is predominantly subhedral).

-orthoclase also seen as anhedral blebs with angular edges between the quartz grains, which could be the effect of different growth rates of simultaneously growing qtz and orthoclase, similar to orthopyroxene and plagioclase.

-chlorite is found disseminated throughout thin section, singular or as a few crystals in clusters. It is massive; cleavage is absent or poor, with low birefringence and parallel extinction. It has associated opaques, zircon, titanite and apatite. The chlorite varies from sun-mm grains in clusters to 2mm for singular larger crystals, which are subhedral and massive.

Modal:

~50 % orthoclase

~35 % quartz

~10 % plagioclase

~5 % biotite

Accessories: ap, titanite, opa, zircon

MIS rhyolitic dyke

AA6-51

N 24°47'04.5" E 072°47'11.9"

Rhyolitic porphyry dyke, with pink kspar phenocrysts (tabular; 1mm-4mm diameter). The groundmass is siliceous.

T/S:

-porphyritic, with phenocrysts of composite subhedral to anhedral plagioclase and orthoclase (1-4 mm) within a groundmass of elongate opaques and quartz (and calcite, rare). This is so fine-grained it is almost indistinguishable.

RANAKPUR CALC-SILICATES

AA6-1A + B

N 24°55'26.7" E 073°24'19.2"

Calc-silicates, Phaneritic (~2-3mm) calcite crystals, interspersed with mafic mineral (biotite/phlogopite), in a granular texture
1A has orange crystal bands, though this is probably just an alteration feature.

T/S: 1A

-this is a calc-silicate, a clinopyroxene-talc-marble, consisting of predominantly calcite /dolomite (~0.5mm-3mm, euhedral, granular texture) with rounded grains of clinopyroxene (cpx) (<0.5mm-1.5mm), elongate, prismatic talc (0.5mm-2mm). Opaque minerals are associated with talc, and titanite is associated with cpx.

-some yellow staining around grain margins, probably Fe-staining.

-calcite shows strain deformation with curved/wavy twins.

Modal:

~84 % calcite

~9.9 % clinopyroxene

~4.1 % talc

~1 % titanite

<1 % opaques

<1 % phlogopite

T/S: 1B

-a marble similar to 1A, but a lot more phlogopite, which is euhedral, 0.5mm-2mm. Opaques also occur as long thin streamers –very characteristic in thin section.

Modal:

~80 % calcite

~11 % phlogopite

~3 % opaques

<1 % titanite

RANAKPUR GRANITOIDS

AA6-2

N 24°55'26.7" E 073°24'19.2"

Phaneritic granite, grey, with euhedral to subhedral fspar, which dominates over the qtz and biotite. Fspar is ~4mm-7mm, with smaller, more rounded qtz and euhedral biotite flakes (~2-3mm diameter).

T/S:

-a fairly granular texture (~1-4 mm), however, a lot of recrystallization textures as well, such as interfingering of grain boundaries, many sub-grains on boundaries as well as ophitic textures and undulatory extinction in qtz.

-mafic minerals (biotite + hornblende) have associated oxides, apatite and zircon and are found disseminated as well as concentrated into clusters.

-the qtz has fractures (which look like exsolution lamellae, making mineral look like orthoclase) and microcline-veins filled with muscovite.

-Plagioclase is the same as qtz, twinning is absent or very faint, but grains are biaxial – (so it is not orthoclase). Microcline is also found, but subordinate to orthoclase.

-Modal:

~32 % plagioclase

~32 % qtz

~15 % orthoclase +/-microcline

~12 % biotite

~4 % hornblende

~3 % oxides

~1 % apatite

~1 % zircon

AA6-3A + B

N 24°55'28.9" E 073°24'20.3"

Similar texture and characteristics as AA6-7

Friable

T/S: 3A

-the slide consists of orthoclase, microcline, plagioclase and qtz, as felsics, with the fspars being predominant.

-grain sizes vary considerably, due to the recrystallization some grains and growth of new ones during deformation. This is shown by undulatory extinction in qtz, embayed and sutured margins in plagioclase. The grain sizes range from 0.3mm-2.5mm with one orthoclase grain ~6mm width.

The mafic mineral is biotite (0.1mm-3mm length) which is euhedral, while feldspars are subhedral to anhedral.

-the biotite has grown around the edges of the other grains and re-entrant angles of >180 degrees are seen.

-euhedral titanite is scattered throughout slide but usually associated biotite, as well as prismatic zircons.

-mymerkitic texture also occurs on the edges of fspar grains.

Modal:

~40 % microcline

~25 % orthoclase
~11 % qtz
~10 % plagioclase
~10 % biotite
~1.5 % titanite
~0.5 % opaque mineral
~1 % phlogo
~1 % zircon

T/S: 3B

-no discernable change from A to B.

AA6-4

N 24°55'28.3" E 073°24'21.5"

Phaneritic, with larger qtz and fspar (greyish white) grains. The fspar grains are very altered/sericitized or perthitic. (up to 4mm diameter., euhedral to subhedral for fspar). The qtz > 1.5 mm, with it sometimes being polycrystalline. The mafic component is disseminated throughout rock, seems to be biotite (euhedral, ~2mm diameter).

T/S:

No discernable change from AA6-3 to this sample, except for presence of hornblende, usually associated with biotite.

~3 % hornblende in sample, other modal proportions are similar to 3. hornblende similar habit to biotite, grows between other grains.

AA6-5

N 24°55'26.5" E 073°24'21.4"

Phaneritic, medium to coarse grained (up to 5mm) qtz (euhedral) and fspar (which looks like they have either alteration or magmatic zoning on rims).

Flecks of mica (biotite scattered throughout sample), which is euhedral, (~1mm-3mm).

Yellow oxide alteration rims seen, a bit friable.

T/S:

-This sample shows a lot of myrmekitic/graphic texture which usually occurs around the edges of grains between 2 fspar grains.

-the fspars range in grain size from 0.5mm to 6mm length, with the smaller grains found between the margins of larger grains together with biotite and hornblende.

-Quartz is subhedral to anhedral, usually infilling btw fspar grains. It exhibits undulatory extinction as well as sutured/embayed margins in relation to the fspars surrounding it.

-large fspar grains (>2mm length) poikilitically enclose anhedral qtz and other smaller fspar grains.

-all fspars are anhedral to subhedral.

Orthoclase is perthitic in some cases, otherwise all fspars usually show a "dirty texture", a lot of bubbles and inclusions.

-get patches of qtz-rich domains as well.

-subequal orthoclase+microcline, subequal plagioclase + qtz.

Modal:

~33 % orthoclase
~27 % microcline
~17 % plagioclase
~15 % qtz
~15 % biotite
~1 % hornblende
~1 % titanite
<1 % opaques

AA6-6

30m E/NE of AA6/4

Similar to AA6-7, but larger grains of fspar, largest grain is ~17mm long, and looks like it has growth-zoning. A bit friable.

T/S:

-somewhat phenocrystic (orthoclase + microcline; ≥ 5 mm), with ~3 phenocrysts.

-the rest of the slide is granular qtz (undulatory extinction) + kspars + plagioclase (rare) + biotite (+/-hornblende).

-alteration is visible macroscopically. When viewing the slide as a whole, fine yellow lines throughout are seen all along grain boundaries, therefore this is not a fresh sample, or the rock is pervasively altered.

-Grains are usually subhedral to anhedral (1-5mm diameter).

-disseminated mafic minerals such as biotite/phlogopite (very light brown pleochroic and euhedral) is found at grain boundaries and triple-point junctions. Titanite (some prismatic) and opaque minerals as well as (sometimes) the blue-green to blue hornblende (subhedral) is found associated with the mica.

-all grains, excepting the mica, are very fractured.

-granophyric intergrowth is usually found at borders between two fspar grains and between fspars and other grains as well.

-Modal:

~35 % orthoclase (perthite)
~25 % qtz
~20 % microcline
~10 % biotite
~6 % plagioclase
~2 % titanite
<1 % opaques
<1 % hornblende

AA6-7

30m E/NE of AA6/4

Phaneritic, equigranular texture (1mm 3mm) with some larger crystals of kspars (pink, 0.6mm to 10mm).

Composed of fspar, qtz and biotite flakes.

Looks like fspar dominates over qtz and biotite.

Altered along grain boundaries, as a yellow rim can be seen.

A bit friable.

T/S:

-same as AA6-5, but get larger grains of microcline/orthoclase, up to 15mm. There is less plagioclase, more microcline and orthoclase.

SUMERPUR GRANITIDS

AA6-16A

N 25°09'31.1" E 073°04'23.3"

Medium-grained (~1mm) granular texture, a lot of qtz, followed by fspar, then biotite (in descending quantity).

T/S:

-Fine-grained (0.5mm-1mm) granular texture with blocky grains of euhedral qtz interspersed with microcline (euhedral to subhedral) and orthoclase (the same), which are slightly on the larger end of the size range.

-biotite is disseminated (anhedral, same size as other grains) and sometimes associated with opaques and titanite, apatite. The muscovite is found within sericitized fspars as well as larger individual euhedral grains disseminated in slide.

Modal:

- ~33 % qtz
- ~20 % orthoclase
- ~12 % plagioclase
- ~8.5 % microcline
- ~11 % biotite
- ~9 % sericitized fspar
- ~6 % muscovite
- <0.5% opaques
- <0.5 % titanite, apatite

AA6-16B

N 25°09'31.1" E 073°04'23.3"

Same as AA6-16A, but with a fine-grained siliceous or mafic enclave, whose boundary is semi-discrete, semi-disseminated.

T/S:

-similar to 16A, with blocky recrystallized qtz, interspersed with tabular to blocky partially sericitized feldspars (with partially embayed margins, subhedral to anhedral). The fspars are usually larger than in 16A, with some ~4mm in length. Generally they are larger than qtz or biotite, which are <0.25mm diameter.

Modal:

- ~30 % qtz
 - ~25 % sericitized plagioclase fspar
 - ~15 % orthoclase
 - ~18 % microcline
 - Biotite
 - Titanite
 - Opaque
 - Muscovite
- } ~12 %

AA6-17

N 25°09'29.5" E 073°04'29.4"

Medium-grained (~1mm-2mm), massive, equigranular with what might be mafic enclaves, which have rims of alteration/radioactive haloes that are straw-yellow.

Rest of rock composed of qtz, plagioclase, kspars and mafic biotite/hornblende, all of which euhedral to subhedral.

Enclaves vary in size from 4mm to 15mm diameter.

T/S:

-texture is "dirty" with a lot of inclusions, and sericitization of the fspars. The fspars are generally larger with them being surrounded by recrystallized qtz and biotite (and/or muscovite).

-the fspar grains vary from 0.5mm-4mm, with the smaller grains being tabular and euhedral, unlike the subhedral (with embayed margins and inclusions) larger grains. The smaller grains are very heavily sericitized in their cores, while the larger are less so.

-the dominant fspar is orthoclase, which is usually perthitic, followed by microcline. Both are sericitized (30-80 %).

-qtz is recrystallized (0.1mm-0.5mm), with, blocky, angular grains in a granular texture. It fills in between the fspars together with the biotite.

-the biotite is disseminated throughout slide (subhedral to euhedral; ≤0.5mm), with abundant radioactive haloes. Some biotite is partially altered to chlorite, while others have opaque minerals growth at the edges of the biotite, as well as fine-grained muscovite.

Modal:

- ~36 % orthoclase
- ~22 % quartz
- ~20 % plagioclase
- ~15% microcline
- ~5 % biotite

~1 % muscovite
~<0.5 % chlorite
~<0.5 % opaques

ERINPURA GRANITOIDS

AA6-18

N 25°06'30.4" E 073°09'07.9"

Augen-gneiss, large phenocrysts of pink-white fspar (5-25mm), separated by bands of biotite. Small crystals of qtz (<2mm).

T/S:

- plagioclase and orthoclase (perthitic, also sericitized) are predominant, and have grown in a granular texture.
- recrystallized qtz subgrains (found between larger grains) which are embayed, have interlocking grain boundaries, as well as undulatory extinction in larger grains are also dominant.
- the mafic mineral component consists of biotite (light to dark brown) which is gathered in clusters at grain boundaries, and is subhedral to euhedral (generally <1mm length).
- some antiperthite is present (plagioclase twinning with exsolution lamellae).
- both plagioclase and orthoclase are poikilitically enclosing smaller euhedral-to-subhedral grains of plagioclase + orthoclase and have microcline-veins of muscovite running through them.
- muscovite also associated with biotite, probably retrograde alteration product. Zircons (<0.1mm) are also found within biotite (can see radioactive haloes), as well as high relief apatite, as well as opaques fine-grained anhedral grown within biotite cleavage planes.

-Modal:

~31 % orthoclase
~31 % plagioclase
~31 % qtz
~6 % biotite
<1 % muscovite
<1 % zircon,apatite, opaques

} sub equal, although plagioclase dominant over others slightly.

AA6-19

N 25°06'01.9" E 073°08'48.7"

Phaneritic, granite-gneiss with augens of fspar (3mm-40 mm length) which are euhedral to subhedral).

Qtz crystals are smaller, with less variance in size (3-8mm), but are more anhedral, probably because qtz is less resistant to flow during metamorphism and deformation.

Bands of mica probably biotite, between felsic grains.

T/S:

- sample shows signs of deformation, including discrete biotite + muscovite (mica) domains interposed with feldspar domains, with the micas having grown and stretched along margins of large (12mm-15 mm) feldspar grains. There is also recrystallized qtz (including sub-grains and interfingering of grain boundaries).
- microcline is predominant (has fuzzy twins, many fractures which are infilled by qtz and sericite, as well as many inclusions)
- there is also what may be magmatic zoning within the feldspar.
- The feldspars also enclose smaller sub-to-anhedral qtz and sub-to-euhedral biotite.
- the boundaries between fspar grains also contain recrystallized qtz together with biotite, muscovite.
- biotite is brown to green, found in clusters (~2mm-4mm across) which are elongate in habit. Opaque minerals are usually associated with the biotite, and the biotite itself has many radioactive haloes within.

Modal:

~72 % microcline
~10 % qtz
~10 % biotite
~5 % plagioclase
~1 % muscovite
~1 % opaque minerals
~1 % radioactive haloes (zircons)

AA6-20

N 25°05'45.7" E 073°08'40.7"

A coarse-grained granite with pink and white fspar grains of up to 5cm in diameter, which are subhedral. Predominantly, the grain size is 3mm-6mm, and these fspar grains are tabular and euhedral. Qtz is anhedral, and surrounds fspar grains together with elongated biotite clusters. These clusters also form slickenside-type surfaces (and hence a foliation) as well

T/S:

- Porphyritic rock, with phenocrysts of orthoclase (perthitic), microcline and plagioclase in a matrix of smaller crystals of the above as well as recrystallized qtz and the biotite.
- phenocrysts are subhedral, with rounded edges (due to dissolution/alteration), have embayed margins and poikilitically enclose many smaller euhedral, tabular, fully sericitized feldspars as well as anhedral quartz blebs.
- phenocrysts vary from ~1 cm to 2mm diameter, while smaller grains (of the same composition) are scattered throughout the slide (usually <1 mm diameter and subhedral).
- biotite is concentrated into large clusters, with large grains being subhedral and smaller euhedral (sub-mm to 2mm). It is also disseminated throughout the rock in single crystals (0.5 mm-1 mm). The biotite contains many inclusions of hexagonal apatite and zircon (radioactive haloes and distinct zircon shapes). Acicular muscovite (<0.5 mm) is associated with the biotite as well, usually at the edges of larger biotite flakes. Titanite (fine-grained massive form) and opaques (subhedral) are rare.

Modal:

~50 % quartz

~20 % orthoclase (perthite)
~12 % plagioclase
~11 % biotite
~6 % microcline
~1 % muscovite
Accessories: Apatite, zircon, titanite & opa

AA6-22

N 24°52'00.3" E 072°50'11.8"

Porphyritic granite-phenocrysts of pink kspar which are euhedral and tabular (~12mm length). The groundmass is medium-grained, whiteish grey fspar, which is subhedral, as well as qtz (subhedral) and mafic clusters, all of which are ~3-4mm across. Inclusions of biotite within the large phenocrysts.

T/S:

- porphyritic, generally phaneritic, (1mm-4mm, but also smaller grains of ~ 0.5mm) in the groundmass and phenocrysts of perthitic microcline and orthoclase, ~7mm-1.5 cm length, which are tabular and have minimal sericitization.
- all other feldspar is fully sericitized, blocky to tabular, subhedral, with more plagioclase than k-feldspar recognizable. The K-feldspar, whether the phenocrysts or smaller grains, is visibly less sericitized than the plagioclase. This could be some effect of crystal composition or composition of fluid that moved through this rock.
- the quartz varies from ~0.1 mm to ~1.5 mm, has undulatory extinction, subgrains, and fills in between the feldspars grains. It also has microcline-veinlets cutting through it, filled with calcite or muscovite (cannot verify), which are ~0.01mm width.
- magmatic hornblende (some evidence of zoning in one grain) is present, ~6 crystals, which are subhedral but retain the diamond shape, ~2mm diameter.
- the shape of hornblende has been retained, but it has been variably altered in the core to chlorite and what may be tremolite.
- chlorite is the main mafic mineral, and can also be seen almost completely replacing biotite and hornblende. It is also present as individual flakes which are euhedral to subhedral (massive, no cleavage). The chlorite itself is being replaced by titanite along cleavage planes. Flakes vary from 0.5mm-2mm length.
- chlorite could be both primary and new growth, and is usually associated with the feldspars, not the quartz.

Modal:

~40 % sericitized plagioclase
~9 % microcline
~7 % orthoclase
~20 % quartz
~7 % chlorite
~1 % hornblende

Accessories: biotite, titanite, trem, opaques, calcite

AA6-23

N 24°50'31.8" E 072°51'16.1"

Very altered and deformed.

Gneiss with pink kspar (subhedral to anhedral, 5mm 15 long).

Bands of platy mafics (probably biotite and muscovite) which define a fabric and flow around large fspar grains.

Smaller qtz grains (2-3mm) interspersed with fspar.

Fspars are fractured/broken up with mafic biotite infilling between fractured segments.

T/S:

- a fine-to-medium-grained rock, with anhedral quartz, subhedral plagioclase (with reacted and embayed/lobate margins and partial sericitisation-20-60 %), orthoclase and microcline as well as phenocryst of orthoclase (perthitic), ~1 cm in length.
- feldspars are the same size as quartz, which has undulatory extinction (~0.1 mm-4 mm), with smaller quartz infilling between the feldspars.
- random orientation of crystals, but mafic biotite in clusters and streamers (2-5mm length) forms a discernable fabric. The biotite is euhedral, prismatic and a dull red-brown to light-brown (~0.2 mm-1.5 mm length). Within the clusters, the biotite has a semi-specific orientation (all usually grown with long axes semi-parallel). There is also yellow Fe-staining around the biotite clusters. Biotite crystals also grow singly between feldspar and quartz grains.
- sillimanite is found within biotite clusters which have a lot of Fe-staining.

Modal:

~40 % plagioclase
~3 % microcline
~7 % orthoclase
~37 % quartz
~12 % biotite
~1 % muscovite

Accessories: opa, titanite, sillimanite

AA6-24

N 24°52'28.0" E 072°52'53.1"

Extremely deformed augen gneiss, almost mylonitic. Augens formed by white fspar + qtz which are strained and flow, having lost their tabular/euhedral shape (flow lengths of minerals ~1040mm length). These grains are separated by platy biotite and/or muscovite.

T/S:

- contains a large amount of mafic minerals, especially biotite and muscovite.
- divided into light and dark bands with dark bands containing elongate biotite + muscovite, as well as phenocrysts of kspar (~2-4mm).
- light domains are dominated by interlocking qtz grains (1-1.5mm diameter; classic strain boundary microcline-structures). The kspar phenocrysts are also found here, as well as smaller fspar grains, similar in size to the qtz.

-a lot of subgrain formation in qtz and also small grains of kspar (microcline+ orthoclase) which are concentrated together. Grain size varies considerably within the light bands.

Modal:

- ~ 13 % Microcline
- ~ 8 % Plagioclase
- ~ 48 % Qtz
- ~20 % biotite
- ~10 % muscovite
- ~<1 % chl

AA6-25

N 24°51'49.8" E 072°56'33.3"

Phaneritic, porphyritic as well, with phenocrysts of salmon-pink kspar which are subhedral (7mm-20mm diameter), with inclusions of biotite. Groundmass is equigranular, massive (2mm-6mm), consisting of predominantly euhedral to subhedral qtz with biotite optically/ poikilitically surrounding the qtz and some fspar.

T/S:

- This section is similar to AA6/23, but the degree of sericitization is much lower, there is also a greater amount of k-feldspar than plagioclase. The biotite clusters (euhedral to subhedral, 0.1 mm-2 mm) are similar, but no yellow Fe-staining or sillimanite.
- there are elongate, subhedral opaques associated with the biotite, as well as apatite and zircon inclusions.
- the biotite itself is sometimes strained and deformed, as can be seen by kinked cleavage planes.
- the plagioclase is, again, more greatly sericitized than the k-feldspars (~30 % sericitization), and varies from subhedral (embayed margins, biotite partially growing into the plagioclase grain) to euhedral and tabular (0.2 mm-6mm length).
- phenocrysts of perthitic orthoclase and microcline (1-2 cm) are present, which are subhedral to euhedral and crossed by fractures. The rest of the k-feldspars are subhedral (1-4 mm).
- the quartz is recrystallized and infills between feldspars, and subgrains at triple point junctions between larger quartz grains are also present.

Modal:

- ~40 % orthoclase
 - ~13 % plagioclase
 - ~8 % microcline
 - ~27 % quartz
 - ~10 % biotite
 - ~1 % apatite
 - ~1 % opaques
- Accessory: zircon

AA6-26

N 24°50'12.2" E 072°59'03.2"

Granite. Medium-grained (all grains <1cm) with subequal amounts of biotite + (qtz and kspar). Both kspar and qtz is euhedral to subhedral and 2mm-10mm in diameter. The biotite is usually found around the grain boundaries of the felsics, usually in clusters.

T/S:

- porphyritic, with phenocrysts of feldspar separated by areas of recrystallized ultra-fine (<0.1 mm) to medium-grained (~1 mm) quartz. Biotite is also present with the quartz, as well as around phenocryst grain boundaries (0.1 mm-0.5 mm).
- opaques are situated with biotite (euhedral to subhedral; 0.05 mm-0.6 mm).
- the ultra-fine crystals might be quartzofeldspathic in nature, it cannot be distinguished.

Modal:

- ~33 % orthoclase
- ~27 % quartz
- ~12 % microcline
- ~5 % biotite
- ~4 % plagioclase
- ~1 % opaque minerals
- ~20 % fine-grained groundmass

SR-1

24°52'29"N 72°52'53"E

Very coarse-grained – pred. Plag, qtz and biotite –almost looks pegmatitic.

T/S:

- rock consists pred. of K-spar, plag/microcline, qtz and mafic component is biotite.
- Large grains of K-spar (3 mm- 1 cm, which are subhedral, perthitic and altered to sericite with new growth of euhedral muscovite crystals) & plag (3mm- 1 cm, similar texture to K-spar with embayed margins in which qtz has grown) which have veins/fractures through them filled with recrystallized qtz, sericite and muscovite (fine-grained < 0.5 mm).
- Qtz is the groundmass & recrystallized with evidence of stress.
- Biot is reddish-brown & sometimes has inclusions of a clear non-pleochroic mineral that has a black radiation halo around it (unknown either zircon/titanite/monazite/xenotime). Opaques and apatite (hexagonal shape) associated with biot.
- alteration products to sericite and muscovite.
- evidence that rock been subjected to stress.
 - Qtz: undulose extinction and subgrains, recrystallization (amoeboid shapes)
 - Biot: wavy cleavage
- modal: ~62 % K-spar
 - ~13 % plag
 - ~8 % biot

~15 % qtz
~2 % opaques(+unknown halo mineral +apatite)

BL-1a

24°54'24"N 72°55'24"E

Phaneritic – micaceous (vermiculite) granite with very minor mafic minerals.

T/S:

-rock consists pred. Of qtz, plag, microcline, orthoclase (all same size, but feldspars more altered in appearance-sericitic- and usually subhedral) & muscovite.

-almost all minerals in t/s show embayed margins ('eaten away') except for muscovite (euhedral).

-Qtz: some large grains (0.7 mm- 3 mm) with undulose extinction, anhedral. Also is partially surr. /sub-ophitic to the plagioclase.

- Plag grain has new growth of muscovite (musc). Grain inside its boundaries but musc is in turn ophitic to either smaller qtz/plag grains.

-Musc: occurs on boundaries of other minerals.

-Modal: ~50 % qtz

~20 % plag

~20 % ortho+ Micro

~10 % musc

DB-1

24°50'34"N 72°51'16"E

Gneiss-(Phaneritic) – micaceous (vermiculite/musc) with pronounced gneissic fabric + phenocrysts of kspar (distorted) with dark bands of mafic minerals (biotite???)

T/S:

-equigranular rock with recrystallization of qtz showed by interfingering of grain boundaries btw adjacent grains and euhedral feldspars

-yellow staining of grain boundaries in plain polarized light (ppl) -maybe oxidation?

-Modal:

~40 % qtz

~20 ortho

~15 % biot

~10 % plag

~10 % micro

~3 % opaques

~1 % musc

~1% zircon

REVDAR RD. (GRANITIDS)

AA6-38

N 24°29'48.6" E 072°45'55.7"

Mylonitic gneiss, very deformed.

Light bands of fspar + qtz (1m-5mm width) separated by darker grey bands of biotite (≤1mm width).

T/S:

-pronounced fabric defined by micas and recrystallized fine-grained qtz + feldspars.

-calcite is subhedral (~2mm diameter) and ophitically encloses chlorite + muscovite.

-muscovite is strained (undulatory extinction) in direction of elongation of fabric.

-there are larger (granoblastic texture) streams of polycrystalline qtz (0.2mm-1mm diameter.), which are lenticular-shaped in the direction of extension, along fabric.

-some remnant microcline and orthoclase phenocrysts (1.5mm-2.5mm), but mostly recrystallized fine-grained mix of orthoclase, plagioclase and qtz-cryptocrystalline-as well as chlorite, biotite and muscovite.

-Modal:

Orthoclase }
Microcline } ~45 % together

~35 % qtz

~10 % biotite + chl

~10 % muscovite

<1 % calcite

AA6-39

N 24°29'48.2" E 072°44'24.4"

A medium to coarse grained granite consisting of whiteish feldspar grains which are very fractured, subhedral to euhedral and 3-9mm across. Qtz grains are subhedral (3-7mm across). The mafic aggregations occur at grain boundaries or junctions. There is Fe-staining throughout the sample.

T/S:

-generally medium-to coarse grained, with larger feldspars (2-4 mm) as well as equigranular-textured quartz together with smaller feldspars (0.75-1 mm).

-larger feldspars have altered margins (with perthitic orthoclase), are subhedral, while the smaller are euhedral and tabular.

-Biotite is usually scattered in small clusters (0.1-0.75 mm length). Usually euhedral, with rare opaques. Some clusters are elongated sub-parallel to each other.

Modal:

~37 % orthoclase

~36 % quartz

~21 % microcline
~4 % plagioclase
Accessory: opaques

AA6-40

N 24°30'07.2" E 072°42'33.5"

Pink granite, consisting pink kspars which are subhedral and very fractured (2-5mm across). These fspars surround qtz grains which are subhedral (~3-4mm across). Get mafic biotite accumulations at grain boundaries of fspars. Fe-staining throughout sample.

T/S:

- size ranges in this sample with generally larger feldspars and on average smaller quartz and biotite grains.
- the biotite is concentrated into clusters, but there is no fabric/elongation. The biotite is euhedral, (0.1-0.8 mm) with associated opaques and euhedral titanite. The biotite is black, may be Fe-staining.
- quartz is granular to subhedral, with sutured blocks (0.15-0.8 mm) and occurs as composite macro-crystals that are similar in size to the feldspars.
- the feldspars are dominated by microcline and orthoclase (minor plagioclase), which are perthitic and sericitized (~50 %). These grains are subhedral, with embayed and ragged margins as well as veins of recrystallized quartz crosscutting grains (1-4.5 mm width).
- these larger grains are sometimes surrounded by a mix of finer-grained quartzofeldspathic material (<0.1 mm).

Modal:

~45 % quartz
~29 % microcline
~23 % orthoclase
~2 % plagioclase
~1 % biotite
Accessory: titanite

AA6-42A

N 24°30'34.2" E 072°41'57.3"

Porphyritic granite, with phenocrysts of fspars which are subhedral, creamy-white (~2mm-15mm), which contain inclusions of dark minerals within fractures in the phenocrysts. These are also partially sericitized. Mafic "streaks" consisting of dark minerals, probably biotite or hornblende, fine-to medium grained and somewhat platy in nature, are also found. The groundmass is a rusty orangeish-pink colour (evidence of Fe-staining) and consists of kspars together with scattered mafic minerals. Qtz is also present as rounded grains (~2mm diameter), but these are not predominant.

T/S:

- a porphyritic sample, with phenocrysts of kspars (microcline+ orthoclase) and qtz, which are 1mm-3mm. there are also mega-phenocrysts of 5mm-1cm of kspars, which are also glomero-porphyritic.
- mafic minerals form elongated clusters and define a fabric visible macroscopically which is also seen within the groundmass. Hornblende is found throughout intergrown with biotite or alone.
- the groundmass has a lot of graphic texture, is extremely fine-grained, with most grains not recognisable (in the sub-1mm range) and consists of qtz, the feldspars (plagioclase+perthitic orthoclase) and mafics.

Modal:

Perthitic orthoclase }
Microcline } ~42 % subequal
~40 % qtz
~10 % biotite
~4 % hornblende
~2 % titanite
~1 % zircons
~1 % opaque minerals
<1 % chl

AA6-42B

N 24°30'34.2" E 072°41'57.3"

Fine-to medium grained predominantly (<0.1mm to 2mm) with a few larger (0.3mm) creamy white fspars.

Very pink, kspars-rich rock, with kspars usually subhedral.

Qtz (~1mm-2mm) is subhedral to anhedral.

Biotite is found in clusters, seems slightly finer-grained than the rest of components.

Alteration shown by yellow rims around minerals.

Subequal fspars+ biotite, less qtz.

T/S:

Equigranular rock, with a lot of quartz and feldspar intergrowth in the form of graphic texture.

- the feldspars have ragged edges with fine-grained recrystallized, material on their edges as well as between larger quartz and feldspar grains.
- feldspars are subhedral to anhedral, sericitized (15 %) and are predominantly k-feldspars.
- the quartz is blocky, euhedral to subhedral.
- all grains vary from 0.1-1 mm, with most averaging in the middle.
- biotite is disseminated, subhedral (0.1-0.3 mm).

Modal:

~39 % orthoclase
~35 % quartz
~20 % microcline
~4 % biotite
~2 % plagioclase
Accessories: titanite, opaques

AA6-47A

N 24°31'32.7" E 072°36'33.0"

Phaneritic, with equigranular orange-stained (altered) fspar (euhedral) and euhedral to subhedral qtz grains (4mm-9mm). Scattered mafic flakes (1-2mm) throughout rock sample.

T/S:

-this is a porphyritic rock, with phenocrysts of feldspar.

-plagioclase and perthitic orthoclase are the main feldspars, and are sericitized (20-40 %). Most feldspar grains vary from 0.75 mm to 7.5 mm. The plagioclase is euhedral tabular to blocky, while the orthoclase is subhedral to anhedral (smaller feldspars ~0.1 mm, which are found with smaller quartz grains).

-the quartz is anhedral, usually <0.75 mm, especially as sub-grains between larger feldspars (undulatory extinction).

-this granite is micaceous, with subhedral muscovite, usually around edges of the feldspar, although it is rare.

-the opaque minerals are found within streamers of Fe-staining.

Modal:

~65 % plagioclase

~30 % quartz

~3 % orthoclase

~1 % muscovite

~ 1 % Accessories: opaques

AA6-47B

N 24°31'32.7" E 072°36'33.0"

Preferential foliation/fabric (with what may be augen-shaped fspars), extremely altered with pervasive iron oxide staining (orange) even on fresh cut surfaces. Also displays avocado-green colour (fspars).

Phaneritic (3mm-6mm length) fspars + qtz (larger than fspars).

Cannot see any mafics, except possible in the veinlets.

T/S:

-this is a very sericitized sample (almost all feldspar is sericitic) and is also porphyritic. There are phenocrysts of perthitic orthoclase and microcline (~2.5 cm) which have very little sericitization. Smaller feldspar grains (~0.2 mm) are found within sericitic masses as well as finer-grained (<0.3 mm) quartz.

-opaques are also found along the streamers of Fe-staining.

-no presence of individual mica grains, only sericite.

Modal:

~60 % sericite

~33 % quartz

~4 % orthoclase

~1 % microcline

~2 % opaques

AA6-48A

N 24°31'17.3" E 072°38'26.0"

A pink rock, kspars-rich, phaneritic (2mm-11mm).

Large kspars grains that are subhedral and look altered together with smaller qtz grains (euhedral to subhedral) as well as mafic clusters (5mm-11mm) of flaky biotite.

Kspars grains look like they have been significantly altered and might have fractures-not clear.

T/S:

-this is a medium- to coarse- grained granite, with grains of feldspar varying between 0.3 mm to 1 cm. orthoclase and microcline are perthitic, while plagioclase is tabular to subhedral.

-the quartz is subhedral to euhedral, and blocky (0.75 mm-2 mm), with smaller (~0.1 mm) sub-grains surrounding edges of quartz. Quartz is also found in veins running through orthoclase.

-biotite is found in blotches of up to 3 mm, surrounded by finer grained (0.1-0.4 mm) euhedral biotite. There is a lot of Fe-staining as well as opaque's and associated titanite within the biotite clusters.

The rock has undergone some strain, as there is the presence of kinked plagioclase, as well as the fact that quartz has undulose extinction and solid-state deformation in the form of recrystallized sub-grains.

Modal:

~49 % orthoclase

~41 % quartz

~5 % plagioclase

~4 % biotite

~ 1 % Accessories: opaques and titanite

AA6-48B

N 24°31'17.3" E 072°38'26.0"

Leucocratic medium to coarse grained aplite dyke, granular texture.

White and pink fspars, + qtz, + (lesser) biotite

T/S:

-this is an equigranular aplite (0.1-0.8 mm) with blocky to subhedral quartz, euhedral tabular plagioclase and subhedral orthoclase and microcline (some larger grains up to 2 mm) grains.

-there is anhedral biotite, which partially grows surrounding other grains (<0.1 mm), which also has euhedral to subhedral opaques, with titanite. The biotite is disseminated.

Modal:

~45 % quartz

~30 % orthoclase

~18 % plagioclase

~4 % microcline

~2 % biotite

~1 % Accessories: opaque's, titanite

AA6-45A

N 24°32'38.4" E 072°35'11.0"

Foliated rock, very mica-rich, almost gneissic-foliation.

Medium-grained (~1mm) stretched out or flattened grains of creamy-white fsp, together with clear Qtz + what looks like flaky vermiculite?

Predominantly Qtz and mica seen, with few bands of white Ksp.

T/S:

-This is a mix of 44B (the muscovite) and 44A (a lot of quartz)

-the quartz is anhedral, with undulatory extinction, fractures and subgrains as well as suturing at boundaries (0.1 mm-subgrains, others up to 2 mm). Usually elongate habit.

-all feldspar is fully sericitized, a few grains where plagioclase twinning can be seen (0.75 mm).

-the muscovite is acicular grains grown between quartz and sericitic feldspar as well as the sericite in the feldspar (up to 0.75 mm). Chlorite is also intergrown with the muscovite, and has Fe-staining, and is massive, with associated opaques.

Modal:

~60 % quartz

~15 % sericitized feldspar (plagioclase)

~22 % muscovite

~2 % chlorite

~1 % Accessory: opaques

AA6-45B

N 24°32'38.4" E 072°35'11.0"

This sample is gneissic in character with fine laminations that are staggered. Silica-rich rock with bands and patches of mafic and felsic minerals. The felsic bands consist of white fsp (1-4mm across) and Qtz (subhedral; 2-5mm). Mafic bands seem to be a mixture of siliceous material and micas.

T/S:

-very similar to 44A, with more quartz and totally sericitized feldspars, less muscovite as individual crystals.

-muscovite is rare, all mica usually chlorite-biotite alteration (0.1-0.5 mm).

-quartz and plagioclase are similar in size (0.1-0.8 mm), while quartz has undulatory extinction, is anhedral, has subgrains and suturing at contacts.

-Garnet found, anhedral, with embayed margins/partially poikilitic to quartz. Garnet fractured.

Modal:

~45 % quartz

~44 % sericitized feldspar (plagioclase)

~7 % biotite

~3 % chlorite

~1 % Accessories: opaques, garnet

SIROHI GRP. Metasediments(REVDAR RD.)

AA6-41

N 24°30'27.2" E 072°42'13.1"

Very fine-grained greenish-grey, may be a siliceous dyke or a metasediment, not too sure.

T/S:

-this section has a lot of Fe-staining as well as opaques associated with this.

-this staining occurs throughout a slide consisting predominantly of quartz. The quartz is found in large grains (0.1-2 mm) which are blocky, and form composite crystals within a matrix of very fine-grained quartz (≤ 0.01 mm).

-the quartz is full of bubbles, giving it a "dirty" texture.

Modal:

~97 % quartz

~3 % Fe-staining + opaques

AA6-43A

N 24°32'09.7" E 072°34'24.8"

Carbonate, flakes of vermiculite/phlogopite, Phaneritic, metasediment, marble, with interlocking granular textured grains.

T/S:

An impure-tremolite-actinolite calc-silicate. The tremolite is acicular, prismatic to subhedral with characteristic cleavage while the talc is euhedral. The calcite is equigranular.

Modal:

~86 % calcite/dolomite

~11 % tremolite

~3 % talc

AA6-43B

N 24°32'09.7" E 072°34'24.8"

Foliated rock, with both light grey and dark green minerals which seem to be flattened/stretched out (maybe a slight fabric) (<0.1cm).

T/S:

- rock is altered, with feldspars totally sericitized. These are plagioclase and orthoclase.
 - the tremolite is also altered, with ragged margins and full of inclusions.
 - the quartz is least affected, forming anhedral crystals, which grow in an elongated habit, forming a fabric.
- Titanite is abundant and prismatic (up to 1 mm).
-some chlorite within feldspars as a replacement mineral.

Modal:

- ~62 % sericitized feldspar (cannot make distinction between k-feldspars and plagioclase)
- ~25 % quartz
- ~10 % tremolite
- ~2 % titanite
- ~1 % chlorite

AA6-44B

N 24°32'39.7" E 072°35'10.1"

Phaneritic (2mm-4mm).

May be a cordierite pegmatite (dark gray mineral in hand specimen).

Has a dark green mineral together with darker black biotite + euhedral Qtz/cord + fsp + lighter mica (muscovite/vermiculite/phlogopite).

T/S:

-An altered sample, with Fe-staining (yellow) along with associated opaque minerals as well as fine-grained muscovite +/- chlorite replacing the feldspars.

- muscovite replaces feldspars (0.2-0.8mm) while some are larger (~1.6 mm) and infill between quartz and feldspar grains.
- microcline (0.75-8 mm) and orthoclase are subhedral, reacted margins, with a lot of replacement muscovite growth (sericite).
- the quartz is anhedral (0.5-7 mm), with undulose extinction.

Modal:

- ~45 % quartz
 - ~45 % microcline
 - ~7 % muscovite
 - ~3 % orthoclase
- Accessory: opaques

AA6-46

N 24°32'38.4" E 072°35'11.0"

Combination of a micaceous, siliceous (maybe quartzite) rock with visible (~1mm-2mm diameter) flecks of muscovite dispersed between interlocking Qtz grains. This is a Phaneritic rock, grains usually ~2-4mm diameter. A mafic mineral, probably biotite, also present between grain boundaries, as well as the presence of Fe-staining at these boundaries.

T/S:

- this sample is predominantly quartz-rich, with muscovite and chlorite as well as some sericite.
- there is little evidence of feldspars, save for the few sericitized portions of the slide..
- muscovite is usually found at the quartz grain boundaries, and is euhedral to subhedral, with intergrown chlorite (0.1 mm-1 mm). There are opaques associated with the chlorite. The quartz is subhedral with undulose extinction and sub-grain formation (0.2 mm-4.5 mm).

Modal:

- ~90 % quartz
 - ~8 % muscovite
 - ~2 % chlorite
- Accessories: opaques, sericite

SWARUPGANJ RD.

AA6-49

N 24°35'24.6" E 072°52'35.4"

Foliated granite, with the foliation defined by platy biotite in elongated blotches. It is Phaneritic, with fspars which are subhedral, 3mm-1mm in length and Qtz, subhedral (~4mm diameter).

A faint yellow colour is present throughout the sample, probably indicative of Fe-staining.

T/S:

-this rock has an equigranular texture (very "dirty" texture too), with subhedral plagioclase and quartz intergrown as well as anhedral orthoclase, ranging from ~0.1 mm-08 mm.

Modal:

- ~40 % quartz
 - ~28 % plagioclase
 - ~28 % orthoclase
 - ~4 % biotite
- Accessory: muscovite, opaque minerals.

AA6-50

N 24°35'24.6" E 072°52'35.4"

Fine-grained, with faintly discernable white crystals of plagioclase and smaller pink crystals of kspars.
Dark, mafic component dominates (although this could also be fine-grained micas as well as Qtz).

T/S:

-this is an amphibolite. The predominant mineral is hornblende (<1 mm), which is acicular to subhedral, with one larger subhedral phenocrysts (~2.5 mm).

-quartz infills gaps between hornblende. Tremolite is also present with the quartz.

Modal:

~93% hornblende

~5 % quartz

~2 % tremolite

KISHENGARH NEPHELINE-SYENITE

AA6-52A

N 26°35'17.0" E 074°53'19.1"

Syenite; plagioclase/kspar (white) = nepheline + biotite/hornblende.

Phaneritic, with a fabric (foliation) formed by platy mafic minerals.

T/S:

-there are fairly discrete patches of hornblende with associated titanite as well as some grains of hornblende that show ophitic textures when enclosing plagioclase (euhedral).

-texture is granoblastic (0.3-1.5mm)

-nepheline is present in the slide, and plagioclase and subordinate microcline.

Modal:

~47 % nepheline

~40 % plagioclase

~7 % hornblende

~3 % titanite

~3 % phlogopite/biotite

AA6-52B

N 26°35'17.0" E 074°53'19.1"

Amphibole schist, prominent foliation, platy dark mineral (probably hornblende), medium to coarse-grained.

T/S:

-a hornblende amphibolite, with intergrown hornblende (light to dark green) and brown biotite (0.1-0.7 mm), with quartz infilling.

Modal:

~60 % hornblende

~25 % quartz

~15 % biotite

APPENDIX C

	MT. ABU												
Sample	AA6/8	AA6/9	AA6/10	AA6/12	AA6/13A	AA6/13B	AA6/14B	AA6/15A	AA6/15B	AA6/27A	AA6/27B	AA6/28	AA6/29
Lithology:	massive granite	massive granite	porphy. granite	foliated granite	foliated granite	foliated granite	foliated granite	massive granite	porphyritic granite	porphyritic granite	foliated granite	porphy. granite	porphyritic granite
CIPW Norms(100 % anhydrous)													
Normative Minerals	Weight % Norm	Weight % Norm	Weight % Norm	Weight % Norm	Weight % Norm	Weight % Norm	Weight % Norm	Weight % Norm	Weight % Norm	Weight % Norm	Weight % Norm	Weight % Norm	Weight % Norm
Quartz	27.09	33.57	26.31	22.4	22.31	25.52	27.89	20.32	24.07	31.04	30.46	22.42	31.7
Plagioclase	32.26	29.88	33.28	31.46	32.94	30.71	31.3	31.11	33.06	30.25	27.34	33.42	30.83
Orthoclase	31.62	31.82	33.65	35.26	33.23	36.42	33.71	36.77	34.83	33.76	34.53	37.05	31.23
Nepheline	0	0	0	0	0	0	0	0	0	0	0	0	0
Corundum	0	0	0	0	0	0	0	0	0	0	0	0	0
Diopside	2.37	0.37	3.26	4.04	5.41	2.85	3.67	3.62	2.09	2.76	2.92	3.11	3.35
Hypersthene	2.83	2.29	0.8	1.88	0	1.45	0.82	1.29	2.34	0.55	0.93	1.09	0.9
Wollastonite	0	0	0	0	0.02	0	0	0	0	0	0	0	0
Acmite	0	0	0	0	0.28	1.87	0.6	0	0	0	1.71	0	0
Na ₂ SiO ₃	0	0	0	0	0	0	0	0	0	0	0.51	0	0
Rutile	0	0	0	0	0	0	0	0	0	0	0	0	0
Ilmenite	0.85	0.47	0.55	0.8	0.57	0.4	0.49	0.76	0.82	0.38	0.36	0.53	0.49
Magnetite	1.87	1.16	1.28	1.83	1.37	0.11	0.92	1.7	1.81	0.86	0	1.16	1.15
Apatite	0.21	0.07	0.12	0.21	0.05	0.12	0.07	0.25	0.23	0.07	0.07	0.14	0.12
Zircon	0.06	0.06	0.06	0.04	0.09	0.06	0.04	0.06	0.07	0.04	0.04	0.03	0.04
Chromite	0.09	0.1	0	0.07	0	0.1	0.1	0	0	0.09	0.09	0.09	0.1
Total	99.25	99.79	99.31	97.99	96.27	99.61	99.61	95.88	99.32	99.8	98.96	99.04	99.91
An	3.7	3.2	1.5	1.4	0.0	0.0	0.0	2.3	4.5	0.6	0.0	1.3	1.1
Ab	28.5	26.7	31.7	30.0	32.9	30.7	31.3	28.9	28.5	29.7	27.3	32.2	29.7
Plag An-content	11.0	10.2	4.4	4.3	0.0	0.0	0.0	6.9	13.1	1.7	0.0	3.6	3.5

	MT. ABU												MIS DYKE
Sample	AA6/33	AA6/34	AA6/35	AA6/36A	AA6/36B	AA6/37	AA6/11	AA6/30B	AA6/31A	AA6/31B	AA6/30A	AA6/21A	AA6-51
Lithology:	foliated	foliated	augen	augen	mylonitic	augen	rhyolite	rhyolite	rhyolite	rhyolite	foliated	massive	rhyolite
	granite	granite	gneiss	gneiss	gneiss	gneiss	dyke	dyke	dyke	dyke	granite	granite	dyke
CIPW Norms(100 % anhydrous)													
Normative Minerals	Weight %	Weight %	Weight %	Weight %	Weight %	Weight %	Weight %	Weight %	Weight %	Weight %	Weight %	Weight %	Weight %
Quartz	37.03	29.92	26.14	26.26	29.07	14.38	28.36	32.47	31.19	31.39	24.89	27.86	10.21
Plagioclase	29.04	27.58	34.69	30.19	33.4	35.19	30.82	27.34	27.21	29.84	30.13	31.22	40.62
Orthoclase	29.02	36.25	33.1	36.23	31.87	38.48	35.53	33.33	34.29	32.15	36.35	34.83	24.81
Nepheline	0	0	0	0	0	0	0	0	0	0	0	0	0
Corundum	0	0	0	0	0	0	0	0	0	0	0	0	0
Diopside	2.42	2.28	1.37	0.15	2.7	5.35	3.36	2.68	2.78	2.18	3.97	1.89	3.3
Hypersthene	0.38	1.71	1.94	3.49	0.59	2.62	0.54	1.17	1.04	1.39	1.08	1.41	9.77
Wollastonite	0	0	0	0	0	0	0	0	0	0	0	0	0
Acmite	1.11	0	0	0	0.4	0	0.65	1.68	1.65	1.71	0	0	0
Na2SiO3	0	0	0	0	0	0	0	0.5	0.32	0.5	0	0	0
Rutile	0	0	0	0	0	0	0	0	0	0	0	0	0
Ilmenite	0.17	0.65	0.63	0.82	0.34	1.04	0.4	0.4	0.32	0.38	0.65	0.61	1.92
Magnetite	0.14	1.26	1.28	1.46	0.6	2.52	0.6	0	0	0	1.38	0.94	5.23
Apatite	0.02	0.14	0.19	0.28	0.07	0.23	0.07	0.07	0.07	0.07	0.19	0.14	0.6
Zircon	0.04	0.06	0.04	0.04	0.04	0.04	0.07	0.06	0.04	0.06	0.04	0.04	0.43
Chromite	0	0.04	0	0.09	0.01	0.07	0.07	0.01	0.01	0.01	0.06	0.1	0.22
Total	99.37	99.89	99.38	99.01	99.09	99.92	100.47	99.71	98.92	99.68	98.74	99.04	97.11
An	0.0	1.1	5.1	2.7	0.0	3.2	0.0	0.0	0.0	0.0	1.2	0.9	7.4
Ab	29.0	26.5	29.6	27.5	33.4	32.0	30.8	27.3	27.2	29.8	28.9	30.3	33.3
Plag An-content	0.0	3.7	13.9	8.4	0.0	8.6	0.0	0.0	0.0	0.0	3.7	2.8	17.3

	ERINPURA											SUMERPUR			
Sample	AA6/18	AA6/19	AA6/20	AA6/22	AA6/23	AA6/24	AA6/24	AA6/25	AA6/26	BL1-A	DB-1	SR-1	AA6/16A	AA6/16B	AA6/17
Lithology:	augen gneiss	augen gneiss	porphy. granite	augen gneiss	granite gneiss	augen gneiss	augen gneiss	porphy. granite	granite	biotite granite	porphy. granite	augen gneiss	massive granite	massive granite	massive granite
CIPW Norms(100 % anhydrous)															
Normative Minerals	Weight % Norm	Weight % Norm	Weight % Norm	Weight % Norm	Weight % Norm	Weight % Norm	Weight % Norm	Weight % Norm	Weight % Norm	Weight % Norm	Weight % Norm	Weight % Norm	Weight % Norm	Weight % Norm	Weight % Norm
Quartz	34.22	30.08	28.28	26.66	36.77	32.02	33.87	20.77	25.16	27.63	33.68	40.17	36.09	29.12	29.28
Plagioclase	36.79	32.8	33.31	39.12	17.23	27.51	28.39	41.12	38.48	39.55	22.44	22.1	26.31	36.5	32
Orthoclase	23.4	27.74	31.05	25.98	19.58	28.46	26.66	27.41	30.35	28.69	30.74	27.55	32.9	27.46	34.92
Nepheline	0	0	0	0	0	0	0	0	0	0	0	0	0	0	0
Corundum	0.06	0.59	0.22	0.29	8.38	3.16	3.6	0.2	0	0.69	5.18	3.31	0	0	0
Diopside	0	0	0	0	0	0	0	0	1.07	0	0	0	1.05	0.1	0.67
Hypersthene	2.6	3.73	4.16	4.96	11.61	5.48	4.7	5.89	2.43	1.04	6.56	4.46	1.83	2.84	2.19
Wollastonite	0	0	0	0	0	0	0	0	0	0	0	0	0	0	0
Acmite	0	0	0	0	0	0	0	0	0	0	0	0	0	0	0
Na ₂ SiO ₃	0	0	0	0	0	0	0	0	0	0	0	0	0	0	0
Rutile	0	0	0	0	0	0	0	0	0	0	0	0	0	0	0
Ilmenite	0.53	0.93	1.01	0.63	1.61	1.01	0.91	1.56	0.59	0.15	1.25	0.76	0.51	0.49	0.46
Magnetite	1.13	1.61	1.55	1.38	3.31	1.75	1.71	2.04	0.9	0.42	2.33	1.62	1.06	0.93	0.75
Apatite	0.14	0.46	0.42	0.28	0.3	0.32	0.28	0.58	0.23	0.74	0.39	0.32	0.12	0.21	0.3
Zircon	0.03	0.06	0.06	0.03	0.04	0.03	0.03	0.03	0.04	0.01	0.03	0.03	0.04	0.03	0.03
Chromite	0	0	0.06	0.09	0.01	0	0.09	0.07	0.09	0.28	0.15	0.13	0.04	0.06	0.07
Total	98.9	98	100.12	99.42	98.84	99.74	100.24	99.67	99.34	99.2	102.75	100.45	99.95	97.74	100.67
An	7.8	7.7	8.2	8.1	0.2	7.0	7.0	13.5	7.3	2.0	5.3	4.7	2.0	7.1	4.7
Ab	29.0	25.0	25.1	31.0	17.0	20.6	21.4	27.7	31.2	37.6	17.2	17.4	24.3	29.4	27.3
Plag An-content	20.2	22.6	23.5	19.9	1.2	24.2	23.5	31.4	18.0	4.7	22.4	20.2	7.3	18.4	13.9

	RANAKPUR						REVDAR RD.	SWARUPGANJ RD.	KISHENGARH
Sample	AA6/2	AA6/3A	AA6/3B	AA6/5	AA6/6	AA6/7	AA6/48B	AA6/49	AA6/52A
Lithology:	grey	grey	grey	grey	grey	grey	aplitic	foliated	nepheline
	granite	granite	granite	granite	granite	granite	dyke	granite	syenite
CIPW Norms(100 % anhydrous)									
Normative Minerals	Weight %	Weight %	Weight %	Weight %	Weight %	Weight %	Weight %	Weight %	Weight %
	Norm	Norm	Norm	Norm	Norm	Norm	Norm	Norm	Norm
Quartz	8.94	12.05	10.93	10.22	13.31	12.37	28.79	36.11	0
Plagioclase	43.18	47.13	47.04	45.43	44.24	46.03	43.15	48.77	13.4
Orthoclase	36.23	33.29	34.71	34.28	33.97	32.96	25.88	9.61	39.95
Nepheline	0	0	0	0	0	0	0	0	32.62
Corundum	0	0	0	0	0	0	0	0	0
Diopside	4.88	1.46	1.88	3.44	2.37	2.12	1.99	3.98	6.08
Hypersthene	2.74	3.46	3.38	2.89	2.42	2.8	0	0.74	0
Wollastonite	0	0	0	0	0	0	0.31	0	0
Acmite	0	0	0	0	0	0	0.81	0	3.79
Na2SiO3	0	0	0	0	0	0	0.54	0	0.48
Rutile	0	0	0	0	0	0	0	0	0
Ilmenite	1.37	1.01	1.03	1.01	0.91	0.99	0.04	0.42	0.57
Magnetite	1.46	1.3	1.3	1.39	1.16	1.28	0	0.75	0
Apatite	0.58	0.56	0.58	0.58	0.44	0.53	0	0.09	0.28
Zircon	0.06	0.06	0.04	0.04	0.04	0.04	0.03	0.01	0.01
Chromite	0.1	0	0	0	0	0	0.01	0.01	0.09
Total	99.54	100.32	100.89	99.28	98.86	99.12	101.55	100.49	99.62
An	7.6	10.4	10.0	9.8	8.4	9.9	0.0	1.2	0.0
Ab	35.6	36.7	37.1	35.6	35.9	36.1	43.1	47.6	13.4
Plag An-content	16.7	21.1	20.2	20.6	18.0	20.5	0.0	2.3	0.0

	REVDAR RD. (ERINPURA-TYPE)							REVDAR RD. (MT. ABU-TYPE)				
Sample	AA6/38	AA6/47A	AA6/47B	AA6/45A	AA6/45B	AA6/43B	AA6/44B	AA6/39	AA6/40	AA6/42A	AA6/42B	AA6/48A
Lithology:	granite	augen	augen	micaceous	granite	granite	pegmatite	augen	massive	porphy	porphy	foliated
	gneiss	gneiss	gneiss	gneiss	gneiss			gneiss	granite	granite	granite	granite
CIPW Norms(100 % anhydrous)												
Normative Minerals	Weight %	Weight %	Weight %	Weight %	Weight %	Weight %	Weight %	Weight %	Weight %	Weight %	Weight %	Weight %
	Norm	Norm	Norm	Norm	Norm	Norm	Norm	Norm	Norm	Norm	Norm	Norm
Quartz	27.95	52.87	58.2	44.37	41.95	19.73	53.87	30.86	24.42	19.75	23.33	30
Plagioclase	41.8	0.51	0.42	7.55	9.6	41.65	15.01	28.07	31.96	31.04	35.28	33.24
Orthoclase	23.99	35.97	31.66	18.83	18.98	4.68	17.37	37.89	36.19	40.23	29.02	29.22
Nepheline	0	0	0	0	0		0	0	0	0	0	0
Corundum	0	4.72	4.18	10.59	9.06		6.72	0	0	0	0	0
Diopside	0.47	0	0	0	0	17.03	0	1.01	1.72	4.76	4.83	2.15
Hypersthene	2.15	2.6	1.6	11.17	11.73		5.4	1.47	2.33	1.42	0	1.77
Wollastonite	0	0	0	0	0	9.55	0	0	0	0	6.74	0
Acmite	0	0	0	0	0		0	0	0	0	0	0
Na2SiO3	0	0	0	0	0		0	0	0	0	0	0
Rutile	0	0	0	0	0		0	0	0	0	0	0
Ilmenite	0.55	0.32	0.27	1.61	1.63	0.93	0.32	0.55	0.65	0.65	0.44	0.53
Magnetite	0.94	1	0.84	3.16	3.1	2.36	1.51	0.75	1.52	1.62	1.03	1.49
Apatite	0.25	0.09	0.02	0.3	0.32	0.32	0.16	0.16	0.09	0.21	0.07	0.05
Zircon	0.03	0.01	0.03	0.04	0.06	0.01	0.01	0.06	0.07	0.06	0.1	0.1
Chromite	0.1	0.01	0.01	0.12	0.1	0.1	0.07	0.03	0.03	0.04	0	0.03
Total	98.23	98.1	97.23	97.74	96.53	96.38	100.44	100.85	98.98	99.78	100.84	98.58
An	8.4	0.1	0.0	0.2	1.0	30.3	0.1	2.9	2.4	0.2	1.4	1.6
Ab	33.4	0.4	0.4	7.4	8.6	4.7	14.9	25.2	29.5	30.9	33.8	31.6
Plag An-content	19.1	16.1	0.0	2.4	9.6	71.6	0.7	9.6	7.2	0.5	3.8	4.5

APPENDIX D

Major and Trace Element Data (Seychelles, MIS and Mt. Abu dolerite samples).

SEYCHELLES GRANITOIDS															
Sample #	%SiO2	%TiO2	%Al2O3	%Fe2O3*	% Fe2O3	% FeO	%MnO	%MgO	%CaO	%Na2O	%K2O	%P2O5	%LOI	%TOTAL	Mg #
LA99M-2	75.65	0.19	12.29	2.39	0.36	1.83	0.08	0.08	0.35	4.19	4.62	0.01	0.35	100.20	0.072
LA99M-3B	58.01	0.94	17.27	8.07	1.21	6.17	0.17	2.86	6.40	4.59	1.50	0.30	0.44	100.55	0.452
LA97M-11B	75.72	0.24	11.77	2.49	0.37	1.90	0.09	0.02	0.49	4.17	4.58	0.02	0.28	99.87	0.018
LA97M-20	70.69	0.49	13.53	3.40	0.51	2.60	0.10	0.54	1.42	4.50	4.60	0.17	0.00	99.43	0.270
LA97M-22	75.46	0.24	12.34	2.20	0.33	1.68	0.07	0.16	0.84	4.08	4.61	0.02	0.44	100.46	0.145
LA97M-23	72.29	0.39	13.81	2.80	0.42	2.14	0.07	0.57	2.02	4.27	3.61	0.09	0.45	100.37	0.322
LA97M-24A	73.84	0.32	12.98	2.52	0.38	1.93	0.07	0.29	1.29	4.09	4.30	0.06	0.30	100.06	0.211
LA97M-25A	72.79	0.33	13.54	2.88	0.43	2.20	0.10	0.41	1.40	5.26	2.84	0.08	0.09	99.72	0.249
LA97M-26D	77.63	0.07	12.62	0.43	0.06	0.33	0.01	0.00	0.68	3.60	5.00	0.01	0.17	100.22	0.000
LA97P-15	73.32	0.31	13.14	2.83	0.42	2.16	0.10	0.36	1.37	5.51	2.57	0.07	0.13	99.71	0.229
LA97A-29	75.87	0.08	12.53	1.23	0.18	0.94	0.04	0.35	0.80	3.74	5.20	0.02	0.43	100.29	0.399
LA97P-4	74.74	0.19	12.36	2.41	0.36	1.84	0.05	0.04	0.90	3.86	5.04	0.02	0.57	100.18	0.037
RT97P-5	73.90	0.21	12.81	2.30	0.35	1.76	0.04	0.07	1.00	3.69	5.58	0.03	0.43	100.06	0.066
LA97L-10	75.55	0.25	12.21	2.04	0.31	1.56	0.04	0.19	0.85	3.09	5.46	0.04	0.92	100.64	0.178
LA97M-9	68.01	0.49	14.58	4.77	0.72	3.65	0.10	0.39	2.41	3.81	4.76	0.11	0.30	99.74	0.160
LA97F-13A	77.99	0.15	12.18	0.69	0.10	0.53	0.03	0.00	0.32	3.77	4.97	0.01	0.13	100.24	0.000
LA97F-13B	71.67	0.37	14.50	2.39	0.36	1.83	0.16	0.39	1.13	4.84	4.48	0.10	0.39	100.42	0.275
LA97F-13C	73.11	0.30	13.22	3.06	0.46	2.34	0.06	0.05	0.88	3.42	5.45	0.03	0.24	99.82	0.037
LA97F-14	71.11	0.51	14.30	3.33	0.50	2.55	0.08	0.52	1.61	4.22	4.22	0.13	0.40	100.43	0.267
LA97R-16	75.31	0.28	12.42	2.30	0.35	1.76	0.04	0.07	0.65	3.14	5.88	0.03	0.87	100.99	0.066
LA99M-3A	73.12	0.26	14.07	2.04	0.31	1.56	0.06	0.43	1.78	4.11	3.41	0.06	0.42	99.76	0.329
LA97M-24B	69.35	0.49	14.78	3.78	0.57	2.89	0.10	0.79	2.46	4.83	3.23	0.15	0.76	100.72	0.327
LA97M-25B	61.04	0.87	17.28	5.38	0.81	4.11	0.30	1.74	3.94	7.62	1.26	0.37	0.06	99.86	0.430
LA97M-26A	58.50	0.79	18.46	6.96	1.04	5.32	0.12	2.00	6.80	4.94	1.11	0.38	0.29	100.35	0.401
LA97M-26B	57.40	0.80	16.13	8.85	1.33	6.77	0.18	3.87	7.17	4.09	1.16	0.28	0.48	100.41	0.505
LA97M-26C	51.58	1.36	17.11	9.42	1.41	7.20	0.15	6.01	8.79	3.49	1.40	0.41	1.71	101.42	0.598
LA97M-26C	51.68	1.35	17.18	9.21	1.38	7.04	0.14	6.04	8.65	3.29	1.58	0.42	1.68	101.22	0.604

<u>MIS granitoids-Jalore</u> (Maheshwari et. al. (2001). Geology and geochemistry of granites around Jaswantpura, Jalore district, southwestern Rajasthan, India, Gondwana Research, 5, 373-379)														
Sample #	%SiO ₂	%TiO ₂	%Al ₂ O ₃	%Fe ₂ O ₃ *	% Fe ₂ O ₃	% FeO	%MnO	%MgO	%CaO	%Na ₂ O	%K ₂ O	%P ₂ O ₅	%TOTAL	Mg #
1	69.3	0.24	14.1	3.5	0.53	2.68	0.05	0.37	0.98	4.3	4.7	0.07	97.61	0.20
2	67.93	0.43	13.72	6.59	0.99	5.04	0.2	0.27	1.68	4.16	4.78	0.06	99.82	0.09
3	71.28	0.32	12.34	5.13	0.77	3.92	0.14	0.21	1.17	5.01	3	0.04	98.64	0.09
4	66.95	0.35	14.23	6.44	0.97	4.93	0.13	0.34	1.83	3.88	4.67	0.05	98.87	0.11
6	71.19	0.23	12.79	3.2	0.48	2.45	0.08	0.23	0.74	3.85	4.95	0.02	97.28	0.14
8	77.09	0.05	12.76	0.95	0.14	0.73	0.01	0.22	0.35	4.45	3.89	0.01	99.78	0.35
9	72.82	0.3	13.1	3.12	0.47	2.39	0.04	0.35	1.13	3.07	5.59	0.06	99.58	0.21
10	69.73	0.36	14.06	5.26	0.79	4.02	0.15	0.25	1.35	4.3	5.24	0.05	100.75	0.10
11	67.25	0.39	13.36	5.88	0.88	4.50	0.116	0.23	1.62	4.13	4.94	0.06	97.98	0.08
13	70.69	0.03	14.96	1.66	0.25	1.27	0.15	0.21	0.36	3.28	7.02	0.02	98.38	0.23
14	72.6	0.2	12.9	2.3	0.35	1.76	0.04	0.28	1	3.3	5.5	0.03	98.15	0.22
15	74.54	0.18	13.32	1.9	0.29	1.45	0.03	0.25	0.91	3.32	5.33	0.03	99.81	0.23
16	74.72	0.12	13.2	2.05	0.31	1.57	0.02	0.23	0.72	3.56	5.08	0.02	99.72	0.21
17	74.12	0.16	13.37	2.21	0.33	1.69	0.05	0.24	0.95	3.87	4.83	0.03	99.83	0.20
18	69.02	0.5	14.04	4.96	0.74	3.79	0.06	0.77	1.71	2.42	5.34	0.14	98.96	0.27
20	76.82	0.07	13.19	0.57	0.09	0.44	0.01	0.2	0.9	4.18	3.86	0.02	99.82	0.45
21	71.52	0.12	11.68	3.63	0.54	2.78	0.13	0.31	9.4	1.69	1.19	0.05	99.72	0.17
22	74.94	0.12	13.08	1.15	0.17	0.88	0.02	0.39	1.36	2.63	4.98	0.03	98.70	0.44
23	67.8	0.54	14.1	5	0.75	3.82	0.07	0.76	1.6	2.2	6.3	0.22	98.59	0.26
24	77.62	0.06	13.07	0.93	0.14	0.71	0.03	0.23	0.74	4.17	4.15	0.01	101.01	0.37
25	64.2	0.73	16.2	3.8	0.57	2.91	0.06	0.48	5.8	2.7	4.9	0.25	99.12	0.23
26	67.46	0.47	14.96	4.52	0.68	3.46	0.07	0.78	1.69	2.51	6.07	0.19	98.72	0.29
27	71.22	0.5	14.23	4.1	0.62	3.14	0.07	1.37	2.42	3.71	2.25	0.1	99.97	0.44
28	74.67	0.05	15.1	0.97	0.15	0.74	0.09	0.27	0.45	4.08	4.21	0.07	99.96	0.39
29	66.9	0.7	14.77	5.16	0.77	3.95	0.09	1.24	2.91	3.13	3.07	0.21	98.18	0.36
30	73.37	0.1	15.07	0.81	0.12	0.62	0.04	0.26	0.58	3.13	5.57	0.16	99.09	0.43
31	70.07	0.27	14.35	2.3	0.35	1.76	0.06	0.21	0.44	3.28	6.76	0.02	97.76	0.18

<u>MIS granitoids-Barmer</u> (Maheshwari et. al. (2001). Geology and petrogenesis of Siwana Peralkaline Granites, west of Barmer, Rajasthan, India, Gondwana Research, 4, 87-95)															
Sample #	%SiO ₂	%TiO ₂	%Al ₂ O ₃	%Fe ₂ O ₃ *	% Fe ₂ O ₃	% FeO	%MnO	%MgO	%CaO	%Na ₂ O	%K ₂ O	%P ₂ O ₅	%LOI	%TOTAL	Mg #
1	76.4	0.2	11.5	2.4	0.36	1.84	0	0	0.5	4.4	4.5	0	0.2	100.10	0.00
2	76.3	0.2	11.3	2.5	0.38	1.91	0	0	0.3	4.7	4.4	0	0.4	100.10	0.00
3	74.8	0.3	10.9	3.6	0.54	2.75	0.1	0.1	1.2	4.1	4.1	0	1	100.20	0.06
4	75.2	0.2	11.1	3.2	0.48	2.45	0.1	0.1	0.8	4.2	4.3	0	0.9	100.10	0.07
5	76.4	0.3	11	3	0.45	2.29	0.1	0	0.3	4.4	4.6	0	0	100.10	0.00
6	75.1	0.2	12.1	3.7	0.56	2.83	0.1	0	0.5	8.1	0.1	0	0.1	100.00	0.00
7	75.3	0.3	11.1	4.1	0.62	3.14	0.1	0.1	0.3	4.6	4	0	0.1	100.00	0.05
8	77.3	0.3	10.6	3.3	0.50	2.52	0	0	0.2	3.7	4.3	0	0.3	100.00	0.00
9	72.2	0.3	12.4	4.3	0.65	3.29	0.1	0.1	0.6	5.1	4.7	0	0.2	100.00	0.05
10	72.4	0.8	11.4	5.5	0.83	4.21	0.1	0.1	0.5	4.8	4.4	0	0.1	100.10	0.04
11	74.3	0.3	11.5	3.1	0.47	2.37	0.1	0.5	1.4	4	4.3	0	0.5	100.00	0.27
12	73.1	0.3	12.5	3.6	0.54	2.75	0.1	0.2	0.7	4.9	4.6	0	0	100.00	0.11
13	74.8	0.2	11.3	4.1	0.62	3.14	0.1	0	0.1	4.8	4.6	0	0.2	100.20	0.00
14	73.9	0.4	10.5	5.8	0.87	4.44	0.1	0	0.2	4.1	4.9	0	0	99.90	0.00
15	75.9	0.3	15.8	4	0.60	3.06	0.1	0	0.3	4.5	4.2	0	0	105.10	0.00
16	73.9	0.2	11.5	4.4	0.66	3.37	0.1	0	0.3	4.4	5.2	0	0.1	100.10	0.00
17	77.6	0.1	11.6	1.6	0.24	1.22	0	0	0.4	5	3.5	0	0.2	100.00	0.00
18	74.4	0.3	11.2	4.1	0.62	3.14	0.1	0.4	0.7	4.5	4.3	0	0.1	100.10	0.19
19	74.6	0.3	12.5	2.9	0.44	2.22	0.1	0.1	0.2	5.3	4	0	0.1	100.10	0.07
20	72.9	0.2	14.4	2.2	0.33	1.68		0	0.3	5.3	4.2	0	0.5	100.00	0.00
21	74.84	0.27	11.18	3.57	0.54	2.73	0.07	0.08	0.49	4.74	4.16	0	0.2	99.60	0.05
22	70.06	0.35	10.66	4.78	0.72	3.66	0.1	0.25	0.7	4.82	4.42	0.07	1.26	97.47	0.11
23	69.79	0.57	8.87	7.62	1.14	5.83	0.14	0.66	0.29	4.23	4.4	0.1	0.85	97.52	0.17

Seychelles Trace Elements														
Seychelles Granitoids														
Sample:	LA99M-2	LA99M-3B	LA97M-11B	LA97M-20	LA97M-22	LA97M-23	LA97M-24A	LA97M-25A	LA97M-26D	LA97P-15	LA97A-29	LA97P-4	RT97P-5	LA97L-10
Ba	1044	629	1213	864	1083	966	1178	1966	334	1770	225	227	119	230
Rb	92.8	43.1	119.5	94.9	151.7	119.5	127.5	46.8	127.4	40.6	158.6	252.4	277.1	352.5
Sr	22.2	458.2	22.1	157.9	56.4	132.4	91.1	140.9	39.4	135.7	35.3	36	36.5	35.2
Ga	20	21	20	18	17	16	18	15	12	17	27.8	24	20	16
Nb	11.8	5.5	13.8	14.7	14.6	13.2	12.2	5.8	7.5	6.6	6.3	33.8	21.8	15.6
Hf	10.3	7	11.4	12.5	10.2	6.8	8.8	11.2	2.8	11.2	8.2	13.3	11	7.4
Zr	330	211	426.2	444.6	307.3	213.8	266.4	423.3	60.1	413.3	62.9	379.7	335.7	201
Y	62.7	41.8	79.2	46.4	63.1	52	58.3	37.1	17.3	41.8	84.3	122.2	92.2	74.1
Th	15.5	6.8	15.6	18.6	19.3	18.2	14.4	7.4	19.7	7.2	15	45.5	38	61
U	3.4	1.4	2.8	2.5	3.8	4.2	2.9	1.3	5.4	1.3	3.2	8.5	6.1	10.2
Ta	0.8	0.3	1.5	1.4	2.4	2.2	1.6	1.4	1.9	1.1	0.8	3.2	2.8	2.5
W	1.2	1.5	324	304	869	552	392	600	488	394	23	283	563	508
Cr	0.9	1.6	0	0	0	0	0	0	0	0	2.1	0	0	0
Ni	1.6	1.3	0	0	0	0	0	0	0	0	1	0	0	0
Co	0	18	68	68	150	96	75	102	95	71	182.8	65	93	93
Sc	6.2	24.9	7.5	9.9	5.2	7.6	8.1	10.4	1.5	11.7	7.3	2.6	3.7	3.6
V	0.53	59.6	4.3	1.05	7.8	26	14.4	10.4	0.6	10.2	1.9	<0.1	2.6	5.8
Cu	0.9	7.7	0	0	0	0	0	0	0.3	0	0	0	0	0
Pb	15.6	9.4	6	9.8	21	18.3	18.7	13.5	28.7	12.8	25.1	35.6	36	42
Zn	96.1	97.6	69.4	99.9	66.8	49.6	66	84.8	3.6	67.9	75.3	103.7	67	41.6
La	62.59	27.07	64	108.09	48	36	44	50	18.82	44	46.8	82.92	81	72
Ce	131.56	60.12	132	204.74	100	73	91	100	35.42	89	104.94	177.02	167	142
Pr	16.45	7.95	16.4	22.51	12.1	8.7	11	12.1	3.55	11.2	14.05	21.56	20	15.9
Nd	63.37	33.73	62	79.26	45	32	41	44	11.57	43	57.05	81.77	72	53
Sm	12.33	7.21	12.1	12.55	8.7	6.5	8	7.5	2.07	8	13.05	17.2	14.3	10.2
Eu	2.21	2.16	2.1	2.2	1.37	1.04	1.44	1.99	0.28	1.97	0.9	1.12	1.3	0.6
Gd	11.97	7.53	12.3	10.86	8.7	6.5	8.6	7	2.04	7.8	13.71	17.62	14.2	9.5
Dy	10.83	7.05	12.1	8.65	9	6.9	8.6	6	2.29	7	13.23	19	13.5	10.2
Ho	2.39	1.6	2.7	1.91	2.1	1.6	1.98	1.35	0.57	1.54	2.85	4.31	3	2.3
Er	6.38	4.2	7.4	5	5.9	4.6	5.5	3.4	1.71	3.9	6.95	12.11	8.2	6.4
Yb	6.98	3.84	7.7	5.29	6.2	5.3	5.9	3.5	2.33	3.8	5.9	11.92	8.1	6.6
Lu	1.06	0.6	1.21	0.84	0.93	0.78	0.89	0.6	0.37	0.59	0.9	1.73	1.16	0.97
S	230	969	34	404	93	22	31	114	174	113	115	0	7	3
As	1	0	1	5	5	4	3	1	8	1	1.4	11	10	14

Seychelles Trace Elements												
Seychelles Granitoids cont.						Seychelles-Intermediate						
Sample:	LA97F-13A	LA97F-13B	LA97F-13C	LA97F-14	LA97F-16	LA99M-3A	LA97M-24B	LA97M-25B	LA97M-26A	LA97M-26B	LA97M-26C	LA97M-26C
Ba	182	441	838	729	366	886	717	699	585	541	542	
Rb	204.8	206.6	191.7	221.4	383.7	116.6	136.1	23.1	32.3	34.3	33.9	
Sr	11.2	80.1	53.6	114.8	24.9	178.8	160.2	190.5	563.8	407.4	1072.2	
Ga	17	19	21	21	20	15	17	19	20	19	21	21
Nb	15.5	29.3	17.9	33.1	21.2	5.2	12.1	16.3	4.7	4.6	2.8	2.9
Hf	5.4	6.6	13	9.7	13.5	4.4	8.3	8.4	10	2.3	2.9	
Zr	131.6	191.7	445.2	317.7	404.2	122	301.3	311.9	350.8	63	134.9	137.3
Y	80.8	126.2	84.7	69.5	127.3	27.5	51.4	89.4	35.5	42.5	21.1	23.2
Th	24.3	26.1	30	38	46	11.7	15.8	4.1	3.9	2	4.3	
U	5.6	4.4	4.4	5.9	6.5	2.7	2.9	1.2	0.9	0.4	0.8	
Ta	2.2	2.1	2.1	3.5	3.5	0.5	0.7	0.5	0.4	0.7	0.2	
W	539	288	565	535	1048	0.9	1.5	1.25	168	307	73	
Cr	0	0.7	0	0	0	0.2	0	0	0	0	86.7	83.7
Ni	0	0	0	0	0	0.8	0.6	0	0	0	34.9	39.2
Co	111	65	105	91	181	4	3	6	49	75	52	27
Sc	1.4	15	7.5	8.5	7.2	5.2	8.6	23.5	20.7	33.2	28.6	29.9
V	<0.1	10.3	1.1	21	3.3	8.41	30.7	12.2	66.3	171	147.9	
Cu	0	0	0	0	0	0	0	0	0	0	21.4	27.1
Pb	32.7	38.3	31	30	43	16.6	19	13.1	8.3	7.1	5.5	
Zn	36.4	122.3	72.4	86.5	74.4	29.6	75	178.7	81.1	101.2	89.2	88.8
La	56.25	51.59	93	87	83	34.69	35.03	25.67	22.8	21	30.51	
Ce	120.98	120.73	180	163	177	80.07	79.72	70.69	51.53	51	66.24	
Pr	15.01	15.41	22	18	22	7.96	10.07	11.63	6.79	7.5	9	
Nd	55.6	60.49	79	61	84	27.33	39.97	58.88	29.48	33	38.12	
Sm	12.8	14.92	14.9	11.2	18.1	4.49	7.91	15.82	6.23	7	7.02	
Eu	0.88	1.24	1.71	1.49	1.28	0.92	1.62	3.57	1.97	1.77	2.39	
Gd	12.26	16.7	14.3	10.4	18.4	4.44	7.56	17.65	6.68	7.1	5.73	
Dy	11.3	18.22	13.2	10.6	19.2	4.13	7.38	15.59	5.56	6.5	3.9	
Ho	2.39	4.12	2.9	2.4	4.3	0.97	1.66	3.33	1.23	1.46	0.78	
Er	6.4	11.4	7.6	6.7	11.7	2.8	4.62	8.2	3.3	3.9	1.89	
Yb	6.43	10.68	7.3	7	11.5	3.31	4.91	7.02	3.11	3.7	1.65	
Lu	0.92	1.56	1.1	1.06	1.67	0.52	0.74	1.07	0.46	0.56	0.26	
S	1910	3393	91	140	29	365	159	722	280	612	894	878
As	12	13	8	8	13	0	4	2	0	0	0	0

<u>MIS (Jalore)-Trace Elements</u>							
Sample	Cr	Ni	Ba	Rb	Sr	Zr	Nb
1	50			117	38	694	35
2	251	12	472	118	63	1175	61
3	239	20	313	113	43	1071	52
4	202	14	413	111	48	1277	51
6	120	21	233	167	13	649	44
8	132	26	62	138	10	107	11
9	219	24	500	232	77	415	24
10	241	26	493	129	48	955	51
11	213	17	478	146	45	1343	59
13	150	22	148	1393	10	32	26
14	50		0	333	45	417	28
15	137	14	301	344	53	355	21
16	385	19	105	466	10	266	32
17	249	15	578	224	51	445	26
18	187	25	704	209	146	389	15
20	127	14	109	141	37	124	11
21	163	20	195	66	183	71	10
22	225	23	561	193	127	90	10
23	228	33	878	253	126	535	24
24	118	12	233	213	14	104	25
25	50			175	346	622	30
26	207	15	767	291	121	489	21
27	109	26	325	227	125	160	12
28	208	23	57	435	10	53	22
29	42	20	365	181	131	355	14
30	180	12	33	267	11	37	10
31	199	16	1015	133	70	619	10

<u>MIS (Barmer)-Trace Elements</u>															
Sample	Cr	Ni	Ba	Rb	Sr	Zr	Nb	Pb	Zn	Co	V	Th	Y	La	Ce
1	3	5	132	140	34	991	22	26	105	1	5	17	156	92	183
2	4	5	27	215	10	729	10	29	214	2	2	15	160	25	67
3	4	5	538	105	29	1135	4	10	119	2	6	12	143	76	147
4	5	5	345	114	23	1328	31	16	208	2	0	17	168	73	143
5	4	5	237	1.7	65	1514	8	22	226	1	5	16	162	86	158
6	3	3	77	1	44	880	13	42	103	1	5	9	115	43	147
7	7	6	158	129	55	2050	51	14	196	3	3	16	178	93	199
8	16	9	158	99	33	2096	39	56	196	3	6	20	231	121	222
9	4	4	129	99	50	1095	8	27	164	3	10	9	122	79	164
10	3	4	70	76	28	1025	36	31	123	2	7	11	100	59	116
11	8	6	130	77	39	396	4	27	93	4	11	1	88	29	9
12	4	5	124	79	44	1218	36	21	193	2	10	14	124	72	155
13	1	6	51	177	28	1316	66	37	270	1	5	41	234	118	237
14	4	6	109	111	29	1301	54	31	182	2	4	14	190	85	189
15	7	5	133	97	10	1487	12	23	145	2	13	12	139	86	163
16	3	5	108	122	11	1462	38	18	176	3	7	8	135	71	150
17	6	4	391	93	30	576	0	24	246	1	3	9	110	37	109
18	5	5	28	7	15	1125	28	24	142	2	10	8	98	89	103
19	3	5	337	111	60	851	11	27	194	2	7	15	139	102	138
20	2	4	422	105	51	781	21	9	60	1	7	11	97	29	68

ABU DOLERITES															
Sample #	%SiO2	%TiO2	%Al2O3	%Fe2O3*	% Fe2O3	% FeO	%MnO	%MgO	%CaO	%Na2O	%K2O	%P2O5	%LOI	%TOTAL	Mg #
R254B-30	45.52	3.41	14.74	14.86	2.97	10.70	0.21	5.82	8.75	2.34	2.78	0.67	0.81	99.10	0.492
R255B-30	44.48	3.33	14.96	14.88	2.98	10.71	0.20	5.78	8.66	2.28	2.81	0.62	0.88	98.00	0.490
R256B-30	44.56	3.30	15.05	14.94	2.99	10.75	0.21	5.99	8.99	2.13	2.73	0.61	1.21	98.51	0.498
R257B-30	45.30	3.74	14.09	15.17	3.03	10.92	0.20	6.17	9.01	2.09	2.22	0.56	0.67	98.55	0.502
R258B-30	42.20	3.78	15.03	16.01	3.20	11.52	0.23	6.07	10.50	2.03	2.75	0.73	0.89	99.33	0.484
R259B-30	43.12	3.63	15.46	15.75	3.15	11.34	0.22	5.93	9.40	2.16	3.34	0.69	0.93	99.70	0.482
R261B-30	45.99	3.27	14.49	14.66	2.93	10.55	0.22	5.48	7.27	1.70	4.07	0.62	1.53	97.77	0.481
R275A-32	41.26	2.68	15.09	14.26	2.85	10.26	0.21	6.42	7.57	1.48	6.00	0.52	4.18	95.49	0.527
R279B-32	43.95	3.89	14.31	16.23	3.25	11.68	0.23	5.55	8.89	1.84	3.43	0.81	0.90	99.13	0.458
R284A-32	41.40	3.93	15.18	16.43	3.29	11.83	0.25	6.32	9.20	1.84	3.49	0.80	1.12	98.84	0.488
RS285B-33	45.17	3.65	14.17	15.46	3.09	11.13	0.22	4.87	7.63	2.14	3.52	0.82	0.74	97.65	0.438
RS286B-33	42.68	3.96	15.12	16.65	3.33	11.99	0.23	5.07	8.30	2.04	3.96	0.92	0.86	98.93	0.430
R287B-33	48.69	3.40	13.06	16.78	3.36	12.08	0.23	4.25	6.83	1.51	3.65	1.04	0.81	99.44	0.385
RS288B-33	46.35	3.60	14.22	15.29	3.06	11.01	0.22	3.69	8.46	2.36	2.81	1.20	0.71	98.20	0.374
RS289b-33	35.74	2.86	10.25	11.52	2.30	8.29	0.16	2.56	29.24	2.28	2.11	0.89	1.08	97.61	0.355
RS291B-33	38.70	3.35	13.61	14.03	2.81	10.10	0.18	4.37	7.32	1.96	3.09	0.78	12.60	87.39	0.435
RS295A-35	46.52	2.64	15.34	15.71	3.14	11.31	0.18	3.17	6.72	2.95	3.61	0.96	0.79	97.80	0.333
RS305b-35	46.07	3.26	15.23	15.07	3.01	10.85	0.21	5.81	8.49	2.75	2.07	0.67	0.80	99.63	0.488
RS306A-35	46.31	2.94	16.74	13.86	2.77	9.98	0.20	5.11	8.93	3.11	1.82	0.64	0.63	99.66	0.477
RS314B-35	43.97	3.81	15.77	16.63	3.33	11.97	0.23	4.54	8.12	2.87	2.67	1.14	0.81	99.75	0.403
RS317A-35	46.26	2.78	16.21	14.17	2.83	10.20	0.18	4.99	8.20	2.76	2.19	0.60	0.68	98.34	0.466
R323A-37	43.49	2.99	13.96	16.76	3.35	12.06	0.25	6.71	8.68	1.48	2.70	0.97	0.80	97.99	0.498
R324A-37	43.16	3.26	14.58	16.79	3.36	12.09	0.27	6.26	10.00	1.86	2.14	1.09	1.03	99.41	0.480
RS327B-37	41.28	3.36	15.77	16.94	3.39	12.19	0.23	6.36	9.73	1.57	2.97	1.13	1.12	99.34	0.482
R328A-37	41.88	3.20	15.37	17.32	3.46	12.47	0.26	6.31	9.22	1.63	3.00	1.09	1.26	99.28	0.474
R335A-38	44.16	2.87	15.41	14.09	2.82	10.14	0.22	7.14	9.91	1.74	2.73	0.68	1.65	98.95	0.556
RS337B-38	40.84	4.10	14.69	17.14	3.43	12.34	0.23	6.52	6.73	1.08	5.44	1.15	1.60	97.92	0.485
RS339a-38	41.11	2.73	15.24	13.56	2.71	9.76	0.20	6.77	7.34	1.51	5.96	0.81	5.30	95.23	0.553
R347A-39	43.09	3.28	13.15	14.63	2.93	10.53	0.22	5.34	11.15	1.81	3.35	0.90	1.36	96.92	0.475
RS349A-39	46.22	3.27	13.39	14.47	2.89	10.42	0.21	5.53	8.73	1.62	3.00	0.92	1.30	97.36	0.486
RS356A-40	43.93	2.61	14.57	13.73	2.75	9.88	0.21	6.99	9.44	1.65	2.74	0.63	2.22	96.50	0.558
RS358A-40	42.66	2.68	16.13	13.04	2.61	9.39	0.20	7.47	10.07	1.76	3.31	0.64	2.55	97.96	0.586
RS366b-40	46.37	2.42	14.95	13.17	2.63	9.48	0.17	5.81	4.95	1.59	5.30	0.59	3.74	95.32	0.522

APPENDIX E

Tables of Ar-Ar age results for samples AA6-9, AA6-18, AA6-2 and AA6-52A.

AA6-9				J=0.0059020							
Step	40/39	38/39	37/39	36/39	³⁹ Ar ¹	F ³⁹ Ar ²	%40* ³	40*/39K	Age	+ 1s.d.	
1	130.974	0.119	0.381	317.223	0.447	0.31	28.40	37.25	358.72	12.73	
2	55.678	0.037	0.204	33.682	1.670	1.46	82.10	45.72	431.24	1.80	
3	51.849	0.027	0.088	4.748	7.728	6.78	97.30	50.43	470.30	0.58	
4	55.421	0.052	1.188	1.452	14.824	16.99	99.40	55.12	508.36	0.18	
5	55.330	0.058	1.307	0.948	19.621	30.50	99.70	55.19	508.95	0.28	
6	55.397	0.062	1.469	1.182	27.321	49.32	99.70	55.21	509.10	0.23	
7	55.170	0.062	1.624	0.873	26.910	67.86	99.90	55.09	508.17	0.28	
8	55.537	0.065	1.780	0.696	8.435	73.66	100.00	55.53	511.70	0.41	
9	55.371	0.071	1.848	0.642	11.427	81.53	100.00	55.39	510.56	0.32	
10	55.379	0.066	1.720	0.946	10.856	89.01	99.80	55.29	509.77	0.35	
11	55.019	0.054	1.367	0.393	3.734	91.58	100.10	55.05	507.83	1.41	
12	55.215	0.063	1.508	1.119	5.685	95.50	99.70	55.05	507.82	0.65	
13	54.632	0.065	1.813	1.429	3.767	98.09	99.60	54.41	502.70	1.05	
14	55.186	0.075	2.439	1.806	2.167	99.59	99.50	54.93	506.91	1.42	
15	55.578	0.056	2.400	5.698	0.601	100.00	97.50	54.17	500.75	4.70	

¹ ³⁹Ar (x 10⁻¹⁶ mols).

² Cumulative ³⁹Ar gas released during the experiment (%).

³ %40* = % radiogenic ⁴⁰Ar of total ⁴⁰Ar released.

AA6-18				J=0.0059150							
Step	40/39	38/39	37/39	36/39	³⁹ Ar ¹	F ³⁹ Ar ²	%40* ³	40*/39K	Age	+ 1s.d.	
1	57.119	0.049	0.070	46.247	4.760	2.27	76.00	43.43	412.74	1.38	
2	55.500	0.040	0.004	3.906	22.924	13.21	97.90	54.32	502.92	0.23	
3	55.786	0.041	0.000	0.968	38.913	31.78	99.40	55.47	512.22	0.60	
4	55.830	0.041	0.000	0.497	36.446	49.18	99.70	55.66	513.69	1.50	
5	55.959	0.043	0.000	0.442	12.179	54.99	99.70	55.80	514.85	0.32	
6	56.083	0.040	0.000	0.570	23.158	66.04	99.70	55.89	515.54	0.29	
7	56.285	0.041	0.000	0.766	8.306	70.00	99.60	56.03	516.71	0.32	
8	56.044	0.041	0.000	0.548	13.396	76.40	99.70	55.86	515.28	0.32	
9	56.235	0.040	0.000	0.598	13.909	83.03	99.60	56.03	516.70	0.54	
10	56.236	0.041	0.082	2.531	6.185	85.99	98.60	55.47	512.20	0.95	
11	56.251	0.042	0.085	2.289	7.908	89.76	98.80	55.56	512.90	0.48	
12	55.821	0.043	0.130	3.181	4.921	92.11	98.30	54.87	507.37	0.70	
13	55.429	0.042	0.171	2.214	3.756	93.90	98.80	54.77	506.55	0.92	
14	57.162	0.042	0.213	2.222	3.964	95.79	98.90	56.51	520.50	0.95	
15	56.941	0.047	0.123	2.292	1.921	96.71	98.80	56.25	518.47	1.64	
16	55.075	0.040	0.075	6.793	1.800	97.57	96.30	53.05	492.64	1.73	
17	57.070	0.038	0.236	6.191	1.580	98.32	96.80	55.24	510.37	1.89	
18	56.040	0.050	0.000	16.226	0.301	98.47	91.40	51.22	477.69	8.47	
19	57.110	0.051	0.454	3.272	1.047	98.97	98.40	56.17	517.84	2.58	
20	57.044	0.054	1.870	4.147	0.472	99.19	98.20	56.03	516.68	5.14	
21	55.561	0.041	0.401	4.047	1.693	100.00	97.90	54.39	503.48	2.11	

¹ ³⁹Ar (x 10⁻¹⁶ mols).

² Cumulative ³⁹Ar gas released during the experiment (%).

³ %40* = % radiogenic ⁴⁰Ar of total ⁴⁰Ar released.

AA6-2		J=0.0058960								
Step	40/39	38/39	37/39	36/39	³⁹ Ar ¹	F ³⁹ Ar ²	%40* ³	40*/39K	Age	+ 1s.d.
1	166.829	0.209	0.037	461.616	3.559	1.27	18.20	30.40	297.58	2.22
2	102.753	0.127	0.000	65.908	12.070	5.59	81.00	83.25	720.83	0.59
3	98.548	0.117	0.016	20.495	28.456	15.78	93.80	92.47	785.46	0.19
4	95.236	0.112	0.005	7.283	42.122	30.85	97.70	93.06	789.53	0.28
5	94.054	0.114	0.000	3.451	12.051	35.17	98.90	93.01	789.18	0.92
6	94.347	0.113	0.003	3.542	24.311	43.87	98.90	93.27	791.01	0.28
7	94.266	0.112	0.009	1.964	14.198	48.95	99.40	93.66	793.66	0.70
8	93.656	0.113	0.007	2.308	19.499	55.93	99.20	92.95	788.77	0.32
9	94.428	0.112	0.021	1.999	22.023	63.81	99.30	93.81	794.71	0.51
10	93.943	0.111	0.008	2.943	11.970	68.09	99.00	93.05	789.45	0.72
11	93.574	0.113	0.011	2.675	17.559	74.38	99.10	92.76	787.47	0.65
12	93.544	0.112	0.007	2.783	17.754	80.73	99.10	92.70	787.03	0.91
13	93.516	0.109	0.029	1.970	15.897	86.42	99.40	92.91	788.52	0.37
14	92.930	0.109	0.053	2.464	11.318	90.47	99.20	92.18	783.50	0.48
15	94.396	0.110	0.004	1.503	7.489	93.15	99.50	93.93	795.48	0.57
16	94.495	0.115	0.000	2.033	5.534	95.13	99.30	93.87	795.08	0.30
17	94.259	0.107	0.026	2.711	3.790	96.49	99.10	93.44	792.12	0.51
18	91.924	0.103	0.000	0.863	1.700	97.10	99.70	91.64	779.77	1.62
19	92.970	0.106	0.000	3.007	2.603	98.03	99.00	92.05	782.62	1.00
20	93.935	0.111	0.000	5.605	1.659	98.62	98.20	92.25	783.97	1.35
21	93.375	0.104	0.000	3.056	3.842	100.00	99.00	92.45	785.31	0.80

¹ ³⁹Ar (x 10⁻¹⁶ mols).

² Cumulative ³⁹Ar gas released during the experiment (%).

³ %40* = % radiogenic ⁴⁰Ar of total ⁴⁰Ar released.

AA6-52A		J=0.0059080								
Step	40/39	38/39	37/39	36/39	³⁹ Ar ¹	F ³⁹ Ar ²	%40* ³	40*/39K	Age	+ 1s.d.
1	6816.031	2.157	0.805	400.872	0.086	0.07	98.30	6701.41	6685.14	21.11
2	512.917	0.259	1.991	50.402	0.553	0.51	97.30	498.87	2478.41	7.69
3	155.505	0.072	1.250	6.791	2.810	2.77	98.80	153.72	1166.31	0.98
4	127.950	0.048	1.160	2.341	12.958	13.18	99.60	127.44	1013.13	0.76
5	121.834	0.045	1.285	1.291	30.695	37.84	99.80	121.65	977.56	0.28
6	118.294	0.045	1.373	0.735	30.607	62.43	100.00	118.28	956.56	0.46
7	123.883	0.044	1.337	1.300	17.308	76.33	99.90	123.71	990.28	0.32
8	118.232	0.045	1.255	2.410	4.872	80.25	99.60	117.71	952.94	0.73
9	117.058	0.041	1.229	2.286	3.853	83.34	99.60	116.57	945.74	1.08
10	120.381	0.045	1.441	2.074	5.424	87.70	99.70	119.99	967.24	0.74
11	151.306	0.055	1.367	3.220	3.495	90.51	99.50	150.59	1148.77	1.46
12	119.895	0.047	1.329	1.726	4.819	94.38	99.70	119.59	964.72	1.61
13	116.820	0.049	1.045	0.031	1.592	95.66	100.10	116.96	948.25	0.99
14	118.405	0.041	0.208	0.098	0.501	96.06	100.00	118.38	957.19	1.53
15	112.348	0.047	0.597	0.120	0.407	96.38	100.00	112.39	919.15	4.52
16	129.151	0.051	1.167	12.733	0.922	97.13	97.20	125.57	1001.72	2.91
17	119.221	0.041	1.350	2.671	3.114	99.63	99.50	118.64	958.77	2.02
18	109.137	0.055	2.398	12.657	0.464	100.00	96.90	105.76	876.17	5.21

¹ ³⁹Ar (x 10⁻¹⁶ mols).

² Cumulative ³⁹Ar gas released during the experiment (%).

³ %40* = % radiogenic ⁴⁰Ar of total ⁴⁰Ar released.